

**DEVELOPMENT OF A PHYSIOLOGY BASED DIFFUSION
MODEL TO PREDICT DERMAL ABSORPTION USING
EXPERIMENTAL INPUT PARAMETERS**

Dissertation

zur Erlangung des Grades des

Doktors der Naturwissenschaften

der Naturwissenschaftlich-Technischen Fakultät III

Chemie, Pharmazie, Bio- und Werkstoffwissenschaften

der Universität des Saarlandes

Von

Steffi Hansen

Saarbrücken 2009

Tag des Kolloquiums: 01 Juli 2009
Dekan: Prof. Dr. Stefan Diebels
Berichterstatter: Prof. Dr. Claus-Michael Lehr (1. Gutachter)
Prof. Dr. Volkhard Helms (2. Gutachter)
Prof. Dr. Rolf Hartmann (Vorsitzender)
Dr. Ulrich F. Schäfer (Akademischer Mitarbeiter)

TABLE OF CONTENTS

TABLE OF CONTENTS	III
SHORT SUMMARY	VII
KURZZUSAMMENFASSUNG	VIII
1 INTRODUCTION	1
1.1 MOTIVATION FOR MODELLING DERMAL ABSORPTION	1
1.2 MORPHOLOGY OF THE SKIN AND SKIN TRANSPORT PATHWAYS	3
1.3 EXPERIMENTAL INVESTIGATION OF DERMAL ABSORPTION	8
1.3.1 <i>Measuring dermal absorption in vitro</i>	8
1.3.2 <i>Evaluation of experimental data</i>	13
1.4 STRATEGIES TO MODEL DERMAL ABSORPTION – STATE OF THE ART	15
1.4.1 <i>Quantitative structure activity relationships (QSAR)</i>	15
1.4.2 <i>Pharmacokinetic models</i>	20
1.4.3 <i>Diffusion models</i>	20
2 AIM OF THE THESIS	33
3 MODEL DEVELOPMENT	35
4 IN SILICO MODEL OF SKIN PENETRATION BASED ON EXPERIMENTALLY DETERMINED INPUT PARAMETERS. PART I: EXPERIMENTAL DETERMINATION OF PARTITION AND DIFFUSION COEFFICIENTS	37
4.1 INTRODUCTION.....	38
4.2 MATERIAL AND METHODS	41
4.2.1 <i>Material</i>	41
4.2.2 <i>Chemicals</i>	41
4.2.3 <i>Composition of buffers</i>	42
4.2.4 <i>Skin samples and skin preparation techniques</i>	42
4.2.5 <i>Lipid coated membranes</i>	42
4.2.6 <i>Characterization of extracted stratum corneum lipids by WAXD</i>	43
4.2.7 <i>Characterization of extracted stratum corneum lipids by DSC</i>	43
4.2.8 <i>Characterization of extracted stratum corneum lipids by HPTLC</i>	44
4.2.9 <i>Determination of drug concentration-skin depth profiles</i>	44
4.2.10 <i>Permeation studies</i>	45
4.2.11 <i>Keratin binding</i>	46
4.2.12 <i>Quantification of flufenamic acid and caffeine</i>	46
4.2.13 <i>Determination of partition coefficients by equilibration experiments</i>	47
4.2.14 <i>Calculation of partition coefficients</i>	49
4.2.15 <i>Calculation of apparent diffusion coefficients</i>	51

4.3	RESULTS.....	52
4.3.1	<i>Characterization of extracted stratum corneum lipids</i>	52
4.3.2	<i>Keratin binding</i>	52
4.3.3	<i>Partition coefficients – directly determined values</i>	53
4.3.4	<i>Partition coefficients – calculated values</i>	57
4.3.5	<i>Diffusion coefficients</i>	58
4.4	DISCUSSION.....	60
4.4.1	<i>Characterization of extracted stratum corneum lipids</i>	60
4.4.2	<i>Partition coefficients – directly determined values</i>	61
4.4.3	<i>Partition coefficients – calculated values</i>	63
4.4.4	<i>Diffusion coefficients</i>	65
4.5	CONCLUSION	67
5	IN SILICO MODEL OF SKIN PENETRATION BASED ON EXPERIMENTALLY DETERMINED INPUT PARAMETERS. PART II: MATHEMATICAL MODELLING OF IN VITRO DIFFUSION EXPERIMENTS.....	69
5.1	INTRODUCTION	70
5.2	MODEL DESCRIPTION.....	71
5.2.1	<i>Model geometry</i>	72
5.2.2	<i>Model equations</i>	73
5.2.3	<i>Aggregation of quantities</i>	75
5.2.4	<i>Numerical techniques</i>	76
5.3	MODEL AND EXPERIMENT	76
5.3.1	<i>Input parameters</i>	76
5.3.2	<i>Corneocyte diffusion</i>	77
5.3.3	<i>Concentration-depth-profiles</i>	79
5.4	RESULTS.....	79
5.4.1	<i>Apparent SC-diffusion coefficient</i>	79
5.4.2	<i>Parameter studies</i>	80
5.4.3	<i>Concentration-depth-profiles</i>	82
5.5	DISCUSSION.....	83
5.5.1	<i>Apparent SC-diffusion coefficient</i>	84
5.5.2	<i>Concentration-depth-profiles</i>	85
5.5.3	<i>Parameters</i>	85
5.6	CONCLUSION.....	87
5.7	APPENDIX A	87
5.7.1	<i>Dimensionless form</i>	88
5.7.2	<i>Flux as a function</i>	89
5.7.3	<i>Effective diffusivity</i>	90

6 THE ROLE OF CORNEOCYTES IN SKIN TRANSPORT REVISED – A COMBINED COMPUTATIONAL AND EXPERIMENTAL APPROACH	91
6.1 INTRODUCTION.....	92
6.2 THEORY	97
6.2.1 <i>Definition of compartments and interfaces</i>	97
6.2.2 <i>Description of compound membrane interaction</i>	99
6.2.3 <i>The special case of non-protein binding substances</i>	101
6.2.4 <i>Calculation of a theoretical stratum corneum-donor partition coefficient</i>	101
6.2.5 <i>Input parameters</i>	102
6.3 MATERIAL AND METHODS	105
6.3.1 <i>Material</i>	105
6.3.2 <i>Chemicals</i>	105
6.3.3 <i>Composition of buffers</i>	106
6.3.4 <i>Skin samples and skin preparation techniques</i>	106
6.3.5 <i>Determination of saturation concentration</i>	107
6.3.6 <i>Keratin binding</i>	107
6.3.7 <i>Determination of partition coefficients by equilibration experiments</i>	108
6.3.8 <i>Quantification of caffeine, flufenamic acid, and testosterone</i>	109
6.3.9 <i>Software</i>	110
6.4 RESULTS.....	110
6.4.1 <i>Hydration</i>	110
6.4.2 <i>Input parameters</i>	111
6.4.3 <i>Mechanism of corneocyte interaction – experimental results</i>	113
6.4.4 <i>Mechanism of corneocyte interaction – comparison of theoretical and experimental results</i>	115
6.5 DISCUSSION	125
6.6 CONCLUSION	128
SUMMARY	IX
ZUSAMMENFASSUNG	XV
REFERENCES	XXII
ABBREVIATIONS.....	XLVII
CURRICULUM VITAE.....	XLIX
LIST OF PUBLICATIONS.....	L
DANKSAGUNG	LV

SHORT SUMMARY

A physiology-based diffusion model is developed to predict drug transport across human skin. It features the “brick-and-mortar”-geometry with homogeneous lipid and corneocyte phases, accessible corneocytes and a homogeneous viable skin layer compartment. Methods are developed to determine all relevant input parameters. Partition and diffusion coefficients are measured using human abdominal skin or are estimated from experimental data, if not directly accessible. Caffeine (CAF) and flufenamic acid (FFA) serve as model drugs. The quality of the model is evaluated by comparing experimental and predicted concentration-depth-profiles. For both CAF and FFA it is found that the corneocytes have a decisive influence on *stratum corneum* affinity and transport.

Therefore, mechanisms of corneocyte-interactions are investigated experimentally and theoretically for the model drugs CAF, FFA, and testosterone (TST). For the non-protein binding CAF the impact of the aqueous compartment on *stratum corneum* partitioning is successfully modelled after introducing a bound water fraction that is non-accessible for compound dissolution. For the lipophilic, keratin binding compounds (FFA, TST) interactions are probably confined to the corneocyte surface. Binding to intracellular keratin is limited by their low aqueous solubility.

KURZZUSAMMENFASSUNG

Ein Physiologie-basiertes Diffusionsmodell zur Vorhersage des Hauttransports wird entwickelt. Die Geometrie basiert auf dem Ziegelstein-Mörtel-Modell, wobei Lipide und Corneocyten sowie die lebenden Hautschichten als homogen und zugänglich für Substanzen angenommen werden. Es werden Methoden entwickelt, um alle relevanten Eingangsparameter für das Modell experimentell zu bestimmen. Verteilungs- und Diffusionskoeffizienten werden an humaner Abdominalhaut gemessen oder, sofern nicht direkt zugänglich, aus experimentellen Daten abgeschätzt. Als Modellsubstanzen dienen Koffein (CAF) und Flufenaminsäure (FFA). Die Modellqualität wird im Vergleich von experimentellen und errechneten Schichttiefenprofilen überprüft. Dies ergab, dass die Corneocyten für sowohl CAF als auch FFA eine entscheidende Rolle bei der Affinität der Substanzen zum *stratum corneum* sowie bei dem Transport über das *stratum corneum* spielen.

Daher werden die Mechanismen der Wechselwirkung mit den Corneocyten für die Modellsubstanzen CAF, FFA und Testosteron (TST) experimentell und theoretisch untersucht. Um die Verteilung von CAF, das nicht an Proteine bindet, in das *stratum corneum* erfolgreich zu modellieren, muss eine gebundene, unzugängliche Wasserphase berücksichtigt werden. Für lipophile, keratinbindende Substanzen (FFA, TST) sind Interaktionen mit den Corneocyten wahrscheinlich begrenzt auf deren Oberfläche. Die Bindung an intrazelluläres Keratin ist aufgrund ihrer geringen Wasserlöslichkeit limitiert.

1 INTRODUCTION

1.1 Motivation for modelling dermal absorption

The skin constitutes one of the largest interfaces between body and environment covering a surface area of approximately 2 m² with adults. On the one hand, the human skin guarantees water homeostasis and shields the body from invasion of pathogens and noxious environmental influences. On the other hand, it is involved in the thermoregulation of the body and serves as an excretory organ. This bifunctional nature of the skin depends on its highly differentiated structure, with the main barrier function being located in the outermost skin layer, the *stratum corneum* (SC).

Whether contact occurs unintended at work, through use of household chemicals, or via application of cosmetics or pharmaceutical products; a variety of different compounds gets into contact with our skin every day. Some may be absorbed or facilitate the absorption of other potentially harmful compounds. Therefore, understanding of skin absorption processes is needed for several reasons.

Safety aspects of chemicals are particularly addressed in the EU REACH program (“Registration, Evaluation, Authorisation, and Restriction of Chemicals”) requesting skin absorption data for toxicological examination. In addition to skin absorption data, substance classification for regulatory purposes also requires skin sensitization, corrosiveness, and photo-toxicity data. The latter ones are also requirements for cosmetical formulations, additional to the knowledge of the invasive behaviour of “active” ingredients in these preparations.

In the field of pharmaceutical sciences, the skin as a delivery route enjoys a high acceptance by patients. In this regard, two different cases have to be distinguished: local delivery to selected skin layers (e.g., antimycotics) and systemic delivery (e.g., hormones). In the context of bioavailability assessment, knowledge on the absorption behaviour of the active compound is essential. For ethical reasons, fundamental skin absorption data can normally not be obtained by conducting *in vivo* studies although *in vivo* studies with human skin must always be considered the “gold-standard”. Therefore, other techniques have been used to obtain the desired information. One option is the use of *in vitro* models and to establish an *in vitro-in vivo* correlation. Some basic information on *in vitro* techniques is provided in a number of documents, such as the Organization for Economic Cooperation and Development (OECD)

guideline 428 (5) in combination with OECD guidance 28 (6), the Scientific Committee on Cosmetic and Non-Food Products Intended for Consumers (SCCNFP) guideline (7), an European Commission (EC) guide (8), and an United States Food and Drug Administration (FDA) guidance (9). However, application of guidance documents to experimental protocols remains challenging and leads to a vast variety of protocols in use which make inter-laboratory comparison still difficult.

The available resources for human skin for *in vitro* studies are limited. This has promoted the search for alternative models. A switch to animal skin, therefore, seems obvious. Species currently in use are mouse, hairless rat, hamster (cheek pouch), snake (shed skin), pig (ear, flank, abdomen or back) and cow (udder). However, differences in SC thickness, number of corneocyte layers, hair density, water content, lipid profile and morphology cause especially rodent skin to be more permeable than human skin, leading to an overemphasis of compound permeability (10). Comparing results different species, human skin finds its closest match in porcine tissue (10-12). While animal skin is still mentioned in the OECD guidance document 28, the explicit use of human skin has later been demanded as the only acceptable surrogate in human risk assessment (5, 11). In addition, a general testing, as well as marketing ban concerning the use of animals for testing cosmetics or their ingredients will come into action in the European Union in September 2009 (13).

To circumvent species differences and testing bans, biotechnologically reconstructed human *epidermis* equivalents are investigated to serve as membranes in permeation experiments as recently reviewed by Netzlaff *et al.* (14). Results of this so-called “German Validation Study” conducted in the years 2003 to 2005 and funded by the “Bundesministerium für Bildung und Forschung” (Federal Ministry for Education and Research) have shown the suitability of such bioengineered human *epidermis* equivalents in permeation studies (15). However, similar to some animal skin models the permeability of these reconstructed human *epidermis* models is much higher than in human skin due to a limited barrier function. Shortcomings of animal and reconstructed *epidermis* models promoted the interest in mathematical prediction of skin absorption. Through the years a large variety of models were developed and greatly improved our understanding of the principles governing skin absorption. The next paragraphs will give an introduction to the skin morphology followed by an overview of the main modelling strategies.

1.2 Morphology of the skin and skin transport pathways

The skin is a multilayer laminate consisting of three histological layers (Figure 1-1):

The subcutis or subcutaneous fatty tissue (*hypodermis*)

The dermis

The *epidermis*, that is itself subdivided into

Basal membrane

Stratum germinativum

Stratum spinosum

Stratum granulosum

Stratum lucidum (only present in plantar and palmar *epidermis*)

Stratum corneum

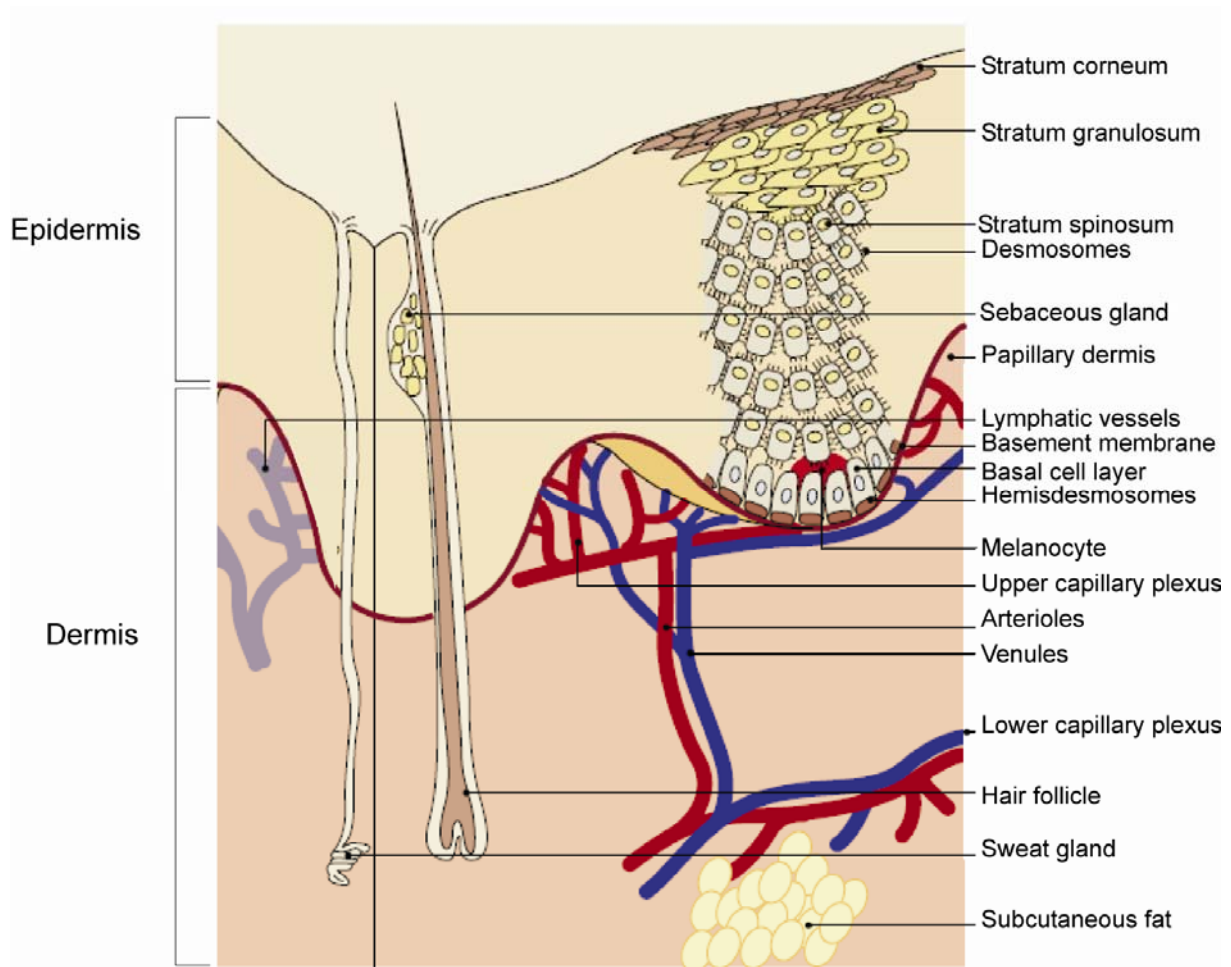


Figure 1-1 Morphology of the skin. Adapted from (16).

The subcutis is composed of loose fat lobules surrounded by connective tissue that is interspersed with blood vessels and nerves and also contains macrophages (17). It

serves as mechanic cushion, isolation, and energy reserve and anchors the skin in the underlying muscle.

The *dermis* is the largest layer of the skin with a thickness of 0.1-0.5 cm depending on body site. The major cells are fibroblasts that produce the compounds of the dermal matrix. This is a gel like mixture of mucopolysaccharides containing collagen and elastin fibres (18). The fibrous structure provides tensile strength and elasticity to the whole skin. Two horizontal capillary plexuses provide the nutrition of the avascular *epidermis*. These are situated at the papillary-reticular junction and at the dermal-hypodermal junction. A more randomly oriented microvasculature supplies skin appendages originating from the *dermis* such as hair follicles and sweat glands (19). Blood and lymphatic vessels fulfil major tasks in removal of waste and metabolic products, immune functions, regulation of body temperature and blood pressure (17). Furthermore, the *dermis* contains sensoric nerves that report pressure, pain and temperature changes.

The basal membrane is situated between *dermis* and *epidermis*. Here keratinic stem cells are situated that are responsible for the skin proliferation. The basal layer further contains several classes of specialised cells. Melanocytes are responsible for the pigmentation not only of skin but also of eyes and hairs. They produce different melanins, high molecular weight polymers of indole quinone, which absorb UV radiation (17). This in turn promotes the melanogenesis and hence leads to skin tanning. Due to the high energy of UV radiation and generation of free radicals excessive sun bathing can lead to melanomas which are one of the most frequent forms of skin cancer. Langerhans cells are also situated in the basal cell layer and accumulate around the hair bulbs (20). These are dendritic cells responsible for presenting antigens, such as contact allergens, to T-lymphocytes in the skin draining lymph nodes. As such they play an important role in contact sensitisation. A final cell population of the basal membrane are Merkel cells. They play a role as sensory receptors of the nervous system as nerve endings are lying closely on the dermal side of the basal membrane (17).

Keratinocytes generated in the basal membrane differentiate during their progress through the different layers of the viable *epidermis* until they are finally desquamated. In the SC desmosomes, that are present in the epidermal layers, are cleaved by proteases leading to desquamation (21, 22). The turnover time of the *epidermis* is approximately 28 days but can be influenced by diseases and environmental effects.

During differentiation the appearance of the cells changes drastically. Directly above the basal layer lies the *stratum spinosum*. Its characteristic spiny appearance is caused by prominent tonofilaments (17). In the outer cell layers keratohyalin and membrane-coating granules appear within the cytosol, marking the transition to the *stratum granulosum*. These contain precursors of the SC intercellular lipid bilayers: glycosylceramides, glycerophospholipids, cholesterol, and sphingosine (23). At the junction between *stratum granulosum* and SC the lamellar granules move to the cell membrane, fuse together and extrude their content into the intercellular space (24). At this step of differentiation the keratinocytes undergo several significant changes that in the end lead to the formation of the highly effective SC barrier.

The SC is the outermost layer of the *epidermis*. It is approximately 10-20 μm thick varying with body site. As most cell organelles including nuclei are degraded during final keratinocyte differentiation it is nonviable *epidermis*. The SC is composed of 15 to 25 layers of tightly packed, flattened cornified cells, embedded into a continuous lipid matrix. The interior of the corneocytes is composed of keratin intermediate filaments. These are cross-linked among each other and to the cornified cell envelope via disulfide bonds by the action of filaggrin (filament aggregating protein). Filaggrin is then disintegrated to amino acids (25). Together with keratin and glycerol (a by-product of the generation of free fatty acids) these amino acids are the natural moisturizing factors providing the water holding capacity of the SC. Compared to the usual water content of tissues of around 70% the typical SC hydration *in vivo* is only about 30% (26, 27). The corneocytes are surrounded by a 10 nm thick cornified cell envelope made of highly crosslinked insoluble proteins, mainly loricrin and small proline-rich protein (1, 28). These proteins are covalently attached to an outer lipid envelope of ω -hydroxyacyl-sphingosines (29) acting as a scaffold for ordering the intercellular lipid bilayers. The composition of the intercellular lipids is unique among epithelia as they contain practically no phospholipids (23). Instead they are made up of ceramides (40 wt%), free fatty acids (12 wt%), cholesterol (25 wt%), and a smaller percentage of cholesterol esters and cholesterol sulphate (30). The relative ratio of the lipid components depends on body site (31). From transmission electron micrographs and small angle x-ray diffraction the lipid lamellae were shown to be oriented parallel to the surface of the corneocytes with repeat distances of 6.4 and 13.4 nm (32-34). These result from a partly or fully interdigitation of ceramides of adjacent bilayers. From wide angle x-ray diffraction and electron refraction studies

large parts of the lipids are known to be present in a crystalline organization of orthorhombic but also slightly looser hexagonal packing (35).

Although it accounts for only a fraction of the overall skin thickness the SC is the most effective barrier of the skin. This can be shown by inflicting a mechanical damage to the SC, e.g. via tape-stripping, sand-paper abrasion or suction blisters which results in a strong increase in permeability (36, 37). Likewise, pathological changes to the SC may affect the permeability: psoriatic plaques are known to be more permeable than healthy skin (38, 39). Nonetheless, favourable physicochemical properties provided, the permeability of intact skin is sufficiently high to be used as an application route in dermatology. Pathways across the membrane are still a matter of debate. As active transporters are absent in the SC there absorption is a passive process. According to the morphology of the SC an inter-cellular, trans-cellular and trans-appendageal (trans-glandular and trans-follicular) route is discussed (Figure 1-2).

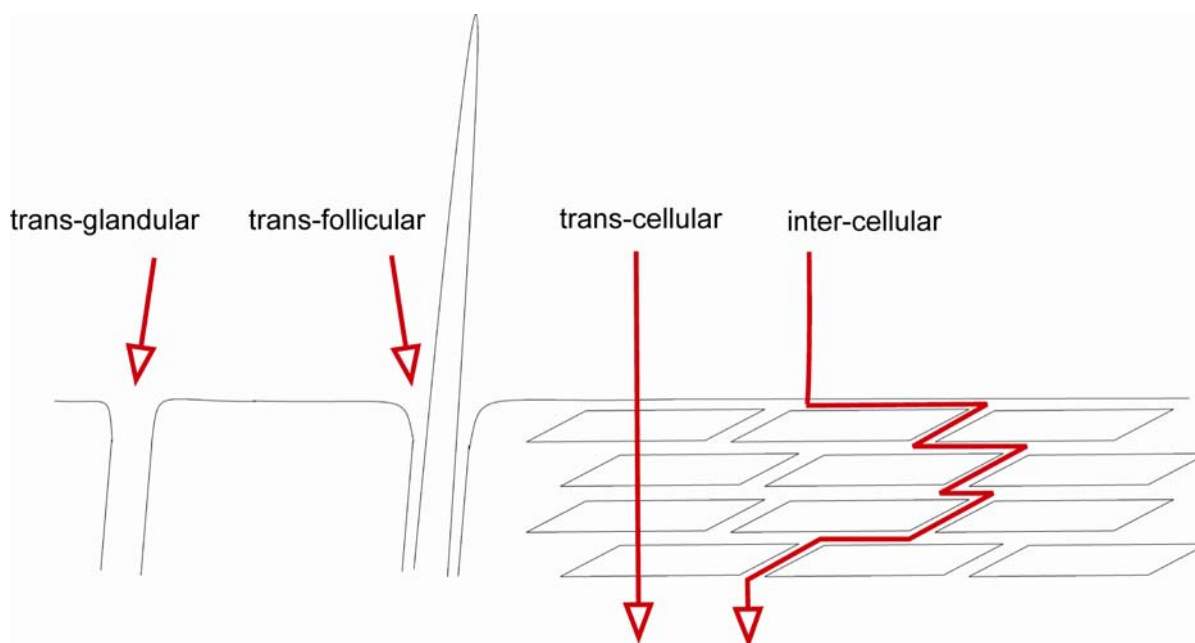


Figure 1-2 Skin permeation pathways. Not drawn to scale. *Stratum corneum* abridged after 4 corneocytes layers.

A huge body of evidence shows that the intercellular lipid pathway plays a dominant role. Thus permeability is strongly enhanced after lipid extraction with organic solvents (40-43). Differential scanning calorimetry, and small and wide angle x-ray diffraction measurements have shown that excipients as well as drugs that act as permeation enhancers modify the crystallinity and organization of the lipid bilayers (44, 45). Several authors noted that inter-individual differences in lipid composition

and organization may be responsible for the high variability reported for drug permeability studies (46-48). Using artificial lipid mixtures de Jager et al. could show that the ceramides are critical for the formation of a long periodicity phase in the artificial lipid bilayers which in turn are essential for achieving barrier properties comparable to natural SC (49).

In contrast the existence of a trans-cellular path was long neglected and is still discussed controversially. The discussion is intimately connected with the discussion of the nature of the hydrophilic passage across the SC. It was argued that at physiological hydration corneocytes do not contain any free water which could enable trans-cellular diffusion. However, it is known that upon exposure to wet air as well as direct contact to water or under occlusive conditions SC takes up water several times its own weight (50, 51). This soon leads to the formation of free water featuring dissolution properties similar to bulk water (26, 52). Boddé et al. showed that aqueous solutions of mercuric chloride applied to dermatomized human breast skin preferably diffuse along the lipid channel, however, with a slight delay, also enter the corneocytes (53). Meanwhile, using microscopical techniques a number of other compounds were witnessed inside the corneocytes (54-56).

The role of appendages was long considered inferior due to their low surface coverage. Recently this value for hair follicles was corrected to be higher than previously assumed (57). Varying with body site a maximum was found at the forehead (1.28%) and a minimum on the forearm (0.09%). The trans-follicular pathway seems to be especially important for the invasion of nanoparticles (58). Small size as well as the natural movement of the hair were reported to be beneficial for the accumulation of the nanoparticles in the follicular opening (58-60). In general, for small molecules the trans-follicular pathway seems to be of less importance although the matter is little understood. Nonetheless, for several compounds the follicular route seems to promote permeability at the beginning of skin absorption while it is overruled by the other higher capacity pathways at later times in the transport process (61-63). Several methods were proposed to investigate the follicular contribution to permeation such as the "SC sandwich" (64); closing hair follicle openings with varnish wax under microscopical control (61); or differential stripping with tape and cyan-acrylate glue (65).

1.3 Experimental investigation of dermal absorption

1.3.1 *Measuring dermal absorption in vitro*

Two different intentions may be pursued with *in vitro* dermal absorption experiments. “Skin permeation” measurements focus on the rate of transport across the skin without looking at processes inside the skin barrier. This is important if a systemic delivery is desired as with transdermal patches delivering drugs such as nicotine, opioid analgesics or sexual hormones across the skin to the circulation. It is equally important for evaluating potential side effects that may result from systemic absorption of topically applied drugs.

In contrast, in “skin penetration” experiments the concentration of an absorbed compound in a certain skin layer or at a specific depth within a single skin layer is measured over time. Therefore, penetration experiments are adequate to investigate local delivery to the skin. This concerns by far the most topical applications for example the treatment of allergic or irritant dermatitis, psoriasis, fungal or bacterial skin infections as well as cosmetic applications of skin care products, repellents or sun-protection.

The difference between permeation and penetration is illustrated in Figure 1-3.

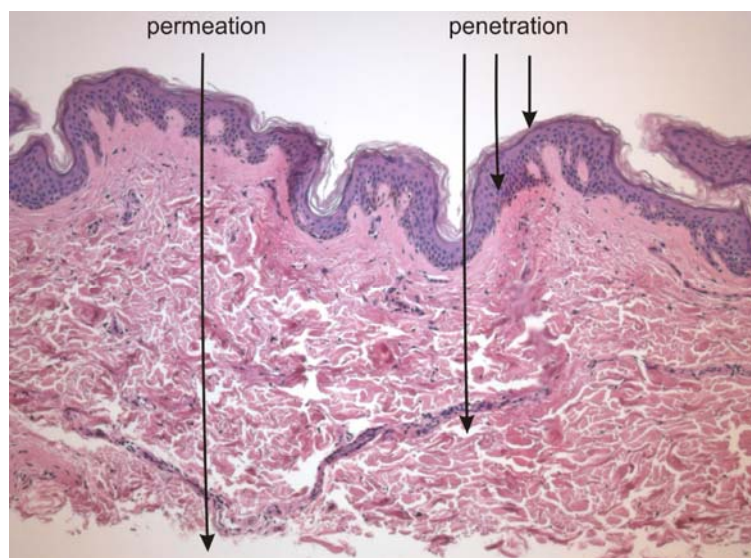


Figure 1-3 Comparison of skin permeation versus penetration. Cross section through human dermatomized skin, x100. Samples are stained with haematoxylin/eosin. Cross sections with a thickness of 4 μm were prepared using a microtome. Pictures courtesy of Leon Muijs.

A very common model for evaluating the *in vitro* skin permeability is the static Franz-type diffusion cell (Figure 1-4). The drug permeability from a donor chamber containing the drug formulation across excised skin or separated skin layers into an acceptor chamber is evaluated. Dosing is possible in infinite (typically $>10 \mu\text{l}/\text{cm}^2$ or $10 \text{ mg}/\text{cm}^2$) or finite manner ($<10 \mu\text{l}/\text{cm}^2$ or $10 \text{ mg}/\text{cm}^2$). Continuous stirring of the acceptor phase minimizes the build-up of non-stirred water layers below the skin membrane. The temperature of the skin surface is held constant at 32°C to mimic the surface temperature of skin *in vivo*. At pre-defined time intervals samples are removed from the acceptor via the sampling port and are analyzed for drug content. Other setups, namely flow-through cells, allow continuous sampling from the acceptor side.

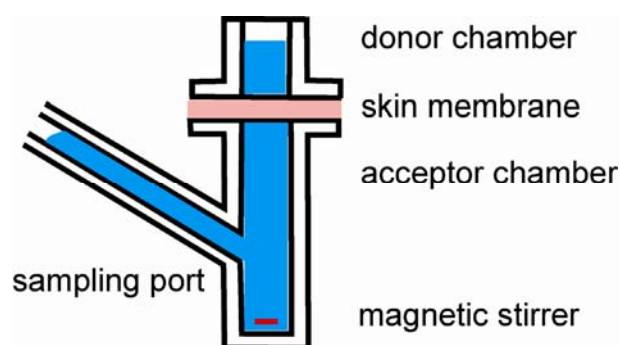


Figure 1-4 Static Franz diffusion cell.

The cumulative drug amount permeated into the acceptor per area is plotted against time. Under infinite dosing the cumulative drug amount in the acceptor increases exponentially during an initial “lag-phase” until the amount permeated per time and area becomes constant at “*steady state*” (Figure 1-5). In contrast, with finite dosing a “*steady state*” is usually precluded as the donor concentration decreases continually during permeation. Therefore the acceptor concentration reaches a plateau before falling off again by dilution through sampling (Figure 1-5).

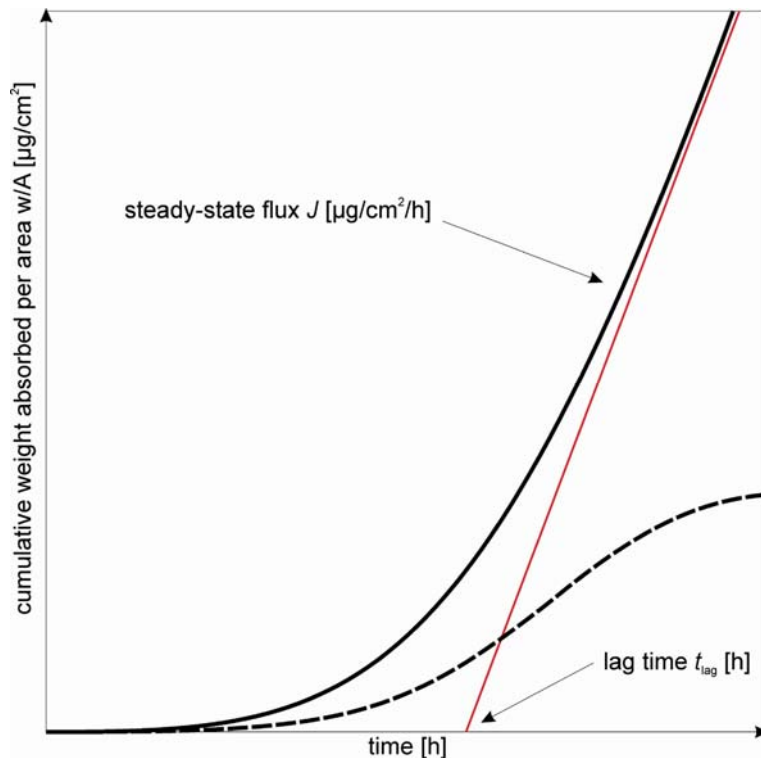


Figure 1-5 Evaluation of skin permeation experiment. The cumulative weight absorbed is plotted against time and approaches a straight line. Infinite dosing (bold black line), linear regression of *steady-state* part of the curve (red line), finite dosing (bold black dashed line).

“Skin penetration” experiments require a processing of the skin following an incubation period. This processing involves destructive methods so that a time-course cannot be evaluated as straight-forward as in permeation experiments.

Drug levels within the SC can be assessed by sampling single corneocyte layers with adhesive tape (Figure 1-6).

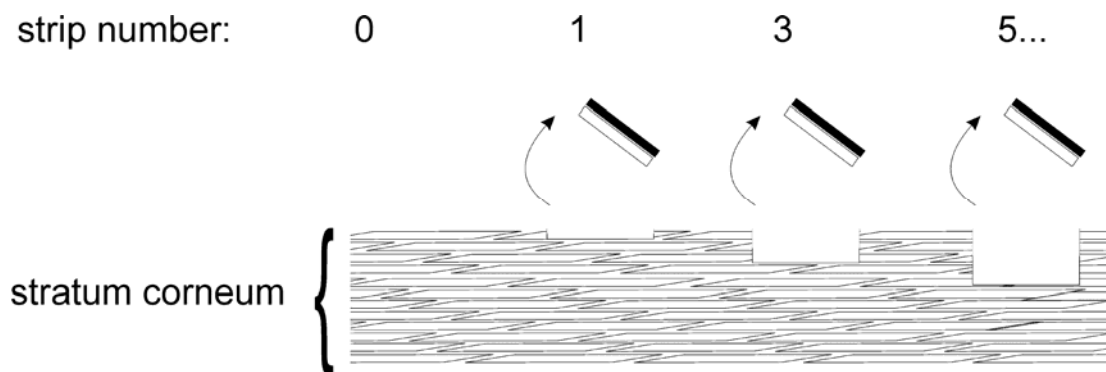


Figure 1-6 Tape-stripping of *stratum corneum*. Full thickness skin abridged after *stratum corneum*. Not drawn to scale. Adapted from (66).

Within the deeper skin layers, that is, the *epidermis* and *dermis*, analogous information can be obtained using biopsy punches. After freezing, the punch biopsies

may be segmented parallel to the surface, by means of a cryo-microtome. The drug is then extracted from the tape-strips or cryo-cuts and quantified by a suitable analytical method, usually scintillation counting (for radioactive compounds) or high performance liquid chromatography. Provided the test substance yields a unique infrared signal, distinguishable from surrounding tissue and formulation components, attenuated total reflectance Fourier-transformation infrared (ATR-FTIR) spectroscopy is a fast, although technically sophisticated alternative method of quantification (67). It has been used to monitor dermal absorption of model substances like 4-cyanophenol, to investigate depth-dependent changes in barrier properties or SC hydration, and investigate the effects of formulation excipients and penetration enhancers, such as oleic acid, on the SC barrier function (68-71).

Results are reported as the drug amount absorbed per square centimetre of SC. In addition, correlating the local drug concentration with the skin depth will result in a detailed insight into the concentration gradient across the membrane, that is, the actual driving force for drug diffusion (Figure 1-7).

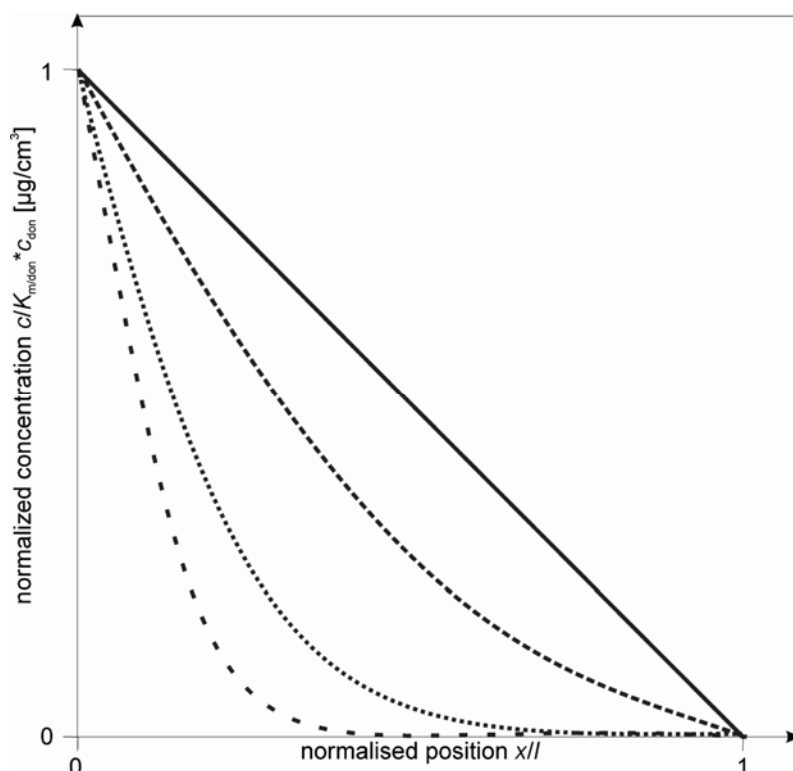


Figure 1-7 Evaluation of skin penetration experiment. Normalized concentration-depth profiles of a drug as a function of time within the membrane of thickness l . $K_{m/don}$ is the membrane partition coefficient, c_{don} is the donor concentration.

Integrating skin concentration-depth profiles over the SC thickness is a measure of the cutaneous bioavailability (72). For comparison conventional *in vivo* methods make use of a pharmacodynamic response in the vasoconstrictor assay or sample from blood and urine. These methods suffer from subjectivity, low sensitivity, and a sophisticated analysis of biological samples among others. In addition, the majority of cutaneously applied drugs are aiming at a local response so that the systemic concentration may not necessarily be representative of the concentration at the target site. The vasoconstrictor or “skin blanching”-assay is an example where a local pharmacodynamic response is evaluated, namely the skin whitening due to a constriction of dermal capillaries. It must be stressed that this response is specific to the local administration of corticosteroids so that the assay cannot be transferred to other drugs. Unfortunately, an FDA guideline proposing tape-stripping as an alternative method to assess the bioequivalence of generics was later drawn back as a consequence of contradictory results of several studies testing the bioequivalence of tretinoin gel products (73, 74).

Lately also optical segmentation methods have been adopted for purposes of skin penetration testing. Confocal laser scanning microscopy (CLSM) localizes a permeating molecule via its fluorescence. Fluorophores in the tissue are excited by a laser and fluorescence is collected particularly from the focal volume of the microscope using a pinhole. To obtain three-dimensional information a sequence of optical sections is collected in axial direction and later re-assembled in the computer. The axial resolution that can be achieved is $\sim 1\ \mu\text{m}$ with a maximum depth into the tissue of $\sim 200\ \mu\text{m}$ depending on transparency to the exciting laser light and scattering of the tissue. CLSM has been used to investigate the penetration of nano- and micro-sized carriers as well as fluorescent molecules qualitatively (58, 75-78). However, achieving quantitative information on concentration and depth is not straightforward as the fluorescence intensity is sensitive to the microscopic environment and subject to photobleaching.

Disadvantages of CLSM such as a low light penetration depth, out-of-focus photodamage, out-of-focus photobleaching and low photon collection efficiency owing to spatial filtering by the pinhole can be overcome by multiphoton fluorophore excitation using near-infrared femtosecond laser pulses and high numerical aperture objectives (79). Multi-photon microscopy has for example been used to investigate

the penetration of PLGA-nanoparticles containing flufenamic acid into human abdominal skin (80).

As with CLSM multi-photon microscopy is restricted to detecting fluorophores. In contrast confocal Raman microscopy opens up possibilities to detect a much greater variety of molecules. The Raman effect is based on inelastic scattering of light by chemical bonds and is shown by nearly all molecules and crystals. At a specific resonance frequency molecular vibrations are triggered that reduce the frequency of the scattered photon. Hence the vibrational spectrum offers chemical information on the illuminated molecule. Confocal Raman microscopy offers a non-invasive possibility to combine highly specific chemical information with three dimensional imaging. Momentarily the lower limit of quantification (LOQ) of around 0.1-1% [w/V] within the focal volume restricts its application. The technique has been used to investigate major compounds of the skin such as water, natural moisturizing factors, skin lipids (81, 82). Also first studies on the penetration of molecules, namely the penetration of metronidazol for the treatment of rosacea, were reported (83).

1.3.2 Evaluation of experimental data

Transport across the main skin barrier, i.e. the SC, is a passive process. Therefore Fick's law of diffusion has been successfully applied to describe skin absorption. Fick's first law assumes the rate of transport per unit area to be proportional to a concentration gradient.

Equation 1-1
$$J = \frac{w}{A} = -D \frac{\partial c}{\partial x}$$

Where J is the flux, which is the rate of transfer per unit area (w/A), D is the diffusion coefficient, c is the concentration of diffusing species (the "diffusant" or "permeant"), and x is the space coordinate.

Fick's second law is a mass balance equation derived from Equation 1-1 (84). Treating skin simplistically as a homogeneous barrier with a constant diffusion coefficient D the diffusion equation is

Equation 1-2
$$\frac{\partial c}{\partial t} = \frac{\partial}{\partial x} \left(D \frac{\partial c}{\partial x} \right) = D \frac{\partial^2 c}{\partial x^2}$$

An approximate solution for the *steady state* (i.e. the tangent to the linear part of the curve in Figure 1-5) is expressed via the linear equation

Equation 1-3
$$J = \frac{D \cdot c}{l} \left(t - \frac{l^2}{6D} \right)$$

Here c is the concentration in the membrane which is related to the measurable concentration in the donor via the membrane-donor partition coefficient according to $c = K_{m/don} \cdot c_{don}$, t is the time, and l is the membrane thickness. The boundary conditions for infinite donor and perfect sink acceptor are $c = \infty$ at $x = 0$ and $c = 0$ at $x = l$. Slope and intercept with the x-axis, i.e. *steady state* flux J and lag-time t_{lag} are used as characteristic descriptors of permeation.

Equation 1-4
$$J = \frac{DK_{m/don}}{l} c_{don}$$

Equation 1-5
$$t_{lag} = \frac{l^2}{6D}$$

Normalizing *steady state* flux for c_{don} gives the apparent permeability coefficient k_P , a parameter only determined by D , $K_{m/don}$, and l , reflecting the interplay of membrane, substance, and formulation:

Equation 1-6
$$k_P = \frac{J}{c_{don}} = \frac{DK_{m/don}}{l}$$

Prerequisite for the outlined procedure are sufficient data points in the *steady state* part of the curve. This can be especially difficult for slow permeating substances as the analysis time *in vitro* is limited due to microbial contamination of the skin. Thus, for $t < 2.4 t_{lag}$ Equation 1-3 is an insufficient approximation of the diffusion equation. In this case an exact solution of Equation 1-2 (84) describing the whole curve is

Equation 1-7
$$J = K_{m/don} c_{don} l \left[\frac{D}{l^2} t - \frac{1}{6} - \frac{2}{\pi^2} \sum_{n=1}^{\infty} \frac{(-1)^n}{n^2} \exp\left(-\frac{Dn^2\pi^2 t}{l^2}\right) \right]$$

A transient solution describing concentration depth profiles within the membrane under infinite dose conditions as measured in penetration experiments is given by (84)

Equation 1-8
$$c(x,t) = K_{m/don} c_{don} \left[\left(1 - \frac{x}{l} \right) - \frac{2}{\pi} \sum_{n=1}^{\infty} \frac{1}{n} \sin\left(\frac{n\pi x}{l}\right) \exp\left(-\frac{Dn^2\pi^2 t}{l^2}\right) \right]$$

Here $c(x,t)$ is the drug concentration at a defined position x within the membrane after a defined incubation time t , c_{don} is the donor concentration, $K_{m/don}$, D , and l are the membrane-donor partition coefficient, the membrane diffusion coefficient and the membrane thickness respectively.

1.4 Strategies to model dermal absorption – state of the art

1.4.1 Quantitative structure activity relationships (QSAR)

Quantitative structure activity relationship models (QSAR) try to correlate a biological effect, in this case the skin absorption, to physicochemical and/or molecular properties, so-called descriptors, that are likely to affect it. This can be achieved based on mechanistic or empirical considerations. Descriptors can either be derived from experiments or calculated from molecular features. Due to the nature of QSARs the outcome of the predictions is always a number value. Therefore QSARs will not allow predicting the development of a process with time. Focussing on the problem of skin absorption this means that predictions are limited to *steady state* parameters.

The majority of QSARs predicting skin absorption are mechanistically based. The QSAR-equation is basically a linear cause-effect relationship that is evaluated by multiple linear regression analysis of a database. From the model equation general information on influences on dermal absorption can be derived, e.g. from positive or negative, linear or exponential coefficients attributed to a certain descriptor. Still, the skin barrier itself is treated as a “black-box” and no primary assumptions on absorption processes are made.

The majority of QSARs is developed for *in vitro* databases reporting logarithmical *steady state* permeability coefficient $\log k_P$. Following the rational of Equation 1-6 molecular descriptors used in QSARs to estimate $\log k_P$ are substitutes for $K_{m/don}$ and D a widely cited example being the Potts and Guy equation (85)

Equation 1-9
$$\log k_P = \log\left(\frac{D_0}{l}\right) + b \cdot \log K_{Oct/w} - c' \cdot MW$$

$\log(D_0/l)$ can be assumed to be a constant, a . Multiple linear regression of $\log k_P$ upon $\log K_{Oct/w}$ and MW provided the following results for a , b , and c' for a database of 93 permeabilities:

Equation 1-10
$$\log k_P = -6.3 + 0.71 \cdot \log K_{Oct/w} - 0.0061 \cdot MW$$

Thus Potts and Guy could explain as good as 70% of the variability of the data, the remaining 30% variability being similar to what were to be expected for experimental $\log k_P$ values (85). A variety of usually very similar models has been proposed for different datasets that are for example reviewed in (18). Similar equations have been proposed by numerous authors.

Part of the remaining variability can be explained if additionally descriptors for protein binding are included (86). For a subset of 37 non-electrolytes Potts and Guy developed a QSAR including only a molecular volume term but no descriptor of compound lipophilicity and added descriptors of solute hydrogen bond acidity ($\sum \alpha_2^H$) and basicity ($\sum \beta_2^H$) achieving $r^2 = 0.94$.

Equation 1-11 $\log k_p = 0.0256MV - 1.72 \sum \alpha_2^H - 3.93 \sum \beta_2^H - 4.85$

Other researchers confirmed the importance of hydrogen bonding as a predictor in QSARs (87, 88). Magee et al. noticed that the impact of hydrogen bonding is increased for highly lipophilic compounds (89).

For comparison in empirical models the cause-effect relationships are intrinsically non-linear and therefore free of primary mechanistic considerations. Still many of the descriptors used in empirical models are the same as applied in mechanistic QSARs so that they are meaningful in the context of skin absorption. Empirical models are justified for multi-factorial biological process such as skin absorption is e.g. influenced by the interplay of permeant, skin and formulation. A prominent method that has repeatedly been used to predict skin permeability are artificial neural networks (ANN) as reviewed recently by Yamashita et al. (90). These are inspired by information processing in the nervous system. The topology of an ANN consists of an input layer, an output layer, and a number of intermediate layers called hidden layers (Figure 1-8).

Each layer has a certain number of units that are cross-linked with the units of the previous and the subsequent layer. These connections are basically the information pathways. Statistical learning methods are used to attach a certain weight to each connection. The units of the input layer can be identical to the descriptors used in mechanistic models. Accordingly, the output layer would be the logarithmical skin permeability coefficient $\log k_p$.

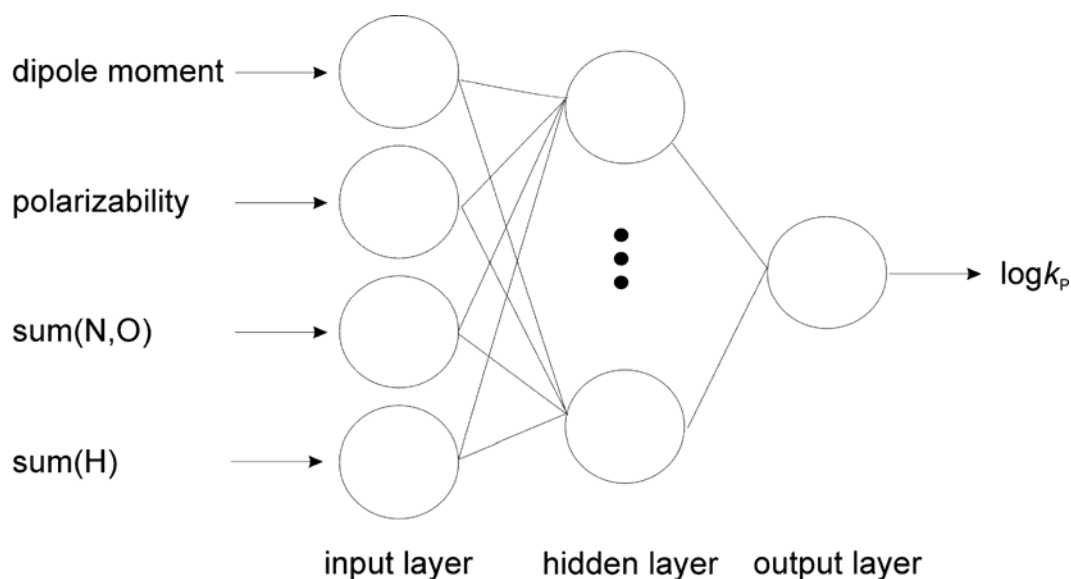


Figure 1-8 Schematic representation of a three-layer artificial neural network. Reproduced from (91).

The quality of QSARs is influenced by homogeneity and size of the database. Especially older databases contain homologous or very closely related series of molecules with only a small number of compounds included, often collected in a single laboratory. This often leads to model equations that rely on a single molecular descriptor due to co-linearity of descriptors such as lipophilicity and molecular weight. This makes it impossible to distinguish between the effects of these two factors on the permeability of large hydrophobic molecules (18). Recent larger databases aimed to avoid this problem by allowing a higher heterogeneity by including data from different sources risking at the same time a higher variability and the inclusion of unreliable data (92, 93). The largest data collections that are the basis for most recent QSARs report $\log k_p$ evaluated across human skin from aqueous vehicles. These are the Flynn database (97 $\log k_p$ values of 94 compounds from 15 different literature sources (94)); the databases collected by Wilschut et al. (123 permeability coefficients of 99 compounds, (95)); and Vecchia and Bunge (170 permeabilities of 127 compounds (96)).

An inherent problem of QSARs is that their applicability is limited by the scope of the database. This concerns the range covered by the descriptors, e.g. penetrant size ($MW < 700$) and polarity ($-1 < \log K_{Oct/w} < 3$) (97) as well as experimental conditions, such as donor vehicle and dosing regime.

QSARs relying on databases of non-aqueous donor vehicle are scarce. In addition, the few that are available report very simple vehicles compared to the complex

semisolid formulations that are used in dermatology and especially in cosmetics. These usually predict maximum flux J_{\max} , i.e. flux achieved from a saturated vehicle, instead of $\log k_P$. In that case c_{don} in Equation 1-4 is substituted for the saturation solubility in the vehicle s_{don} .

$$\text{Equation 1-12} \quad J_{\max} = \frac{DK_{\text{m/don}}}{l} s_{\text{don}}$$

J_{\max} and k_P can be transformed into each other via s_{don} .

$$\text{Equation 1-13} \quad J_{\max} = k_P s_{\text{don}}$$

Early databases report very homogeneous compounds such as alcohols and phenols (98, 99). A maximum flux database for 278 compounds has recently been published online with the inclusion criteria published in an accompanying paper (100).

$K_{\text{m/don}}$ can be expanded to $s_{\text{m}}/s_{\text{don}}$, where s_{m} is the saturation solubility in the membrane, Equation 1-12 can be simplified as

$$\text{Equation 1-14} \quad J_{\max} = \frac{D}{l} s_{\text{m}}$$

Equation 1-14 implicates that maximum flux is independent of the donor vehicle and only depends on the solubility of the permeant in the membrane. Therefore, maximum flux QSARs are of particular value as they apply to all vehicles that do not interact with the skin. Especially for risk assessment J_{\max} is more suitable than k_P as it can be used to estimate the performance of a vehicle.

Kasting et al. (101) suggested that $s_{\text{m}} = (s_{\text{Oct}})^b$ so that

$$\text{Equation 1-15} \quad \log J_{\max} = a + b \cdot \log s_{\text{Oct}} - c \cdot \text{MV}$$

whereas Sloan and coworkers (102) emphasised the importance of aqueous zones of the SC membrane for transport and suggested

$$\text{Equation 1-16} \quad \log J_{\max} = a + b \cdot \log s_{\text{Oct}} + (1 - b) \cdot \log s_{\text{w}} - c \cdot \text{MV}$$

They successfully applied Equation 1-16 (or derivatives of it employing $\log s_{\text{IPM}}$ or $\log s_{\text{MO}}$ instead of $\log s_{\text{Oct}}$ where IPM denotes isopropylmyristate and MO mineral oil) to fit a large diverse database of flux from aqueous vehicles (103, 104) as well as several datasets with non-aqueous vehicles such as IPM, propylene glycol and MO (102, 105-108). This could not be expected as both Equation 1-15 and Equation 1-16 rely on the assumption that vehicle and membrane do not interact whereas effects on all parameters of Equation 1-12, i.e. D , $K_{\text{m/don}}$ and l , were reported for the investigated vehicles (109).

A major draw-back of QSARs developed for *in vitro* databases is that they are not immediately applicable to predict *in vivo* skin absorption. There additional mechanisms such as elimination from the site of action, dermal metabolism, and a different membrane hydration state play a role (110). In addition to making adjustments for non-aqueous vehicles predictions of *in vivo* skin absorption have to consider finite dosing. A finite dose depletes during the course of the experiment and the flux increases until it reaches a maximum before falling off again. Calculation of a true *steady state* flux J_{ss} and a *steady state* permeability coefficient k_P is precluded due to the non-existence of a *steady state* as well as continually changing donor concentrations. Therefore the significance of a predicted $\log k_P$ according to the lines above is of limited value for the *in vivo* situation (111).

Hostynek and Magee (97) proposed an alternative method to evaluate finite dose experiments. They defined a finite dose maximum flux $J_{max'}$ as the maximum % dose absorbed per time and area which is not to be confused with *in vitro* maximum flux achieved at saturation of the vehicle and which is basically a *steady state* entity (Equation 1-17). Here “% dose” is defined in terms of “fraction absorbed of dose applied”. It can be used to calculate an equivalent to a *steady state* permeability coefficient: the maximum permeability coefficient $k_{Pmax'}$ was derived by dividing $J_{max'}$ by the applied dose (Equation 1-18).

Equation 1-17 $J_{max'} = \%dose_{max'}/t[h]$

Equation 1-18 $k_{Pmax'} = J_{max'}/\text{applied dose}$

They proposed a QSAR to predict $\log k_{Pmax'}$ that apart from molecular descriptors for lipophilicity, size and hydrogen bonding also included descriptors for vehicle and occlusion state to better account for *in vivo* exposure scenarios ($r^2 = 0.69$). The database comprised of 51 values of $\log k_{Pmax'}$ estimated from urinary excretion levels for a total of 28 compounds (13 phenols, 4 steroids and 11 structural unrelated compounds) applied as ethanol or acetone solution; non-, semi-, or fully occluded (97). A correlation of $\log k_{Pmax'}$ with *steady state* permeability coefficients $\log k_P$ predicted according to a modified Potts and Guy equation using only descriptors for lipophilicity and molecular size performed surprisingly well ($r^2 = 0.62$) (97). Still, the application to a larger more diverse database of *in vivo* measured permeabilities especially for therapeutically relevant vehicles remains to be shown.

1.4.2 *Pharmacokinetic models*

In pharmacokinetic models the skin layers are described as one or two well stirred compartments. Additional compartments symbolize the vehicle and the systemic circulation (or the receptor solution if the model shall be applied to diffusion cell experiments). Exchange between compartments is modeled via first order rate constants. Using ordinary differential equations provides average concentration inside a respective compartment at a specific time. Pharmacokinetic models of the skin can be combined with compartmental models of the body to account for systemic distribution and elimination.

Pharmacokinetic models are often used for parameter studies where the influence of systematic changes in critical parameters (e.g. changes in cutaneous blood flow due to vasoconstriction or changes in skin hydration due to application of an occlusive dressing) on absorption and elimination is simulated (112-115). This allows visualizing effects that could be difficult to investigate experimentally.

Alternatively the model equations can be fit to experimental data in order to determine rate constants of specific compounds (116, 117). It has been attempted to relate these rate constants to physiological (cutaneous blood flow, skin thickness) and physico-chemical parameters (apparent permeability-, diffusion-, and partition coefficients, flux, or lag time). As described in the previous section several of these parameters can be related to physico-chemical properties of permeants such as molecular weight and size so that the model can later be used in a predictive way.

A major drawback of pharmacokinetic models is that the membrane is treated as a “black box” so that no information on absorption mechanisms and transport pathways is available. Nonetheless, pharmacokinetic dermal clearance models can be useful in combination with diffusion models of the upper skin layers for *in vivo* simulations (118).

1.4.3 *Diffusion models*

In comparison to QSAR and pharmacokinetic models that were presented before, diffusion models go beyond reproducing the skin membrane as a “black box”. The skin morphology and skin transport mechanisms are mirrored in the geometry of the model membrane and the descriptors used by the diffusion model. Similarly to mechanistic QSARs, Fick’s law is used to describe skin transport. *Steady state* solutions allow the prediction of lag-time, *steady state* flux and permeability

coefficient. In order to achieve a local and temporal resolution of the diffusion process Fick's law is solved in space and time dimensions. The resulting partial differential equations are using finite difference, finite element or other numerical techniques if analytical solutions of the diffusion equation become too complicated. In addition to *steady state* parameters non-*steady state* diffusion models also allow the prediction of transient processes such as the concentration at a specific time and position inside membrane, donor, or acceptor (of an *in vitro* diffusion cell apparatus or the systemic circulation). Therefore among the modelling strategies introduced so far, non-*steady state* diffusion models are best suited to provide information on skin absorption mechanisms.

The descriptors used in the predictions can be related to experimentally determined values. These include the membrane geometry which is derived from microscopical investigations and diffusion and partition coefficients in most cases. The microscopical resolution of the skin in the *in silico* model will be determined by the available computational power and by the degree to which reliable estimates of model input parameters can be generated. An evaluation of the predictive capability can effectively be achieved by comparing results of the predictions with experimentally generated validation data.

In the following, published diffusion models will be analyzed and evaluated under these aspects. Requirements will be unearthed that will be the basis for the development of the experimentally based and validated diffusion model presented in this thesis.

Table 1-1 Features of 1D-diffusion models. (non-ss: non-*steady state*; cdp: concentration-depth-profiles; sim: simulation; phys.-chem.: physico-chemical; exp.: experimental; cum.: cumulative; ---: not performed;)

Source	Model complexity					Input data			Validation of predictions
	Skin layers	Non-ss	cdp	sim	Special	Fit to 1D	Phys.-chem.	exp.	
Chandrasekaran et al. 1980; (119)	1				Binding			x	Compare $D_{ss}/D_{t_{lag}}$ vs. c_{don} to exp. data
Anissimov et al. 1999; (120)	1	x		x	Acceptor sampling rate, acceptor volume, clearance				Shape of cum. amount absorbed vs. time compared qualitatively to exp. data
Kasting et al. 2006; (121)	1	x		x	Finite dose, Volatile permeants				---
Kubota et al. 1993; (122)	1	x			Binding	x			compare cum. amount absorbed vs. time to exp. data
Kasting 2001; (111)	1	x		x	Finite dose	x			Fit model to exp. cum. amount absorbed vs. time; compare J_{max} and % of dose absorbed vs. dose to exp. data
Tang et al. 2002; (123)	1	x			Hydration effects	x			compare cum. amount absorbed vs. time to exp. data
Watkinson et al. 1992; (124)	1	x	x	x	Variable diffusion coefficient				Shape of cdp at ss compared qualitatively to exp. cdp
Gumel et al. 1998; (125)	1	x	x	x	Binding			x; (119)	compare graphical and analytical estimates of t_{lag}
Kalia et al. 2001; (72)	1	x	x	x	Drug release from vehicle				---
Anissimov et al. 2001; (126)	1	x	x	x	Finite dose, Clearance				model fitted to exp. flux vs. time data and cum. amount absorbed vs. time data; fit and exp. compared qualitatively
Anissimov et al. 2004; (124, 127)	1	x	x	x	Variable diffusion and/or partition coefficient				model fitted to exp. cdp; fit and exp. compared qualitatively
Pirot et al. 1997; (128)	1	x	x			x			compare J_{ss} and k_p to values derived from fitting to cdp at ss
Rim et al. 2005; (129)	1	x	x	x	Penetration enhancer Binding	x		x; (119)	compare J_{ss} vs. c_{don} to exp. data from (119); compare J_{ss} vs. time to exp. data
Tojo et al. 1987; (130)	2							x	compare solubility in SC to exp. data
Krüse et al. 2007; (131)	2	x		x	Exposure scenarios, Finite dose	x			compare cum. amount absorbed vs. time to exp. data
Manitz et al. 1998; (132)	3	x	x		Penetration enhancers and reducers			x; (130)	---

Table 1-2 Features of 2D- and 3D- single layer diffusion models. (cor.: corneocytes; non-ss: non-*steady state*; cdp: concentration-depth-profiles; sim: simulation; phys.-chem.: physico-chemical; exp.: experimental; coeff.: coefficient; MO: mineral oil; DPPC: dipalmitoyl phosphatidyl choline; ---: not performed)

Source	Model complexity								Input data			Validation of predictions
	2D	3D	Lipid diffusion heterogeneous	Cor. accessible	Non-ss	Cdp	Sim	Special	Fit to 1D	Phys.-chem.	exp.	
Frasch et al. 2003; (133)	x						x					---
Johnson et al 1997; (134)	x		x							x		compare graph of lateral diffusion coeff. vs. MW (n=120) to exp. data (n=6)
Mitragotri 2003; (135)	x		x							x		compare log k_p to literature data, n=83
Barbero et al. 2006; (136)	x			x			x					---
Michaels et al 1975; (137)	x			x			x			x		fit model to exp. K_p vs. $K_{MO/W}$ data
Poulin et al. 2001; (138)	x			x						x		compare log k_p to literature data, n=47
Wang et al. 2006; (110)	x		x	x			x	Hydration		x		compare to a 2D model with isotropic lipid phase (139); compare mass transfer coeff. to exp. data for DPPC (140)
Wang et al. 2007; (141)	x		x	x				Hydration		x		compare log k_p to literature data, n=95
Heisig et al. 1996 ; (142)	x			x	x	x	x					compare shape of cdp to microscopical results for HgCl ₂ (53); compare estimates of t_{lag} for different geometries to homogeneous model and literature
Barbero et al. 2005; (143)	x			x	x	x	x					---
George et al. 2004; (144)	x			isotropic SC	x	x	x	Binding				---
George et al. 2005; (145)	x			isotropic SC	x	x	x	Binding			x; (119)	compare t_{lag} to a 1D model; (125)
Chen et al. 2008; (146)	x			x	x	x				x		compare cdp to exp. tape-stripping; (147)
Rim et al. 2007; (148)		x			x		x					---
Feuchter et al. (149)		x		x	x	x	x					---

INTRODUCTION

Table 1-1 and Table 1-2 give an overview over published diffusion models. Although these lists are far from being exhaustive, they provide a representative cross-section of published models. Three aspects are analyzed: (i) model complexity, (ii) source of input data, and (iii) validation of the predictions.

The models are ordered by the complexity of the underlying membrane geometry, into one-dimensional (Table 1-1) and multi-dimensional models (Table 1-2) and by the number of skin layers that are included. The extent of the predictions is outlined shortly. In this context “ss” stands for models predicting *steady state* parameters. For geometrically simple models non-*steady state* expressions are very common while the majority of two-dimensional models are limited to *steady state* predictions.

It is pointed out if non-*steady state* skin concentration-depth-profiles are included in the predictions. These provide time and space resolved concentrations inside the skin which contain information on skin absorption mechanisms. The prediction of SC concentration-depth profiles is particularly relevant to interpretation of studies using tape-stripping.

A number of published approaches aim to improve the predictability of realistic exposure scenarios with the final goal to create a model for flexible *in vivo* applications. Especially 1D-diffusion models have been used to investigate specific questions of skin absorption. These include effects within the tissue such as hydration (123, 150), adsorption of permeants to a limited number of binding sites (119, 122, 125, 145), and the influence of permeation enhancers or reducers (129, 132); as well as effects within donor and acceptor such as finite dosing (111, 121, 131, 151), the permeation of volatile compounds (121), and clearance (120, 126).

It is further indicated if simulation studies have been performed (120, 142, 152). By systematically varying input parameters of interest influences on permeation and penetration are investigated. Despite not using any experimental data these studies can be extremely valuable. Especially for complex, multi-dimensional models it is often difficult or impossible to perform the same studies experimentally to the degree required by the model as will be discussed later.

Hardly surprisingly the discussion about the nature of the lipophilic and hydrophilic pathways across the SC is carried on in the published diffusion models leading to a vast variety of modelling strategies.

INTRODUCTION

One-dimensional models assume a homogeneous membrane. This implies that transport characteristics are independent of the position in the membrane resulting in a single pathway that is taken by all molecules. Although oversimplifying the highly complex skin absorption process such models were successfully used e.g. to explain trans-epidermal water loss (TEWL) (153). One-dimensional models with variable diffusion- and/or partition coefficient were proposed to account for the vertical heterogeneity of the SC (124, 127). Morphological evidence for depth dependent changes in diffusivity and membrane affinity can be found in changes in intercellular lipid conformational ordering (124) and in the progressive degradation of corneodesmosomes towards the skin surface. This was proposed to lead to a different cellular cohesion within stratum disjunctum and stratum conjunctum (22) and differences in hydration capacity of the corneocytes situated at different depths in the horny layer (51).

A *steady state* expression that integrates parallel diffusion pathways is achieved by adapting Ohm's law to the diffusion problem (Figure 1-9). Parallel diffusion pathways are described as resistors connected in parallel so that the conductivity (or permeability) of the membrane equals the sum of the conductivity of the individual pathways.

Equation 1-19
$$k_{P,\text{tot}} = \sum_{n=1}^N k_{P,n}$$

Accordingly, consecutive diffusion barriers can be modelled as serial resistors. Resistance R and permeability are related via $k_P = 1/R$. This is used in multi-layer models that include the viable *epidermis* and/or the *dermis* to account for a diffusion hindrance of highly lipophilic compounds by the more hydrophilic skin layers (130, 154, 155).

Equation 1-20
$$R_{\text{tot}} = \sum_{n=1}^N R_n$$

This requires at least one vertical partition step that accounts for the change in lipophilicity between SC and *epidermis*. Each layer is characterized by a specific apparent diffusivity. For comparison, in single layer models the model membrane represents the SC or the *epidermis* with an adjacent acceptor compartment that provides a perfect sink or a defined clearance rate.

INTRODUCTION

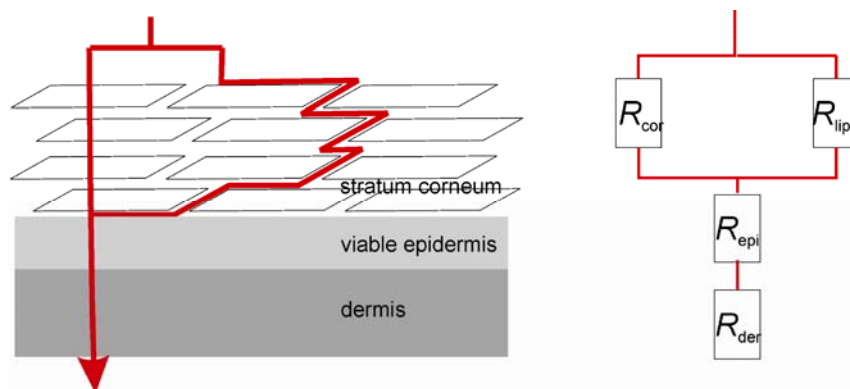


Figure 1-9 Permeation pathways and resistances in a two-dimensional skin model.

Probably the majority of heterogeneous diffusion models are based on the “brick-and-mortar” geometry. These mimic the biphasic SC structure as a brick wall with the corneocytes being the “bricks” completely embedded by the lipid bilayers being the “mortar”. As recently reviewed, shape and structuring of cellular and lipid phase may differ widely between individual models as does the representation of lipophilic and hydrophilic pathways across the membrane (110).

The source of the input data for the various models can be categorized into three groups, namely those derived from (i) fitting to a one-dimensional solution of Fick’s law, (ii) physico-chemical properties and (iii) those measured experimentally.

The input parameters for a single layer homogeneous model membrane in contact with a donor and acceptor solution are membrane thickness, membrane-donor and membrane-acceptor partition coefficients and membrane diffusion coefficient. Equation 1-4 to Equation 1-7 provide the adequate solutions to model concentrations in the acceptor compartment. Fitting Equation 1-8 to tape-stripping data the SC-donor partition coefficient $K_{SC/don}$ and the characteristic SC diffusion parameter D_{SC}/l^2 are derived. Assuming the tortuosity of the pathway to be negligible l equals the nominal membrane thickness so that D_{SC} can be calculated. *In vivo* l can be derived from the TEWL (153). Fitted parameters can re-enter the model e.g. to perform predictions of special exposure scenarios.

Pirot et al. used estimates of $K_{SC/don}$ and D_{SC} from Equation 1-8 for a short term exposure to extrapolate on *steady state* concentration depth profiles (128). This is useful for example when evaluating potentially harmful compounds to minimize the exposure time.

INTRODUCTION

Krüse et al. investigated possibilities of predicting *in vitro* finite dose exposure scenarios using $K_{SC/don}$ and D_{SC} determined by fitting a one dimensional multi-layer diffusion model to *in vitro*, infinite dose data (131). The benefit of the approach is that infinite dose experiments are easier to perform as defined constant conditions are applied during the experiment. Also, they are less challenging concerning sensitivity of the analytical method involved.

However, due to the morphological heterogeneity of the skin $K_{SC/don}$ and D_{SC} are apparent parameters. This means that the affinity or diffusivity of a permeant is averaged over the whole SC. Therefore a fitting strategy is useless for deriving input parameters for multi-dimensional models with a microscopical resolution of the skin absorption process. These rely primarily on input parameters that are derived from physico-chemical properties, mainly lipophilicity and molecular size (Table 1-2). Which input parameters are required in detail will of course depend on the complexity of the model. A typical single-layer brick-and-mortar based model is depicted in Figure 1-10 with partition and diffusion schemes. In the model in Figure 1-10 the corneocytes are assumed to be accessible, partition and diffusion properties of lipids and corneocytes are homogeneous. The membrane is in contact with a well stirred infinite donor and a perfect sink acceptor that both do not contribute to the barrier resistance. Thus input on lipid-donor ($K_{lip/don}$) and corneocyte-lipid partition coefficients ($K_{cor/lip}$) and lipid (D_{lip}) and corneocyte diffusion coefficients (D_{cor}) is required together with the donor concentration and geometrical information on the membrane dimensions.

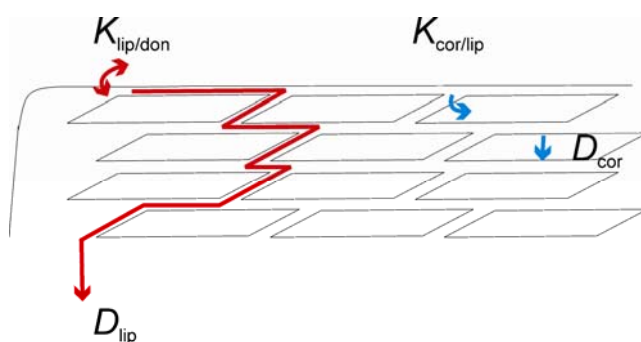


Figure 1-10 Partition and diffusion coefficients required in a brick-and-mortar model. Not drawn to scale, *stratum corneum* abridged after four layers of corneocytes.

Membrane-donor partition coefficients are often replaced by solvent-solvent partition coefficients with simple organic lipophilic solvents aiming to mimic the solvent

INTRODUCTION

properties of the rate limiting membrane, the SC. Mostly this is the octanol-water partition coefficient ($K_{Oct/w}$) but also mineral oil, olive oil or isopropyl myristate were proposed as model lipid phase (85, 107, 137). Exponential relationships of the form

Equation 1-21 $K_{m/don} = aK_{Oct/w}^b$

aim to account for a change in transport pathway with permeant lipophilicity. An exponent below one signals the SC lipophilicity to be lower than octanol. Accordingly, lipid- and corneocyte-aqueous donor partition coefficients $K_{lip/don}$ and $K_{cor/don}$ have been calculated using varying sets for the regression parameters a and b (110, 135, 141, 156).

Equation 1-22 $K_{lip/don} = 0.35 \cdot K_{Oct/w}^{0.81}$

Equation 1-23 $K_{cor/don} = 5.6 \cdot K_{Oct/w}^{0.27}$

Dividing $K_{cor/don}$ by $K_{lip/don}$ we obtain $K_{cor/lip}$. Basically, all such relationships available in the literature were developed for the same very small datasets consisting of a homologous series of hydrocortisone esters and a series of methyl substituted p-cresols (157, 158). Anderson et al. determined $K_{lip/don}$ and $K_{cor/don}$ in equilibration experiments with SC lipids extracted from human skin or delipidized SC sheets (157, 158). The original set of estimates on $K_{lip/don}$ was later supplemented by 9 other substances (5 steroids, octanol, decanol, naphthol and lidocaine) by Mitragotri (159). However, Mitragotri measured the drug release from a piece of SC that had previously been saturated with the drug and fitted the release profile to a one-dimensional solution of Fick's law to receive $K_{lip/don}$. This assumes partitioning and diffusion to be confined to the intercellular region of the SC lipid bilayers. Taking into account recent insights in the location of SC transport pathways it must be expected that the derived value for $K_{lip/don}$ represents not only the affinity to the SC lipids but also to the corneocytes. Later analyses often use combinations of the directly measured and fitted data decreasing the significance of the work (146, 160).

Estimates according to Equation 1-22 and Equation 1-23 will provide apparent partition coefficients again averaged over the lipids or corneocytes respectively. For example $K_{cor/don}$ will not differentiate between uptake into the corneocyte interior or adsorption to the corneocyte surface. Furthermore estimates according to Equation 1-23 will always apply to fully hydrated membranes. This is representative of the situation in the *in vitro* diffusion cell experiments but not of the *in vivo* situation.

For the diffusion in solvents D can be assessed from the Stokes-Einstein equation

Equation 1-24
$$D = \frac{k_B T}{6 \cdot \pi \eta r}$$

Here k_B is the Boltzman constant, T is the temperature, η is the dynamic solvent viscosity and r is the radius of the diffusant assuming a spherical shape of the molecule. Poulin et al. used Equation 1-24 to receive D_{lip} supplementing η by the viscosity of olive oil (138).

From other lipid bilayer systems, notably liposomes, it is known that solute transport is highly anisotropic and size dependent. Thus the structural heterogeneity of the lipid bilayers should translate into spatial variations in partition and diffusion coefficients. For a relatively small set of fluorescent labels and molecular oxygen lateral diffusion coefficients in human SC lipids were determined by FRAP (fluorescence recovery after photobleaching) or EPR (electron paramagnetic resonance spectroscopy) (156). Johnson et al. proposed that lateral diffusion coefficients sufficiently explain the SC permeability. This advocates for a continuous path across the SC that can be travelled by lateral diffusion. However, Johnson et al. used a single-layer brick-and-mortar model with impenetrable corneocytes which casts doubt on their conclusion as the observed result could also result from ignoring trans-corneocyte diffusion (Table 1-2). Thereupon, several models were published assuming anisotropic lipid diffusion treating the problem in different ways.

Mitragotri expressed the *steady state* SC permeability as the sum of the permeability via lateral diffusion of lipid components, free volume diffusion, and diffusion via shunts such as skin appendages, and aqueous pores, i.e. imperfections of the lipid bilayers (135).

Equation 1-25
$$k_{P,SC} = k_{P,lateral} + k_{P,free\ volume} + k_{P,shunt} + k_{P,pores}$$

Equation 1-25 assumes transport to be confined to the lipid region or the skin appendages while the corneocytes are impermeable. Thus the corneocytes simply serve as obstacles reducing diffusive area and increasing path length (133, 156). Preferences for one or more of the pathways will be determined by size and lipophilicity of the permeants (135). Lateral and free volume diffusion coefficients were estimated from scaled particle theory. This theory relates diffusion coefficients to the work required to create a cavity in a lipid bilayer to allow solute motion (135). Diffusion is described as a statistical process assuming that a molecule of a defined size requires the formation of a sufficiently large hole right next to it:

Equation 1-26 $D = D_0 \exp(-c \cdot MV)$

Here c is a constant inversely proportional to the average free-volume available for diffusion, MV is the molecular volume of the diffusant, and D_0 is the diffusivity of a hypothetical molecule with vanishingly small MV (85). This requires information on the size of the permeant and on structural information of the lipid bilayers. The latter were adopted from bilayers of the model lipid dipalmitoyl phosphatidylcholine. These are probably not fully representative of the SC lipid bilayer composition and organisation (see section 1.2).

Heterogeneous lipid diffusion was also realized in the model of Wang et al. (110), however fully relying on input parameters derived from relationships that had been developed for human skin (110, 134, 135). In addition, they assumed the corneocytes to be accessible for all solutes and therefore consider a different nature of lipophilic and hydrophilic pathways

Equation 1-27 $k_{P,SC} = k_{P,comp} + k_{P,polar}$

Here $k_{P,comp}$ is the permeability across defect-free SC due to lateral diffusion in the plane of the lipid bilayers, trans-bilayer crossing, and hindered diffusion across the keratin network within the corneocytes. By differentiation between lateral bilayer diffusion and trans-bilayer crossing lipid diffusion is considered to be anisotropic. $k_{P,polar}$ is the contribution of defects and finds its closest comparison in Mitragotri's analysis in $k_{P,shunt}$ and $k_{P,pores}$ (110, 141).

In contrast to the intercellular lipid bilayers, corneocyte diffusion is usually considered to be isotropic. It is described as a fraction of the diffusivity in water D_{aqu} in order to account for the presence of intra-cellular keratin fibres. Early analyses compare the corneocyte interior to an aqueous gel taking D_{cor} to be roughly one-tenth of D_{aqu} . For compounds with a molecular weight between 300 and 500 Da a value of $2 \times 10^{-7} \text{ cm}^2/\text{s}$ was considered appropriate (137, 161). Other authors used hindered diffusion theory in media with fibrous obstacles to find a factor to relate D_{cor} to D_{aqu} . This theory acknowledges steric as well as hydrodynamic hindrance due to the keratin microfibrils (110). For the diffusion of small compounds in polymers as well as in different cell membranes it could be shown that the relationship between molecular size and diffusion coefficient is exponential rather than linear (162).

Equation 1-28 $D = D_0 MW_{rel}^{-c}$

INTRODUCTION

D_0 and c are constants characteristic of the polymer or membrane at a defined temperature and MW_{rel} is the molecular weight of the diffusing compound relative to a reference molecule. This relationship was used to describe corneocyte diffusion where the keratin polymeric network slows down transport compared to diffusion in bulk water.

Whether the underlying assumptions of the above approximations are appropriate is often questionable, even more so if the predictions are not validated adequately. This is mostly a consequence of non-availability of alternative experimental methods to determine the input data in the resolution required by multi-dimensional models. As can be seen in Table 1-1 and Table 1-2 only a minority of models rely on experimentally determined input data. These are foremost one-dimensional models as descriptors such as membrane-donor partition coefficient $K_{m/don}$ or apparent membrane diffusivity D_m can be measured relatively easily in equilibration and/or diffusion experiments. Experimental techniques for measuring partition coefficients in the resolution of a multi-dimensional model have been published (52). However, the set of hydrocortisone esters and methyl substituted p-cresols by Raykar et al. is currently the only one reporting experimental data on $K_{lip/don}$ and $K_{cor/don}$ (157, 158). To our knowledge these were never used in a diffusion model for predicting skin absorption. Suitable experimental methods for estimating the remaining input parameters for a two-dimensional model are still missing and have to be developed.

The last column in Table 1-1 and Table 1-2 deals with the validation of the predictions. The focus is here on the validation of the outcome and not of the descriptors used as input. Also we refrain from discussing the validation of the computation (e.g. numerical calculations that are validated via analytical solutions). In case of *steady state* models these are the same parameters as used in QSARs i.e. $(\log) k_P$, J_{ss} , and in addition the lag-time t_{lag} . The main benefit is that *steady state* parameters are available in reasonably large databases for at least a number of vehicles and with satisfactory accuracy as described in section 1.3.1. Several models have been applied to predict permeability coefficients for a large number of compounds (e.g. Mitragotri (135), Johnson et al. (134), Wang et al. (141)). Requiring detailed input data for all compounds these models are invariably based on input data derived from physico-chemical properties of the permeants. The disadvantages of *steady state* predictions have been discussed at great length in section 1.3.1. In

INTRODUCTION

addition it shall be noted that k_P , J_{ss} and t_{lag} are condensed parameters which can mask experimental errors, even more so if logarithmical values are used. A more rigorous model validation is achieved for non-*steady state* predictions. These usually imply cumulative amount permeated into the acceptor compartment, or flux versus time profiles. These can easily be acquired in a simple diffusion experiment so that their use as validation tools is relatively common among the modeling strategies.

In contrast, models predicting concentration-skin depth profiles necessarily imply tape-stripping to generate the validation data. These are much rarer cited in literature due to the extensively higher work load involved as this is a destructive technique. The only analyses validating their model with concentration depth profiles by comparing with experimental data are the 1D-model of Pirot et al. for the diffusion of 4-cyanophenol (128). Chen et al. are actually using the same dataset for the validation while working with a two-dimensional model (146). Unfortunately their brick-and-model suffers from corneocyte-offset ratio that is not representative of human skin.

In summary, with increasing model complexity three major problems occur that up to now could not be solved satisfactorily. Despite years of research our insight into the mechanisms of skin penetration is still incomplete. While individual points have been focussed repeatedly from different angles, others remain “uncharted territory”. This is especially true for the heavily discussed question of the localisation of the hydrophilic pathway(s) and the treatment of the corneocytes. As a consequence the first and most important question is which properties of the skin membrane and mechanisms of permeation are relevant and thus need to be included.

Second, reliable input data for models displaying skin absorption at micrometer-scale is missing. In many cases approximations are used to unknown expense of the model accuracy. So far the degree of resolution achievable in the computation is not available in the experiment.

And third, although a number of very detailed models are available these are often not validated adequately. This hampers the value of the predictions as the accuracy of the model cannot be evaluated objectively.

2 AIM OF THE THESIS

Diffusion models are the most promising among the modelling strategies for predicting skin absorption. Especially since latest developments in computer technology allow to develop diffusion models with an increasing complexity that achieve a more and more realistic representation of the complex diffusion environment of human skin. Accurately predicting skin absorption is relevant in a variety of fields such as pharmaceuticals, cosmetics and risk assessment.

In order to build a reliable model the quality of input and validation data set are decisive. They are preferably collected in experiments with human skin. However, complex diffusion models relying on a reliable experimentally derived dataset and validated on an experimental basis are currently not available. Therefore, the aim of the thesis was to develop such an experimentally founded diffusion model with geometry and transport characteristics mimicking the situation in human skin.

The following strategy has been used. First a model was proposed that according to current knowledge will likely provide a realistic representation of skin absorption (Chapter 03). Then methods were developed to measure all input parameters experimentally with human skin (Chapter 4). These data were generated for two model compounds. As model compounds FFA and CAF were selected that feature different physicochemical properties and therefore different skin absorption characteristics. The model predictions were validated by comparing concentration-depth profiles produced in the simulation with experimentally generated tape-stripping profiles (Chapter 4 and 5). Discrepancies between model and experiment hint at previously unconsidered influences that should then be investigated experimentally (Chapter 6) in order to be implemented in the model.

The computational work was performed in the group “Simulation in Technology” at Heidelberg University directed by Prof. Dr. Gabriel Wittum. Numerical techniques to solve the diffusion equation for the non-*steady state* problem of drug diffusion are well established in this group. These had already been applied to the problem of skin absorption in a two-dimensional diffusion model of the human SC earlier by Heisig et al. (142). The original model had a “brick-and-mortar” geometry assuming homogeneous corneocyte and lipid phases with permeable corneocytes and constant partition and diffusion coefficients.

However, the original model had only been applied for theoretical simulation studies while the predictive capability had never been evaluated on an experimental level. Now this model will be developed further and put on an experimental basis.

The thesis will be divided into 4 chapters entitled:

Chapter 3 “Model development”

Chapter 4 “In silico model of skin penetration based on experimentally determined input parameters. Part I: Experimental determination of partition and diffusion coefficients”

Chapter 5 “In silico model of skin penetration based on experimentally determined input parameters. Part II: Mathematical modelling of *in vitro* diffusion experiments”

Chapter 6 “The role of corneocytes in skin transport revised – a combined computational and experimental approach”

3 MODEL DEVELOPMENT

In this section a model will be proposed that according to current knowledge provides a realistic representation of absorption through human skin. At first the relevant morphological and geometrical features of human skin need to be rebuilt in the model membrane. The model should be general, i.e. it should apply to a maximum variety of molecular penetrants. Note that this excludes transport of particulate formulations which allows us to ignore the contribution of appendageal transport. As outlined in section 1.2 the trans-appendageal route is especially important for the absorption of nano-particulate carriers whereas it plays a negligible role for the absorption of molecular penetrants save but during the very initial phase. For the majority of molecules the SC is the main barrier. For highly lipophilic compounds an additional hindrance by an unfavourable partitioning into the hydrophilic viable deeper skin layers (DSL) will have to be considered (154). Therefore in order to integrate this particular group of compounds a two-layer model is required. A first layer represents the SC. Below, a second layer represents the DSL. This will be a homogeneous compartment representing both the viable epidermal layers as well as the *dermis*. Despite that both strata contain different physiologically specialized cell populations the main properties determining permeability will be very comparable for both. These are notably their elevated hydrophilicity compared to the highly lipophilic SC and the presence of fibres which will influence the diffusion coefficient. For comparison it is common practice in skin permeation studies to work with heat separated *epidermis* as well as split skin or dermatomized skin which contains parts of the *dermis* in addition to the *epidermis*.

As repeatedly shown the SC geometry (such as form, dimensions and offset ratio of the corneocytes, dimensions of the lipid channel) is essential for the exceptional barrier properties of the skin (136, 142, 143). Therefore, multi-dimensional models must be considered superior to a homogeneous representation of the skin membrane. As outlined in section 1.2 there is increasing evidence that a trans-cellular pathway needs to be considered for at least some permeants. Therefore, models considering accessible corneocytes will be applicable to a wider range of compounds. In conclusion the model SC will feature the classic “brick-and-mortar” geometry with the dimensions derived from microscopical investigations with human skin. An unsolved question is which degree of structuring of the individual SC phases

is relevant for permeation. From the previous chapter it is clear that a consultation of literature cannot help at this task. There is no conclusive decision on how the internal heterogeneity of the SC should be treated. In contrast among the wide variety of two-dimensional models this problem is treated very differently. Keep in mind for example the elaborate treatment of anisotropic transport in the lipid phase by Mitragotri or hindered transport across corneocytes by Wang et al. (110, 135, 141). The approach pursued in the course of this work will be to start with the simplest possible option, i.e. by assuming homogeneous lipid and corneocyte phases. Therefore the descriptors used in the model will be: (i) the lipid-donor partition coefficient $K_{lip/don}$; (ii) the corneocyte-lipid partition coefficient $K_{cor/lip}$; (iii) the DSL-lipid partition coefficient $K_{DSL/lip}$; (iv) the lipid diffusion coefficient D_{lip} ; (v) the corneocyte diffusion coefficient D_{cor} ; (vi) and the DSL diffusion coefficient D_{DSL} . All input parameters used in the predictions will be of experimental origin (either measured directly or if this is not possible derived from experimental data). The accuracy of the predictions will be evaluated by comparing experimental and predicted time resolved skin concentration-depth profiles. Therefore, approximations such as used by model descriptors that are derived from physico-chemical properties of the permeants will be avoided. This approach will allow detecting shortcomings of the model such as would be provoked by an insufficient representation of model membrane heterogeneity. These will then have to be investigated in order to be integrated in the model and improve the predictions.

4 *IN SILICO* MODEL OF SKIN PENETRATION BASED ON EXPERIMENTALLY DETERMINED INPUT PARAMETERS. PART I: EXPERIMENTAL DETERMINATION OF PARTITION AND DIFFUSION COEFFICIENTS

Parts of this chapter have been published as:

S. Hansen, A. Henning, A. Naegel, M. Heisig, G. Wittum, D. Neumann, K.H. Kostka, J. Zbytovska, C.M. Lehr, U.F. Schaefer, *In silico* model of skin penetration based on experimentally determined input parameters. Part I: Experimental determination of partition and diffusion coefficients, Eur J Pharm Biopharm 68 (2008) 352-67 DOI: 10.1016/j.ejpb.2007.05.012.

The author of the thesis made the following contributions to the publication.

Planned, performed and interpreted all major experiments. Wrote the manuscript.

4.1 INTRODUCTION

Pharmaceutical and cosmetic industries as well as governmental institutions share a common interest in skin investigation such as bioavailability studies, risk assessment of products and consumer protection among others. *In vivo* studies with humans are considered the “gold-standard”. As these are tied to ethical, analytical and economic concerns much effort has been put into developing reliable *in vitro* methods preferentially using human skin. Still the high demand for human skin conflicts with an insufficient availability. Thus, animal or bioengineered skin is often used alternatively. However, large interspecies variabilities and insufficient barrier formation limit their significance for the situation in man.

Therefore mathematical modeling may be a potential alternative. *In silico* approaches include predicting the apparent permeability coefficient k_P of various substances from easily accessible physical constants like descriptors for molecular weight, lipophilicity and solvation parameters (85, 163-165). Furthermore one- or two-compartmental pharmacokinetic models determine rate constants from physicochemical and physiological skin properties such as partition and diffusion coefficients, blood flow and skin thickness (114). These allow for estimating the absolute amount present within a certain compartment after a defined time. Apart from that diffusion models additionally predict drug concentrations locally and temporally by solving the partial differential equations of Fick’s 2nd law of diffusion (166). These models describe skin penetration as a series of partition and diffusion steps which may be quantified in terms of partition coefficients K and diffusion coefficients D .

Several diffusion models with a varying degree of complexity are currently in use. Accordingly the estimation of model parameters becomes more and more challenging. The simplest cases consider a homogeneous SC such as the two dimensional multi-layer diffusion model of Manitz et al. (132). Here input data on $K_{SC/don}$, $K_{SC/Epi}$, $K_{Epi/Der}$, D_{don} , D_{SC} and D_{DSL} are sufficient. These are readily available for several compounds from literature (130, 154). Subscripts indicate the respective skin layers involved in the partition or diffusion process (don, SC, lip, cor, Epi, Der and, DSL for donor, SC, intercellular SC lipids, corneocytes, *epidermis*, *dermis* and, DSL, i.e. viable *epidermis* plus *dermis*). More sophisticated models describe the SC geometry as “brick-and-mortar”, the corneocytes being bricks and the lipids acting as intercellular mortar (137). If only the lipoidal pathway is considered this requires input

data on $K_{lip/don}$, and D_{lip} (134). As so far partition coefficients with extracted SC lipids have only been measured for a single set of compounds several usually very similar correlations of $K_{lip/don}$ with $K_{Oct/w}$ according to a power law (linear free energy relationship) have been suggested (150, 157, 160). Direct measurements of lateral diffusion coefficients of a small set of larger compounds (223-787 Da) and molecular oxygen in extracted SC lipids have been attempted by fluorescence recovery after photobleaching (FRAP) (156, 167). From this work also a general relationship of D_{lip} on molecular weight could be discerned. If apart from that the model allows corneocyte access it becomes crucial to break down the consecutive partition and diffusion steps experimentally according to the anatomical heterogeneity of skin. Similarly to $K_{lip/don}$ Nitsche et al. related $K_{cor/don}$ to $K_{Oct/w}$ via a power law (150). Estimates of D_{cor} have been proposed on the basis of Phillips et al.'s analysis of hindered diffusion in media with fibrous obstacles and for the special case of water by spin-echo NMR measurements of mobile protons in guinea pig footpad SC (168, 169). Using a two-dimensional brick and mortar diffusion model with homogeneous lipid and corneocytes phases Heisig et al. were able to simulate non-*steady state* drug permeation through the SC (142). Based on realistic dimensions the time resolved location of a drug within the SC was examined by systematically varying $K_{cor/lip}$, D_{lip} , and D_{cor} . An accurate resolution of the lipid channel has been attempted in (110). The authors introduced the dimensionless parameter R to quantify the relative extents of lateral lipid diffusion and trans-bilayer hopping.

However, up to now an adequate conjunction of all these elements is missing, i.e. a brick-and-mortar diffusion model that is based on experimental input data on all relevant partition and diffusion coefficients and that is validated on the basis of experimental concentration-skin depth profiles.

Therefore, we further elaborate the model of Heisig et al. (142). By now the model has been extended by increasing the number of corneocyte layers to 16 and adding a homogeneous epidermal/dermal compartment (cf. section 5). Thus the model membrane is composed of three different phases: corneocytes, surrounding lipids and the DSL. A graphical representation of the relevant parameters is depicted in Figure 4-1.

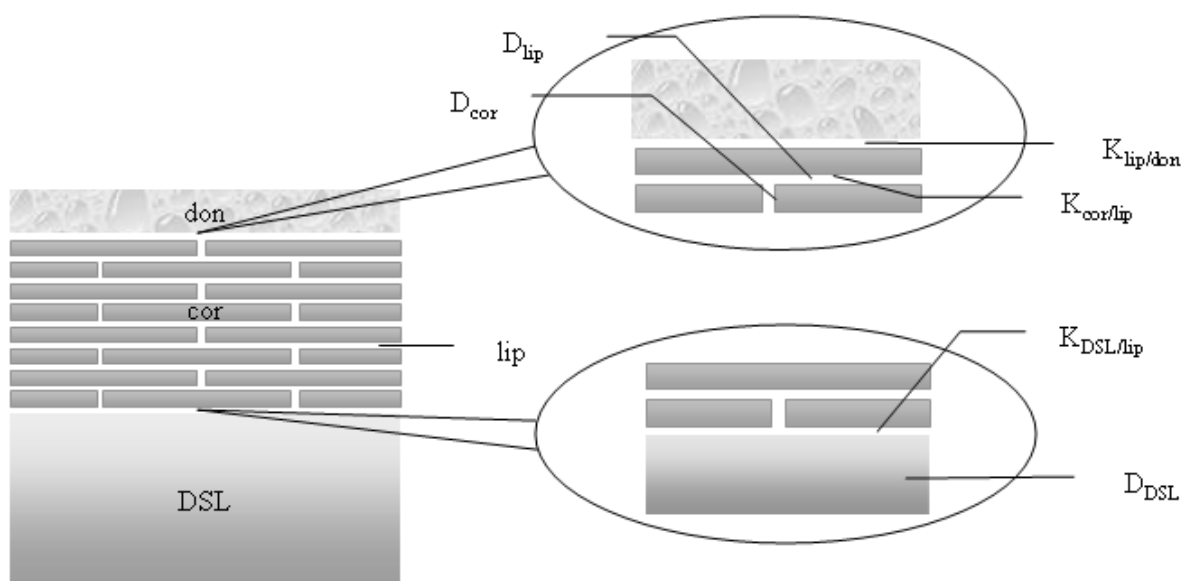


Figure 4-1 Schematic picture of skin anatomy and the main partition and diffusion coefficients involved in skin transport.

It is assumed that transport within a phase is due to Fick's second law. On the interfaces between two phases partition coefficients $K_{cor/lip}$ and $K_{DSL/lip}$ allow for an abrupt change in concentration. The flux across an interface is continuous due to mass conservation. For detailed information on model geometry, relation to measured physical quantities and applied numerical methods refer to chapter 5. This study presents experimental methods and calculation techniques to determine partition and diffusion coefficients in detail as needed for the *in silico* diffusion model presented in chapter 5.

Table 4-1 Overview over partition and diffusion coefficients needed for conclusive *in silico* diffusion modeling of skin transport and their acquisition method. Direct parameters may be determined in experiments. Derived parameters are not directly accessible experimentally but may be determined from experimentally available data. These together with a reference of the calculation method are presented under "source".

coefficients	direct	derived	source
$K_{lip/don}$	x		
$K_{cor/lip}$		x	$(K_{SC/don} ; K_{lip/don} ; \text{Equation 4-9})$
$K_{DSL/lip}$		x	$(K_{cor/lip} ; K_{SC/DSL} ; \text{Equation 4-10})$
D_{lip}	x		
D_{cor}		x	$(D_{SC} ; D_{lip} ; K_{cor/lip} ; (170))$
D_{DSL}	x		

Several input parameters such as $K_{lip/don}$, D_{lip} and D_{DSL} are determined experimentally. Other parameters needed for conclusive description of skin absorption, i.e. $K_{cor/lip}$ and $K_{DSL/lip}$, cannot be measured directly and therefore are estimated from accessible experimental data (Table 4-1). Furthermore time dependent concentration-depth profiles through the SC and the DSL are measured. These are employed to validate the calculated drug penetration profiles in chapter 5.

4.2 MATERIAL AND METHODS

4.2.1 *Material*

The following materials and equipment were used: static Franz diffusion cells type 6G-01-00-15-12 (Perme Gear, Riegelsville, PA); BCA-assay kit (Sigma Aldrich GmbH, Steinheim, Germany); dialysis membrane MW-cut-off 12-14 kDa (Medicell International Ltd, London, Great Britain, VWR Darmstadt, Germany); Centriscart I cut-off 20 kDa (Sartorius AG, Goettingen, Germany), Durapore® membrane filters, polyvinylidene fluoride, 0.22 µm, 5 cm (Millipore, Schwalbach, Germany); Multifilm Kristallklar (Beiersdorf AG, Hamburg, Germany); cryomicrotome (HR Mark II, model 1978. SLEE, Mainz, Germany); centrifuge (Universal 30RF Hettich Zentrifugen, Tuttlingen, Germany); freeze dryer (Alpha 2-4 LSC, Christ, Osterode, Germany); thickness meter (model 5041, type (VRZ) with tactile probe (MT) 10B; accuracy ±1 µm; Heidenhain Company, Taunreut, Germany).

4.2.2 *Chemicals*

The following chemicals were used: FFA (MW 281.24 g/mol; $\log K_{Oct/w}$ 4.8; pKa 3.9 (171)) CAF (MW 194.2 g/mol; $\log K_{Oct/w}$ -0.083; pKa 1.39 (172)), sodium chloride, potassium chloride, methanol, chloroform, trypsin type I from bovine pancreas, standard and reference lipids for HPTLC analysis: ceramide III and IV, triolein, oleic acid, cholesterol and cholesteryl oleate were provided by Sigma Aldrich GmbH, Steinheim, Germany. Sodium azide, acetonitrile and sodium monohydrogen phosphate dihydrate were provided by Fluka Chemie AG, Buchs, Germany. Citric acid monohydrate, potassium dihydrogen phosphate, orthophosphoric acid, diethyl ether, n-hexane, glacial acetic acid 100%, petrolether, isopropanol, HPTLC plates, silicagel 60 non-fluorescent, copper sulphate pentahydrate were provided by Merck, Darmstadt, Germany. Keratin from bovine hoof and horn was provided by ICN biomedicals, Aurora, Ohio.

4.2.3 Composition of buffers

All buffer substances were of analytical grade and were prepared with purified water. Phosphate buffered saline (PBS) pH 7.4: 1 l contains $\text{Na}_2\text{HPO}_4 \cdot 2\text{H}_2\text{O}$ 1.44 g, KH_2PO_4 0.2 g, NaCl 8 g, KCl 0.2 g.

Soerensen phosphate buffer pH 7.4: 1 l contains $\text{Na}_2\text{HPO}_4 \cdot 2\text{H}_2\text{O}$ 9.2 g, KH_2PO_4 2 g.

Buffer pH 2.2: 1 l contains citric acid monohydrate 20.8 g, $\text{Na}_2\text{HPO}_4 \cdot 2\text{H}_2\text{O}$ 0.4 g.

Buffer pH 2.6: 1 l contains orthophosphoric acid 1.16 ml, KH_2PO_4 2.04 g.

4.2.4 Skin samples and skin preparation techniques

Skin samples were taken from Caucasian female donors undergoing abdominal surgery with the approval of the ethic committee of the Caritas-Hospital Lebach, Germany. After removal of subcutaneous fatty tissue full thickness skin was stored at -26°C for a maximum of 6 months after surgery. For details see Wagner et al. (173).

4.2.4.1 Preparation of stratum corneum sheets

SC sheets were prepared according to the method of Kligman (174) by two times 24 h immersion of cleaned full thickness skin pieces of approximately 12 cm^2 in 0.15% (w/v) trypsin in PBS. In between as well as afterwards the pieces were washed three times with PBS and finally freeze dried. Freeze dried membranes were kept in a freezer at -18°C for a maximum of 6 months after surgery.

4.2.4.2 Preparation of corneocyte sheets

Isolated freeze dried SC sheets were delipidized with 5 ml chloroform/methanol (2:1 v/v) under occasional agitation. After 24 h delipidized membranes were removed from the extraction solution, washed three times in chloroform/methanol (2:1 v/v) and allowed to dry on air under ambient conditions.

4.2.4.3 Preparation of dermis sheets

Heat separation of full thickness skin was done according to Kligman (174) by 90 s immersion in water of 60°C . The *epidermis* was peeled off with forceps. Leftovers only comprised of *dermis*.

4.2.5 Lipid coated membranes

SC lipids were extracted by 24 h immersion of SC in 5 ml chloroform/methanol (2:1 v/v). Organic solvents were removed in a nitrogen stream. Lipids of three donor skins

(each of a surface area of roughly 60-80 cm²) were combined, re-dissolved in chloroform/methanol (2:1 v/v) and adjusted to a final concentration of 2.5% (w/v). Durapore® membrane filters were cut into 8 approximately equal pieces (surface area per piece about 4.9 cm²) with a scalpel and were coated by 30 times dipping into this solution. After each dip organic solvents were allowed to evaporate. Coated membranes were equilibrated at 70 °C for 10 min (175). Filters were stored in a drying cabinet at 32 °C for 2-5 d before use as such treatment results in the lowest variability of permeability and partition data (3).

The reproducibility of the coating was ascertained by measuring the increase of thickness and mass. Membrane thickness was determined with a thickness meter equipped with a tactile probe to an accuracy of ±1 µm averaging values measured at 5 different sites (before: 114 ± 6 µm; after coating: 203 ± 23 µm). Membrane weight was determined with an analytical balance to an accuracy of ±0.01 mg (before: 15.82 ± 0.25 mg; after coating: 38.35 ± 2.77 mg).

4.2.6 Characterization of extracted stratum corneum lipids by WAXD

Wide angle X-ray powder diffraction data were collected at room temperature with an X'Pert PRO PRO θ - θ powder diffractometer (PANalytical, The Netherlands) with parafocusing Bragg-Brentano geometry using CuK α radiation (λ = 1.5418 Å, U = 40 kV, I = 30 mA). Data were scanned over the angular range of 15-30° (2 θ) with a Xe gas proportional detector equipped with a secondary curved monochromator. Data evaluation was performed in the software package HighScore Plus.

Lamellar spacings, d , were calculated according to $d = n\lambda/2\sin\theta$, where n is the diffraction order, λ the wavelength of the X-ray beam and θ the scattering angle.

4.2.7 Characterization of extracted stratum corneum lipids by DSC

Differential scanning calorimetry was performed using a thermal analysis data system (DSC Q100, TA Instruments, Alzenau, Germany). The instrument was calibrated using indium as standard. Samples of 3 - 6 mg were heated in sealed aluminium pans from 0 to 120 °C at a scanning rate of 5 °C/min under nitrogen purge, with an empty aluminium pan as reference.

4.2.8 Characterization of extracted stratum corneum lipids by HPTLC

Separation and quantification of extracted SC lipids has been performed exactly as described elsewhere (176). In short, dried and weighed extracted SC lipids were diluted with chloroform/methanol 2:1 to an appropriate degree and 1 - 5 µl were applied to HPTLC silica gel plates together with standard solutions (Triolein and oleic acid 0.7 - 15 µg; sterols and ceramides 0.7 - 7 µg). Solvent systems and quantification methods were the same as described by Netzlaff et al. (176).

4.2.9 Determination of drug concentration-skin depth profiles

SC- and DSL- concentration-depth profiles were analyzed by tape-stripping of the SC and cryo-sectioning of the DSL (173). Briefly, full thickness skin was incubated in static Franz diffusion cells with a diffusion area of 1.76 cm² and an acceptor volume of 12 ml at 32 ± 1 °C. Soerensen phosphate buffer pH 7.4 containing 0.05% w/v sodium azide was employed for both donor and acceptor solutions. In preliminary experiments it was ascertained that preservation with 0.05% w/v sodium azide did neither influence analytics nor penetration. Infinite dose conditions were ascertained using a donor volume of 500 µl containing 1 mg/ml of FFA or 12.5 mg/ml of CAF. A higher donor concentration was chosen for CAF due to analytical reasons. For both chemicals this corresponds to ≈50% of saturation concentration. In no experiment the donor concentration decreased more than 10% of the initial value. The acceptor concentration reached a maximum of 0.99% for FFA and 0.22% for CAF of the saturation concentration (i.e. 1.97% and 0.43% of the donor concentration, respectively) after the maximum incubation time of 24 h. Thus at all times acceptor concentrations were smaller than 10% of the saturation concentration, so that perfect sink conditions were assured. After 1, 2, 6, 14 or 24 h remaining donor was removed and the surface was cleaned with dry cotton-swabs. Afterwards the skin was horizontally segmented first by tape-stripping followed by cryo-cutting according to Wagner et al. (173). As a slight modification the first two instead of only one strip were discarded to prevent potential contamination by residual drug on the skin surface. Due to analytical reasons tape-strips were combined in pools according to the following scheme: #1+2 = discarded, #3-5 = pool 1, #6-10 = pool 2, #11-15 pool 3, #16-20 = pool 4. Surface parallel cuts of the DSL were collected according to the following scheme: #1 = incomplete cuts, #2-5 = 4 x 25 µm sections, #6-

9 = 4 x 25 μm sections, #10-11 = 2 x 25 μm sections and #12 = rest of the residual tissue.

FFA was extracted by 2 h shaking at room temperature with HPLC mobile phase. CAF was extracted in a shaking water bath for 2 h at 60 °C with phosphate buffer pH 2.6 (identical to buffer used in HPLC mobile phase). Strips were extracted with 3 ml of solvent whereas 1.5 ml was used for cuts for both substances. The recovery of the extraction method is $95.35 \pm 4.8.1\%$ for FFA (173) and $87.37 \pm 5.07\%$ for CAF. Concentration-skin depth profiles for the SC were determined for an incubation time of 1, 2 and 6 h and for the DSL for 1, 2, 6, 14 and 24 h. For each time point and each drug three to four replicates were performed. For the SC the extract concentration is related to the SC concentration via the volume of SC removed. The SC volume per tape strip is calculated from the stripping area (1.767 cm^2) and the SC thickness per tape strip. The latter is determined microscopically via a highly standardized method (173, 177). For the DSL the extract concentration is related to the DSL concentration via weighing assuming a density of hydrated tissue of 1 g/cm^3 .

The concentration of substance extracted from a pool of strips or cuts is plotted in the middle of the respective depth segment. Skin depths were calculated as given by Wagner et al. (173).

4.2.10 Permeation studies

Steady state flux J_{ss} of FFA and CAF through SC, *dermis* or SC-lipids were measured in a separate Franz diffusion cell experiments using the respective membrane by taking samples from the acceptor compartment at time intervals of 1-36 h. Experimental conditions were as described under “Determination of drug concentration-skin depth profiles”. For both compounds the donor concentration was 1 mg/ml. J_{ss} was calculated from the linear proportion of plotting the cumulative amount of substance transported per area versus time using a minimum of 5 data points according to a validated method as described in (178). For experiments with lipid coated membrane filters it was assumed that transport is only possible via the pores of the filter (porosity = 70% of the total filter volume according to the manufacturer). Only the area of the pores (i.e. 70% of the total area) was considered for calculation of J_{ss} . Permeation experiments with uncoated filters that had been treated analogous to the coated membranes (30 times dipping in methanol/chloroform 2:1; equilibration at 70 °C for 10 min; storage at 32 °C for 2-5 d)

showed no significant resistance of the filter material. This proved that the barrier is formed by the lipids.

4.2.11 Keratin binding

Prior to the experiment water soluble low molecular weight keratin fractions resulting from the manufacturing process were removed by classical dialysis using dialysis tubing with a molecular weight cut-off of 12-14 kDa. Removal of soluble keratin fraction was considered to be complete if a BCA-assay in the supernatant performed according to the standard protocol provided by the manufacturer was negative (linear concentration range 0.2-1 mg/ml or 5-25 µg of total protein, detection limit 0.01 µg/ml). Insoluble keratin fractions were retrieved by freeze-drying.

Increasing ratios of the respective substance to keratin (0.6, 1, 10, 50, 100, 200, 300, 400, 500, 1000 µg/mg) were incubated on a magnetic stirrer (500 rpm) at 32 °C, over 24 h, i.e. until equilibration. 1.5 ml of the suspension was transferred to centriscart tubes (MW-cut-off 20 kDa) and centrifuged for 25 min at 2795 g. The supernatant was diluted with Soerensen buffer pH 7.4 to an appropriate concentration and transferred into HPLC vials and the concentration of unbound substance was determined by HPLC. Samples containing only substance solution without keratin were subjected to the identical procedure and represented 100% free concentration.

4.2.12 Quantification of flufenamic acid and caffeine

Samples were analysed by RP-HPLC using an isocratic Dionex HPLC system (Lichrospher® RP-18 column/ 125 x 4 mm/ 5µm with a LiChroCART® 4-4 guard column (Merck-Hitachi, Darmstadt); Software: chromeleon 6.50 SP2 build 9.68.

FFA: mobile phase: 80:20 (v/v), methanol/ buffer pH 2.2; retention time: 3.5 ± 0.2 min; flow rate: 1.2 ml/min; injection volume: 50 µl; detection wavelength: 284 nm; detection limit: 15 ng/ml; quantification limit: 50 ng/ml.

CAF: mobile phase: 90:10 (v/v) buffer pH 2.6/acetonitrile; retention time: 5.1 ± 0.2 min; flow rate: 1.2 ml/min; injection volume: 50 µl; detection wavelength: 270 nm; detection limit: 15 ng/ml; quantification limit: 50 ng/ml.

For both compounds a calibration was performed using external standards with 0.05-25 µg/ml dissolved in Soerensen buffer pH 7.4. For extraction experiments standards were dissolved in the respective extraction fluid. If necessary, unknown samples

were diluted to an appropriate concentration with the same medium as the samples prior to analysis.

4.2.13 Determination of partition coefficients by equilibration experiments

4.2.13.1 Decrease of donor concentration (Method 1a)

The partition coefficient K_{ij} between two phases i and j is the proportion of substance concentration [w/V] between a receiving phase i and a donating phase j:

Equation 4-1
$$K_{ij} = \frac{c_i}{c_j}$$

Relating Equation 4-1 to skin partition coefficients c_i and c_j are the concentrations in the respective skin compartment or the donor, respectively. Assuming a density of 1 g/cm³ for aqueous donor, SC, cor, lip and DSL (179) the volume of the skin compartment and the donor directly translates into the mass. Method 1a determines the concentration in the receiving skin compartment from the concentration decrease in the incubation solution where w_0 and w_{End} are weight of substance within the incubation solution before and after equilibration; w_i is the dry mass of the respective skin compartment i.e. SC, cor, lip (i.e. the mass of lipid on the membrane filter disc) or DSL and w_j is the mass of the incubation solution.

Equation 4-2
$$K_{ij} = \frac{(w_0 - w_{\text{End}})w_j}{w_{\text{End}}w_i}$$

$K_{\text{SC/don}}$, $K_{\text{cor/don}}$, $K_{\text{lip/don}}$ and $K_{\text{DSL/don}}$ were measured based on the method introduced by Raykar et al. by equilibration experiments (52). In contrast to Raykar et al. the original method for determining $K_{\text{lip/don}}$ was modified by coating Durapore® membrane filters with SC lipids rather than using test tube walls where they were deposited during removal of the organic solvent. The filters were prepared identically to the ones used in permeation experiments for determining D_{lip} (q.v.). This ensured setup properties like lipid organisation to be most comparable between these complementary sets of experiments. Briefly SC, delipidized SC, lipid coated filters, or prepared *dermis* sheets were immersed in 10 ml Soerensen buffer pH 7.4 with 0.05% w/v sodium azide containing either 10, 50, 100 or 1000 µg/ml CAF or 10, 50 or 1000 µg/ml FFA and allowed to equilibrate at 32 °C for 24 h. Afterwards samples were drawn and analyzed for drug contents.

To exclude unspecific adsorption the test tubes and in case of $K_{lip/don}$ non-coated membrane filters were incubated with the drug solution alone. Furthermore to exclude that substances interfering with analytics are extracted by the solvent system, the membranes were soaked with the pure buffer solution for 24 h and underwent the same procedure as the drug containing solutions. All control tests proved negative.

4.2.13.2 Extraction of specimen (Method 1b)

The amount of substance partitioned into the respective skin compartment may further be determined directly by extraction (180, 181). The corresponding partition coefficient $K_{SC/don}$, $K_{cor/don}$, $K_{lip/don}$, and $K_{DSL/don}$ may then be calculated substituting $(w_0 - w_{End})$ in Equation 4-2 by the extracted mass of substance (w_{Ex}) Equation 4-3.

Equation 4-3
$$K_{i/j} = \frac{w_{Ex} w_j}{w_{End} w_i}$$

Briefly, samples were taken out of the incubation solution, washed three times in Soerensen-buffer pH 7.4 and blotted dry between filter papers. The samples were put into screw-top scintillation vials. The lids were secured with a Teflon septum. Extraction agents and conditions were the same as described for skin penetration studies. For both compounds the extraction steps were repeated until the extract concentration was below the detection limit of the HPLC.

Control samples composed either of the analyte dissolved in buffer without any skin or lipid coated filter or of the respective skin sample, or lipid coated filter immersed in pure buffer solution were subjected to an analogous procedure.

To check for completeness of extraction dried untreated or delipidized SC sheets of 2 x 3 cm were spiked with ethanolic solutions of FFA or CAF (20 µl containing 5-100 µg FFA or 1-50 µg CAF). The solvent was allowed to evaporate at ambient conditions. Samples were extracted as described above. 92-107% (w/w) FFA from untreated SC, 99-105% (w/w) FFA from corneocytes, 91-108% (w/w) CAF from untreated SC and 93-110% (w/w) CAF from corneocytes were recovered.

4.2.14 Calculation of partition coefficients

4.2.14.1 Estimation of the stratum corneum-donor partition coefficient $K_{SC/don}$ from penetration experiments (Method 2)

The concentration-SC depth profile of a substance (i.e. $c(x,t)$ as a function of position x and time t) can be computed by using an appropriate solution to Fick's 2nd law of diffusion. Such a solution which was repeatedly applied for estimating diffusion coefficients in SC is given by Equation 4-4 "long times" (128, 182, 183). Equation 4-4 converges rapidly for $D_{SC} t/l^2 > 1$.

Equation 4-4

$$c(x,t) = K_{SC/don} c_{don} \left\{ 1 - \frac{x}{l} \right\} - \sum_{n=1}^{\infty} \frac{2}{n\pi} K_{SC/don} c_{don} \sin\left(\frac{n\pi x}{l}\right) \exp\left(\frac{-D_{SC} n^2 \pi^2 t}{l^2}\right)$$

Here, l is the SC thickness (FFA: 14 μm , CAF: 15 μm), $K_{SC/don}$ is the partition coefficient between SC and donor vehicle and D_{SC} is the diffusion coefficient in the SC.

At "short times" an appropriate solution is given by Equation 4-5. For $D_{SC} t/l^2 \leq 1$, Equation 4-5 converges quickly and therefore is a suitable solution for Fick's 2nd law of diffusion "at short times" (184).

Equation 4-5

$$c(x,t) = K_{SC/don} c_{don} \sum_{n=0}^{\infty} \left\{ \operatorname{erf} \frac{(2n+2)l+x}{2\sqrt{Dt}} - \operatorname{erf} \frac{2nl-x}{2\sqrt{Dt}} \right\}$$

Both Equation 4-4 and Equation 4-5 assume a homogeneous membrane with an infinite donor and a perfect sink below the membrane, that is the concentrations at the top and the bottom of the SC are $c(0,t) = K_{SC/don} c_{don}$ and $c(l,t) = 0 \mu\text{g}/\text{cm}^3$, respectively. (Equation 4-4 is basically identical to Equation 1-8.)

The values of $K_{SC/don}$ and D_{SC} for the 1, 2 and 6 h concentration profiles of FFA and CAF were determined in a two-step process. First, a simple grid-search was made where the diffusion coefficient D_{SC} was varied from $10^{-5} \text{ cm}^2/\text{s}$ to $10^{-16} \text{ cm}^2/\text{s}$ and the partition coefficient $K_{SC/don}$ from 1.0 to 300.0. For each pair of $D_{SC}/K_{SC/don}$ values the root-mean square deviation between the experimental and calculated values was computed to assess the quality of this potential solution. The best 100 results for each substance and incubation time were then subjected to a non-linear optimization routine to find the optimal values for D_{SC} and $K_{SC/don}$. This procedure assumes that D_{SC} is not a function of depth, but rather may vary with time. Thus, potential time-

dependent influences of changes in the SC properties on the diffusion may be discovered and taken into account. This especially relates to swelling which is typically observed within the first hours of a Franz diffusion cell experiment when using aqueous acceptor media (173).

Due to the restrictions concerning the extraction procedure of the tape-stripping method explained in section 4.2.9 only four data points along the x-axis were available for fitting. The infinite series was truncated after when the machine accuracy was reached. For example, in the case of Equation 4-5, the series was truncated when the next summand would have been less than the product of the current sum and the machine epsilon ε (185).

4.2.14.2 Estimation of the stratum corneum viable deeper skin layers partition coefficient $K_{SC/DSL}$ from penetration experiments

The ratio of the concentration at the bottom layer of the SC c_{exSC} , (i.e. within the last pool of tape-strips) and the topmost layer of the viable *epidermis* c_{inDSL} , (i.e. the first pool of cuts) gives $K_{SC/DSL}$ Equation 4-6.

Equation 4-6
$$K_{SC/DSL} = \frac{c_{exSC}}{c_{inDSL}}$$

Using aqueous donor media the SC becomes increasingly fragile with prolonged incubation time until it finally comes off in large flaps rather than in distinct corneocyte layers. Therefore tape-stripping is only possible for incubation times up to 6 h while cryo-cutting of DSL is still possible after 24 h. Thus experimental data on c_{exSC} is available only up to 6 h whereas data on c_{inDSL} is also available for longer times. As c_{exSC} proved to be constant after 1 h for FFA and 2 h for CAF no further changes of c_{exSC} are to be expected after longer incubation. For this reason the mean c_{exSC} of 1-6 h or 2-6 h was applied for calculating $K_{SC/DSL}$ for 14 and 24 h, respectively.

4.2.14.3 Estimation of corneocyte-lipid-and lipid-deeper skin layers partition coefficient $K_{cor/lip}$ and $K_{DSL/lip}$

By definition the (volume) concentration in the SC can be expressed using the relative volume fractions of the lipid and corneocyte phase φ_{lip} and φ_{cor}

Equation 4-7
$$c_{SC} = (\varphi_{lip} + \varphi_{cor} K_{cor/lip}) c_{lip}$$

Consequently,

Equation 4-8
$$K_{SC/don} = (\varphi_{lip} + \varphi_{cor} K_{cor/lip}) K_{lip/don}$$

holds. $K_{\text{cor/lip}}$ is estimated from $K_{\text{SC/don}}$ and $K_{\text{lip/don}}$ using Equation 4-9.

$$\text{Equation 4-9} \quad K_{\text{cor/lip}} = \frac{1}{\varphi_{\text{cor}}} \left(\frac{K_{\text{SC/don}}}{K_{\text{lip/don}}} - \varphi_{\text{lip}} \right)$$

Realistic values for the volume fractions of the lipid and corneocyte phase are $\varphi_{\text{lip}} = 0.1$ and $\varphi_{\text{cor}} = 0.9$ respectively. These values result from the model geometry used for *in silico* simulations and are founded empirically (170).

Analogously, $K_{\text{DSL/lip}}$ is estimated from $K_{\text{SC/DSL}}$ and $K_{\text{cor/lip}}$:

$$\text{Equation 4-10} \quad K_{\text{DSL/lip}} = \left(\frac{\varphi_{\text{lip}} + \varphi_{\text{cor}} K_{\text{cor/lip}}}{K_{\text{SC/DSL}}} \right)$$

As $K_{\text{SC/DSL}}$ proved to be time dependent, only values at 24 h of incubation were considered. After 24 h $K_{\text{SC/DSL}}$ was constant for both FFA and CAF.

4.2.15 Calculation of apparent diffusion coefficients

According to the *steady state* diffusion equation the *steady state* flux J_{ss} is defined as the product of the negative of the apparent diffusion coefficient D and the concentration gradient dc/dx (Equation 4-11). Rewriting dc/dx in Equation 4-11 as the product of the initial donor concentration c_0 and the membrane-donor partition coefficient $K_{i/j}$ divided by the membrane thickness h and rearranging Equation 4-11, D is calculated (Equation 4-12) (154, 186).

$$\text{Equation 4-11} \quad J_{\text{ss}} = -D \frac{dc}{dx}$$

$$\text{Equation 4-12} \quad D = -\frac{J_{\text{ss}} h}{K_{i/j} c_0}$$

Substituting the variables in Equation 4-12 with experimental data on J_{ss} , the values of $K_{i/j}$, c_0 , and h for the respective apparent diffusion compartment (i.e. lip, DSL, SC) D_{lip} , D_{DSL} and D_{SC} were assessed. In particular D_{lip} was determined using $K_{\text{lip/don}}$ (method 1a), c_0 the donor concentration of the transport experiment, and h the thickness of the lipid coated filter (q.v.).

D_{DSL} was calculated using $K_{\text{SC/DSL}}$ after equilibration (24 h), and the concentration in the lowest SC segment c_{ExSC} . The thickness h represents the thickness of fully swollen *dermis* (FFA: 3.78 ± 0.27 mm, CAF: 3.83 ± 0.47 mm; mean \pm sd of 5 different sites per piece).

D_{SC} was calculated using $K_{\text{lip/don}}$ (method 1a), the initial concentration used in the transport experiment c_0 , and a SC thickness h of 15 μm .

4.3 RESULTS

4.3.1 *Characterization of extracted stratum corneum lipids*

4.3.1.1 Characterization of extracted stratum corneum lipids by WAXD

Strong reflections at spacing of 0.41 nm and 0.37 nm confirmed an orthorhombic lateral packing of extracted SC-lipids (187). Concomitantly, a broad peak at about 0.4 nm spacing indicated parts of the lipids to be present in an amorphous or liquid crystalline state.

4.3.1.2 Characterization of extracted stratum corneum lipids by DSC

Mixtures of extracted SC lipids produced endothermic transitions at 35 ± 4 °C and 68 ± 3 °C. The blank Durapore® membrane filter showed no transitions in the inspected temperature range. Durapore® membrane filters coated with mixtures of extracted SC lipids showed an endothermic transition at 71 ± 4 °C. Due to the low mass of lipids relative to the mass of the filter the weaker transition at around 35 °C was only present in 1 of 5 samples.

4.3.1.3 Characterization of extracted stratum corneum lipids by HPTLC

The extracted lipid mixture was composed of $4.1 \pm 1.6\%$ cholesterol, $3.3 \pm 1.1\%$ cholesterol esters, $32.6 \pm 2.1\%$ triglycerides, $4.3 \pm 1.4\%$ free fatty acids and $4.3 \pm 1.5\%$ ceramides (total mass of lipid extracted = 100%, n = 6).

4.3.2 *Keratin binding*

FFA exhibits a concentration dependent keratin binding (Fig. 8). Within the observed concentration range the dependence of the bound ($\mu\text{g}/\text{mg}$ keratin) versus free concentration ($\mu\text{g}/\text{ml}$) at equilibrium at 32 °C may be expressed by a Langmuir adsorption isotherm ($r^2 = 0.983$, $\chi^2 = 2.5$). The maximum weight of FFA that may be bound by 1 mg of keratin is 77.03 ± 7.81 μg . For CAF keratin binding is negligible (Figure 4-2).

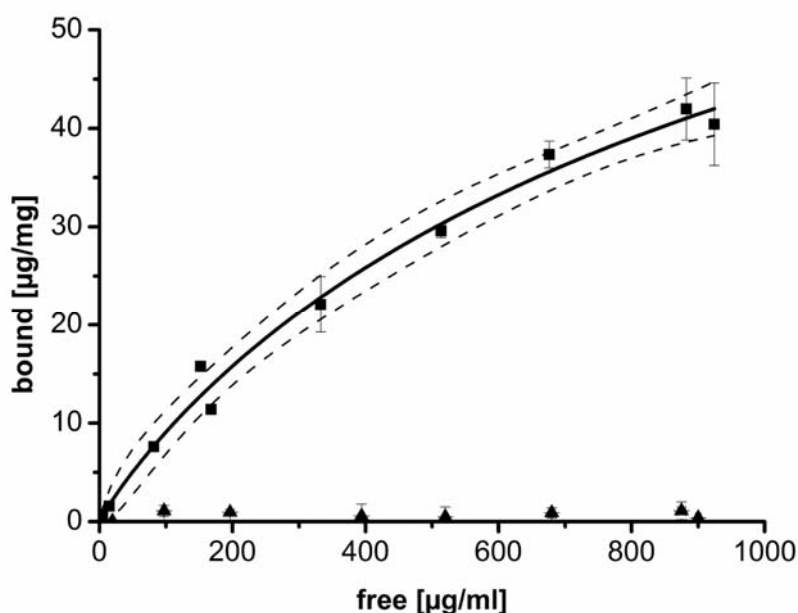


Figure 4-2 The weight of substance bound per mg keratin is plotted against the equilibrium concentration of free substance within the incubation solution. Keratin binding data of flufenamic acid (filled squares) is fitted to a Langmuir-adsorption isotherm (solid line) and confidence bands (dashed lines). Caffeine binding to keratin is negligible (filled triangle). (mean±sd)

4.3.3 Partition coefficients – directly determined values

4.3.3.1 *K*_{SC/don}

Equilibration experiments showed a preferred partitioning of FFA from Soerensen phosphate buffer into the SC (Table 4-2). Extraction (method 1b) proved the decrease of incubation solution (method 1a) to be due to a substance transfer into the SC.

Table 4-2 Partition coefficients of flufenamic acid and caffeine between different skin membranes (i) and phosphate buffer pH 7.4 (don) were measured by equilibration experiments and calculated from the decrease of donor concentration (method 1a, denoted as $^*K_{i/don}$) or from extraction (method 1b, denoted as $^{\#}K_{i/don}$). (mean±sd, n = number of repetitions, n.a. not analyzed)

i	flufenamic acid $^*K_{i/don}$	flufenamic acid $^{\#}K_{i/don}$	caffeine $^*K_{i/don}$	caffeine $^{\#}K_{i/don}$
SC	16.20±4.89 (n=9)	16.36±3.58 (n=12)	4.51±2.73 (n=22)	5.62±0.61 (n=22)
cor	n.a.	19.67±7.11 (n=3)	2.74±1.94 (n=9)	3.76±0.97 (n=9)
lip	20.32±0.54 (n=4)	23.15±0.51 (n=4)	2.15±0.42 (n=4)	n.a.
DSL	5.58±0.94 (n=6)	10.38±2.51 (n=6)	-2.22±2.59 (n=14)	5.10±2.04 (n=14)

$K_{SC/don}$ of FFA could further be retrieved from fitting tape-stripping profiles to Equation 4-4 (method 2, Figure 4-3 and Table 4-3). This fit seems appropriate for the 6 h profile whereas the elevated FFA concentrations found in the lower SC layers after 1 and 2 h are represented less efficiently. Estimates of $K_{SC/don}$ are somewhat lower than values measured by equilibration experiments however, considering the well known inter- and intra-individual variability of skin the results are still within a comparable range.

Table 4-3 *Stratum corneum*-donor partition coefficient and *stratum corneum* diffusion coefficient for flufenamic acid and caffeine were estimated from fitting the 1, 2 and 6 h concentration-*stratum corneum* depth profiles to Equation 4-4 (denoted as $**K_{SC/don}$ and $**D_{SC}$). (mean \pm sd)

t [h]	flufenamic acid $**K_{SC/don}$	flufenamic acid $**D_{SC}$ [cm ² /h]	caffeine $**K_{SC/don}$	caffeine $**D_{SC}$ [cm ² /h]
1	9.46 \pm 2.34	7.89 \pm 3.60*10 ⁻⁸	2.92 \pm 0.58	3.97 \pm 1.06*10 ⁻⁸
2	8.12 \pm 1.27	4.75 \pm 1.44*10 ⁻⁸	4.62 \pm 0.70	2.98 \pm 0.73*10 ⁻⁸
6	5.88 \pm 0.40	3.95 \pm 0.64*10 ⁻⁸	4.70 \pm 0.23	1.82 \pm 0.17*10 ⁻⁸

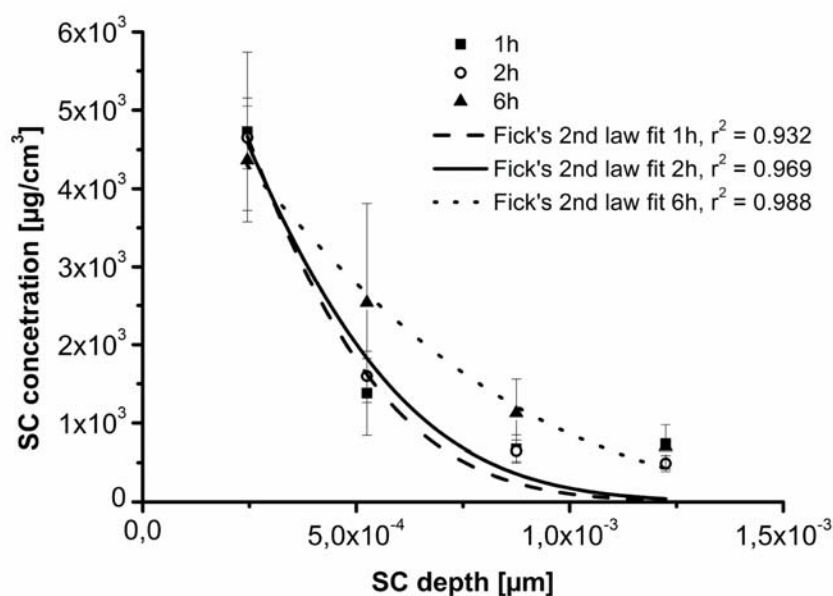


Figure 4-3 Tape stripping of the *stratum corneum* after 1 (filled square), 2 (open circle) and 6 h (filled triangle) incubation with flufenamic acid. The concentration-*stratum corneum* depth profiles are fitted to Equation 4-4. (mean \pm sd)

Like FFA, CAF showed a preferred partitioning from aqueous medium into the SC however, to a lesser extent (Table 4-2). Values measured with method 1b slightly exceed method 1a. Again $K_{SC/don}$ was also estimated from concentration-SC depth

profiles (method 2) (Figure 4-4 and Table 4-3). Estimates of method 2 excellently match results of method 1a and 1b.

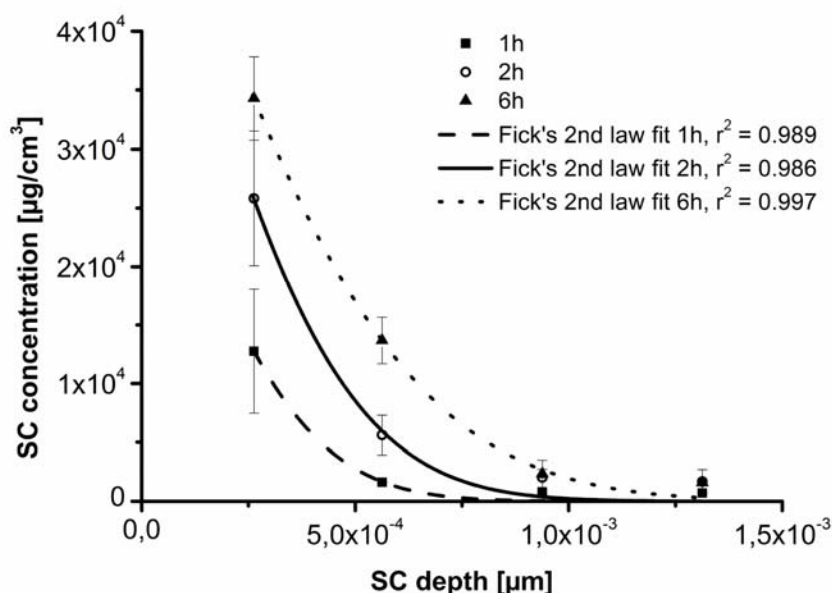


Figure 4-4 Tape stripping of the *stratum corneum* after 1 (filled square), 2 (open circle) and 6 h (filled triangle) incubation with caffeine. The concentration-*stratum corneum* depth profiles are fitted to Equation 4-4. (mean±sd)

4.3.3.2 $K_{cor/don}$

Both FFA and CAF preferably partition from Soerensen phosphate buffer pH 7.4 to delipidized SC sheets (Table 4-2). $K_{cor/don}$ of FFA exceeds CAF 5 - 7 times. For CAF values measured with method 1b slightly, though not significantly, exceed method 1a.

4.3.3.3 $K_{lip/don}$

For FFA both methods 1a and 1b are in a comparable range and suggest a preferred partitioning of FFA from Soerensen phosphate buffer pH 7.4 to SC-lipids (Table 4-2). CAF also favours the lipophilic environment although $K_{lip/don}$ is only about one tenth of FFA.

4.3.3.4 $K_{DSL/don}$

$K_{DSL/don}$ suggests a preferred partitioning between aqueous donor and viable skin layers for both compounds (Table 4-2). Incubating *dermis* sheets with CAF solutions caused only non-descript concentration changes fluctuating around zero resulting in

an exceptionally large standard deviation. For both compounds significantly higher amounts could be extracted from the viable skin layers than would have been estimated from the decrease of donor solution.

4.3.3.5 $K_{SC/DSL}$

Figure 4-5 and Figure 4-6 show from bottom to top the time dependency of c_{ExSC} , c_{inDSL} and $K_{SC/DSL}$ for FFA and CAF. This allows determining $K_{SC/DSL}$ when equilibrium of partition between SC and deeper skin layers has been established. The equilibrium value of $K_{SC/DSL}$ will later be used to calculate $K_{lip/DSL}$ (q.v.). For FFA, due to constant concentrations within the bottom layer of the SC and rising concentrations at the onset of the DSL, $K_{SC/DSL}$ decreases steadily until it converges to a constant value after about 14 - 24 h (Figure 4-5). The ratio of substance concentration of c_{ExSC} to c_{inDSL} is approximately 3:1 after 24 h. For CAF after initial changes of c_{ExSC} and c_{inDSL} $K_{SC/DSL}$ of CAF levels off to a ratio of 27:1 (Figure 4-6).

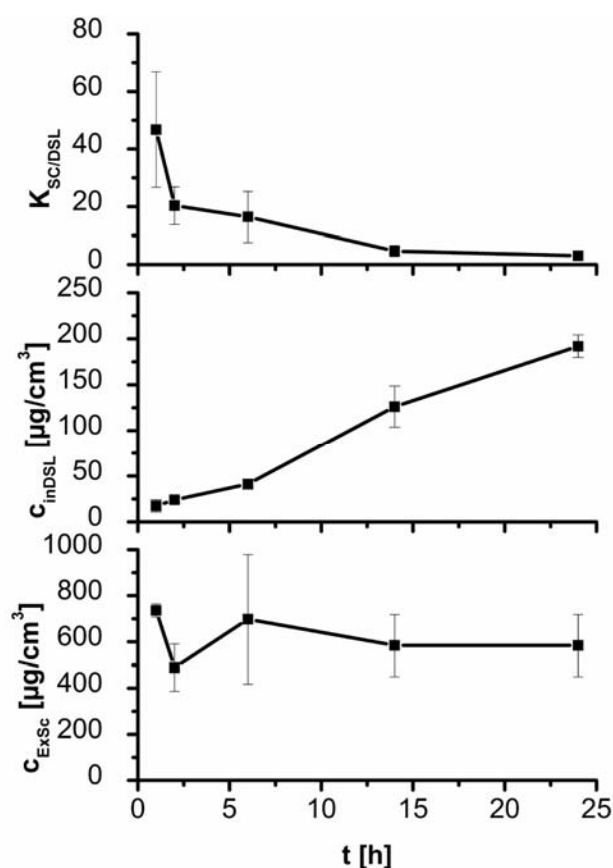


Figure 4-5 Flufenamic acid: Time-dependency of the *stratum corneum*-viable deeper skin layers partition coefficient (top), the concentration in the bottom *stratum corneum* layer as analyzed by tape-stripping (down) and concentration in the top layer of the viable deeper skin layers as analyzed by cryo-sectioning (middle). (mean \pm sd)

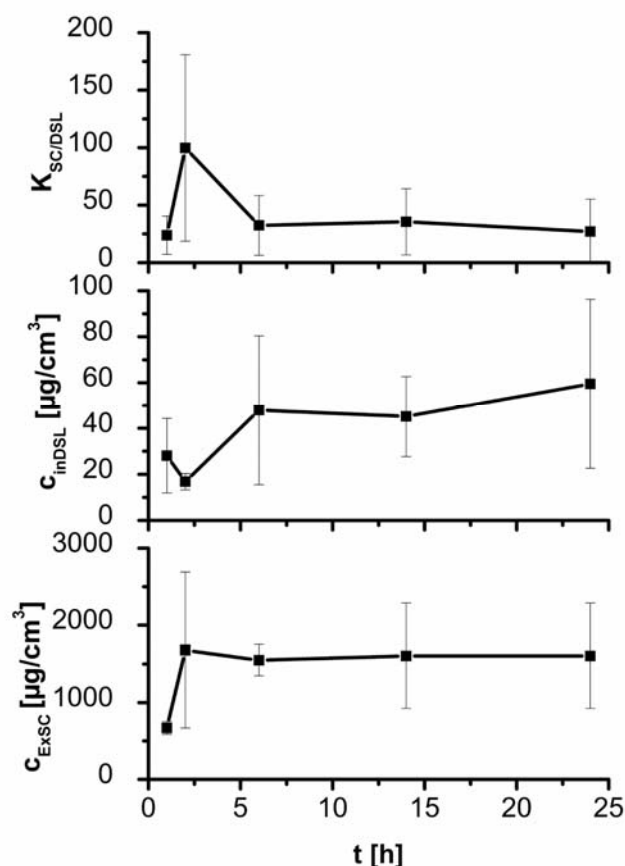


Figure 4-6 Caffeine: Time-dependency of the *stratum corneum*-viable deeper skin layers partition coefficient (top), the concentration in the bottom *stratum corneum* layer as analyzed by tape-stripping (down) and concentration in the top layer of the viable deeper skin layers as analyzed by cryo-sectioning (middle). (mean \pm sd)

4.3.4 Partition coefficients – calculated values

4.3.4.1 $K_{cor/lip}$

Calculations of $K_{cor/lip}$ based on experimental values for $K_{SC/don}$ and $K_{lip/don}$ (Table 4-4). $K_{SC/don}$ was acquired in 3 different ways. Since the results from equilibration measurements (method 1a and b, Table 4-2) were very similar $^*K_{SC/don}$ determined by method 1a was chosen for the calculation. In addition $K_{cor/lip}$ was calculated based on 6 h values of $^{**}K_{SC/don}$ as these were best represented by Equation 4-4 (Figure 4-3, Figure 4-4 and Table 4-3). Independent of the input data $K_{cor/lip}$ shows FFA to partition reluctantly from a lipophilic into a hydrophilic environment. In contrast to FFA corneocyte uptake of CAF dominates over lipids.

Table 4-4 The corneocyte-lipid partition coefficient was calculated from the *stratum corneum*-donor- and the lipid-donor partition coefficient (Equation 4-9). The viable deeper skin layers-lipid partition coefficient was calculated from *stratum corneum*-viable deeper skin layers partition coefficient and the corneocyte-lipid partition coefficient (Equation 4-10). The second column indicates which values were considered for calculation.

coefficients	source	flufenamic acid	caffeine
$K_{\text{cor/lip}}$	$*K_{\text{SC/don 1a}}; *K_{\text{lip/don 1a}}$	0.77±0.08	2.22±1.78
	$**K_{\text{SC/don 2}}; *K_{\text{lip/don 1a}}$	0.21±0.02	2.32±0.57
$K_{\text{DSL/lip}}$	$K_{\text{SC/DSL}}; K_{\text{cor/lip 1a/1a}}$	0.26±0.10	0.08±0.14
	$K_{\text{SC/DSL}}; K_{\text{cor/lip 2/1a}}$	0.10±0.04	0.08±0.10

4.3.4.2 $K_{\text{DSL/lip}}$

$K_{\text{DSL/lip}}$ suggests partitioning from SC-lipids to DSL of both FFA and CAF to be in the same range. Both compounds prefer the lipophilic environment of the SC lipids to the more hydrophilic viable skin layers (Table 4-4).

4.3.5 Diffusion coefficients

Figure 4-7 shows typical weight permeated per area versus time plots for FFA and CAF. *Steady state* flux of FFA through mainly lipophilic compartments, i.e. SC and lipids is ten or five times higher than that of CAF, whereas its *steady state* flux through the more hydrophilic DSL is only one-tenth of CAF (Table 4-5). As expected from their similar molecular weight (see material section) usually apparent diffusion coefficients of both compounds are of the same order of magnitude within a distinct compartment and increase from SC to lipids to viable skin layers.

Table 4-5 The *steady state* flux and diffusion coefficient for flufenamic acid and caffeine for stratum corneum, viable deeper sin layers and stratum corneum-lipids. The diffusion coefficient is calculated from the *steady state* diffusion equation using *steady state* flux and the product of the concentration in the respective donating compartment (i.e. 1 mg/ml for all experiments), the partition coefficient into the membrane and the membrane thickness. (mean ± sd; n = number of repetitions)

	flufenamic acid	flufenamic acid	caffeine	caffeine
	$J_{\text{ss}} [\mu\text{g}/\text{cm}^2/\text{h}]$	$D [\text{cm}^2/\text{h}]$	$J_{\text{ss}} [\mu\text{g}/\text{cm}^2/\text{h}]$	$D [\text{cm}^2/\text{h}]$
lip	108.66±6.51 (n=4)	$1.1\pm0.2\cdot10^{-4}$	21.89±2.0 (n=4)	$2.1\pm0.7\cdot10^{-4}$
DSL	2.50±0.70 (n=8)	$4.9\pm4.3\cdot10^{-3}$	25.65±4.8 (n=3)	$2.3\pm4.0\cdot10^{-3}$
SC	2.31±0.96 (n=8)	$1.7\pm0.8\cdot10^{-7}$	0.21±0.1 (n=7)	$1.4\pm0.4\cdot10^{-7}$

D_{SC} was further estimated from the decrease of $c(x,t)$ as a function of depth by fitting SC concentration-depth profiles to Equation 4-4 (Table 4-3). For both compounds D_{SC} decreases with time. These results range about one order of magnitude lower than values calculated on the basis of *steady state* flux (Table 4-5).

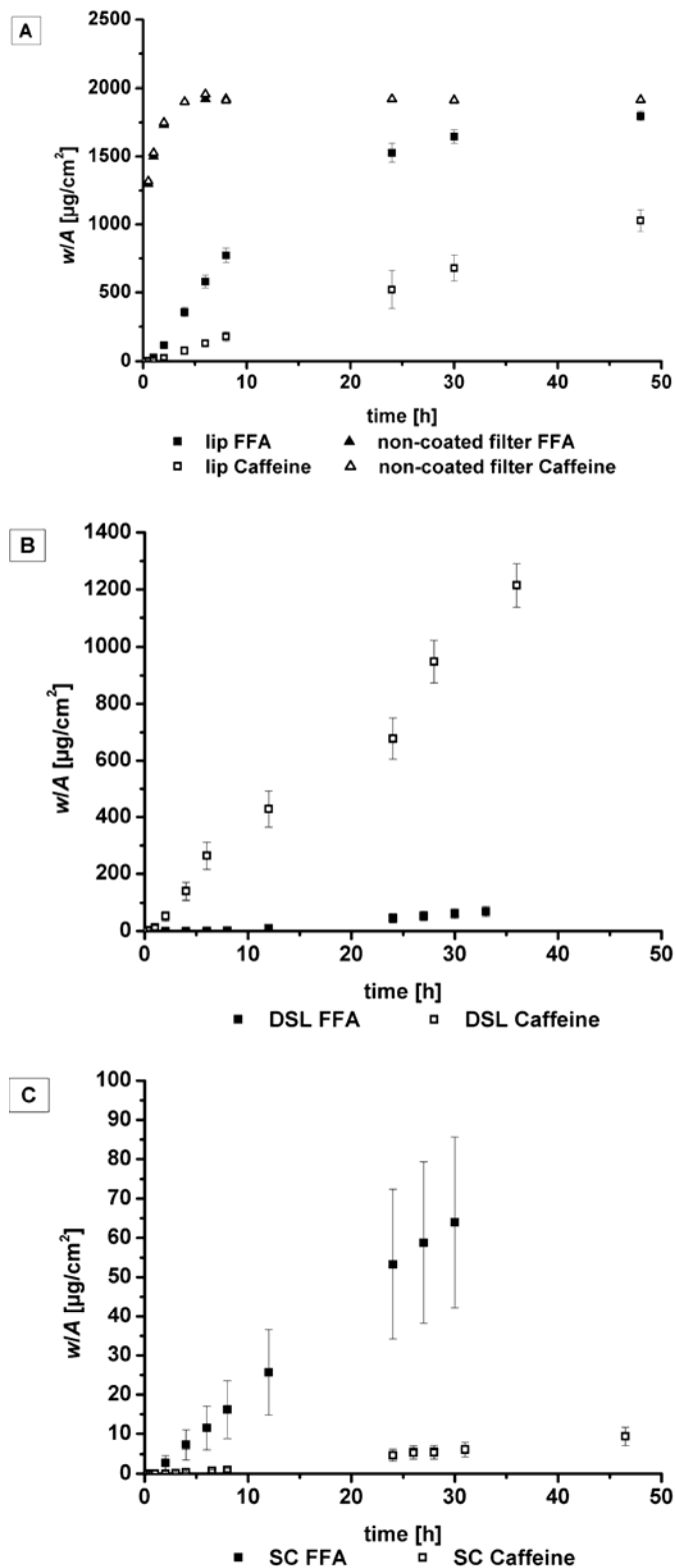


Figure 4-7 Typical weight permeated per area versus time plots of flufenamic acid (closed square) and caffeine (open square) across (A) lipid coated membrane filters, (B) viable deeper skin layers and (C) stratum corneum. (A) further includes weight permeated per area versus time plots of flufenamic acid (closed triangle) and caffeine (open triangle) across non-coated membrane filters.

4.4 DISCUSSION

Experimental data on relevant skin transport parameters of two test substances, FFA and CAF, were collected for the validation of an advanced two-dimensional skin penetration model (170). This included the SC- and DSL-concentration-depth-profiles, partition coefficients and diffusion coefficients. It was further sought to experimentally break down the consecutive partition and diffusion steps according to the anatomical and functional heterogeneity of the SC.

4.4.1 *Characterization of extracted stratum corneum lipids*

4.4.1.1 Characterization of extracted stratum corneum lipids by WAXD

The presence of orthorhombic crystalline structures showed that the lateral packing of the extracted SC lipids is representative of intact SC (187). Together with a lamellar organization of the SC lipid bilayers an orthorhombic lateral packing has been proposed to be crucial for the exceptional barrier properties of skin (188). Concomitantly significant amounts of amorphous lipids were detected that might result from the fairly large amounts of triglycerides within the samples (see 4.4.1.3).

4.4.1.2 Characterization of extracted stratum corneum lipids by DSC

Two of the four endothermic transitions described for human SC were found. The first at around 35 °C has previously been implicated with a disordering of the lateral packing from orthorhombic to hexagonal and hexagonal to liquid crystalline phase. The second one at approximately 70 °C results from a disordering of the lamellar structure (189). For intact SC two more transitions were reported by other authors (190). As these result from lipids covalently attached to proteins and protein denaturation they are not to be expected in isolated skin lipids.

4.4.1.3 Characterization of extracted stratum corneum lipids by HPTLC

The composition of SC lipid mixtures was found to be comparable to findings of other authors. For female abdominal skin de Paepe et al. report very similar ratios of triglycerides, cholesterol esters and ceramides III and IV, as well as free fatty acids contents within the same order of magnitude (191). The relatively larger cholesterol fraction reported by this group might be explained by age related variations. The high amounts of triglycerides are not surprising since skin originated from plastic surgery is always contaminated with triglycerides as shown by Wertz et al. (192).

4.4.2 Partition coefficients – directly determined values

4.4.2.1 $K_{SC/don}$

The uptake of substances from a topical formulation is governed by a partition process between topical formulation and uppermost skin layer, i.e. the SC. This may be quantified in terms of a partition coefficient $K_{SC/don}$. Conventionally $K_{SC/don}$ is measured by equilibration experiments where isolated SC is incubated with the respective donor formulation. In skin penetration or permeation experiments as well as in *in vivo* application of drug formulations a concentration ratio identical to this partition coefficient attunes rapidly at the onset of the SC. Within the SC directly below the zone of equilibrium the substance concentration will decrease rapidly due to a concentration gradient over the membrane.

It could be shown that $K_{SC/don}$ determined by equilibration measurements may be retrieved directly from tape-stripping experiments by fitting concentration-SC depth profiles to Equation 4-4 (Table 4-3). For FFA this method gives slightly lower values than results from equilibration experiments (Table 4-2 and Table 4-3). Customary the first one or two tape-strips are discarded due to contamination with the donor solution. Bommannan et al. identified this region to be critical for diffusion processes within the SC (193). They investigated the SC barrier function by infrared spectroscopy and found a disorder of the SC intercellular lipids that decreases throughout the first three tape-strips and then becomes constant. Recently these findings could be transferred to *in vitro* tape-stripping of skin. Mueller et al. found biphasic SC concentration-depth profiles at *steady state* for the diffusion of clobetasol propionate from saturated solutions containing 20% v/v propylene glycol over heat separated *epidermis* (194). They attributed this behaviour to an increased corneocyte uptake or an increased intercellular solubility within the SC disjunctum (194). This may involve a decrease of the SC diffusion coefficient in the same region causing the curvature of concentration-depth profiles to be steeper over the first three tapes than from tape four onwards. In contrast Equation 4-4 tacitly assumes constant diffusion and partition properties throughout the whole SC.

Additionally the significance of fitting the penetration data to Equation 4-4 is limited for FFA for short incubation times. Assuming perfect sink conditions at the outflow of the SC it does not represent the elevated concentration found in the lower SC after 1 and 2 h of incubation (Figure 4-3). Oppositely, a fit to Equation 4-4 nicely represents

the 6 h profile of FFA. It seems that a so far non-specified mechanism promotes the penetration of FFA at the beginning of the diffusion process and is later compensated for by Fick'ian diffusion. It may be speculated that the special properties of FFA such as binding to keratin or its pH sensitive lipophilicity and solubility may be held responsible for this behaviour.

For CAF estimates on $K_{SC/don}$ from SC concentration-depth profiles excellently match results of equilibration measurements (Table 4-2 and Table 4-3). CAF does not seem to be as sensitive to depth dependent alterations in lipid fluidity within the upper SC as FFA. As the alterations of the SC ordering reported by Bommannan et al. predominantly concern the intercellular lipid channel substances using the lipid pathway should be affected more than others. This might explain why estimates of method 2 for FFA deviate from equilibration experiments while estimates for CAF do not.

4.4.2.2 $K_{lip/don}$

For the *in silico* model an accurate anatomical break down of partition processes was sought. As all corneocyte layers are embedded in a continuous lipid layer the boundary layer towards the donor solution is in fact lipoidal rather than cellular. Therefore $K_{lip/don}$ instead of $K_{SC/don}$ is needed to correctly describe the partitioning at the top of the SC. So far, measurements of lipid partition coefficients are only known from the original works of Raykar et al. (52). $K_{lip/don}$ was determined in equilibration experiments employing extracted human SC-lipids brought up onto Durapore® membrane filter supports. Lipid coated membranes have previously been used by other authors in permeation studies (175, 195, 196). Usually artificial lipid mixtures or lipids of animal origin were used. To our knowledge this is the first occasion that these were prepared completely from extracted human SC-lipids and were employed to measure partition coefficients.

4.4.2.3 $K_{SC/DSL}$

Especially for lipophilic substances the partition step at the interface between lipophilic SC and more hydrophilic viable *epidermis/dermis* may represent an additional hindrance against drug permeation. For FFA the increase in c_{inDSL} (Figure 4-5, middle) may partly be explained by a water uptake into the viable skin layers during incubation in the Franz diffusion cell. This leads to a visible swelling. The

increased volume of water contains additional substance. A concomitant decrease in pH from 8 to 7.4 should not impair FFA solubility (pK_a 3.9 (171)) (197). In addition the partitioning process is superimposed by binding of FFA to viable skin layer proteins. Up to saturation of binding sites this leads to an over-proportional increase of c_{inDSL} and a concomitant decrease of $K_{SC/DSL}$ (Figure 4-5, middle and top). After 24 h $K_{SC/DSL}$ then becomes constant. This value is used for calculating $K_{DSL/lip}$. In contrast, CAF does not bind to proteinaceous structures (Figure 4-2) and consequently shows no time dependency of c_{ExSc} , c_{inDSL} or $K_{SC/DSL}$ (Figure 4-6). For the sake of consistency again the 24 h values were used to calculate $K_{DSL/lip}$.

4.4.3 Partition coefficients – calculated values

4.4.3.1 $K_{cor/lip}$

According to Equation 4-9 $K_{cor/lip}$ was calculated as a secondary derived parameter employing experimental data on $K_{SC/don}$ and $K_{lip/don}$ and considering realistic relative volume fractions of the lipid and corneocyte phase, φ_{lip} and φ_{cor} .

By systematically varying φ_{lip} and φ_{cor} it can be shown that naturally occurring variations in lipid channel dimensions have only a limited impact on $K_{cor/lip}$. For example variation of φ_{lip} of $\pm 20\%$ reflects in a change of $*K_{cor/lip} \pm 0.7\%$ and $**K_{cor/lip} \pm 9.5\%$ for FFA and $*K_{cor/lip} \pm 1.4\%$ and $**K_{cor/lip} \pm 1.3\%$ for CAF.

As recently reported by Nitsche et al. for highly lipophilic compounds, i.e. with a $\log K_{Oct/w} > 5$ experimental results of $K_{SC/don}$ are largely sensitive to the lipid content and composition of the used skin samples hampering the significance of estimates of corneocyte hold-up based on $K_{SC/don}$ (150). This problem was circumvented by determining both $K_{SC/don}$ and $K_{lip/don}$ experimentally in analogous setups using identical sets of donor skins and validated preparation techniques. One of the prerequisites of Equation 4-9 is

Equation 4-13
$$K_{SC/don} = \varphi_{lip} K_{lip/don} + \varphi_{cor} K_{cor/don}$$

Substituting $K_{lip/don}$ and $K_{cor/don}$ with experimental results from equilibration measurements (method 1) a theoretical $K_{SC/don}$ may be calculated. Thus the theoretical $K_{SC/don}$ of FFA is 20.02 ± 7.68 (based on $K_{lip/don}$ and $K_{cor/don}$ determined by method 1b, i.e. extraction of skin specimen) and 2.68 ± 2.42 for CAF (based on $K_{lip/don}$ and $K_{cor/don}$ determined by method 1a). These theoretical values of $K_{SC/don}$ are

both in very good agreement with experimental results which indicates that a calculation of $K_{\text{cor/lip}}$ on this basis is valid.

Our analyses show that some degree of corneocyte uptake may be claimed for both FFA and CAF (Table 4-4). In accordance with their octanol-water partition coefficients $K_{\text{cor/lip}}$ of CAF is higher than that of FFA. It must be kept in mind that alternatively to partitioning into the corneocytes part or all of the substance could bind to proteins of the cornified envelope or to keratin. Especially FFA proved a likely candidate for protein binding whereas no binding was detected for CAF (Figure 4-2).

4.4.3.2 $K_{\text{DSL/lip}}$

Again an accurate anatomical break down of partition steps was sought. Therefore our method for calculating $K_{\text{cor/lip}}$ was expanded to the partition step at the interface DSL-lipid (Equation 4-10). According to the compound lipophilicity partitioning from SC-lipids to viable *epidermis* of FFA should be hampered whereas CAF should prefer the DSL. Thus $K_{\text{DSL/lip}}$ of FFA is to be expected lower than that of CAF. Our results suggest otherwise (Table 4-4). First, this mirrors the improved solubility of weak acids like FFA under moderate alkaline conditions within the DSL. Second, a high binding of FFA to proteins of the viable skin layers, such as collagen, elastin or melanin, will further raise the concentration within the DSL of this particular substance and hence will increase $K_{\text{DSL/lip}}$. This behavior may be investigated by measuring $K_{\text{DSL/don}}$. Incubating *dermis* sheets with FFA led to a measurable decrease in the concentration of the incubation solution (method 1a, Table 4-2). Still, extracted amounts were up to two times higher than would have been estimated from analyzing the decrease of the donor concentration (method 1b, Table 4-2). In contrast, for CAF no relevant decrease in concentration of the incubation solution could be detected. Still, significant amounts of CAF were extracted from the DSL. Consequently FFA enters the DSL by partitioning or binding to proteins and also by water of hydration while CAF will only be dissolved in water of hydration and will not bind to epidermal or dermal proteins. Third, this hints that the solubility of hydrophilic substances like CAF in SC lipids may be much better than usually assumed.

4.4.4 Diffusion coefficients

4.4.4.1 D_{lip}

Lipid coated membranes have widely been used for diffusion measurements. In contrast to our study most of the cited experiments were performed with lipid mixtures of artificial or animal origin (175, 198). De Jager et al. could demonstrate that especially lamellar organisation and lateral packing are highly sensitive to lipid composition and manufacturing conditions (199). This problem was circumvented by using lipids extracted from human SC. By D_{SC} measurements it could be shown that the thermal behaviour and thus the crystallinity of the extracted SC lipids on the membrane support is very similar to the *in vivo* situation. What is more WAXD measurements revealed that a significant portion of the lipids is present in an orthorhombical crystalline state. However, due to the presence of amorphous lipids and the absence of corneocytes the 3D structure of the lipids on the filters will probably be different from the *in vivo* situation. Thus D_{lip} can only be an approximation. Furthermore co-extracted triglycerides might act as a possible penetration enhancer in permeation experiments (177) and thus may lead to an overemphasis of D_{SC} and D_{lip} . However, our measured values for D_{lip} queue nicely with literature data on lipid diffusion coefficients. Lange-Lieckfeldt and Lee reported that ratios ranging from 10^2 - 10^4 with lipid diffusion rates of 10^{-8} - 10^{-9} cm²/s result from SC geometry reflecting the tortuous diffusion pathway and the low diffusion area (198). The ratio of D_{lip}/D_{SC} was $6.4 * 10^2$ (D_{SC} determined according to Equation 4-12 or $1.4 * 10^4$, $2.3 * 10^4$, $2.8 * 10^4$ (D_{SC} for 1, 2 and 6 h determined according to Equation 4-4 for FFA and $1.5 * 10^3$ (D_{SC} determined according to Equation 4-12 or $5.3 * 10^3$, $0.7 * 10^3$, $1.2 * 10^4$ (D_{SC} for 1, 2 and 6 h determined according to Equation 4-4 for CAF (Table 4-3 and Table 4-5). This does not necessarily imply impenetrable corneocytes. They still may act as a reservoir if the rate of transport is lowest within intercellular lipids and hence determines the overall diffusion velocity through the SC. Further, our measured values for D_{lip} are in good agreement with lateral diffusion coefficients measured with a fluorescence recovery technique in extracted SC lipids (156). Diffusion within the plane of the lipid bilayers is believed to be considerably slower than perpendicular to it. However, Johnson et al. found lateral- but not trans-bilayer diffusion coefficients are sufficient to explain the overall resistance of solute permeation through the SC (134). In addition it has been suggested that lipid bilayers

might be oriented not strictly parallel to the corneocytes possibly allowing a continuous pathway for lateral diffusion (110).

In view of these facts it is justified to employ our measured apparent lipid diffusion coefficients as direct input data for the *in silico* model presented in the accompanying paper (170). This assumes constant diffusion properties within all lipid bilayers irrespective of the SC depth.

4.4.4.2 D_{DSL}

Cross et al. reported for a series of aliphatic alcohols an additional partition step between *epidermis* and *dermis* significantly influencing maximum flux and apparent permeability coefficient if compound $\log K_{Oct/w}$ was 2 and higher (154). Consequently for CAF no additional hindrance is to be expected ($\log K_{Oct/w} = 0.083$ (172)). Likewise may be assumed for FFA, as this is completely ionized within the fully swollen *epidermis* and *dermis* (197). If transport is indeed homogeneous throughout the whole viable skin layers the *steady state* concentration gradient should be linear. Experimental data on the *steady state* DSL-concentration gradient is available from surface parallel segmentation of the DSL (Figure 4-8). Substituting dc/dx and $J_{ss,DSL}$ in Equation 4-12 directly by experimental data it is possible to calculate D_{DSL} . For FFA linear regression of 24 h DSL-cryo-cutting data revealed a slope of the $6.34 \cdot 10^2 \mu\text{g}/\text{cm}^4$ with the intercept with the y-axis at $1.80 \cdot 10^2 \mu\text{g}/\text{cm}^3$ and a reasonable r^2 of 0.823. Thus D_{DSL} calculates to $3.9 \cdot 10^{-3} \pm 1.7 \cdot 10^{-3}$ which is very similar to estimates on the basis of J_{ssDSL} , $K_{SC/DSL}$, c_{ExSC} and h_{DSL} (Table 4-5). Therefore diffusion properties are indeed homogeneous through the viable skin layers for FFA. Consequently our calculated values for D_{DSL} for both FFA and CAF may be used as direct input data for mathematical modeling of skin penetration (170).

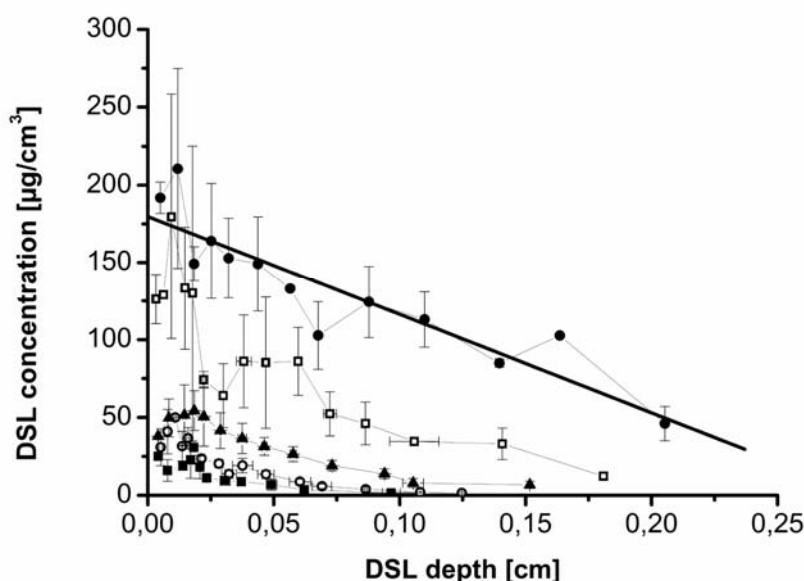


Figure 4-8 Cryo-sectioning of viable deeper skin layers after 1 (filled square), 2 (open circle), 6 (filled triangle), 14 (open square) and 24 h (filled circle) for flufenamic acid with linear regression of the 24 h graph (bold line) assuming constant membrane properties at *steady state*. (mean \pm sd)

4.4.4.3 D_{SC}

Estimates of D_{SC} from fitting the 1, 2 and 6 h concentration-SC depth profiles to Equation 4-4 suggest a decreasing diffusion velocity with time for both FFA and CAF. As already mentioned water uptake may impact on the SC diffusion properties. On first sight our results seem contradictory to the well known permeation enhancing effect of water which is probably due to a disruption of intercellular SC lipids (200). However, this effect may probably be antagonized by a concomitant increase in path length due to swelling of corneocytes. As a significant proportion of both compounds was found to partition into the corneocytes a decrease in D_{SC} seems a possible logical consequence. In contrast to D_{lip} and D_{DSL} , D_{SC} cannot be used as direct input for *in silico* modeling due to the inhomogeneous character of the SC. However, the accompanying study shows that D_{SC} together with D_{lip} and $K_{cor/lip}$ is a powerful tool to estimate D_{cor} (170).

4.5 CONCLUSION

Skin transport of drug substances from a topical formulation may be described in terms of partition and diffusion coefficients that account for abrupt changes in the environmental lipophilicity and diffusion characteristics of the medium. This study

describes methods and data to measure the relevant partition and diffusion steps involved in skin transport taking into account its anatomical heterogeneity. While several coefficients such as $K_{\text{lip/don}}$, D_{lip} and D_{DSL} may be measured experimentally, others such as $K_{\text{cor/lip}}$, $K_{\text{DSL/lip}}$ and D_{cor} can only be determined indirectly. Equations are presented to calculate $K_{\text{cor/lip}}$ and $K_{\text{DSL/lip}}$ from experimentally available data. For two compounds with different physicochemical properties, i.e. FFA and CAF the complete data set has been collected for the case of diffusion from an aqueous donor buffered at pH 7.4 across human skin. Where available, experimental and calculated coefficients were compared to literature data and were found to be consistent.

5 *IN SILICO* MODEL OF SKIN PENETRATION BASED ON EXPERIMENTALLY DETERMINED INPUT PARAMETERS. PART II: MATHEMATICAL MODELLING OF *IN VITRO* DIFFUSION EXPERIMENTS

Parts of this chapter have been published as:

A. Naegel, S. Hansen, D. Neumann, C.M. Lehr, U.F. Schaefer, G. Wittum, M. Heisig, *In silico* model of skin penetration based on experimentally determined input parameters. Part II: Mathematical modelling of *in vitro* diffusion experiments. Identification of critical input parameters, Eur J Pharm Biopharm 68 (2008) 368-79 DOI:10.1016/j.ejpb.2007.05.018.

The author of the thesis made the following contributions to the publication.

Significantly contributed to the development of the theoretical concept realized in the diffusion model. Planned, performed and interpreted all experiments.

5.1 Introduction

Recently, there has been much interest in mathematical models and numerical methods available to predict dermal absorption *in-silico* in order to avoid unnecessary and costly *in-vitro* and *in-vivo* testing (201, 202). To a great extent, this is due to ethical difficulties resulting in a lack of sufficient amounts of human skin. The use of animal skin is limited by animal healthcare regulations and anatomical difference. Economic and time constraints must be considered as well, especially with respect to increasing legislation in the risk assessment of industrial chemicals (203). Therefore, mathematical modelling and numerical simulation of drug transport through human skin gain key roles in the investigation of dermal and transdermal drug delivery as well as risk assessment of chemical exposure.

Today, most of the pharmacokinetic models are based on one or more compartments describing the skin layers and the vehicle (112-115, 117, 204). The drug concentration in each of these layers is modelled by an ordinary differential equation, which does not provide information about the drug concentrations in the layers of the SC and the deeper skin layers (DSL). Furthermore, the parameters like diffusion coefficients and partition coefficients for these equations are model- and system-dependent allowing no direct input for computational simulation of skin transport.

A further mathematical approach for modelling are diffusion models which consist of partial differential equations describing drug delivery in space and time according to Fick's laws of diffusion (110, 132, 133, 136, 139, 142-145, 205-212). These models are based on first principles, such as balance of mass. Resolving the structure, they have the great advantage that the parameters, e.g., diffusion and partition coefficients, are system-independent, allowing a system-independent parameter identification. Therefore, the effects of different parameters like corneocyte permeability, corneocyte alignment, diffusion and partition coefficients on skin transport can be studied *in-silico* on arbitrary skin geometries.

Recently, due to advances in simulation techniques, diffusion models running on fully resolved two-dimensional or even three-dimensional geometries have become feasible. A great part of these models are so-called "brick-and-mortar" models (110, 130, 133, 134, 137, 139, 142, 143, 166, 198, 212-214). The bricks and mortar correspond to the corneocytes and the surrounding intercellular lipid bilayers,

respectively. A very good survey of existing “brick-and-mortar” models is given by Wang et al. (110).

It was shown several years ago (142) that including the heterogeneous structure of the SC in the geometry is crucial for the barrier function of the membrane. This two-dimensional diffusion model allows to calculate the time-dependent spatial distribution of drugs in the different skin layers and to illustrate the diffusional pathway in the SC. These illustrations are very similar to photographs of SC visualised using two-photon fluorescence microscopy (54, 55, 215).

This section presents an extension of the two-dimensional diffusion model presented by Heisig et al. (142) by increasing the number of corneocyte layers to 16 and adding a homogeneous epidermal/dermal compartment. The experimental data on partition coefficient $K_{lip/don}$ as well as diffusion coefficients D_{lip} and D_{DSL} that have been introduced in the previous chapter (4) are used as input parameters in the 2D-model to evaluate drug concentration-SC/DSL-depth profiles *in silico*. Experimentally not accessible partition coefficients $K_{cor/lip}$ and $K_{DSL/lip}$ are derived from experimental data on $K_{SC/don}$, $K_{lip/don}$, and $K_{SC/DSL}$ as described in section 4.2.14. A method is presented to derive diffusion coefficient D_{cor} from experimental data on $K_{lip/don}$, D_{lip} , and D_{SC} by assuming constant partition and diffusion coefficients. As model drugs one lipophilic, however ionisable substance (FFA) and one hydrophilic non-ionisable compound (CAF) are used. A comparison of the concentration-SC/DSL-depth profiles obtained by *in vitro* and *in silico* experiments is presented and discussed.

5.2 Model description

This section formulates a mathematical description of a Franz diffusion cell experiment for one substance under infinite dose conditions. In particular, it introduces notation used in the remainder of the work. At first, a description of the model geometry is given. The next subsection formulates the distribution of the substance, or more precisely its concentration, in terms of a partial differential equation. How this model is related to physical quantities measured in the experiment is derived afterwards. The section concludes with a brief description of the numerical methods which were applied in the solution process.

5.2.1 Model geometry

The model is based on the two-dimensional *brick-and-mortar model* which was used for the SC in (142). A full-thickness or *extended skin model* is derived from this model by adding a homogeneous compartment of constant size for the deeper skin layers (DSL). This compartment guarantees proper outflow conditions at the interface between SC and *epidermis*. It does not focus on a precise resolution of the processes in *epidermis* and *dermis*. This simplification is admissible as far as only a structural resolution of the SC and the barrier property of full thickness skin are concerned. The resulting geometry of the extended skin model is depicted in Figure 5-1.

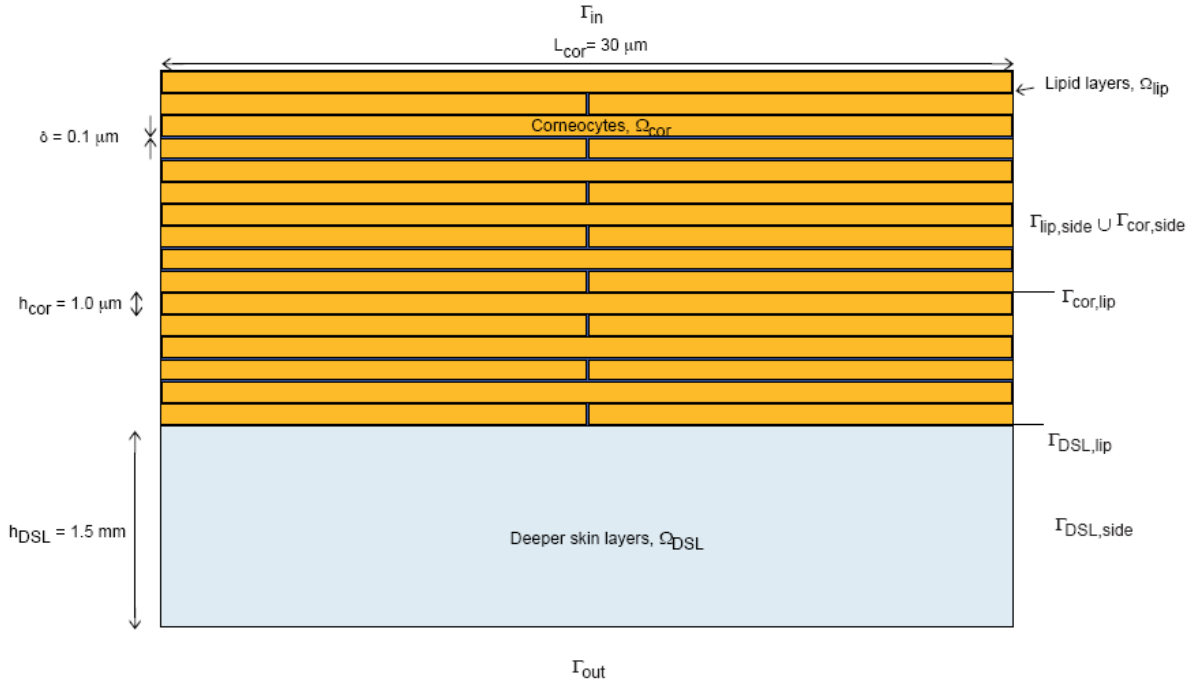


Figure 5-1 The extended brick-and-mortar model for human *stratum corneum* and viable *epidermis* and *dermis*. Diffusion occurs through lipid layers, corneocytes and viable deeper skin layers. Interfaces, domains and parameters are given in Table 5-1.

Formally, the domain consists of three different phases Ω_{cor} , Ω_{lip} , and Ω_{DSL} , representing either the corneocytes, the surrounding lipid matrix or the DSL. The corneocytes are fully staggered in $n = 16$ layers. The remaining geometric parameters are the diameter of lipid channel $\delta = 0.1 \mu\text{m}$, the corneocyte height $h_{cor} = 1 \mu\text{m}$, the corneocyte width $L_{cor} = 30 \mu\text{m}$, and the height of the DSL compartment $h_{DSL} = 1.5 \text{ mm}$. These parameters are summarised in Table 5-1.

Table 5-1 Description of the model geometry

Description of the model geometry	
\square	Lipid layers thickness
L_{cor}	Corneocyte length
h_{cor}	Corneocyte height
h_{DSL}	Height of DSL compartment
\mathcal{L}_k	k th SC layer
d_k	Average depth of \mathcal{L}_k ; distance of the centre mass of \mathcal{L}_k to the top surface Γ_{in}

The neighbouring phases are separated by two interfaces $\Gamma_{\text{cor/lip}}$ and $\Gamma_{\text{DSL/lip}}$ respectively. The corneocytes and the deeper skin layers do not share a common interface. The domain is confined by boundaries Γ_{in} , Γ_{out} , and Γ_{side} . For the remainder of this work an index set $I = \{\text{cor}, \text{lip}, \text{DSL}\}$ will be used in order to avoid an unnecessarily abundant notation. Subdomains and interfaces are then, for instance, referred to by the symbols Ω_i , and Γ_{ij} for $i \neq j$ and $i, j \in I$ (Table 5-2).

Table 5-2 Domains and interfaces of the model membrane

Domains and interfaces	Symbol	Diffusion coefficient	Partition coefficient	Concentration
(Donor compartment)		n.a.		c_{don}
Interface	Γ_{in}		$K_{\text{lip/don}}$	
Lipid layers	Ω_{lip}	D_{lip}		c_{lip}
Interface	$\Gamma_{\text{cor/lip}}$		$K_{\text{cor/lip}}$	
Corneocytes	Ω_{cor}	D_{cor}		c_{cor}
\vdots				
Interface	$\Gamma_{\text{DSL/lip}}$		$K_{\text{DSL/lip}}$	
Deeper skin layers	Ω_{DSL}	D_{DSL}		c_{DSL}
Interface	Γ_{out}		$K_{\text{DSL/acc}}$	
(Receptor compartment)		n.a.		c_{acc}

5.2.2 Model equations

It is assumed that transport in each phase is due to Fick's second law of diffusion,

Equation 5-1 $\delta_t c_i(x, t) - \text{div}(D_i \nabla c_i(x, t)) = 0$

for $t > 0$, $x \in \Omega_i$, $i \in I$. On the interfaces between the phases two different types of transmission conditions apply. Partitioning between the different phases is modelled using a partition coefficient $K_{i/j}$,

Equation 5-2
$$c_i(x, t) = K_{i,j} c_j(x, t)$$

for $t > 0$, $x \in \Gamma_{i,j}$, $i \neq j$. As for several hydrophilic and also some lipophilic compounds their intra-corneocyte presences has been visualized, $K_{cor/lip} \neq 0$ needs to be considered at the lipid-corneocyte interface (53, 54, 56, 216). Additionally, the flux across an interface must be continuous due to mass conservation, which means that

Equation 5-3
$$(D_i \nabla c_i(x, t) + D_j \nabla c_j(x, t)) \cdot n(x) = 0$$

holds for $t > 0$, $x \in \Gamma_{i,j}$, $i \neq j$ and any normal n to $\Gamma_{i/j}$. The initial values used are given by

Equation 5-4
$$c_i(x, 0) = 0$$

For $x \in \Omega_i$, $i \in I$. The boundary conditions are given by

Equation 5-5
$$c_{lip}(x, t) = c_{lip}^{(in)}, x \in \Gamma_{in}$$

Equation 5-6
$$c_{DSL}(x, t) = c_{DSL}^{(out)}, x \in \Gamma_{out}$$

Equation 5-7
$$\frac{\partial c_i}{\partial n}(x, t) = 0, x \in \Gamma_{i,side}, i \in \{lip, cor\}$$

and

Equation 5-8
$$\frac{\partial c_{DSL}}{\partial n}(x, t) = 0, x \in \Gamma_{DSL,side},$$

for $t > 0$. The concentrations on the outer boundaries are usually induced by concentrations in the donor and the acceptor compartments, c_{don} and c_{acc} . On this model they are assumed to be constant and have constant partition coefficients as well:

Equation 5-9
$$c_{lip}^{(in)} = K_{lip/don} c_{don},$$

Equation 5-10
$$c_{DSL}^{(out)} = K_{DSL/acc} c_{acc}.$$

The original brick-and-mortar model is obtained by removing the subdomain Ω_{DSL} and by an identification of the interfaces $\Gamma_{DSL/lip}$ and Γ_{out} . In this case, the condition in Equation 5-8 becomes empty and Equation 5-6 and Equation 5-10 must be substituted by

Equation 5-11
$$c_{lip}(x, t) = c_{lip}^{(out)}, x \in \Gamma_{out}$$

Equation 5-12 $c_{lip}^{(out)} = K_{lip/acc} c_{acc}$.

Note that protein binding effects of the keratin-filled corneocytes, as reported, e.g. by (217), are not included in the model. This can be done, e.g., by adding a factor before the time derivative in Equation 5-1 for $i = cor$.

5.2.3 Aggregation of quantities

For each time $t > 0$ the amount of substance passing through the interface $\Gamma \subset \delta\Omega_{lip}$ is given by

Equation 5-13 $j(\Gamma, t) = - \int_{\Gamma} (D_{lip} \nabla c_{lip}(x, t)) \cdot n d\mu$

When Γ is a part of $\delta\Omega$, n should be chosen as an outward normal to obtain a proper direction of the flow. As it is often desirable to normalise this quantity with respect to an area of unit size, the flux is defined by

Equation 5-14 $J(\Gamma, t) = \frac{j(\Gamma, t)}{A(\Gamma)}$.

Here $A(\cdot)$ refers to the area operator. In Franz-cell diffusion experiments, membranes are often characterised by the *steady state* flux $J_{\infty} = \lim_{t \rightarrow \infty} J(\Gamma_{in}, t)$. In the experiment, concentrations are always aggregated by inspecting pools of strips, each assigned to a certain depth of the SC (as described in section 4.2.9). To compare the results, the same must be done in the simulation. For $k = 1, \dots, 16$, we define the k th SC layer by $\mathcal{L}_k \{x \in \Omega : (k-1)(h_{cor} + \delta) \leq \text{dist}(x, \Gamma_{in}) \leq k(h_{cor} + \delta)\}$. This definition involves the distance between $x \in \Omega$ and Γ_{in} , which is given by $\text{dist}(x, \Gamma_{in}) = \min_{y \in \Gamma_{in}} |x - y|$. The (average) depth of \mathcal{L}_k within the SC is

Equation 5-15 $d_k = \left(k - \frac{1}{2}\right)(h_{cor} + \delta)$

which is the average distance between \mathcal{L}_k and Γ_{in} . The average concentration \bar{c}_k in \mathcal{L}_k is defined by

Equation 5-16 $\bar{c}_k = \frac{1}{\int_{\mathcal{L}_k} 1 dx} \int_{\mathcal{L}_k} c(x) dx,$

where $c(x) \equiv c_i(x)$ for $x \in \Omega_i, i \in \{cor, lip\}$. Plotting the pairs (d_k, \bar{c}_k) for $k = 1, \dots, 16$ results in discrete concentration-depth-profile.

5.2.4 Numerical techniques

Before computations can be performed, the system has to be transformed to a dimensionless form. The dimensionless partial differential equation is then solved numerically. Computations were performed by Arne Naegel et al. as described in (170) using the Rothe method: first the time is discretised using a fractional-step- θ -scheme. The resulting two-dimensional problem is solved using a finite-volume-scheme. The whole process leads to a large system of equations which are solved using an algebraic-multigrid method. By transforming the variable back into the original dimensions, the desired quantities can be computed.

5.3 Model and experiment

This section gives a summary of facts to be kept in mind, when comparing experiment and simulation. Though the model discussed so far neither includes a donor nor an acceptor compartment. Equation 5-9 and Equation 5-10 already describe a Franz diffusion cell with infinite dose conditions. For reasons of simplification, perfect sink conditions will be assumed in the deeper skin regions, i.e.

$$c_{\text{DSL}}^{\text{out}} = c_{\text{acc}} = 0, \text{ for the remainder of this work.}$$

5.3.1 Input parameters

The computational model relies on seven input parameters. The membrane is characterised by the diffusion coefficients D_{lip} , D_{cor} , and D_{DSL} and the partition coefficients $K_{\text{cor/lip}}$, and $K_{\text{DSL/lip}}$. An additional partition coefficient $K_{\text{lip/don}}$ and a constant concentration c_{don} describe the donor compartment (Equation 5-9).

Section 4 described how D_{DSL} , D_{lip} , and $K_{\text{lip/don}}$ can directly be determined in an experiment. The quantity c_{don} is a free input parameter. In the case of the tape stripping experiment it is given by the concentration used in the donor compartment. The remaining three parameters D_{cor} , $K_{\text{cor/lip}}$, and $K_{\text{DSL/lip}}$ are hidden from direct access due to the heterogeneous structure and the small length scales of the SC membrane. In general, only average concentrations are available for the SC. Using a definition in analogy to Equation 5-16, this yields an apparent partition coefficient $K_{\text{SC/don}}$ between donor and the first layer of the SC membrane. Nevertheless, this yields access to the partition coefficients $K_{\text{cor/lip}}$ and $K_{\text{DSL/lip}}$ by using the relative volume fractions of lipids and corneocytes in the SC as described in section 4.2.14.3.

A similar approach must be taken to determine the diffusion coefficient in the corneocytes D_{cor} . While D_{lip} and D_{DSL} are determined, e.g., by flux experiments (section 4.2.15), this does not carry over to D_{cor} . Yet this quantity can be derived from *steady state* flux through the SC membrane. Until the end of the following subsection, the model is restricted to an SC-only geometry. On this membrane it is possible to define an apparent diffusion coefficient D_{SC} : for a homogeneous medium $D_{\text{SC}} = D_{\text{lip}} = D_{\text{cor}}$ and $K_{\text{cor/lip}} = 1$ hold, and the *steady state* flux is given by Fick's first law of diffusion:

$$\text{Equation 5-17} \quad J_{\infty}^{\text{hom}} = -(D_{\text{lip}} \nabla c_{\text{lip}}) \cdot n = -D_{\text{lip}} \frac{c_{\text{lip}}^{(\text{out})} - c_{\text{lip}}^{(\text{in})}}{h_{\text{SC}}}$$

For a heterogeneous membrane the apparent diffusion coefficient D_{SC} can be defined analogously, of course. It is implicitly given by the *steady state* flux:

$$\text{Equation 5-18} \quad J_{\infty} = -D_{\text{SC}} \frac{c_{\text{lip}}^{(\text{out})} - c_{\text{lip}}^{(\text{in})}}{h_{\text{SC}}}$$

Solving for D_{SC} finally yields

$$\text{Equation 5-19} \quad D_{\text{SC}} = \frac{J_{\infty} \cdot h_{\text{SC}}}{c_{\text{lip}}^{(\text{out})} - c_{\text{lip}}^{(\text{in})}},$$

where the right hand side of this equation is accessible in both simulation and experiment. An immediate consequence of Equation 5-17 and Equation 5-18 is the identity

$$\text{Equation 5-20} \quad J_{\infty} = \frac{D_{\text{SC}}}{D_{\text{lip}}} J_{\infty}^{(\text{hom})},$$

which explains the (artificial) definition of D_{SC} . The quotient $D_{\text{SC}}/D_{\text{lip}}$ is the constant indicating, how the flux through the heterogeneous SC membrane differs from a homogeneous membrane with the same thickness. This interpretation will be used in the subsequent subsections to derive a value for D_{cor} .

5.3.2 Corneocyte diffusion

For a fixed geometry the flux J_{∞} is described by a function which is linear in D_{lip} and additionally depends on the variable

$$\text{Equation 5-21} \quad \xi = \frac{D_{\text{SC}}}{D_{\text{lip}}} K_{\text{cor/lip}}$$

only. By definition, (see Equation 5-19), the same must be true for the apparent diffusion coefficient. This behaviour is mentioned earlier in the literature (110, 137, 139) using a variable $\sigma = 1/\xi$. A short and rigorous proof of this fact is presented by Arne Nägel in (170). The argumentation is valid for all models based on diffusion equations, and is in particular independent of geometric assumptions, e.g., the shape of the corneocytes.

The role of the dimensionless variable ξ should be elucidated: It is defined by the product of the speed of diffusion within the corneocytes, which is evaluated relatively to the lipids, and the partition coefficient between those two phases. When it comes to membrane permeability, both quantities can be traded into each other. Slow corneocyte diffusion can be compensated by an increase in the partitioning into the corneocytes and vice versa, little partitioning can be compensated by faster diffusion. In particular two limit cases are of interest. For $\xi \rightarrow 0$ an impermeable corneocyte membrane is obtained; there is neither a partitioning of substance into the corneocytes nor diffusion within. Analogously $\xi \rightarrow \infty$ characterises a highly permeable corneocyte membrane; an infinite amount partitions into the corneocytes and shows an instantaneous diffusion behaviour.

These two cases lead to the minimal and maximal apparent SC-diffusion coefficient which are denote by $D_{SC,0}$ and $D_{SC,\infty}$, respectively. Both coefficients depend on the geometry. As diffusion in the homogeneous membrane is typically in between those cases, the constants should satisfy the inequality $D_{SC,0} < D_{lip} < D_{SC,\infty}$. For the brick- and mortar geometries in this work the relation between D_{SC} and ξ is given in terms of the very efficient approximation

Equation 5-22
$$D_{SC}(\xi) \approx D_{SC,0} + \frac{D_{SC,\infty} - D_{SC,0}}{1 + \left(\frac{D_{SC,\infty} - D_{lip}}{D_{SC,\infty} - D_{SC,0}} \right) / \xi}.$$

The derivation is again found in (170). The right hand side of the equation characterises a function of ξ of sigmoid shape on a logarithmical scale, with a range in the interval $[D_{SC,0}, D_{SC,\infty}]$. Solving Equation 5-22 for a given D_{SC} yields

Equation 5-23
$$D_{SC}(\xi) \approx \left(\frac{D_{SC,\infty} - D_{lip}}{D_{lip} - D_{SC,0}} \right) / \left(\frac{D_{SC,\infty} - D_{SC}}{D_{SC} - D_{SC,0}} \right).$$

Based in this approximation and Equation 5-21, estimates for D_{cor} are available given D_{lip} , D_{SC} and $K_{\text{cor/lip}}$.

5.3.3 Concentration-depth-profiles

The simulation, as described by Equation 5-13 in this work and the experiment, as described in section 4, allow deriving concentration-depth-profiles. Input data for both test compounds are derived from two different experimental setups which are also discussed in section 2 extensively. Both methods use the same techniques to determine D_{lip} , D_{DSL} , and $K_{\text{lip/don}}$. They differ in the way to determine $K_{\text{SC/don}}$, which affects $K_{\text{cor/lip}}$, $K_{\text{DSL/lip}}$, and D_{cor} . The first method, denoted by (M1), derives the partition coefficients from an equilibrium experiment, in which concentrations are determined by measuring the loss of substance in the donor compartment. Alternatively, one can measure the substance extracted from the skin, yielding similar results (see also section 4.2.11). In a second method, denoted by (M2), the partition coefficient between donor and SC is obtained from a fit to the well-known solution of the one-dimensional heat equation (see section 4.2.14.1). The latter approach in particular also yields values for D_{SC} (see section 4.2.15). As these turn out to be below the minimal membrane specific quantity $D_{\text{SC},0}$, they were not considered in determining D_{cor} according to Equation 5-23.

5.4 Results

5.4.1 Apparent SC-diffusion coefficient

The illustration in Figure 5-2 shows a plot of $D_{\text{SC}}/D_{\text{lip}}$ as a function of ξ for the model membrane which is denoted by membrane A. The discrete data points are obtained from numerical simulation directly, while the continuous approximation corresponds to the right-hand side of Equation 5-22. The geometry-dependent constants are $D_{\text{SC},0}/D_{\text{lip}} = 0.0004675$ and $D_{\text{SC},\infty}/D_{\text{lip}} = 11.0000000$.

To visualise the influence of changes in the geometry, membranes with different geometric parameters are considered as well. In a first step the lipid layer thickness of the model membrane is reduced by a factor of two, i.e., $\delta = 0.05 \mu\text{m}$ (membrane B). In a second step, the relative cell overlap is gradually changed down to an overlap of zero. The minimal horizontal length of overlap of two neighbouring corneocyte blocks is $v = \frac{1}{2}(L_{\text{cor}} + \delta)$ (model membrane A, fully staggered),

$v = \frac{1}{4}(L_{cor} + \delta)$ (membrane C), $v = \frac{1}{8}(L_{cor} + \delta)$ (membrane D) and $v = 0.0 \mu m$

(membrane E, zero overlap), respectively. In all cases the continuous functions show an excellent agreement to the discrete data. Hence, the latter ones are omitted in the illustration for the sake of clarity.

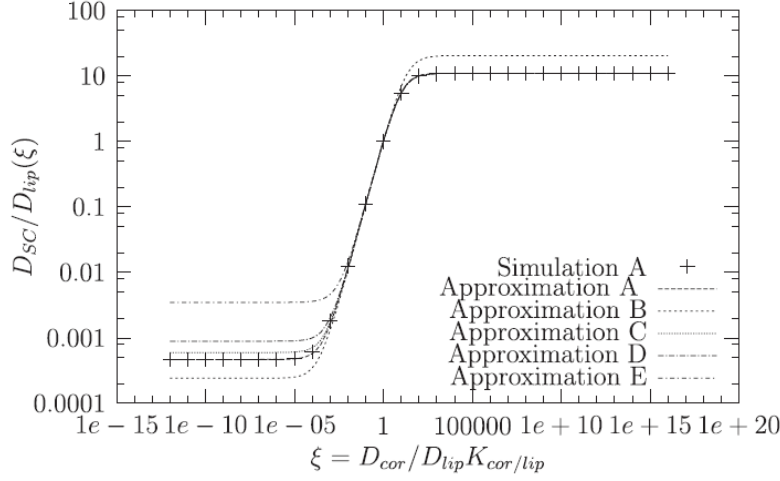


Figure 5-2 The apparent diffusion coefficient D_{SC}/D_{lip} for the model SC geometry is described as a function of $\xi = D_{cor}/D_{lip} K_{cor/lip}$. Simulated discrete data and corresponding approximation (model membrane, shown as membrane A, $\delta = 100$ nm, $v = \frac{1}{2}(L_{cor} + \delta)$). Additionally: approximation for membrane B using a thinner lipid layer ($\delta = 50$ nm, $v = \frac{1}{2}(L_{cor} + \delta)$) and approximations for membranes C–E with a decreased horizontal overlap ($\delta = 100$ nm and $v = \frac{1}{2}(L_{cor} + \delta)$, $v = \frac{1}{4}(L_{cor} + \delta)$, $v = \frac{1}{8}(L_{cor} + \delta)$). In all cases $L_{cor} = 30 \mu m$ was used.).

5.4.2 Parameter studies

To visualise the influence of changes in the values of D_{cor}/D_{lip} and $K_{cor/lip}$, parameter studies have been conducted. A representative test set of parameters consisted of values of

$$K_{cor/lip} \in \{0.01, 0.1, 1, 10\}$$

and

$$\frac{D_{cor}}{D_{lip}} \in \{10^{-5}, 10^{-3}, 10^{-1}\}$$

This results in nine concentration–SC-depth profiles which are shown in Figure 5-3. Due to the influence on the concentration, they are grouped in three triples according to the $K_{cor/lip}$ value in ascending order. The remaining parameters in this study are

given by $K_{lip/don} c_{don} = 1 \mu g/ml$, $K_{lip/DSL} = 1.0$, and $\frac{D_{DSL}}{D_{lip}} = 100.0$.

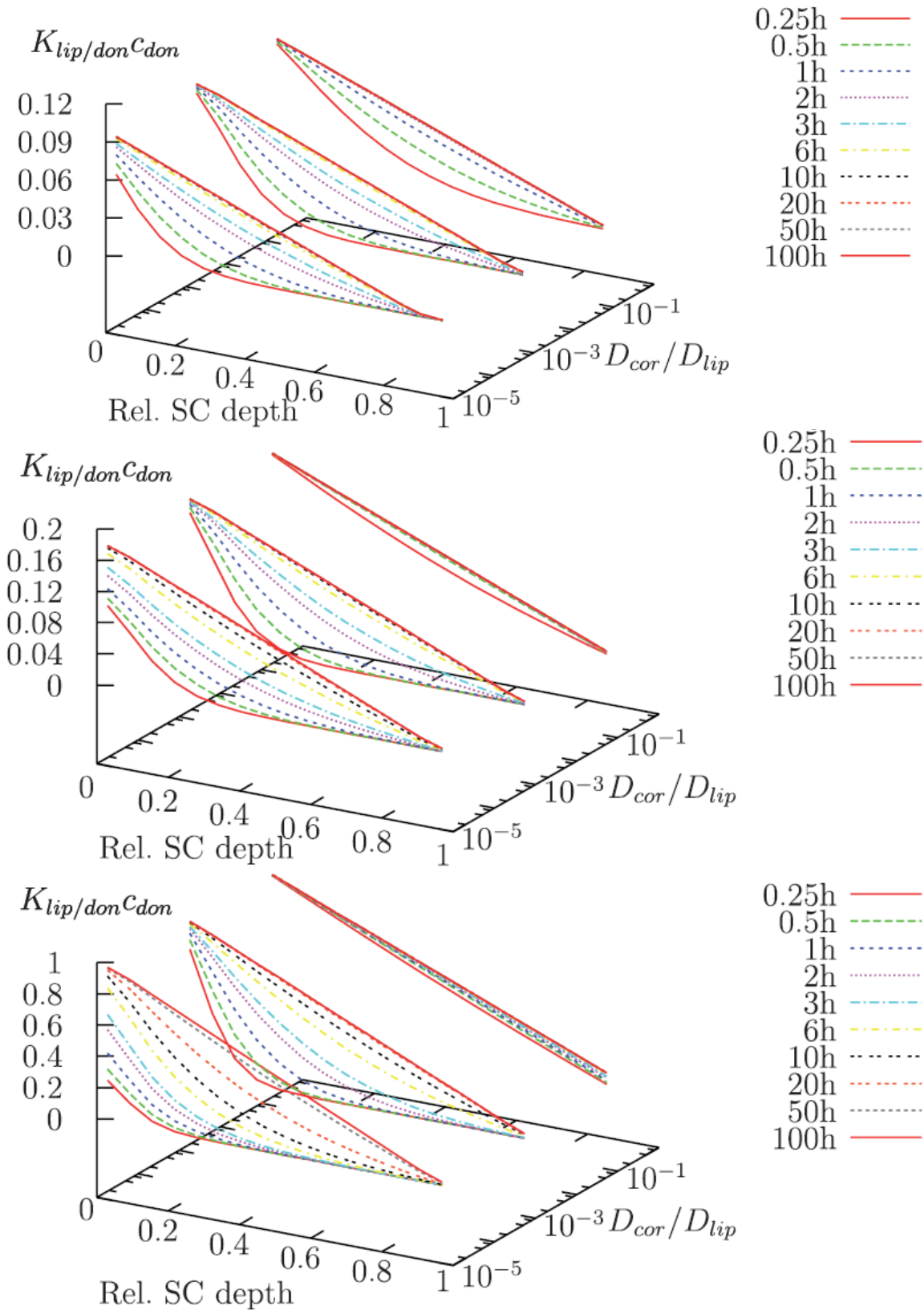


Figure 5-3 Time dependence of concentration–SC-depth profiles for $K_{cor/lip} = 0.01, 0.1, 1.0$ (from top to bottom) and various values for $D_{cor}/D_{lip} = 10^{-1}, 10^{-3}, 10^{-5}$. Concentrations are shown relative to $K_{lip/don} c_{don} = 1 \mu\text{g/ml}$. Parameters in DSL compartment: $K_{lip/DSL} = 1$, $D_{DSL}/D_{lip} = 100$. Times are normalised to $D_{lip} = 1.0 \mu\text{m}^2/\text{s} = 3.6 \cdot 10^{-5} \text{ cm}^2/\text{h}$.

5.4.3 Concentration-depth-profiles

A summary of the input data is given in Table 5-3. The table is extended by two rows for the speed of diffusion in the corneocytes. The value D_{cor} is determined according to Equation 5-23. As this derivation is sensitive with respect to errors in the input data, an alternative estimate is introduced. This is denoted by D_{cor}^* and its value is obtained from D_{cor} by a reduction of one (CAF) and two (FFA) orders of magnitude, respectively. This latter mentioned quantity is used to generate the concentration-depth-profiles which are shown in Figure 5-4. For each model substance results are plotted separately for incubation times of 1 h, 2 h and 6 h (from top to bottom) with FFA on the left hand side and CAF on the right hand side. As the input data for FFA contain a comparatively large value of $K_{\text{SC/don}}$ for (M1), an overestimation for $K_{\text{cor/lip}}$ is obtained. Hence, these results are excluded from the illustrations.

Table 5-3 Experimental input parameters for simulation. Mean values according to section 4. D_{cor} and D_{cor}^* determined according to section 5.3.2.

Parameter		Substance			
		Flufenamic acid		Caffeine	
D_{lip} [cm ² /h]	4.9×10^{-3}	1.1×10^{-4}		2.1×10^{-4}	
D_{SC} [cm ² /h]		1.7×10^{-7}		1.4×10^{-7}	
D_{DSL} [cm ² /h]		2.3×10^{-3}			
$K_{lip/don}$		20.32		2.15	
c_{don} [mg/ml]		1.0		12.5	
		Experimental method			
	(M1)	(M2)	(M1)	(M2)	
$K_{SC/don}$	16.20	5.88	4.51	4.70	
$K_{cor/lip}$	0.77	0.21	2.22	2.32	
$K_{DSL/lip}$	0.26	0.10	0.08	0.08	
D_{cor} [cm ² /h]	1.4×10^{-7}	5.1×10^{-7}	1.8×10^{-8}	1.7×10^{-8}	
D_{cor}^* [cm ² /h]	1.4×10^{-9}	5.1×10^{-9}	1.8×10^{-9}	1.7×10^{-9}	

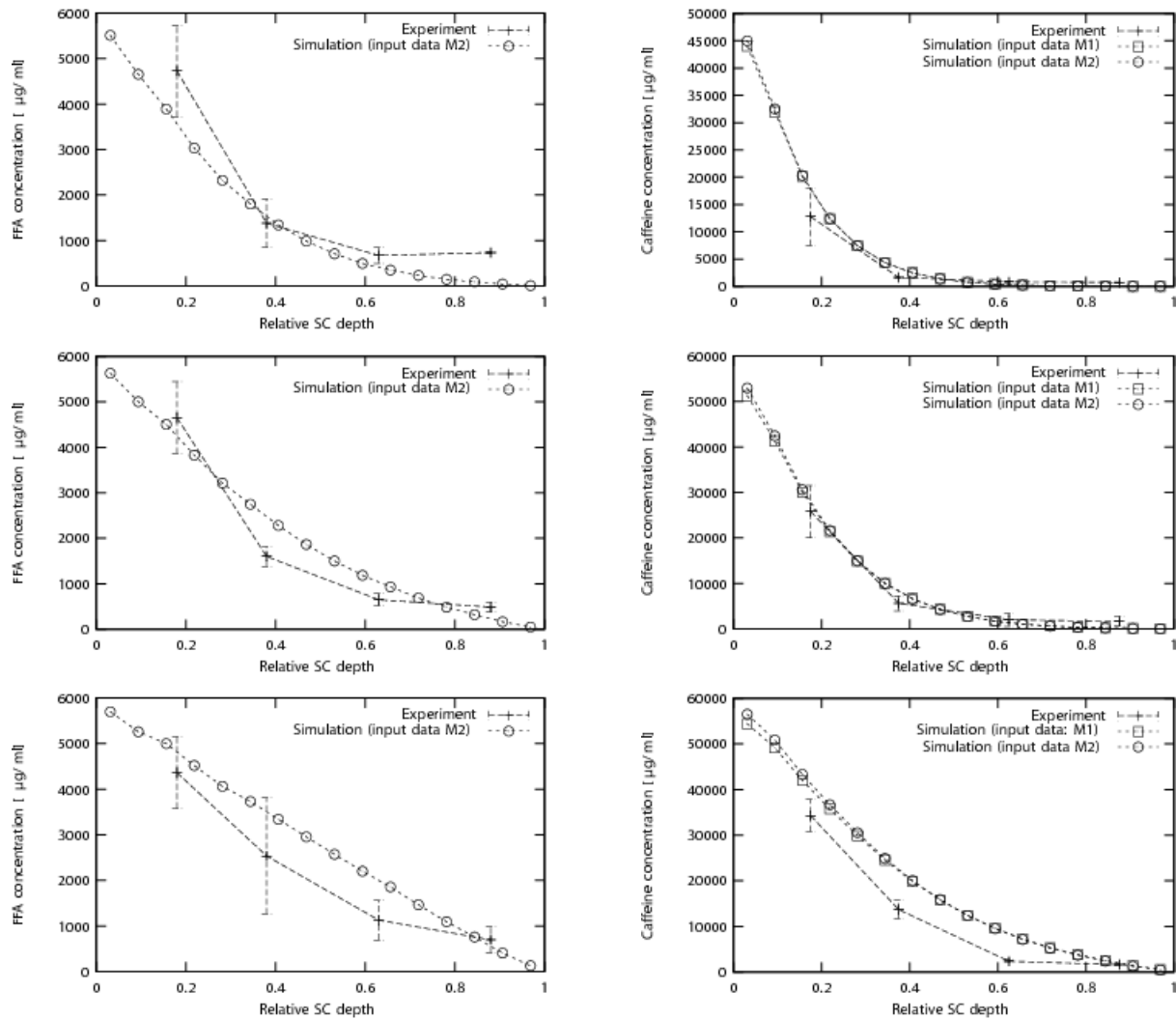


Figure 5-4 Comparison of experimental and computational results on concentration-depth-profiles of (left hand side, top to bottom) flufenamic acid at 1, 2, and 6 h incubation time and (right hand side, top to bottom) caffeine at 1, 2, and 6 h incubation time.

5.5 Discussion

While neglecting geometric information, the model presented in this work is based on first principles only. This is independent of the substance and yields excellent predictive qualities as long as the relevant parameters are determined accurately enough. Of course, this can be achieved mathematically by using parameter estimation and inverse modelling. However, this limits the predictive power of the model, as it relies on an *a-posteriori* analysis. In order to avoid this, an experimental access to the relevant model coefficients is preferred in the study at hand.

The rationale for the choice of the test compounds is to show that the model is applicable independently of a substance's hydrophilic and lipophilic character,

respectively. The main restriction is that the substances must show Fickian type diffusion behaviour. Therefore, a key assumption in this work is that both substances diffuse freely through the whole membrane. Note that although the molecular weight is not incorporated in the model directly, it naturally influences the diffusion properties. This may impair the applicability of the model for molecules with a particularly large molecular weight. Finally, keratin binding of FFA is not included in the model.

5.5.1 Apparent SC-diffusion coefficient

A comparison of membranes A and B in Figure 5-2 yields that a change in the relative lipid layer thickness affects the scaling of the approximating function. A reduction of d increases the maximal values for $D_{SC,\infty}/D_{lip}$ and decreases the minimal values for $D_{SC,0}/D_{lip}$. On the contrary, variations in the overlap of the corneocyte cells, as described by the graphs for membranes A, and C–E, affects the lower bound $D_{SC,0}/D_{lip}$ only. The latter observation explains, for instance, the differences in the barrier function between species (e.g., human vs. rat), between human skin and human skin equivalents as well as between normal and diseased skin.

For large values $\xi > 0.1$, the graphs for membranes A and C–E almost coincide. In the lower regimes, $\xi < 0.1$, especially membrane E, the case of overlap zero, is significantly different from the other cases. With respect to the data presented in Table 5-3, it must be mentioned that the experimental results are gathered in the lower regimes ($D_{SC}/D_{lip} = 1.5 \times 10^{-3}$ for FFA, and $D_{SC}/D_{lip} = 6.7 \times 10^{-4}$ for CAF). This observation has two drawbacks: Firstly, the variation of geometric parameters in section 5.4.1 shows that changes in the geometry affect the dependence of D_{SC}/D_{lip} on ξ . The smaller the horizontal overlap is, the larger becomes the minimal effective membrane permeability. In this case, the resulting n (and consequently also D_{cor}) is reduced. Secondly, the computation of ξ is ill conditioned for $D_{sc} \rightarrow D_{sc,0}$. In Figure 5-2 this is seen easily for small values of ξ , which correspond to almost identical values of D_{SC}/D_{lip} .

Despite these shortcomings it should be stressed that the concept and the results presented in sections 5.3.2 and 5.4.1 extend to a multitude of membranes in cell biology and are applicable for all membranes of biphasic character.

5.5.2 Concentration-depth-profiles

The results for FFA are shown on the left hand side of Figure 5-4 from top to bottom with increasing incubation times. The development of the profiles in time is similar for both simulation and experiment; the only exception is the linear profile for the simulation after 6 h. This is an indicator that *steady state* is reached after 6 h, which is not observed in the experiment. The quantitative precision is quite accurate, though not perfectly within the range of the experimental error. For CAF, shown on the right hand side of Figure 5-4, the concentrations of the simulations show significantly better agreements with the experiment and are close to the range of experimental accuracy. Due to the similarity of input data for (M1) and (M2) for $K_{SC/don}$, the result of the simulations can hardly be distinguished.

Compared to the small incubation times of 1 and 2 h, experiment and simulation show comparatively large differences for an incubation time of 6 h. This is firstly caused by technical problems of the tape stripping technique. With increasing incubation times water enters into the SC and leads to a degradation of the structure. As a consequence, the spatial resolution of the tape stripping profiles is losing accuracy. Secondly, the mathematical model is lacking precision as it does not include swelling effects. As reported by Richter et al. (51), especially the thickness of the lowermost SC layers can be affected by water content. As such behaviour is not included in the simulation, this may lead to an underestimation of the layer volume, and hence to an overestimation of the concentration. This is in particular true for the lowermost SC layers. Especially for FFA the results of simulation and experiment differ in this region. One reason can be the comparatively large depth of the DSL compartment. The smaller this compartment, the tighter is the coupling between the end of the membrane and the lowest SC layers.

Last it must be mentioned that one basic assumption of this work are equally sized and fully staggered SC layers. The effect of layers differing in their thicknesses will be subject to future research. The model also does not cover that the uppermost skin layer in the SC disjunctum is packed less tight than in the lower SC layers.

5.5.3 Parameters

One input parameter of particular importance is the diffusion coefficient in the lipids: due to the introduced normalisation, all times in the simulation depend on D_{lip} . This is critical, as this is an apparent quantity itself. It is known, cf. (92), that lateral diffusion

along the lipid bilayers is much faster than vertical diffusion through the lipid bilayers. Therefore, the experimental value for D_{lip} must be regarded to be an averaged value already, which represents all micro scale effects of diffusion in the SC. This is implicitly taken into account in the analysis at hand. It is the major advantage of this approach that this average quantity is feasible experimentally, while it is uncertain, if diffusion is Fickian at all on much smaller scales.

The second important unknown is the diffusion coefficient D_{cor} . Although it is difficult to access this quantity experimentally, the method presented in section 5.3.2 yields reasonable estimates. Yet, as shown by Naegel et al. (170), the method is sensitive against geometric information, such as the relative corneocyte overlap and the lipid layer thickness. The necessity to reduce D_{cor} can be due to differences in the cell alignment. Although the cells are fully staggered in the model membrane used for the simulation, it is unlikely that this is exactly the case in natural geometries (218). Instead, already a slight perturbation of the optimal overlap leads to an increase of $D_{SC,0}$ as could be shown by Naegel et al. (170). For a constant observed value for D_{SC} , this corresponds to lower values for D_{cor} .

One of the first computer simulation studies to consider penetrant concentration-depth-profiles in the SC was the one from Watkinson et al. (124). These authors modelled concentration-distance-profiles for the case of heterogeneous SC, however their analysis is only applicable to the *steady state* transport. They argued that the diffusion coefficient decreases from outer to inner layers of the SC. Using variable diffusion and partition coefficient models Anissimov and Roberts (127) showed in a previous study that partition coefficient heterogeneity had a more profound effect on predicted fluxes than diffusion coefficient heterogeneity. In a further paper, cf. (194), they argued that the clobetasol propionate tape stripping data were most consistent with the partition coefficient decreasing exponentially for half the SC and then becoming a constant for the remaining SC. The analysis of Naegel et al. (170) shows, how diffusion in the corneocytes and partitioning are interrelated and can be compensated by one another. Although constant coefficients were used, good agreements of simulation and experiment are obtained.

The different values of $K_{SC/don}$ and thus $K_{cor/lip}$ for (M1) and (M2) for FFA in Table 5-3 require further investigations. One reason may be effects of protein binding, which is caused by compounds attaching to keratin fragments inside the corneocytes. This behaviour is not included in the model. However, it is known, e.g., from (219), that in

the *steady state* this is equivalent to a reduction of D_{cor} . This is the reason, why the correction of D_{cor} was chosen to be stronger for FFA than for CAF.

The time dependent interplay between D_{cor} and $K_{\text{cor/lip}}$ or (M1) and (M2) for FFA is visualised in Figure 5-3. It can be observed that the larger the value of $K_{\text{cor/lip}}$ the more extreme the reaction to changes in $D_{\text{cor}}/D_{\text{lip}}$. This is what must be expected: with increasing $K_{\text{cor/lip}}$, the corneocytes become more and more important for the storage capacity of the SC. When the diffusion in the corneocytes is slow, the reservoirs fill up slowly. With respect to the SC-depth the influence in the uppermost layers is the strongest in this case.

5.6 Conclusion

This study presented an *in silico* simulation of drug diffusion in an *in vitro* diffusion experiment under infinite dose conditions. It is based on experimental input data as determined in section 4. The substances considered in this work are FFA and CAF, which serve as representatives for lipophilic and hydrophilic compounds, respectively.

By a comparison of experiment and simulation it was shown, which parameters are critical when performing simulations. The analysis of the underlying model leads to improved insights how the *steady state* flux through the SC membrane on the one hand and the interaction of diffusion in and partitioning between lipid and corneocyte on the other hand are coupled. It is shown, how a corrected interpretation of the input parameters leads to very good agreements of the concentration–depth-profiles of experiment and simulation.

The future work will include enlarging the set of substances as well as studying the effect of protein binding on the permeability properties of the human skin. Additionally, it must be shown whether the achieved tools are also valid in three-dimensional models.

5.7 Appendix A

For the sake of a better understanding, the following passage tries to give a brief overview over the numerical and mathematical methods. For a vector field $\mathbf{F}: \Omega \subset \mathbb{R}^2 \rightarrow \mathbb{R}^2$ in two-dimensional space with components $\mathbf{F} = (F_1, F_2)$, the divergence is given by

$$\operatorname{div} \mathbf{F}(x) = \frac{\delta F_1(x)}{\delta x_1} + \frac{\delta F_2(x)}{\delta x_2}.$$

This corresponds to the limit case of the surface integral which is normalised by the volume for infinitely small volumes. Regarding the derivation of the formulas of the diffusion equations of the form $-\operatorname{div}(\alpha \nabla u) = f$ in Ω the reader may want to refer to standard literature from physics, cf. (220). A comprehensible mathematical overview on this topic, which also considers the effect of the transmission conditions, can be found, e.g., in (84).

5.7.1 Dimensionless form

By dividing the concentrations c_i by a density ρ , we obtain a dimensionless variable $u_i = c_i/\rho$. At the same time a characteristic length scale λ and a characteristic time scale τ are introduced. The diffusion coefficients can then be written as

$$\text{Equation 5-24} \quad D_i = \alpha_i \frac{\lambda^2}{\tau}$$

with a dimensionless scalar value $\lambda_i > 0$. For the time being it is assumed that $\lambda = 1 \mu\text{m}$. The characteristic time scale τ is chosen, such that $\alpha_{\text{lip}} = 1$ and consequently

$$\text{Equation 5-25} \quad D_i = D_{\text{lip}} (\alpha_i \nabla_y u_i) = 0$$

for $i \in \{\text{cor}, \text{lip}, \text{DSL}, \text{SC}\}$. The variables are then coupled by

$$c_i(x, t) = \rho u_i(y, s)$$

where

$$\text{Equation 5-26} \quad t = s \cdot \tau \text{ and } x_k = y_k \cdot \lambda$$

for each component k of the vector. As it becomes obvious in Equation 5-26 all domains and interfaces also undergo a transformation. Therefore, Ω_i , $\Gamma_{i,j}$ are substituted by their dimensionless counterparts $\hat{\Omega}_i$; $\hat{\Gamma}_{i,j}$. The dimensionless form of Equation 5-1 is then, for instance, given by

$$\delta_s u_i - \operatorname{div}_y (\alpha_i \nabla_y u_i) = 0$$

for $s > 0$, $y \in \hat{\Omega}_i$, and $i \in I$. Analogous results hold for the other equations, as can be verified in a straightforward manner. The equations of the dimensionless formulation are formally identical, but the diffusion coefficients α_i , $i \in I$ are given relative to D_{lip} . As an obvious implication, the time scale is inversely proportional to D_{lip} , e.g., a

reduplication of all diffusion coefficients is equivalent to accelerating the time scale by a factor of two. Yet, due to Equation 5-25 a transformation to physical quantities remains easy, see Section 5.7.2 for further examples. A list of the parameters used in the dimensionless formulation is found in Table 5-4.

Table 5-4 Parameters of the dimensionless formulation

$u_{lip}, u_{cor}, u_{DSL}$	Dimensionless drug concentration in lipid, corneocyte and deeper skin layers
$\alpha_{cor}, \alpha_{SC}, \alpha_{DSL}$	Dimensionless diffusion coefficients relative to D_{lip} , e.g., $\alpha_{cor} = D_{cor}/D_{lip}$
$\hat{\Omega}_{lip}, \hat{\Omega}_{cor}, \hat{\Omega}_{DSL}$	Domains after transformation
$\hat{r}_{lip,cor}, \hat{r}_{lip,DSL}$	Interior interfaces after transformation
$\hat{r}_{lin}, \hat{r}_{side}, \hat{r}_{out}$	Exterior interfaces after transformation
λ, τ	Characteristic length and time scale

5.7.2 Flux as a function

Within this subsection the computational domain is restricted to the SC again. The flux and the permeability for this membrane are functions of α_{cor} and $K_{cor/lip}$. Within the model both variables are positive constants, $\alpha_{cor}, K_{cor/lip} > 0$. Using the transformation $u_{cor} = K_{cor/lip} \bar{u}_{cor}$ a substitution of u_{cor} by \bar{u}_{cor} results in

$$\delta_s u_{lip} - \text{div}_y (\alpha_{lip} \nabla_y u_{lip}) = 0 \text{ in } \hat{\Omega}_{lip},$$

$$K_{cor/lip} (\delta_s \bar{u}_{cor}) - \text{div}_y (\xi \nabla_y \bar{u}_{cor}) = 0 \text{ in } \hat{\Omega}_{lip}$$

and

$$(\alpha_{lip} \nabla_y u_{lip} + \xi \nabla_y \bar{u}_{cor}) \cdot n = 0,$$

$$u_{cor} = \bar{u}_{cor} \text{ on } \hat{r}_{lip,cor}$$

with $\xi = \alpha_{cor} K_{cor/lip}$. Note that the piecewise defined function

$$u(x) = \begin{cases} u_{lip}(x), & x \in \hat{\Omega}_{lip} \\ \bar{u}_{cor}(x), & x \in \hat{\Omega}_{cor} \end{cases}$$

is continuous. As the solution u_{lip} in the lipid channel is not affected by this transformation, the flux

$$J_{\infty} = \frac{D_{lip} \rho}{A(\hat{r}_{out})} \lim_{s \rightarrow \infty} \int_{\hat{r}_{out}} \nabla_y u_{lip}(y, s) \cdot n d\mu$$

is also an invariant of the transformation. Consequently all membranes with identical values of n yield the same fluxes. By definition, this carries over to the permeability

and the effective diffusion coefficient of the SC. The latter one is from now on denoted by $\alpha_{SC} = D_{SC}/D_{lip}$. It should be stressed that the whole argumentation is independent of the dimension and the shape of the geometry.

5.7.3 Effective diffusivity

Plotting the discrete data of α_{SC} as a function of ξ results in a graph of sigmoid shape which is bounded between $\alpha_{SC,0}$ and $\alpha_{SC,\infty}$, cf. Figure 5-2 (Simulation A). If α_{SC} can be represented by a continuous function, this representation must be of the type

$$\text{Equation 5-27} \quad \alpha_{SC}(\xi) = \alpha_{SC,0} + \frac{\alpha_{SC,\infty} - \alpha_{SC,0}}{1 + \exp(\Phi(\xi))},$$

where $\Phi : \mathbb{R} \rightarrow \mathbb{R}$ is continuous, and satisfies

$$\lim_{\xi \rightarrow 0} \Phi(\xi) = \infty \quad \text{and} \quad \lim_{\xi \rightarrow 1} \Phi(\xi) = -\infty$$

One approach is to use an affine linear transformation of the form

$$\Phi(\xi) = \frac{\beta - \ln \xi}{y}$$

with $\beta, y \in \mathbb{R}$ and $y > 0$. A homogeneous membrane leads to the constraint $\alpha_{SC}(1) = 1$, which is equivalent to the identity

$$y = \beta / \ln \left(\frac{\alpha_{SC,\infty} - 1}{1 - \alpha_{SC,0}} \right)$$

Inserting this into Equation 5-27 yields

$$\alpha_{SC}(\xi) = \alpha_{SC,0} + \frac{\alpha_{SC,\infty} - \alpha_{SC,0}}{1 + \left(\frac{\alpha_{SC,\infty} - 1}{1 - \alpha_{SC,0}} \right)^{\left(\frac{1 - \ln \xi}{\beta} \right)}}$$

The positive constant β depends on the geometry and characterises the inflection point of the graph. For the geometry considered in this work, a non-linear regression

analysis yields that $\beta \approx \ln \left(\frac{\alpha_{SC,\infty} - 1}{1 - \alpha_{SC,0}} \right)$ is a good approximation and consequently

$$\alpha_{SC}(\xi) = \alpha_{SC,0} + \frac{\alpha_{SC,\infty} - \alpha_{SC,0}}{1 + \left(\frac{\alpha_{SC,\infty} - 1}{1 - \alpha_{SC,0}} \right) / \xi}$$

The latter is equivalent to Equation 5-22, since $\alpha_{SC} = D_{SC}/D_{lip}$ holds, due to Equation 5-25.

6 THE ROLE OF CORNEOCYTES IN SKIN TRANSPORT REVISED – A COMBINED COMPUTATIONAL AND EXPERIMENTAL APPROACH

Parts of this chapter have been published as:

S. Hansen, A. Henning, A. Naegel, M. Heisig, G. Wittum, D. Neumann, K.H. Kostka, Peter Meiers, C.M. Lehr, U.F. Schaefer. The role of corneocytes in skin transport revised – a combined computational and experimental approach. *Pharmaceutical Research* (2009) accepted DOI: 10.1007/s11095-009-9849-7.

The author of the thesis made the following contributions to the publication.

Developed the theoretical concept. Planned, performed, and interpreted all experiments. Planned, performed, and interpreted the calculations. Wrote the manuscript.

6.1 INTRODUCTION

In the pharmaceutical field of drug application it is well established that occlusion effectively enhances skin permeation of hydrophilic compounds by increasing the partitioning into the SC (221). This principle is used in occlusive semisolid formulations and transdermal patches. SC hydration may further vary due to patient skin type (seborrhoic/sebostatic), exposure to sun, wind, cold, air-conditioning, chemicals or cosmetics among many others. However, there is an ongoing debate on the mechanisms involved in these effects. Especially the potential influence of compound-corneocyte interaction on permeation through human SC (SC) is under discussion. For small lipophilic molecules, interactions with keratin or other proteins are usually neglected as there is a common consent that transport occurs mainly via the intercellular lipids. For hydrophilic molecules, corneocytes may offer an additional pathway across the SC, such as through the controversially discussed continuous desmosome-corneocyte route (58, 61, 64, 222-225). Meanwhile, there is significant evidence that the corneocytes are accessible for - at least a few - permeants. It is unquestionable that water enters the corneocytes very effectively (26, 50). In addition, several larger hydrophilic and even lipophilic molecules (usually dyes) were visualized inside the corneocytes either by conventional or high speed two-photon microscopy (56, 226). Boddé et al. found hints that disintegrating desmosomes serve as an entrance through the cornified envelope into the corneocytes in the apical SC (53). In the light of these results, the neglect of compound-corneocyte interaction is challenged. This is even more substantial for predictive models of SC permeability or SC flux.

The gain in knowledge about the SC structure and the permeant-barrier interaction is reflected in the development of increasingly sophisticated morphology based mathematical models for skin transport. In the simplest case, the SC morphology is approximated by a brick-and-mortar model with an inaccessible intra-cellular phase. Here, the corneocytes (bricks) simply serve as obstacles reducing diffusive area and increasing path length (133, 156). Some of these models mimic the anisotropic structure of the SC lipid bilayers (31, 34, 196, 227) by using anisotropic transport in lateral and trans-bilayer direction (110, 133, 135, 156). Other elaborate models implement a trans-corneocyte pathway assuming a homogeneous interior and isotropic intra-cellular transport (110, 137, 139, 142, 166, 170). Finally, Wang et al.

used hindered diffusion theory to estimate the corneocyte diffusion coefficient D_{cor} in order to account for intra-corneocyte keratin forming fibrous obstacles (141, 168, 169).

Despite these obvious advances the available experimental data on compound-corneocyte interactions are still scarce and too inaccurate to validate morphologically exact diffusion models. For which substances do corneocyte interactions take place? Which structures are responsible for the interactions? Which compound properties are relevant for interactions with specific structural elements of the corneocytes? And finally, how could these be evaluated quantitatively?

Corneocytes are filled with a protein network of keratin intermediate filaments and are surrounded by a cornified protein envelope (cpe) (1). Together with small hydrophilic hygroscopic molecules - the natural moisturizing factors (e.g. urea, amino acids, and lactic acid) - keratin provides the major water holding capacity of the SC thus regulating skin flexibility, firmness, and smoothness. Hence, water present in healthy skin *in vivo*, i.e. about 15-30% per weight of dry SC (27) is tightly bound (228-230). Through occlusion or in a very humid environment additional water (up to several times the weight of the dry tissue) may be taken up by the corneocytes. Finally, water intercalates between intercellular lipids to occasionally form water pools of vesicle-like structure but without causing any major disruption of the lipid bilayers (231, 232). Corneodesmosomes mediate cellular contact between adjacent corneocytes and provide SC cohesion until they are gradually degraded during desquamation within the stratum disjunctum. In summary, interactions of a penetrating molecule with the SC are possible with (i) intercellular lipids; (ii) keratin and proteins of the corneodesmosomes or the cornified protein envelope; (iii) water.

The primary interaction of a compound with intercellular lipids or water is dissolution of the substance in the liquid phase. At equilibrium, the ratio of concentrations between two adjacent non-miscible media, is determined by the partition coefficient, i.e. the ratio of solubility in both phases. In contrast, small molecules interact with proteins by forming complexes. In simple cases, the number of protein-bound molecules may be calculated from a Langmuir isotherm. For concentrations far away from saturation of binding sites the relationship between free and bound concentration is sufficiently described by a linear relationship, i.e. in terms of a partition coefficient. Approaching saturation the concentration of bound substance becomes independent of free concentration visible as a plateau.

Previous models that take into account the anatomical heterogeneity of SC in detail assume that interactions with the protein phase are regulated by a partition coefficient (52, 150). These apply in the limit that compound concentrations are low and far away from saturation. However, non-linear concentration influences indicating saturable processes are being repeatedly reported in literature. These include binding studies using isolated keratin protein (233, 234) as well as SC-donor partition coefficients ($K_{SC/don}$) of a number of compounds (such as doxycyclin (233), primaquine (234), timolol (122), testosterone, hydrocortisone, estradiol, progesterone (180), cyanophenol, iodophenol, and pentyloxyphenol (180)). Even for studies where no non-linear concentration dependence is reported (235-237) this may be an effect of a low protein binding constant or that potential protein binding compounds are denied access to the binding sites, as for example keratin is mainly found intra-cellular. The same effect would be caused by an insufficient compound solubility in the surrounding tissue as then the maximum binding capacity cannot be achieved. The non-linear development of the binding isotherm may further be overcompensated by non-saturable partitioning. This concept has first been introduced for the adsorption of gases to glassy polymers as the “dual sorption”-theory but may be ubiquitously applied to processes with concurrent mobile and fixed species of the same compound irrespective of the mechanism of immobilization (238). Chandrasekaran et al. transferred the concept to the interaction with human epidermal membranes and SC using the example of scopolamine (119). They described the process as a combination of dissolution creating mobile, freely diffusible molecules and adsorption producing non-mobile molecules that cannot contribute to the diffusion process (119). Between mobile and non-mobile species a rapid exchange compared to the diffusion time-scale and a local equilibrium is assumed. The authors however assumed the whole membrane to participate in dissolution and binding of drug molecules. The aim is now to relate mobile and fixed drug species to specific SC substructures.

Lately we established experimental methods to quantify the tendency of compounds to interact with the corneocytes in terms of a corneocyte-intercellular lipids partition coefficient ($K_{cor/lip}$) (239). Although this method provides a general idea of the overall extent of corneocyte uptake, it does not allow insight into the mechanism of interaction. The question is how to analyze the contributions of the individual structural elements of the SC experimentally. Techniques have been reported how to

adopt equilibration experiments so as to determine a compound's affinity to SC lipids. However, to our knowledge only two data-sets of experimentally measured partition coefficients into extracted SC lipids are reported for a very limited set of compounds. These are a series of 11 hydrocortisone esters from Raykar et al. and CAF and FFA from our own works (52, 239). Usually this problem is circumvented by employing a correlation between the lipid-donor partition coefficient ($K_{lip/don}$) and the octanol-water partition coefficient ($K_{Oct/w}$) according to a power law (linear free energy relationship) (150, 156, 160).

Similar correlations have also been proposed to exist between the corneocytes-water partition coefficient ($K_{cor/w}$) and $K_{Oct/w}$ (52, 150, 157, 240). Furthermore, partition coefficients into delipidized SC and callus shavings have been proposed as a model to investigate compound binding to corneocyte proteins (52, 180, 217). There are several shortcomings of these methods. Lipid extraction with methanol/chloroform cannot remove the ω -OH-acylceramides covalently attached to the cpe (29). This may lead to an overestimation of protein binding of lipophilic compounds. Treatment with organic solvents will denature the corneocyte proteins so that binding properties will most probably be very different from intact SC. Finally, like intact SC delipidized SC and callus will hydrate significantly during incubation with aqueous media so that again it is not obvious whether substance uptake is due to protein binding or dissolution in the corneocyte water phase. These shortcomings may be overcome by using isolated pulverized animal keratin instead. Binding studies using keratin from bovine hoof and horn have been done in the past with a focus on fungicides and anti-malaria drugs (233, 234, 241, 242). The pattern of keratin proteins depends on species, tissues, as well as states of terminal differentiation (243, 244). The amino acid composition of human and bovine epidermal keratins is relatively comparable which most probably reflects identical function (245).

Uptake into aqueous SC domains has so far only been investigated indirectly by comparing SC-water partition coefficients estimated from the decrease of the donor concentration (method 1) and from the extraction of the SC after equilibrium (method 2) (52). This method is based on the assumption that the dissolution properties of water inside the SC are identical to bulk water. Recently, it was shown that significant portions of water are tightly bound to SC structures and are therefore unavailable for compound dissolution (228-230). Ignoring bound water leads to wrong estimates of $K_{SC/don}$ according to method 1 and therefore of the uptake into aqueous domains of

the SC (246, 247). The aim is now to investigate partitioning into aqueous SC domains directly by measuring $K_{SC/don}$ at clearly defined hydration levels. This will be possible by switching to a non-aqueous donor such as low viscous paraffin (LVP) to avoid the uncontrolled excessive hydration that happens with an aqueous donor. SC may now be used dry or gradually hydrated and a series of equilibration experiments may be performed with SC of known water content as displayed in Figure 4.1. At zero hydration the SC-LVP partition coefficient ($K_{SC/LVP}$) will exclusively be determined by the intercellular lipids and accessible proteins (Figure 4.1B). With increasing hydration $K_{SC/LVP}$ should be influenced depending on the affinity of the molecule to water if the aqueous domain is accessible for drug molecules (Figure 4.1C). By measuring $K_{SC/LVP}$ at different hydration levels it can be tested whether water uptake has a linear influence on $K_{SC/LVP}$ indicative of a partitioning process.

We could recently show that corneocyte interactions need to be taken into account for both the hydrophilic CAF ($\log K_{Oct/w}$ -0.08) and the lipophilic FFA ($\log K_{Oct/w}$ 4.8) (239). In the case of FFA, keratin binding had been suspected to be responsible for the observed corneocyte interaction while this could be ruled out for CAF (239). Apart from that dissolution within the aqueous corneocyte domain is imaginable for both compounds CAF being highly soluble in water and FFA being a weak acid exhibiting a pH dependent aqueous solubility (pK_a 3.8; (171)). Naegel and coworkers demonstrated the significance of the corneocyte involvement for the shape of the SC concentration-depth profiles of both FFA and CAF through numerical modeling on the basis of experimental input values on all relevant partition and diffusion coefficients (170). For both compounds their mechanism of corneocyte interaction shall now be clarified. The original set of compounds has been extended by TST ($\log K_{Oct/w}$ 3.32) as it is practically insoluble in water but stands a good chance to bind to keratin due to its high lipophilicity. TST is in contrast to FFA non-ionizable and therefore its aqueous solubility is independent of pH. In addition, CAF and TST are typical examples of reference compounds recommend by the internationally accepted guidelines 427 and 428 of the Organization for Economic Cooperation and Development (OECD) for performing system suitability tests for skin permeation experiments (5, 6). For all three compounds $K_{SC/LVP}$ was measured as a function of SC hydration and donor concentration.

In order to interpret the experimental results quantitatively two constitutive compartmental models of SC are formulated. These allow an easy prediction of

$K_{SC/don}$ as a function of membrane composition, in detail SC hydration, and donor concentration. The spatial resolution is given by the compartments that are defined and is limited by the degree to which reliable estimates of input parameters are available. To quantify compound interactions with individual compartments the two elements of the “dual-sorption”-theory (119), i.e. non-saturable dissolution and saturable binding were applied to individual compartments in terms of partition coefficients and Langmuir binding isotherms. Input data was either experimentally derived or found in theoretical parameter studies. Calculations are evaluated by comparing results with independently determined experimental $K_{SC/LVP}$. Discrepancies between measurements and predictions are investigated by systematically varying critical input parameters.

6.2 THEORY

6.2.1 Definition of compartments and interfaces

We assume a compartmental composition of the SC of lipids and corneocytes, Ω_{lip} and Ω_{cor} . Two main states of the SC will be discussed. These are “hydrated SC” (SC,hyd) and “dry SC” (SC,dry). The latter is an artificial state obtained by freeze-drying of excised SC which is only relevant for the *in vitro* situation. Nonetheless, it will be useful for illustrating the effect of SC water content and protein binding. “SC,dry” is composed of a lipid and a protein compartment

Equation 6-1
$$\Omega_{SC,dry} = \Omega_{lip} + \Omega_{pro}$$

“SC,hyd” additionally contains an aqueous compartment

Equation 6-2
$$\Omega_{SC,hyd} = \Omega_{SC,dry} + \Omega_{aqu}$$

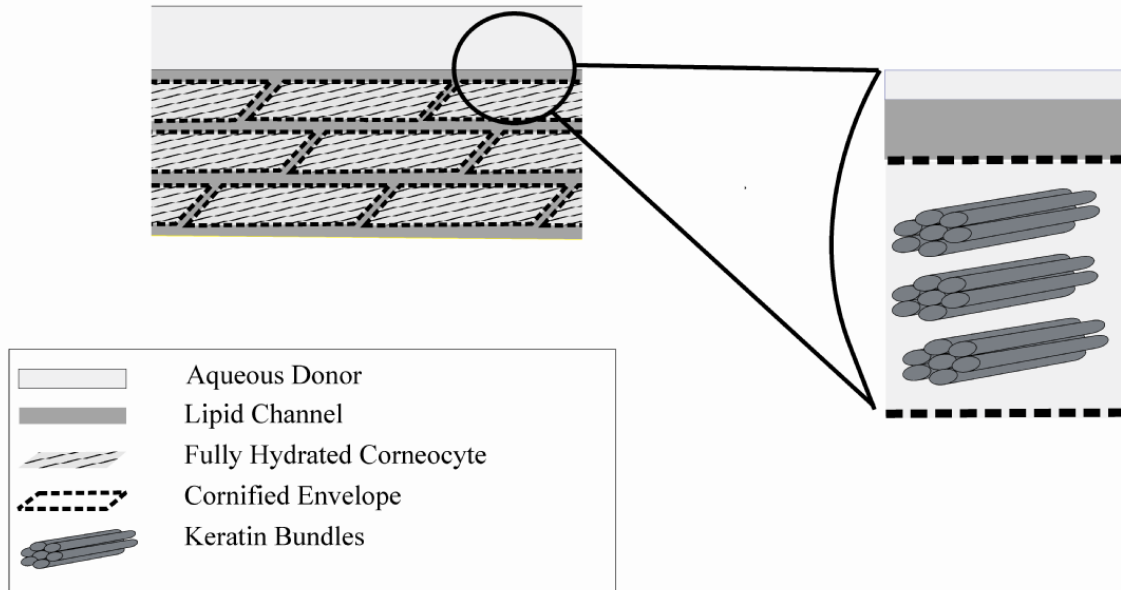
Such a compartmental composition in dry and hydrated state will be discussed as “Model 1” (M1). As an extension of M1 Ω_{pro} will be further subdivided into a keratin and a cornified envelope sub-compartment in “Model 2” (M2)

Equation 6-3
$$\Omega_{pro} = \Omega_{ker} + \Omega_{cpe}$$

The composition of the M1 and M2 model membrane at dry and hydrated state is depicted in Figure 6-1.

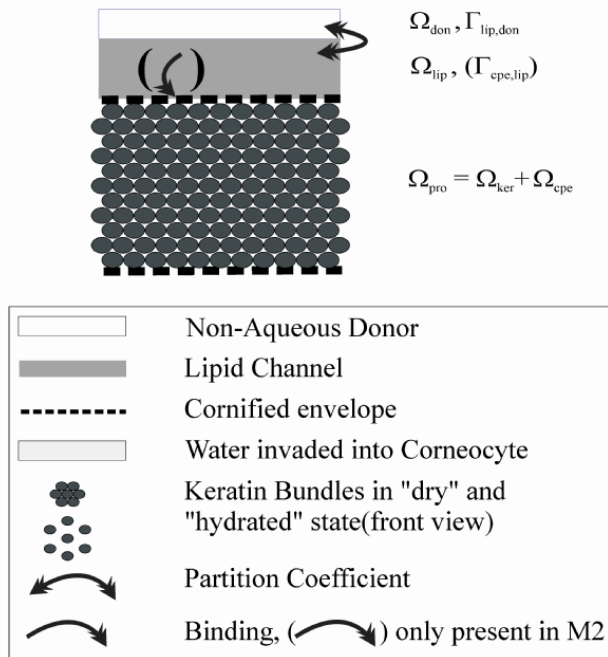
A:

The first three corneocyte layers of SC are shown in contact with an aqueous donor medium. Magnified view into a fully hydrated corneocyte with keratin bundles, cornified envelope, water of hydration, adjacent lipid channel and aqueous donor.



B:

Cross-section of “dry SC” in contact with a non-aqueous donor. Magnified view into a dry corneocyte with adjacent lipid channel and non-aqueous donor. Compartments and interfaces.



C:

Cross-section of “hydrated SC” in contact with a non-aqueous donor. Magnified view into a hydrated corneocyte with adjacent lipid channel and non-aqueous donor. Compartments and interfaces.

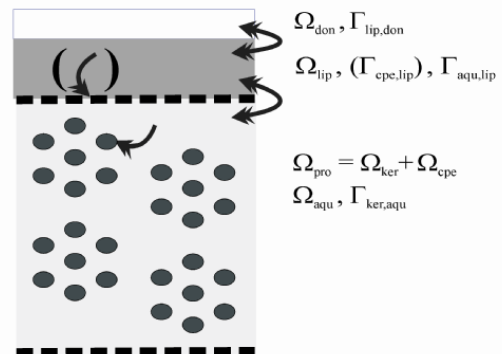


Figure 6-1 A: Upon contact with an aqueous donor water invades into the corneocytes. B and C: Incubating excised *stratum corneum* with a non-aqueous donor such as low viscous paraffin allows working at a defined hydration state. Compartments and interfaces used in the compartmental models of “dry *stratum corneum*” (B) and “hydrated *stratum corneum*” (C). Not drawn to scale.

The membrane is in contact with an inert donor medium Ω_{don} . Adjacent compartments are separated by interfaces $\Gamma_{lip,don}$, $\Gamma_{aqu,lip}$, $\Gamma_{pro,lip}$ and $\Gamma_{pro,aqu}$ in M1 and $\Gamma_{lip,don}$, $\Gamma_{aqu,lip}$, $\Gamma_{ker,aqu}$ and $\Gamma_{cpe,lip}$ in M2. By definition Ω_{aqu} and Ω_{cpe} do not share a common interface. The theoretical interface $\Gamma_{cpe,ker}$ is ignored as direct substance exchange between two solids is considered impossible. An index set $I = \{don, lip, aqu, pro, ker, cpe\}$ will be used to avoid unnecessary abundant notation. Compartments and interfaces are then referred to by the symbol Ω_i and $\Gamma_{i,j}$ for $i \neq j$ and $i, j \in I$ (Table 6-1). The composition of the model membrane with the described compartments and interfaces at dry and hydrated state is depicted in Fig. 1.

Table 6-1 Compartments and interfaces of the model membrane in M1 and M2

Compartments and interfaces	symbols	partition coefficients and binding constants	concentrations	model
Donor compartment	Ω_{don}	$K_{lip/don}$ no interaction	c_{don}	M1 SC,dry
Interface	$\Gamma_{lip,don}$			
Lipid layers	Ω_{lip}		c_{lip}	
Interfaces	$\Gamma_{pro,lip}$			
Aqueous compartment	$\Gamma_{aqu,lip}$	$K_{aqu/lip}$	c_{aqu} c_{pro}	M1 SC,hyd
Interface	Ω_{aqu}	k_{pro} and $c_{max,pro}$		
Protein compartment	$\Gamma_{pro,aqu}$			
	Ω_{pro}			
Donor compartment	Ω_{don}	$K_{lip/don}$ $K_{aqu/lip}$, k_{cpe} and $c_{max,cpe}$	c_{don}	M2 SC,dry
Interface	$\Gamma_{lip,don}$			
Lipid layers	Ω_{lip}		c_{lip}	
Interfaces	$\Gamma_{aqu,lip}$ and $\Gamma_{cpe,lip}$		c_{cpe}	
Cornified envelope	Ω_{cpe}			
Aqueous compartment	Ω_{aqu}	k_{ker} and $c_{max,ker}$	c_{aqu}	M2 SC,hyd
Interface	$\Gamma_{ker,aqu}$			
Keratin compartment	Ω_{ker}		c_{ker}	

6.2.2 Description of compound membrane interaction

M1 and M2 apply to equilibrium conditions. We consider the whole SC volume accessible for compounds which is expressed in the following set of equations for M1 (Equation 6-4 and Equation 6-5) and M2 (Equation 6-6 and Equation 6-7) at dry and hydrated state

Equation 6-4
$$c_{SC,dry} = \phi_{SC,dry}^{lip} c_{lip} + \phi_{SC,dry}^{pro} c_{pro}$$

Equation 6-5
$$c_{SC,hyd} = \phi_{SC,hyd}^{lip} c_{lip} + \phi_{SC,hyd}^{pro} c_{pro} + \phi_{SC,hyd}^{aqu} c_{aqu}$$

Equation 6-6
$$c_{SC,dry} = \phi_{SC,dry}^{lip} c_{lip} + \phi_{SC,dry}^{ker} c_{ker} + \phi_{SC,dry}^{cpe} c_{cpe}$$

Equation 6-7
$$c_{SC,hyd} = \phi_{SC,hyd}^{lip} c_{lip} + \phi_{SC,hyd}^{ker} c_{ker} + \phi_{SC,hyd}^{cpe} c_{cpe} + \phi_{SC,hyd}^{aqu} c_{aqu}$$

with the concentration of a substance within a compartment being defined as $c_i = w/V_i$, i.e. as the weight of the substance in the compartment relative to its volume. The volume fractions of the compartments relatively to the volume of the SC are defined as $\phi_{SC}^i = V_i/V_{SC}$. Although substantial portions of water are known to be tightly bound to proteins as a starting point we assume all water to be available for compound dissolution. This is in agreement with SC partitioning experiments performed with sucrose by Raykar et al. who could not find proof of an inaccessible water fraction within human SC (52).

Substance-compartment interactions are modelled depending on the nature of the compartment. At $\Gamma_{lip,don}$ and $\Gamma_{aqu,lip}$ partition coefficients K_{ij} are applied. That is:

Equation 6-8
$$c_i(x) = K_{ij} c_j(x)$$

holds for $x \in \Gamma_{i,j}$, with $(i,j) \in \{(lip,don), (aqu,lip)\}$.

In contrast, for all protein compartments Ω_{pro} , Ω_{ker} and Ω_{cpe} we follow the rationale by Chandrasekaran et al. who suggested a non-linear dependence assuming a limited number of available binding sites and described the relationship between protein-bound and free concentration by a Langmuir-isotherm (119)

Equation 6-9
$$c_i(x) = \frac{k_i c_{max,i} c_j(x)}{1 + k_i c_j(x)}$$

for $x \in \Gamma_{i,j}$, with $(i,j) = (pro,aqu)$ for M1 and $(i,j) \in \{(ker,aqu), (cpe,lip)\}$ for M2. In this sense for M1 we assume $\Gamma_{pro,lip}$ to be an “inert” interface and protein binding only via $\Gamma_{pro,aqu}$. Due to the coupling of Ω_{aqu} , Ω_{lip} , and Ω_{don} via $K_{aqu/lip}$ and $K_{lip/don}$ at $\Gamma_{aqu,lip}$ and $\Gamma_{lip,don}$ the free (and thus also the bound) concentrations will be a function of c_{don} :

Equation 6-10
$$c_{aqu} = K_{aqu/lip} c_{lip} = K_{aqu,lip} K_{lip/don} c_{don} = K_{aqu/don} c_{don}$$

Equation 6-11
$$c_{lip} = K_{lip/don} c_{don}$$

From an anatomical standpoint direct lipid-protein contact can only reasonably be assumed between SC lipids and the cpe or corneodesmosomes. As a first approach in M2 we are concentrating on the cpe for the simple reason that information on its dimensions are available from literature (1).

This has severe consequences for the description of c_{SC} . For M1 the concentration within “SC,dry” and “SC,hyd” are given by

Equation 6-12 $c_{SC,dry} = \varphi_{SC,hyd}^{lip} K_{lip/don} c_{don}$

as $\Omega_{aqu} = \emptyset$, and consequently $c_{aqu} = c_{pro} = 0$, and by

Equation 6-13

$$c_{SC,hyd} = \varphi_{SC,hyd}^{lip} K_{lip/don} c_{don} + \varphi_{SC,hyd}^{pro} \frac{k_{pro} c_{max,pro} K_{aqu/don} c_{don}}{1 + k_{pro} K_{aqu/don} c_{don}} + \varphi_{SC,hyd}^{aqu} K_{aqu/don} c_{don}$$

For M2 $c_{SC,dry}$ and $c_{SC,hyd}$ are described as

Equation 6-14 $c_{SC,dry} = \varphi_{SC,dry}^{lip} K_{lip/don} c_{don} + \varphi_{SC,dry}^{cpe} \frac{k_{cpe} c_{max,cpe} K_{lip/don} c_{don}}{1 + k_{cpe} K_{lip/don} c_{don}}$

as $\Omega_{aqu} = \emptyset$, $c_{aqu} = c_{ker} = 0$ and by

Equation 6-15

$$c_{SC,hyd} = \varphi_{SC,hyd}^{lip} K_{lip,don} c_{don} + \varphi_{SC,hyd}^{ker} \frac{k_{ker} c_{max,ker} K_{aqu,don} c_{don}}{1 + k_{ker} K_{aqu,don} c_{don}} + \varphi_{SC,hyd}^{cpe} \frac{k_{cpe} c_{max,cpe} K_{lip,don} c_{don}}{1 + k_{cpe} K_{lip,don} c_{don}} + \varphi_{SC,hyd}^{aqu} K_{aqu,don} c_{don}$$

Note that in Equation 6-9 $c_i(x)$ depends only on the concentration $c_j(x)$ but not on the volume fraction φ_{SC}^i . In other words at high SC hydration when water intercalates between lipids the bound concentration will still be correctly described by Equation 6-9 despite that parts of Ω_{aqu} share no interface with Ω_{pro} or Ω_{cpe} . This of course only true if the number of binding sites is independent of φ_{SC}^{aqu} .

6.2.3 The special case of non-protein binding substances

In the special case of non-protein binding substances, the maximum concentrations $c_{max,i}$ are identically zero. Therefore, the terms corresponding to the Langmuir isotherms vanish and, for both M1 and M2, the same result is obtained for $c_{SC,dry}$ (Equation 6-12) and $c_{SC,hyd}$

Equation 6-16 $c_{SC,hyd} = \varphi_{SC,hyd}^{lip} K_{lip,don} c_{don} + \varphi_{SC,hyd}^{aqu} K_{aqu,don} c_{don}$

respectively.

6.2.4 Calculation of a theoretical stratum corneum-donor partition coefficient

The theoretical SC-donor partition coefficient is calculated by applying Equation 6-8 to the whole SC membrane and rearranging for $K_{SC/don}$

Equation 6-17 $K_{SC/don} = \frac{c_{SC}}{c_{don}}$

Accordingly, in Equations 4-5 to 4-9 c_{SC} is divided by c_{don} to calculate $K_{SC,hyd}$ and $K_{SC,dry}$ for M1 (Equation 6-18 and Equation 6-19), M2 (Equation 6-20 and Equation 6-21) and non-keratin binding substances (Equation 6-22).

Equation 6-18 $K_{SC,dry/don} = \phi_{SC,dry}^{lip} K_{lip/don}$

Equation 6-19 $K_{SC,hyd/don} = \phi_{SC,hyd}^{lip} K_{lip/don} + \phi_{SC,hyd}^{pro} \frac{k_{pro} c_{max,pro} K_{aqu/don}}{1 + k_{pro} K_{aqu/don} c_{don}} + \phi_{SC,hyd}^{aqu} K_{aqu/don}$

Equation 6-20 $K_{SC,dry/don} = \phi_{SC,dry}^{lip} K_{lip/don} + \phi_{SC,dry}^{cpe} \frac{k_{cpe} c_{max,cpe} K_{lip/don}}{1 + k_{cpe} K_{lip/don} c_{don}}$

Equation 6-21

$$K_{SC,hyd/don} = \phi_{SC,hyd}^{lip} K_{lip/don} + \phi_{SC,hyd}^{ker} \frac{k_{ker} c_{max,ker} K_{aqu/don}}{1 + k_{ker} K_{aqu/don} c_{don}} + \phi_{SC,hyd}^{cpe} \frac{k_{cpe} c_{max,cpe} K_{lip/don}}{1 + k_{cpe} K_{lip/don} c_{don}} + \phi_{SC,hyd}^{aqu} K_{aqu/don}$$

Equation 6-22 $K_{SC,hyd/don} = \phi_{SC,hyd}^{lip} K_{lip,don} + \phi_{SC,hyd}^{aqu} K_{aqu,don}$

In order to compare calculated with experimental results values of $K_{SC,hyd/don}$ need to be transformed to $K_{SC,dry/don}$ via (for the derivation see *insert I*):

Equation 6-23 $K_{SC,dry/don} = \frac{K_{SC,hyd/don}}{\phi_{SC,hyd}^{SC,dry}}$

Insert I - Transformation of partition coefficients

According to Equation 6-17 the partition coefficients $K_{SC,dry/don}$ and $K_{SC,hyd/don}$ can be written as

$$K_{SC,dry/don} = \frac{c_{SC,dry}}{c_{don}} = \frac{w/V_{SC,dry}}{w/V_{don}}$$

$$K_{SC,hyd/don} = \frac{c_{SC,hyd}}{c_{don}} = \frac{w/V_{SC,hyd}}{w/V_{don}}$$

So that $K_{SC,dry/don}$ and $K_{SC,hyd/don}$ are related via

$$K_{SC,dry/don} = K_{SC,hyd/don} \frac{V_{SC,hyd}}{V_{SC,dry}} = K_{SC,hyd/don} \frac{1}{\phi_{SC,hyd}^{SC,dry}}$$

6.2.5 Input parameters

The following paragraph relates the terms in Equations 4-18 to 4-22 to experimentally measured parameters for the special case of LVP as donor medium and for CAF, FFA, and TST as model compounds.

6.2.5.1 The stratum corneum lipid-low viscous paraffin partition coefficient $K_{lip/LVP}$

According to the definition of the partition coefficient in Equation 6-8 the upper limit is determined by the ratio of the saturation concentrations within the two phases (s_i and s_j). In this sense $K_{lip/LVP}$ can be expressed as in Equation 6-24. In an earlier publication for CAF and FFA we measured $K_{lip/don}$ for don being Soerensen phosphate buffer pH 7.4 (Soer,7.4) (Equation 6-25) (239). Rearranging Equation 6-25 for s_{lip} and substituting it into Equation 6-24 $K_{lip/LVP}$ is calculated from the measured quantities $K_{lip/Soer,7.4}$, $s_{Soer,7.4}$, and s_{LVP} (Equation 6-26).

$$K_{lip/LVP} = \frac{s_{lip}}{s_{LVP}}$$

Equation 6-24

$$K_{lip/Soer,7.4} = \frac{s_{lip}}{s_{Soer,7.4}}$$

Equation 6-25

$$K_{lip/LVP} = \frac{K_{lip/Soer,7.4} s_{Soer,7.4}}{s_{LVP}}$$

Equation 6-26

For TST no experimental data on $K_{lip/Soer,7.4}$ were available so that first the lipid-water partition coefficient $K_{lip/w}$ was inferred from the octanol-water partition coefficient $K_{Oct/w}$ as proposed in (150) (Equation 6-27). The aqueous solubility of TST being pH independent $K_{lip/w}$ was taken to be identical to $K_{lip/Soer,7.4}$ so that $K_{lip/LVP}$ could then be calculated according to Equation 6-26.

$$K_{lip/w} = (K_{Oct/w})^{0.78}$$

Equation 6-27

Equation 6-27 is subject to uncertainty as it relies on a fitting procedure and depends on the diversity and accuracy of the underlying database. A number of similar correlations of the general form

$$K_{lip/w} = a(K_{Oct/w})^b$$

Equation 6-28

have been proposed. Taking $a = 1$ values for b were suggested in the range of 0.70 to 0.78 (85, 134, 150, 160, 248). Considering both a and b as being variable, values as high as 0.91 have been suggested for b (52). The exponent of 0.78 was chosen because it was derived for a database of experimentally determined SC lipid-water partition coefficients. A comparison of calculated values of $K_{lip/w}$ for CAF and FFA with experimentally determined values shall serve as a test of consistency of estimates of Equation 6-27. For CAF and FFA Equation 6-27 predicts $K_{lip/w}$ to be 0.87 and 38.37 while experimental values were 2.15 ± 0.42 and 20.32 ± 0.54 respectively

(note that for FFA the prediction was corrected for pH 7.4 as this was used in the experiment (239)). Despite the experimental and theoretical uncertainty Equation 6-27 seems to be a valuable instrument to estimate $K_{lip/w}$ for TST where no experimental results are available.

6.2.5.2 The aqueous compartment-low viscous paraffin partition coefficient $K_{aqu/LVP}$

$K_{aqu/LVP}$ was calculated for CAF, FFA, and TST as proposed for $K_{lip/LVP}$ from the saturation concentrations in aqu and LVP. The solvent properties of aqu were supposed to be essentially like bulk water. For CAF and TST the aqueous solubility is independent of pH so that $s_{Soer,7.4}$ seems a reasonable experimental approximation for s_{aqu} . In contrast for FFA a pH correction was necessary. Depending on the analytical method opinions on corneocyte pH vary ranging from moderately acidic (pH 5.5-6.5; employing surface parallel pH electrodes combined with tape-stripping (197)) to practically neutral (measuring the fluorescence lifetime of pH-sensitive dyes, e.g. 2',7'-bis-(2-carboxyethyl)-5-(and-6)-carboxyfluorescein (216)). Due to the lipophilicity of the fluorescent dye the latter method exclusively probes the intercellular lipid channel while information on the corneocyte pH is most probably not available. Therefore 5.5 and 6.5 seem a reasonable estimate for the lower and upper margin of the corneocyte pH. Accordingly the lower margin of $K_{aqu/LVP}$ was calculated for FFA using $s_{Soer,5.5}$ and the upper margin of $K_{aqu/LVP}$ was calculated using $s_{Soer,6.5}$. All analyses for FFA were performed for both pH-values.

6.2.5.3 The Langmuir isotherm describing keratin binding

In M1 the binding properties of the protein compartment will simplistically be described as keratin. Experimental data on $q_{max,ker}$ and k_{ker} measured with keratin from bovine hoof and horn is available from literature for CAF and FFA (239) or presented here for TST. The maximum binding capacity of a protein is usually reported in terms of its loading $q_{max,i}$, i.e. as a weight fraction relatively to the weight of the protein [w/w] rather than as a concentration $c_{max,i}$ relatively to the volume of the protein [w/V]. $q_{max,i}$ is related to $c_{max,i}$ via the protein density:

Equation 6-29
$$c_{max,ker} = \frac{w}{V_{ker}} = \frac{w}{w_{ker}} \rho_{ker} = q_{max,ker} \rho_{ker}$$

It has been argued that with swelling keratin uncoils and exposes additional binding sites (249). Reported values for $q_{max,ker}$ and k_{ker} correspond to maximally expanded

keratin as experiments were performed in “Soer,7.4”. This might be a source for errors in the case of “dry SC”. This is avoided by restricting keratin binding to be only possible in hydrated SC.

6.2.5.4 The Langmuir isotherm describing binding to the cornified protein envelope

In M2 binding to SC proteins is subdivided into binding to intra-cellular keratin accessible (as in M1) only from the aqueous compartment and binding to the cpe accessible only from the lipid compartment. For $q_{\max, \text{ker}}$ and k_{ker} experimental data is readily available. In contrast, there are no studies reporting the maximum binding capacity $q_{\max, \text{cpe}}$ or the binding constant to the cpe k_{cpe} . Therefore we performed a theoretical parameter study where different combinations of $q_{\max, \text{cpe}}$ (1, 10, 50, and 100 $\mu\text{g}/\text{mg}$) and k_{cpe} (10^{-3} $\text{ml}/\mu\text{g}$ and 10^3 $\text{ml}/\mu\text{g}$) were tested. Although these values are arbitrarily founded however, they may serve to illustrate the potential of protein binding via the SC lipids in a range of possible protein binding constants and binding capacities.

6.3 MATERIAL AND METHODS

6.3.1 *Material*

The following materials and equipment were used: dialysis membrane MW-cut-off 25 kDa (Medicell International Ltd, London, Great Britain, VWR Darmstadt, Germany); Centrisart I cut-off 20 kDa (Sartorius AG, Goettingen, Germany); scintillation vials borosilicate glass with screw cap (VWR, Darmstadt, Germany); freeze-dryer (Alpha 2-4 LSC, Christ, Osterode, Germany); UV/VIS spectrophotometer (Lambda 35, Perkin Elmer, Rodgau-Jürgesheim, Germany); Hellma® precision cells made of Quartz SUPRASIL®, type 100-QS-10 (Hellma®, Muehlheim, Germany).

6.3.2 *Chemicals*

4-Androsten-17 β -ol-3-on (i.e. TST), FFA, CAF, sodium chloride, potassium chloride, methanol, a bicinchoninic acid kit for protein determination and Trypsin type I from bovine pancreas were supplied by Sigma Aldrich GmbH, Steinheim, Germany. Acetonitrile and sodium monohydrogen phosphate dihydrate were supplied by Fluka Chemie AG, Buchs, Germany. Low viscous paraffin (density at 20 °C 0.818-0.875 g/cm^3 ; dynamic viscosity 25-80 mPas), citric acid monohydrate, potassium dihydrogen phosphate, orthophosphoric acid were supplied by Merck, Darmstadt,

Germany. Keratin from bovine hoof and horn was supplied by ICN biomedical, Aurora, Ohio.

6.3.3 Composition of buffers

All buffer substances were of analytical grade and were prepared with purified water. Phosphate buffered saline (PBS) pH 7.4: 1 l contains $\text{Na}_2\text{HPO}_4 \cdot 2\text{H}_2\text{O}$ 1.44 g, KH_2PO_4 0.2 g, NaCl 8 g, KCl 0.2 g.

Soerensen phosphate buffer: is composed of x parts 0.15 M Na_2HPO_4 , and 100-x parts 0.15 M KH_2PO_4 (pH 5.5: x = 3.5; pH 6.5: x = 30; pH 7.4: x = 80.3).

Buffer pH 2.2: 1 l contains citric acid monohydrate 20.8 g, $\text{Na}_2\text{HPO}_4 \cdot 2\text{H}_2\text{O}$ 0.4 g.

Buffer pH 2.6: 1 l contains orthophosphoric acid 1.16 ml, KH_2PO_4 2.04 g.

6.3.4 Skin samples and skin preparation techniques

Skin samples were taken from Caucasian female donors undergoing abdominal surgery with the approval of the ethic committee of the Caritas-Hospital Lebach, Germany. After removal of subcutaneous fatty tissue full thickness skin was stored at -26°C for a maximum of 6 months after surgery. For details see Wagner et al. (173).

6.3.4.1 Preparation of stratum corneum sheets

SC sheets were prepared according to the method of Kligman (174) by two times 24 h immersion of cleaned full thickness skin pieces of approximately 12 cm^2 in 0.15% (w/V) trypsin in PBS. In between as well as afterwards the pieces were washed 3 times with PBS and finally freeze-dried. Samples were kept at -26°C overnight to guarantee complete freezing and then equilibrated inside the single chamber system at -40°C . Main drying was performed overnight at 0.050 mbar, with a shelf temperature of 20°C and a condenser temperature of -80°C . For the final drying for two hours the vacuum was elevated to 0.001 mbar keeping shelf and condenser temperature as during main drying. During the entire procedure the temperature of condenser and shelf was permanently monitored. Dried SC samples had a parchment like, crumple and brittle appearance. Freeze-dried membranes were kept in a freezer at -18°C for a maximum of 6 months after surgery.

6.3.4.2 Preparation of hydrated stratum corneum

A gradual hydration of SC sheets was achieved by equilibrating freeze-dried SC sheets of known weight over a 15.32% w/w sodium chloride solution or pure water or

immersion in water for 24 h at 32 °C in desiccators. The hydrated SC sheets were weighed again (in the case of SC sheets immersed in water these were blotted dry between paper filters before weighing). The level of hydration was calculated as follows: % w/w = 100 x (weight hydrated SC – weight dried SC) / weight dried SC.

6.3.5 Determination of saturation concentration

An excess of CAF, FFA or TST was suspended in 5 ml Soerensen buffer pH 5.5; 6.5; 7.4 or LVP in a screw top scintillation vial. The lid was secured with a Teflon disk. The mixture was stirred at 500 rpm, at 32 °C for at least 24 h. Stirring was stopped and the samples were further kept at 32 °C until non-dissolved substance had settled down completely. Samples were drawn from the supernatant without disturbing the sediment and centrifuged for 5 min at 2795 g. During centrifugation the temperature of the samples did not change. The samples were diluted to an appropriate concentration, and analyzed via HPLC or UV spectroscopy. Preliminary experiments had shown that saturation was complete within 24 h and no filtration was needed.

6.3.6 Keratin binding

Prior to the experiment water soluble low molecular weight keratin fractions resulting from the manufacturing process were removed by classical dialysis using dialysis tubing with a molecular weight cut-off of 25 kDa. Removal of soluble keratin fraction was considered to be complete if a BCA-assay in the supernatant performed according to the standard protocol provided by the manufacturer was negative (linear concentration range 0.2-1 mg/ml or 5-25 µg of total protein, detection limit 0.01 µg/ml). Insoluble keratin fractions were retrieved by freeze-drying.

Increasing ratios of TST to keratin (eleven steps in the range of 0.025 – 4.68 µg/mg keratin) were incubated on a magnetic stirrer (500 rpm) at 32 °C, over 24 h, i.e. until equilibration. 1.0 ml of the suspension were transferred to centrisart tubes (MW-cut-off 20 kDa) and centrifuged for 20 min at 2795 g at 25 °C. The supernatant was diluted with Soerensen buffer pH 7.4 to an appropriate concentration and transferred into HPLC vials and the concentration of unbound substance was determined by HPLC. Samples containing only substance solution without keratin were subjected to the identical procedure and represented 100% free concentration.

6.3.7 Determination of partition coefficients by equilibration experiments

The substance concentration within the SC was determined from the decrease of the substance weight within the donor volume during incubation and normalized to the dry volume of SC where w_0 and w_{End} are the substance weight within LVP before and after equilibration

Equation 6-30
$$K_{\text{SC,dry/don}} = \frac{(w_0 - w_{\text{End}})/V_{\text{SC,dry}}}{w_{\text{End}}/V_{\text{LVP}}}$$

$V_{\text{SC,dry}}$ was determined from weighing freeze-dried SC by normalizing to the density of dry SC: 1.3 g/cm³ (2).

6.3.7.1 Influence of concentration of incubation solution

$K_{\text{SC/don}}$ was measured based on the equilibration method introduced by Raykar et al. (52). The concentration dependence of $K_{\text{SC/don}}$ was evaluated in a broad concentration range with dry^(d) SC and for the “hydrated state” with SC hydrated over pure water^(h) and additionally for exemplary concentrations for SC hydrated above sodium chloride^(NaCl) and by bathing in water^(H) as described in 6.3.4.2 (dry weight 6.95-25.45 mg per piece). An SC sheet was immersed in 2 ml LVP containing 32.20-92.15 µg/ml^(d,h), 57.93-75.49 µg/ml^(NaCl), and 57.93 µg/ml^(H) CAF; 12.12-403.37 µg/ml^(d), 39.17-403.37 µg/ml^(h), 12.12 µg/ml^(NaCl) and 12.12-48.92 µg/ml^(H) FFA; 9.60-414.45 µg/ml^(d,h), and 9.60-188.87 µg/ml^(NaCl,H) TST and allowed to equilibrate at 32 °C for 24 h.

To exclude unspecific adsorption to the test tubes these were incubated with the drug solution alone. Furthermore, to exclude that substances interfering with analytics are extracted by the solvent, a piece of SC was soaked with the vehicle for 24 h and underwent the same procedure as the drug containing solutions.

All partition coefficients are reported relative to the volume of dry SC independent of the hydration state of the SC.

6.3.7.2 Influence of hydration

SC either freeze-dried or gradually hydrated as described in 3.4.3 were subjected to the procedure as described in 4.7.1. A minimum of four repetitions was performed for each hydration state. Afterwards samples were drawn from the LVP and analyzed for drug contents via UV spectroscopy.

6.3.8 *Quantification of caffeine, flufenamic acid, and testosterone*

6.3.8.1 Extraction of testosterone from low viscous paraffin

The extraction method substitutes the UV quantification below the lower limit of quantification. The equilibration experiment was performed as described above. After establishing equilibrium 1 ml of the donor were transferred into a glass test tube and 2 ml of methanol were added. The mixture was vortexed intensely and the non-miscible phases were allowed to separate at room temperature. A sample was drawn from the upper phase (methanol) and analyzed by HPLC/UV-Vis. If necessary, samples were diluted prior to the analysis. In preliminary experiments the extraction efficiency in the concentration range of 10-200 µg/ml had been found to be $95 \pm 5\%$. The extraction was performed at c_{don} 9.6, 24.1, and 188.87 µg/ml using $n = 5$ for each concentration and each hydration method as well as “dry” SC resulting in overall 60 samples. The samples at 188.87 µg/ml serve as a control that the results of the extraction method are not different from the UV measurement and therefore can be combined. A t-test comparing results from extraction experiments at 188.87 µg/ml with all results from UV measurements above 50 µg/ml found no statistical differences on the 95% confidence level.

6.3.8.2 UV-spectroscopy

Samples dissolved in LVP were analyzed by UV-spectroscopy at 270 nm, 284 nm, and 250 nm (CAF, FFA, and TST, respectively) after adding dichloromethane (DCM) up to a final ratio of LVP : DCM of 1 : 10. For all compounds a calibration was performed using external standards containing 3.75 - 20 µg/ml CAF (limit of quantification LOQ: 3 µg/ml), 3.125 - 15 µg/ml FFA (LOQ: 1 µg/ml), or 5 - 15 µg/ml TST (LOQ: 5 µg/ml) dissolved in the same medium as the unknown samples, i.e. 10% V/V LVP/DCM. If necessary, unknown samples were diluted to an appropriate concentration with 10% V/V LVP/DCM. UV cuvettes were sealed with parafilm and aluminium foil to prevent evaporation of the volatile DCM.

6.3.8.3 HPLC

Samples dissolved in (Soer,7.4) or methanol were analysed by RP-HPLC using an isocratic Dionex HPLC system (Lichrospher® RP-18 column/ 125 x 4 mm/ 5µm with

a LiChroCART® 4-4 guard column (Merck-Hitachi, Darmstadt); Software: chromeleon 6.50 SP2 build 9.68.

CAF: mobile phase: 90:10 (V/V) buffer pH 2.6/acetonitrile; retention time: 5.1 ± 0.2 min; flow rate: 1.2 ml/min; injection volume: 50 μ l; detection wavelength: 270 nm; detection limit: 10 ng/ml; quantification limit: 50 ng/ml

FFA: mobile phase: 80:20 (V/V), methanol/ buffer pH 2.2; retention time: 3.5 ± 0.2 min; flow rate: 1.2 ml/min; injection volume: 50 μ l; detection wavelength: 284 nm; detection limit: 15 ng/ml; quantification limit: 50 ng/ml

TST: mobile phase: 70:30 methanol/ water (V/V); retention time: 4.8 min \pm 0.2 min; flow rate: 1.2 ml/min; injection volume: 50 μ l; detection wavelength: 250 nm; detection limit: 15 ng/ml; quantification limit: 50 ng/ml

For all compounds a calibration was performed using external standards with 0.05-25 μ g/ml dissolved in the same medium as the unknown samples, i.e. Soerensen buffer pH 7.4 or methanol. If necessary, unknown samples were diluted to an appropriate concentration with the same medium prior to analysis.

6.3.9 Software

All calculations were performed with Origin 7.5G SR3, OriginLab Corporation, Northampton, MA, USA.

6.4 RESULTS

6.4.1 Hydration

The aim was to span a wide range of hydration states. This could be realised by hydrating SC sheets above or within salt solutions or pure water. Different salt solutions or a saturated atmosphere have repeatedly been used for hydrating skin. Commonly, sodium bromide 27% wt/wt (50), saturated sodium carbonate (50), potassium carbonate 5.7-1.4 M (250, 251), and saturated barium chloride (252) are used to generate specific relative humidities in a vapor sealed environment. The mole fraction of a sodium bromide 27% wt/wt solution is equivalent to a sodium chloride 15.32% wt/wt solution, i.e. 2.62 M. Due to thermodynamic equilibrium SC hydration should basically be the same after equilibration above water in a saturated atmosphere and after immersion. However, there is microscopical evidence that swelling is profoundly different in humid air and after immersion, the latter resulting in significant water uptake into selective zones of the SC (51). The immersion

procedure is relevant for the measurement of partition coefficient experiments with aqueous vehicles and for *in vitro* Franz-diffusion cell experiments with aqueous donor and acceptor media. In order to investigate possible influences on $K_{SC/don}$ we additionally investigated SC that had been hydrated in a saturated atmosphere. Here, no influence on the SC structure had been reported (51).

Equilibration of SC sheets over 15.32% w/w sodium chloride solution, pure water or immersion in water resulted in hydration of 31 - 79% w/w ($n = 16$), 46 - 212% w/w ($n = 83$), and 445-780% w/w ($n = 25$). The SC hydration is highly sensitive to small changes in the relative humidity of the environment especially during weighting. Therefore the SC water content that was reached with one hydration method varied rather largely. Furthermore these variations may be due to varying quantities of natural moisturizing factors between skins of different patients. For the evaluation of partition coefficients the accurate level of hydration of each individual SC sheet was taken into account instead of using a mean hydration level for all SC sheets hydrated with the same method.

6.4.2 Input parameters

Table 6-2 gives an overview over the sources and results of the input parameters needed for the compartmental models M1 and M2 as introduced in section 6.2. Data gathered from the literature are marked as such. Further data that have been determined in the course of this work are presented in detail below.

Table 6-2 Sources and results of input parameters used in M1 and M2 for caffeine, flufenamic acid, and testosterone.

	CAF	FFA	TST
$K_{lip/Soer}$	^a 2.15 ± 0.42	^a 20.32 ± 0.54	n.a.
s_{aqu} [mg/ml]	24.87 ± 0.90	pH 6.5: 0.43 ± 0.014 pH 5.5: 0.041 ± 0.002	0.02 ± 0.001
s_{LVP} [mg/ml]	$0.134 \pm 3.31 \cdot 10^{-3}$	1.18 ± 0.05	0.50 ± 0.06
$K_{lip/LVP}$	399.03	35.40	15.67
$K_{aqu/LVP}$	185.6	pH 6.5: 0.36 pH 5.5: 0.035	0.047
$q_{max,ker}$ [μ g/mg]	n.a.	^a 77.03 ± 7.08	2.16 ± 1.36
k_{ker} [ml/ μ g]	n.a.	^a $1.28 \cdot 10^{-3} \pm 2.4 \cdot 10^{-4}$	0.0517 ± 0.045

(a (239); n.a. not available)

6.4.2.1 Determination of saturation concentration

The solubility in Soer,7.4 and LVP is as expected from the compound lipophilicity i.e. Soer,7.4: CAF > TST; LVP: FFA > TST > CAF (Table 6-2). As a weak acid the aqueous solubility of FFA is pH dependent and higher at pH 6.5 than at pH 5.5.

6.4.2.2 Keratin binding of testosterone

TST exhibits a concentration dependent keratin binding (Figure 6-2). The dependence of the bound ($\mu\text{g}/\text{mg}$ keratin) versus free concentration ($\mu\text{g}/\text{ml}$) at equilibrium at 32 °C may be expressed by a Langmuir adsorption isotherm (Equation 6-9). The Langmuir adsorption constant k_{ker} and the maximum loading capacity $q_{\text{max,ker}}$ could be determined by non-linear regression (Table 6-2; $\chi^2 = 0.00879$; $r^2 = 0.888$). However, due to the low aqueous solubility of TST the predicted $q_{\text{max,ker}}$ cannot be confirmed experimentally. The uncertainty of $q_{\text{max,ker}}$ is irrelevant in the models as by definition of the maximum free concentration available for keratin binding equals the aqueous solubility of TST (compare section 6.2.1). At low ratios of compound to protein the linear part of the isotherm applies.

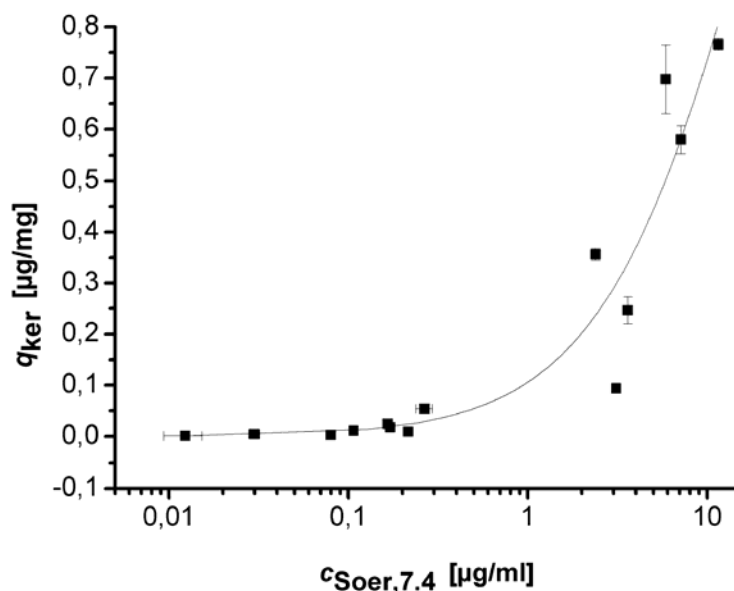


Figure 6-2 The Langmuir isotherm accurately represents the concentration dependence of testosterone binding to keratin. ($n = 3$ for each level of $c_{\text{Soer,7.4}}$; standard deviation displayed as error bars; for most points the size of the error bars falls within the size of the symbols)

6.4.3 Mechanism of corneocyte interaction – experimental results

Experimentally, two ways of substance-corneocyte interactions can be identified at least qualitatively. These are an involvement of SC water and binding to proteins. As described a non-aqueous donor allows working with SC at defined water content so that the role of hydration on the SC-donor partition coefficient can be investigated. Figure 6-3A shows that only $K_{SC,dry/don}$ of the highly water soluble CAF depends on $\omega_{SC,dry}^{aqu}$. For the lipophilic poorly water soluble compounds FFA and TST the degree of membrane hydration does not influence the SC partition coefficient (Figure 6-3B and C). Therefore, for the lipophilic compounds we will not distinguish between the hydration methods in the further course of this article. It is further evident that with increasing hydration $K_{SC,dry/don}$ of CAF is significantly higher than $K_{SC,dry/don}$ of FFA and TST indicating a higher affinity to hydrated SC of CAF compared to FFA and TST.

Furthermore a dependence of $K_{SC,dry/don}$ on c_{don} indicates an underlying saturable process such as binding to a limited number of available protein binding sites. Figure 6-4 shows the results for FFA and TST which were already known to bind to isolated bovine keratin in a saturable fashion. Only for FFA a concentration dependence of $K_{SC,dry/don}$ is present. For TST this was not the case within the analytically accessible concentration range. For both compounds a concentration dependence of $K_{SC,dry/don}$ is present in the concentration range below 50-100 µg/ml. This is more pronounced for FFA than for TST. As expected $K_{SC,dry/don}$ of the non-keratin binding CAF does not depend on concentration at a defined $\omega_{SC,dry}^{aqu}$ (results not shown).

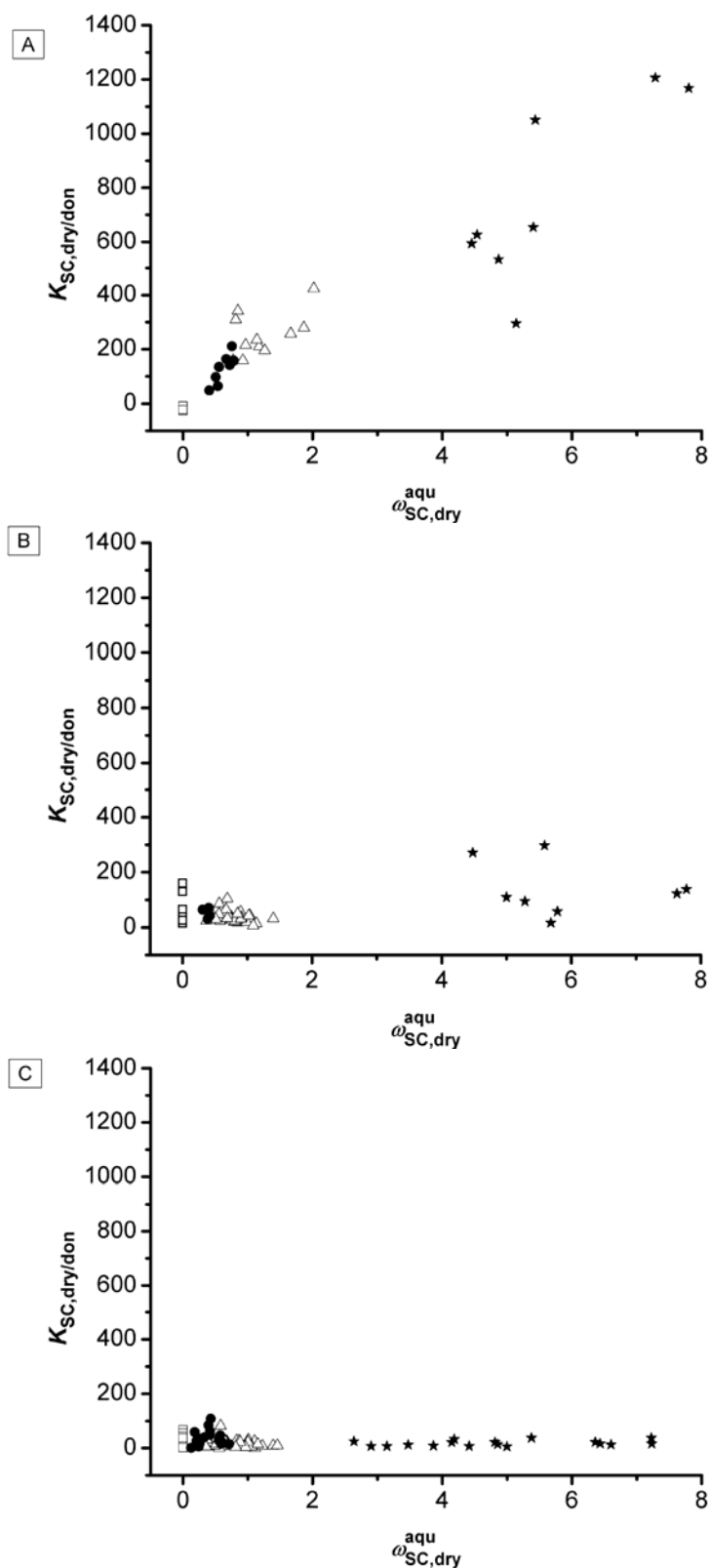


Figure 6-3 Experimentally measured $K_{SC,dry/don}$ of the hydrophilic caffeine (A) increases with progressive *stratum corneum* hydration. For the lipophilic compounds flufenamic acid (B) and testosterone (C) *stratum corneum* hydration has no influence on $K_{SC,dry/don}$. (open square: dry *stratum corneum*, filled circle: hydrated above sodium chloride, open triangle: hydrated above water, filled star: hydrated in water)

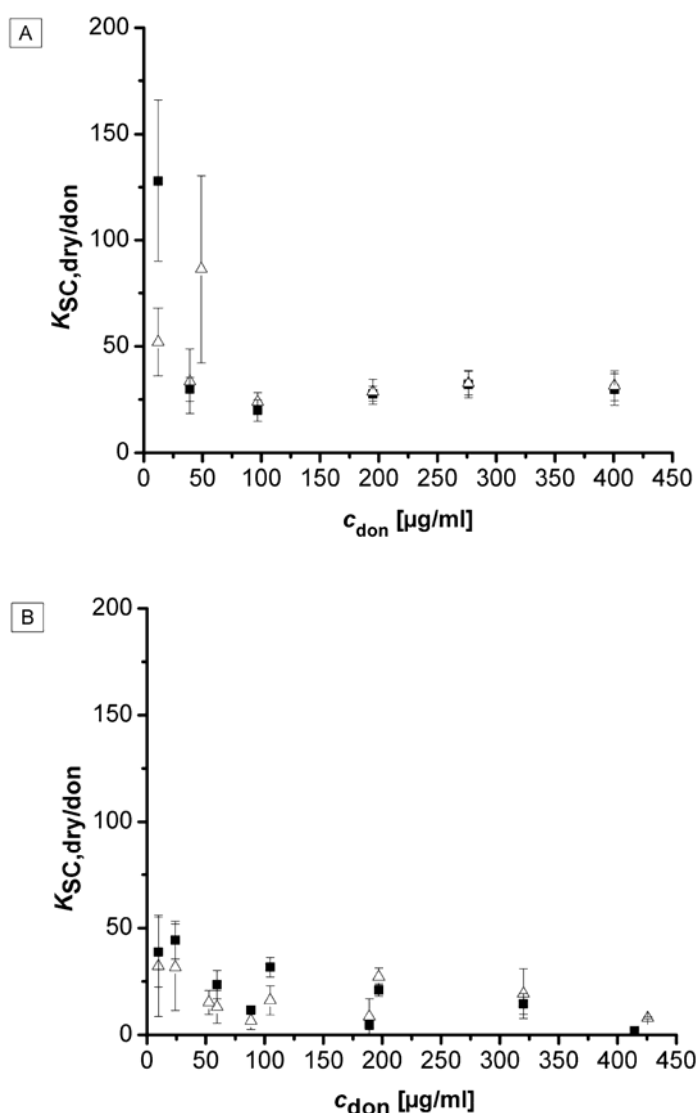


Figure 6-4 $K_{SC,dry/don}$ of keratin binding substances flufenamic acid (A) and testosterone (B) were measured as a function of donor concentration. $K_{SC,dry/don}$ increases in the lower concentration range whereas it is relatively constant at high concentrations. The different symbols indicate the applied hydration method (filled square: dry *stratum corneum*, open triangle: hydrated *stratum corneum*; $n = 2-15$; standard deviation displayed as error bars).

6.4.4 Mechanism of corneocyte interaction – comparison of theoretical and experimental results

6.4.4.1 Non-keratin binding compounds: caffeine

Figure 6-5A compares experimentally determined $K_{SC,dry/don}$ measured at different SC hydration levels (open squares) with the values predicted (bold solid line) according to Equation 6-18 (dry SC) and Equation 6-22 and Equation 6-23 (hydrated SC). Remember that for non-keratin binding substance there is no difference between M1

and M2. For the predictions the same range of $\omega_{SC,dry}^{aqu}$ was chosen as in the experiment. In both experiment and prediction $K_{SC,dry/don}$ depends linearly on $\omega_{SC,dry}^{aqu}$. A linear regression provides for the experimental results a slope of 137.11 ± 9.11 and an offset of 31.45 ± 25.99 (expressed as mean \pm se; $r^2 = 0.869$). The slope signifies the increase of $K_{SC,dry/don}$ due to an uptake of 1 g water per 100 g dry SC. The offset is determined by $K_{SC,dry/don}$ at zero hydration which indicates the affinity of CAF to the lipid compartment. Due to the substantial scatter of the experimental data the estimated offset is subject to a high variation. The compartmental model overestimates the impact of $\omega_{SC,dry}^{aqu}$ on $K_{SC,dry/don}$ and suggests a steeper slope than seen *in vitro* as well as a higher offset. Predicted values for slope and offset are 241.28 and 159.94 (compare to section 6.4.3).

For CAF it could be shown earlier that it does not bind to keratin. Therefore no concentration dependence of $K_{SC,dry/don}$ was expected. Nonetheless, to confirm the theory a range of concentrations was tested. Any influence of concentration on partitioning should have produced a deviance from the theory. This was not the case as shown e.g. in Figure 6-5.

Two possible influencing factors were investigated on a theoretical level in order to evaluate their potential to influence the affinity of CAF to the aqueous compartment. This is first s_{aqu} that directly enters $K_{aqu/don}$ (see 6.2.5.2). The influence of a systematic decrease of s_{aqu} on $K_{SC,dry/don}$ at increasing $\omega_{SC,dry}^{aqu}$ in steps of 5 mg/ml starting with $s_{Soer\ 7.4}$ is shown in Figure 6-5B. As s_{aqu} is reduced a progressive hydration leads to a more shallow increase of $K_{SC,dry/don}$ with $\omega_{SC,dry}^{aqu}$ with s_{aqu} best mimicking the experimental slope.

As a second influencing factor the volume fraction of the aqueous phase available for compound uptake was investigated. So far we considered the whole aqueous phase accessible for compound dissolution although it is well known that substantial portions of water are bound to SC proteins and natural moisturizing factors. It has long been recognized for liposomes that water that is bound strongly to lecithin is non-accessible for compound partitioning (247). This concept has also been adopted for hydration of SC keratin (26). Hadgraft et al. as well as others determined a portion of $\omega_{SC,dry}^{aqu,bound}$ as bound water ($\omega_{SC,dry}^{aqu,bound}$ being the weight of bound water per weight of dry SC) which would consequently be unavailable for partitioning. Any additional

water is considered free water with dissolution properties exactly as bulk water. A bound water fraction can easily be implemented into the model. $\omega_{SC,dry}^{aqu,bound}$ is transferred to $\phi_{SC,hyd}^{aqu,bound}$ as described in *insert II* which is then subtracted from $\phi_{SC,hyd}^{aqu}$:

Equation 6-31

$$K_{SC,dry/don} = \frac{\phi_{SC,hyd}^{lip} K_{lip/don} + \left(\phi_{SC,hyd}^{aqu} - \phi_{SC,hyd}^{aqu,bound} \right) K_{aqu/don}}{\phi_{SC,hyd}^{SC,dry}}$$

To illustrate the dependence of $K_{SC,dry/don}$ on $\omega_{SC,dry}^{aqu,bound}$ the level of $\phi_{SC,hyd}^{aqu,bound}$ was varied (Figure 6-5C). For $\phi_{SC,dry}^{aqu} \leq \phi_{SC,dry}^{aqu,bound}$ the modulus in Equation 6-31 is zero so that the term describing the affinity to the aqueous compartment is deleted. In other words if the number of water molecules within the SC is smaller than the number of water binding sites then all water will be bound and none will be available for compound dissolution. $K_{SC,dry/don}$ will now exclusively be determined by uptake into the SC lipids and $K_{SC,dry/don}$ against $\omega_{SC,dry}^{aqu}$ gives a straight line parallel to the x-axis (Figure 6-5C). For $\phi_{SC,dry}^{aqu} > \phi_{SC,dry}^{aqu,bound}$ any additional water will again be available for compound dissolution and $K_{SC,dry/don}$ increases linearly with $\omega_{SC,dry}^{aqu}$ (Figure 6-5C). However, the slope will depend on the height of $\omega_{SC,dry}^{aqu,bound}$. $\omega_{SC,dry}^{aqu,bound} = 0.34$ is indicated by a bold dotted line. Figure 6-5D compares the estimate for $\omega_{SC,dry}^{aqu,bound} = 0.34$ (bold dotted line) and $s_{aqu} = 15$ mg/ml with the experimental data (open squares). Both correction strategies offer an equally good representation of the slope of the experimental data. The problem of overemphasising the offset of the experimental curve is not solved by either correction strategy.

Insert II - The volume fractions of the SC compartments

Conventionally water, lipid or protein content within SC is expressed as weight fractions relative to the weight of dry SC, for example $\omega_{SC,dry}^{lip} = w_{lip} / w_{SC,dry}$. For convenience and easy comparison with other authors we also use weight fractions for representation of data. However, for calculations we need volume fractions relative to the volume of dry as well as hydrated SC. This section will explain how weight and volume fractions are related. The derivation of $\phi_{SC,hyd}^i$ from $\omega_{SC,dry}^i$ will be shown here exemplarily for $\phi_{SC,hyd}^{lip}$ for M1 but can be done analogously for all other compartments as well as for M2. We assume dry SC to be composed of 30% w/w lipids, i.e. $\omega_{SC,dry}^{lip} = 0.3$ and 70% w/w proteins: $\omega_{SC,dry}^{pro} = \omega_{SC,dry}^{SC,dry} - \omega_{SC,dry}^{lip} = 1 - \omega_{SC,dry}^{lip} = 0.7$. These are empirical values recorded in our lab *in vitro* for female abdominal skin of 14 different patients in 136 samples by lipid extraction of freeze-dried SC and weighing. $\omega_{SC,dry}^{cpe}$ was previously determined to be 0.07 (1) so that $\omega_{SC,dry}^{ker} = \omega_{SC,dry}^{pro} - \omega_{SC,dry}^{cpe} = 0.63$. Due to the definition in Equation 6-2 we obtain $\omega_{SC,hyd}^{lip} = w_{lip} / (w_{SC,dry} + w_{aqu})$ where the last identity results from dividing both numerator and denominator by $w_{SC,dry}$:

$$\omega_{SC,hyd}^{lip} = w_{lip} / (w_{SC,dry} (w_{SC,dry} / w_{SC,dry} + w_{aqu} / w_{SC,dry})) = \omega_{SC,dry}^{lip} / (1 + \omega_{SC,hyd}^{aqu}).$$

Therefore, $\omega_{SC,hyd}^i$ varies depending on the extent of SC hydration $\omega_{SC,hyd}^{aqu}$ in contrast to $\omega_{SC,dry}^i$ which is always constant. Relating this relationship to the specific densities the volume fractions of the respective compartments are calculated: $\phi_{SC,hyd}^{lip} = \omega_{SC,hyd}^{lip} \rho_{SC,hyd} / \rho_{lip}$ with the density of

hydrated SC defined as $\rho_{SC,hyd} = 1 / (w_{SC,dry}^{lip} / \rho_{lip} + w_{SC,dry}^{pro} / \rho_{pro} + w_{SC,dry}^{aqu} / \rho_{aqu})$. For dry SC and SC lipids the following densities are reported in literature: $\rho_{SC,dry} = 1.3 \text{ g/cm}^3$, and $\rho_{lip} = 0.973 \text{ g/cm}^3$ (2, 3). The density of SC proteins can be calculated from $\rho_{SC,dry}$ as shown here for M1: $\rho_{SC,dry} = w_{SC,dry} / V_{SC,dry} = w_{SC,dry} / (w_{lip} / \rho_{lip} + w_{pro} / \rho_{pro})$. Dividing both numerator and denominator by $w_{SC,dry}$ this relationship may be expressed in terms of weight fractions:

$$\rho_{SC,dry} = w_{SC,dry} / (w_{SC,dry} (w_{lip} / (w_{SC,dry} \rho_{lip}) + w_{pro} / (w_{SC,dry} \rho_{pro}))) = 1 / (w_{SC,dry}^{lip} / \rho_{lip} + w_{SC,dry}^{pro} / \rho_{pro})$$

After reorganisation for ρ_{pro} the protein density was calculated as 1.52 g/cm^3 . This value is well within the experimentally determined range (4). We assumed ρ_{ker} and ρ_{cpe} to be equal to ρ_{pro} .

$$\rho_{pro} = \omega_{SC,dry}^{pro} / (1 / \rho_{SC,dry} - \omega_{SC,dry}^{lip} / \rho_{lip})$$

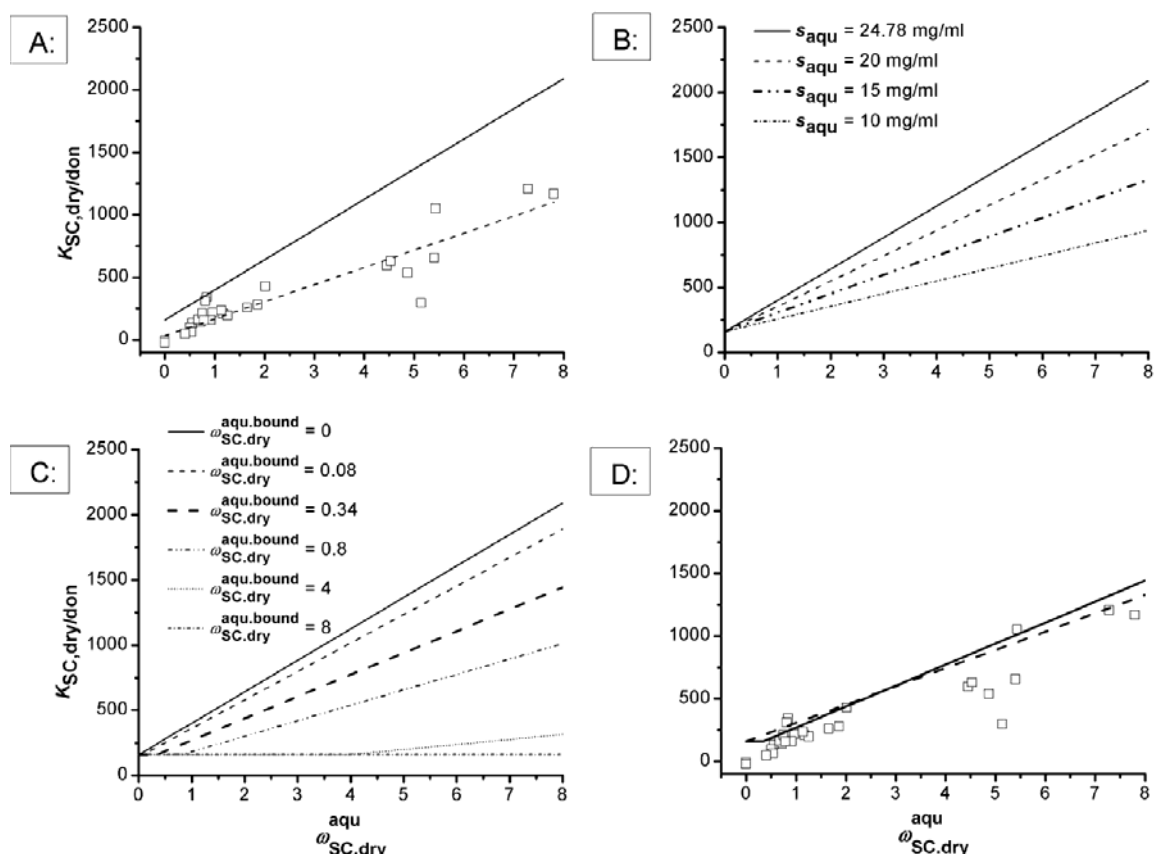


Figure 6-5 Comparison of experimental and calculated $K_{SC,dry/don}$ as a function of $\omega_{SC,dry}^{aqu}$ for caffeine. (A): The model overestimates the impact of hydration on $K_{SC,dry/don}$ (open squares: experiment; dashed line: linear fit of experimentally determined $K_{SC,dry/don}$ against $\omega_{SC,dry}^{aqu}$; straight line: calculated $K_{SC,dry/don}$ for $0 \leq \omega_{SC,dry}^{aqu} \leq 8$). (B and C) results of the optimization strategies: (B: effect of a reduction of s_{aqu} ; C: effect of an increasing bound water fraction). (D): The experimental data is compared to optimized predictions. (open squares: experiment; bold dashed line: s_{aqu} reduced to 15 mg/ml; bold straight line: bound water fraction of $\omega_{SC,dry}^{aqu} = 0.34$.)

6.4.4.2 Keratin binding compounds: flufenamic acid and testosterone

Figure 6-6A compares predictions of M1 (Equation 6-18 and Equation 6-19) with experimental results on the dependency of $K_{SC,dry/don}$ on c_{don} for varying degrees of SC hydration in the range of $\omega_{SC,dry}^{aqu} = 0 - 8$. Experimental data are shown as means and standard deviation for dry (open squares) and hydrated SC (open triangles: hydrated above water; filled circle: SC hydrated above NaCl solution; filled star: SC hydrated within water). Results predicted with M1 are shown as lines (bold dashed line: $\omega_{SC,dry}^{aqu} = 0$).

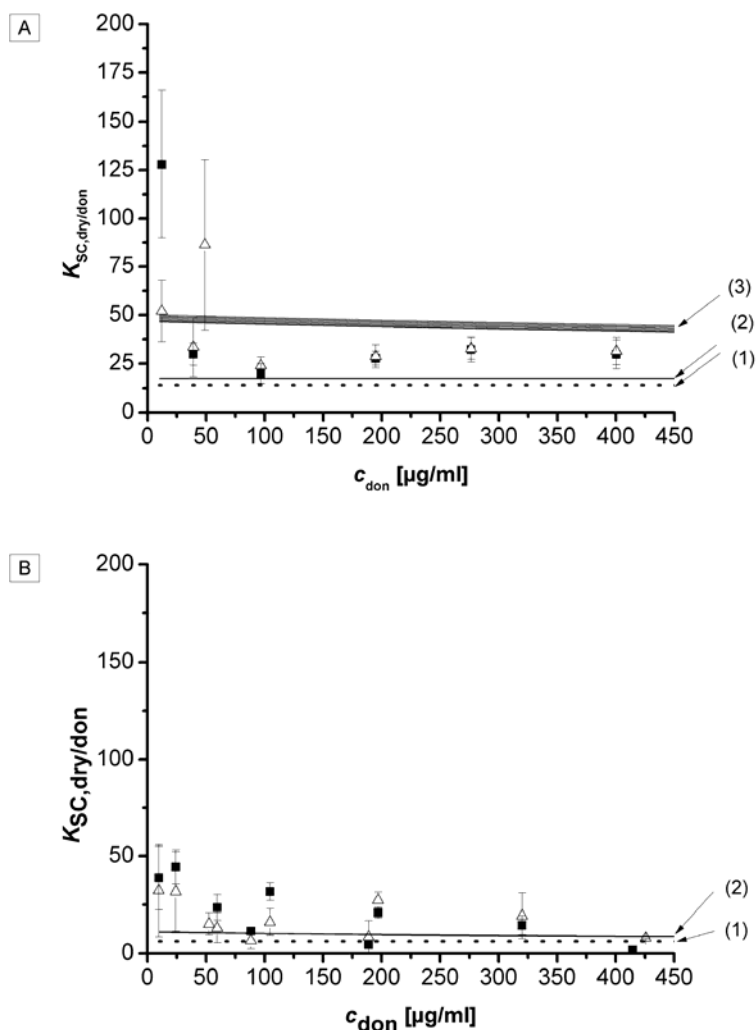


Figure 6-6 M1: Comparison of experimental and calculated $K_{SC,dry/don}$ as a function of c_{don} for varying $\omega_{SC,dry}^{aqu}$ for A: flufenamic acid and B: testosterone. (Experimental results: dry *stratum corneum* (filled square); *stratum corneum* hydrated (open triangle)). Calculated results, Fig. 5A: (1) $\omega_{SC,dry}^{aqu} = 0$; (2) $pH_{aqu} = 5.5$; $0 < \omega_{SC,dry}^{aqu} \leq 8$; (3) $pH_{aqu} = 6.5$; $0 < \omega_{SC,dry}^{aqu} \leq 8$; Fig. 5B: (1) $\omega_{SC,dry}^{aqu} = 0$; (2) $0 < \omega_{SC,dry}^{aqu} \leq 8$.) For flufenamic acid the influence of the pH_{aqu} was investigated using the upper and lower margin determined by a tape-stripping method with surface parallel pH electrodes (197).

Figure 6-6A gives the results for FFA. Here additionally two different values for pH_{aqu} were considered. In M1 according to Equation 6-18 $K_{SC,dry/don}$ for dry SC is exclusively influenced by the compound affinity to the lipid compartment. As the lipid concentration c_{lip} is described via a simple proportionality (Equation 6-8) M1 predicts $K_{SC,dry/don}$ of dry SC to be independent of c_{don} . M1 implicates a donor concentration dependence only for hydrated SC which is accounted for by a Langmuir isotherm (Equation 6-9). Considering a pH_{aqu} of 5.5 (which was approximately the lower margin of pH-values investigated in SC (197)) the solubility of FFA in the aqueous

compartment is very low (Table 6-2). This leads to a very low $K_{\text{aqu/don}}$ which enters Equation 6-19 in the term describing the compound affinity to the aqueous phase and the Langmuir isotherm quantifying protein binding. Therefore at $\text{pH}_{\text{aqu}} 5.5$ M1 predicts $K_{\text{SC,dry/don}}$ to be practically independent of SC hydration and independent of donor concentration. At $\text{pH}_{\text{aqu}} 6.5$, which would be approximately the upper margin of pH values investigated in human SC (197), $K_{\text{aqu/don}}$ is an order of magnitude higher than at $\text{pH}_{\text{aqu}} 5.5$. The effect on $K_{\text{SC,dry/don}}$ is however still limited. Compared to dry SC M1 predicts that hydration of the SC provokes a four to five times elevated $K_{\text{SC,dry/don}}$. Finally, the absolute level of hydration is rather unimportant such as in the range of $0 < \omega_{\text{SC,dry}}^{\text{aqu}} \leq 8$ an increasing $\omega_{\text{SC,dry}}^{\text{aqu}}$ influences $K_{\text{SC,dry/don}}$ negligibly (Figure 6-6). The range of $K_{\text{SC,dry/don}}$ predicted by M1 within the pH_{aqu} range of 5.5 and 6.5 includes the major portion of the experimental values. At $\text{pH}_{\text{aqu}} 5.5$ M1 further correctly predicts the independency of hydration. However, obviously in both cases M1 is not able to correctly express the concentration dependence of $K_{\text{SC,dry/don}}$ at low c_{don} that was seen in the experiment.

Figure 6-6B shows the results for TST. Here experimental partition coefficients were in the range of 2 to 32. M1 predicts $K_{\text{SC,dry/don}}$ of 6.28 for dry SC and 8.47 to 11.42 for hydrated SC. Both are independent of $\omega_{\text{SC,dry}}^{\text{aqu}}$ as well as c_{don} . Due to the similar $K_{\text{aqu/don}}$ of FFA at $\text{pH}_{\text{aqu}} 5.5$ and TST the influence of hydration on $K_{\text{SC,dry/don}}$ is similarly negligible as for FFA.

Figure 6-6B shows the results for TST. Experimental partition coefficients were in the range of 1.81 ± 0.24 to 50.13 ± 22.53 . In the concentration range below $50 \mu\text{g/ml}$ $K_{\text{SC,dry/don}}$ increases with decreasing c_{don} . In contrast M1 predicts $K_{\text{SC,dry/don}}$ of 6.28 for dry SC and 8.47 to 11.42 for hydrated SC, both being independent of $\omega_{\text{SC,dry}}^{\text{aqu}}$ as well as c_{don} . Due to the similar $K_{\text{aqu/don}}$ of FFA at $\text{pH}_{\text{aqu}} 5.5$ and TST the influence of hydration on $K_{\text{SC,dry/don}}$ is similarly negligible as for FFA.

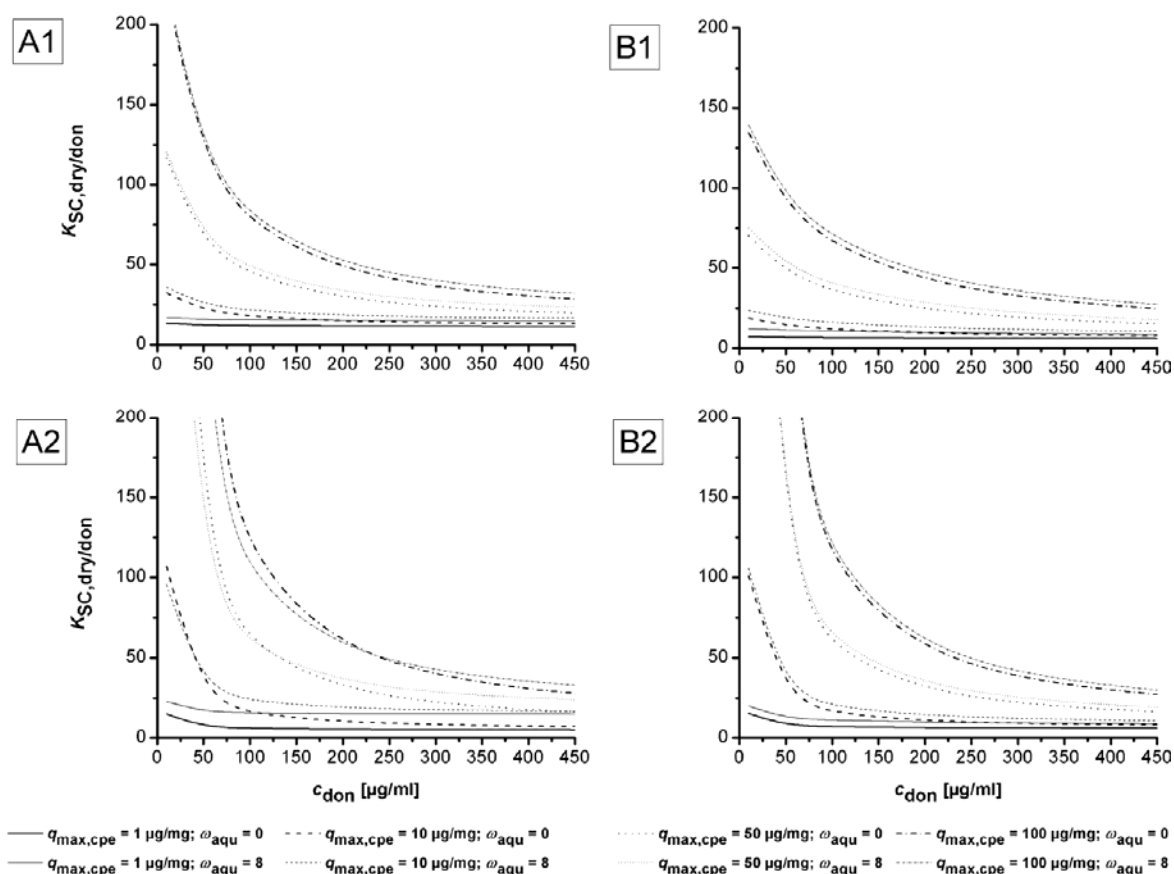


Figure 6-7 M2; systematic variation of the cornified envelope maximum binding capacity $q_{max,cpe}$ (1, 10, 50, and 100 $\mu\text{g/mg}$) and the cornified envelope binding constant k_{cpe} A: FFA; B: TST. A1 + B1 $k_{cpe} = 10^{-3} \text{ ml}/\mu\text{g}$. A2 + B2 $k_{cpe} = 10^3 \text{ ml}/\mu\text{g}$. (bold lines: $\omega_{SC,dry}^{aqu} = 0$; thin lines: $\omega_{SC,dry}^{aqu} = 8$)

The predictions of M2 (Equation 6-20 and Equation 6-21) are shown in Figure 6-7 (left hand-side FFA, right hand-side TST). Figure 6-7A1 and B1 were calculated assuming $k_{cpe} = 10^{-3} \text{ ml}/\mu\text{g}$ which would be considered as a kind of lower margin where the compound affinity to the cpe is very limited. This is combined with different levels of maximum binding capacity $q_{max,cpe}$ of 1, 10, 50, and 100 $\mu\text{g/mg}$, i.e. from a rather moderate to a substantial maximum binding capacity. Furthermore the influence of the aqueous compartment was considered by predicting $K_{SC,dry/don}$ for the lower and upper limit of SC hydration i.e. $\omega_{SC,dry}^{aqu} = 0$ (bold lines) and $\omega_{SC,dry}^{aqu} = 8$ (thin lines). (A1 and B1) At $k_{cpe} = 10^{-3} \text{ ml}/\mu\text{g}$ a $q_{max,cpe} = 1 \mu\text{g/mg}$ is not sufficient to provoke a concentration dependence of $K_{SC,dry/don}$. With increasing $q_{max,cpe}$ two effects are obvious: (i) the concentration dependence at low c_{don} becomes more pronounced, i.e. the slope of $K_{SC,dry/don}$ against c_{don} becomes steeper, (ii) $K_{SC,dry/don}$ in the whole concentration range is increased, with the increase being more pronounced at lower

c_{don} . An increase in $q_{max,cpe}$ however does not lead to an increased influence of $\omega_{SC,dry}^{aqu}$ on $K_{SC,dry/don}$. These trends are evident both in the predictions for FFA and TST. For TST at identical combinations of k_{cpe} and $q_{max,cpe}$ the slope of the curve at low c_{don} , i.e. in the range where the cpe shows its influence is slightly less steep than with FFA.

Figure 6-7A2 and B2 were calculated assuming $k_{cpe} = 10^3$ ml/ μ g i.e. an upper margin marking a high compound affinity to the cpe. This is again combined with different levels of $q_{max,cpe}$ of 1, 10, 50, and 100 μ g/mg. Again the influence of the aqueous compartment was considered by calculating the results for the lower and upper limit of SC hydration $\omega_{SC,dry}^{aqu} = 0$ (bold lines) and $\omega_{SC,dry}^{aqu} = 8$ (thin lines). Now, already even for $q_{max,cpe} = 1$ mg/mg there is a (however limited) non-linear concentration influence on $K_{SC,dry/don}$. In general compared to the estimates with $k_{cpe} = 10^{-3}$ ml/ μ g (i) the absolute height of the predicted $K_{SC,dry/don}$ is higher, especially in the lower range of c_{don} , (ii) the slope of $K_{SC,dry/don}$ against c_{don} is steeper (the first partially being a consequence of the second).

In Figure 6-8A1 and B1 the experimental results are shown together with that combination of $q_{max,cpe}$ and k_{cpe} that achieves the best prediction according to M2 (again A marks the results for FFA while B will be TST). These are for both FFA at pH_{aqu} 5.5 and TST: $q_{max,cpe} = 10$ μ g/mg and $k_{cpe} = 10^3$ ml/ μ g. There will probably be further suitable combinations of $q_{max,cpe}$ and k_{cpe} being able to correctly express the experimental results. Therefore it was tested whether the binding parameters measured with bovine keratin could serve to give a first estimate of the binding properties of the cpe (Figure 6-8A2 and B2). For FFA these estimates express the experimental results at low c_{don} less correctly than the “optimized” set of $q_{max,cpe}$ and k_{cpe} . However, the overall range of the experimental values is expressed in the simulation.

It shall be noted that in case of TST all results of M2 predict a concentration dependence of $K_{SC,dry/don}$ at c_{don} lower than the concentration range investigated in the experiment. Further investigations will require methods with a higher analytical sensitivity to confirm this prediction. For TST the estimate using $q_{max,ker}$ and k_{ker} for describing the binding properties of the cpe expresses the experimental data better than the “optimized” set of $q_{max,cpe}$ and k_{cpe} .

In summary, M2 however, not M1 is able to predict the concentration dependence of $K_{SC,dry/don}$ that is seen in the experiment. It shall be noted that the predicted influence of hydration on $K_{SC,dry/don}$ for protein binding permeants with limited water solubility is profoundly different from hydrophilic compounds. For protein binding compounds hydration acts in a two-state fashion: there is a visible difference in $K_{SC,dry/don}$ at zero hydration ($\omega_{SC,dry}^{aqu} = 0$) compared to any other hydration state ($\omega_{SC,dry}^{aqu} > 0$). However, there is practically no differentiation according to the actual water weight fraction at $\omega_{SC,dry}^{aqu} > 0$. This is equally predicted by model M1 and M2 for both FFA and TST and is depicted e.g. in Figs. 6-8. This is also in line with Figure 6-3B and C which shows that the hydration method does not influence $K_{SC,dry/don}$ of FFA and TST.

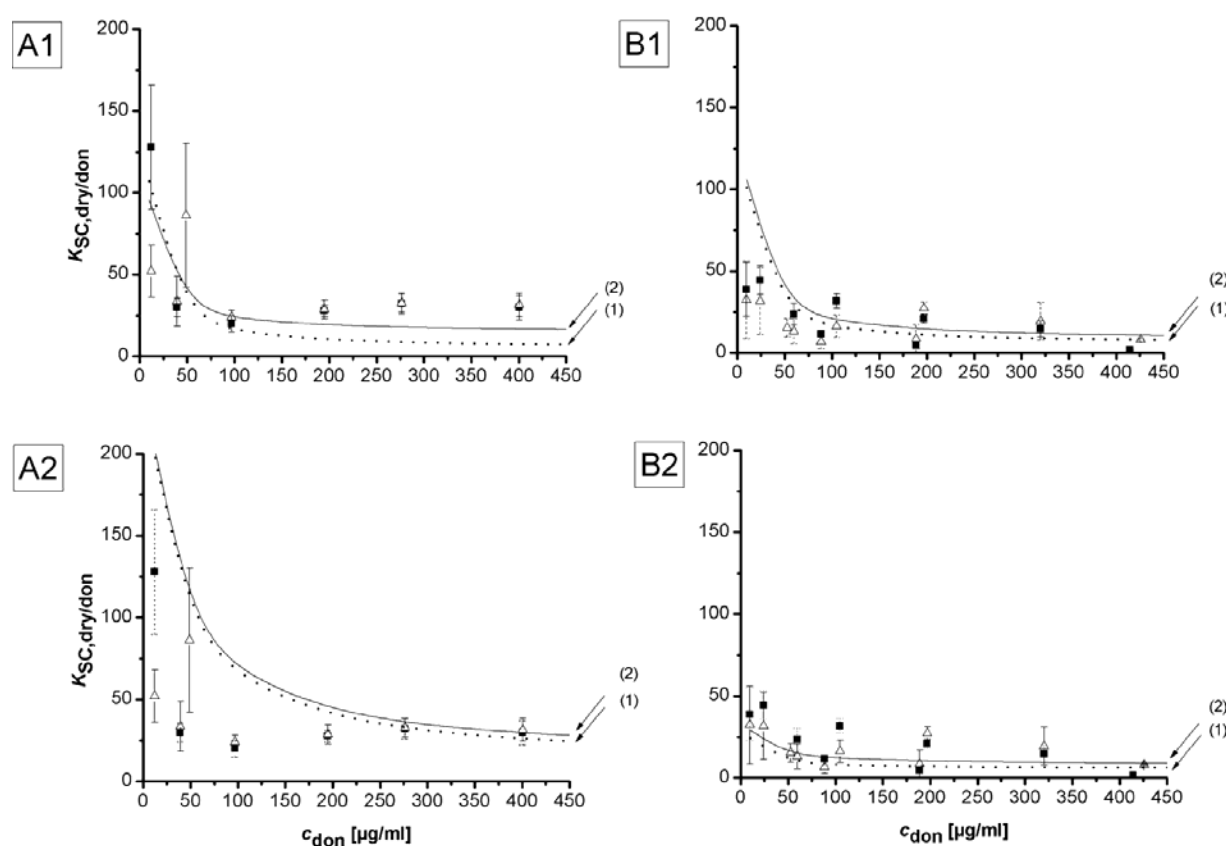


Figure 6-8 M2; comparison of experimental results of flufenamic acid and testosterone with optimized binding parameters for cpe (A1: flufenamic acid: $q_{max,cpe} = 10 \mu\text{g}/\text{mg}$, $k_{cpe} = 103 \text{ ml}/\mu\text{g}$, $\text{pH}_{aqu} = 5.5$; B1: testosterone: $q_{max,cpe} = 10 \mu\text{g}/\text{mg}$, $k_{cpe} = 103 \text{ ml}/\mu\text{g}$). Assuming the binding properties of the cornified envelope proteins to be identical to keratin, i.e. $q_{max,cpe} = q_{max,ker}$ and $k_{cpe} = k_{ker}$ was a good first estimate of $K_{SC,dry/don}$ (A2: flufenamic acid, B2: testosterone). (Experimental results: dry *stratum corneum* (filled square); hydrated *stratum corneum* (open triangle)). Calculated results: (1) $\omega_{SC,dry}^{aqu} = 0$; (2) $\omega_{SC,dry}^{aqu} = 8$).

6.5 DISCUSSION

After the present experimental findings there can be no doubt that hydration plays a central role in SC partitioning of water soluble molecules. Obviously CAF has a higher SC affinity than FFA and TST. At first sight this is contradictory to predictions that foot on a positive correlation between $\log K_{\text{Oct/w}}$ and the apparent permeability coefficient (85, 89, 253). This means that a hydrophilic compound such as CAF permeates the skin poorly due to a low affinity to the highly lipophilic character of the SC. This is evidently true for aqueous donor media. In addition the cited QSARs (quantitative structure permeability relationships) rely on a lipid permeation pathway that excludes the trans-cellular route.

It is well established that occlusion effectively enhances skin permeation of hydrophilic compounds by increasing the partitioning into the SC (202). The theoretical analysis offers a very simple method to predict the influence of the SC water content on SC partitioning. In addition, the presented experimental setup allows an easy investigation of the effect of hydration on $K_{\text{SC,dry/LVP}}$. In contrast, the Franz cell, an experimental setup that is often used in *in vitro* skin permeability measurements, is not suited for addressing this kind of question as the skin membrane will always be fully hydrated through the aqueous acceptor medium.

As a first approach to describe the interactions of CAF with the aqueous domain quantitatively the dissolution properties were assumed to be comparable to physiological buffer. However, this led to an overestimation of the impact of hydration on $K_{\text{SC,dry/don}}$. Two strategies were followed in order to reduce the affinity of CAF to the aqueous compartment. Both the reduction of the aqueous solubility and the introduction of a non-accessible water fraction could successfully reduce the slope of $K_{\text{SC,dry/don}}$ with $\omega_{\text{SC,dry}}^{\text{aqu}}$. The aqueous solubility of CAF depends on temperature, and may be increased by the presence of organic acids or their alkali salts, e.g., benzoates, salicylates or citrates while no such effect is reported for phosphate ions contained in the Soerensen buffer (172). Although Kasting et al. advocated for a shallow transition from bound to free water state which could result in a likewise shallow transition of dissolution properties a two-state analysis was sufficient to reduce the dependence of $K_{\text{SC,dry/don}}$ on $\omega_{\text{SC,dry}}^{\text{aqu}}$ to values as found *in vitro* (26, 249). The picture may be significantly complicated if the binding sites of water and drug compounds are identical. Then the magnitude of the binding constant would

determine whether the drug is possibly able to displace water from its binding site. However both strategies fail to reduce the overestimated offset of the predicted $K_{SC,dry/don}$ at $\omega_{SC,dry}^{aqu} = 0$ as this is only influenced by the compound affinity to the lipid compartment (Equation 6-18). According to section 6.2.5.1 this was calculated from $K_{lip/Soer,7.4}$, $s_{Soer,7.4}$, and s_{LVP} . Prerequisite for Equation 6-26 is that all interacting phases are non-miscible. It is known that at high hydration water intercalates into SC lipids. The improved hydrophilicity of the lipid bilayer could promote the lipid affinity of hydrophilic compounds such as CAF such that the experimental value for $K_{lip/Soer,7.4}$ is slightly overestimated. Equally, a penetration of LVP into SC lipids should lower the affinity of CAF to the SC lipids as the solubility of CAF in LVP is significantly lower than in SC lipids ($K_{lip/LVP}$ of CAF is highly positive). Both mechanisms could account for an overestimation of $K_{lip/LVP}$ of CAF and thus of $K_{SC,dry/don}$ at $\omega_{SC,dry}^{aqu} = 0$.

For a number of compounds adsorption to isolated keratin powder was reported (233, 234, 241, 242). The question is whether keratin binding is possible in the morphological context of the membrane. Due to the unique morphology of the human SC a direct contact between keratin and intercellular lipids is highly unlikely (29). Therefore in M1 the possibility of lipid-protein interactions was ruled out completely. Instead it was assumed that compound keratin interactions will be mediated via intra-corneocyte water which in turn communicates with intercellular lipids. However, potentially protein binding compounds usually are lipophilic and therefore poorly water soluble. This was tested with the two keratin binding compounds FFA and TST that differ in their maximum binding capacity and keratin affinity constant. Varying pH_{aqu} predictions of M1 effectively showed that if there are substantial FFA concentrations within the corneocyte water $K_{SC,dry/don}$ will not so much be concentration dependent but sensitive to SC hydration. It is therefore highly unlikely that FFA enters intra-corneocyte water to a significant extent. It remains to be analysed whether the weakly acidic corneocyte pH could facilitate the corneocyte solubility of bases and thus mediate keratin access of lipophilic bases. This could provide the explanation for the significant concentration dependence of $K_{SC,dry/don}$ of scopolamine (119) although this may also have been a consequence of binding to the cpe.

Summing up these findings the concentration dependence of $K_{SC,dry/don}$ seen in the experiment is much more likely to be a consequence of protein access directly via

the lipids and not via the detour of the aqueous corneocyte phase. This can only reasonably be assumed for structures as the cpe and corneodesmosomes although we did not consider the corneodesmosomes explicitly in our analysis. Compared to the major SC component keratin such structures encompass only a very small fraction of the whole SC (1). Therefore the main question addressed with M2 was whether this might be enough to account for the measured effects. Our theoretical parameter study systematically varying the binding parameters to the cpe could show that this is indeed possible if not likely. As this approach is not feasible for applying the model to a larger database $q_{\max, \text{ker}}$ and k_{ker} could be used as estimates for $q_{\max, \text{cpe}}$ and k_{cpe} . This relies of course on the assumption that the binding properties of the cpe can be expressed by keratin at all, as keratin is only one of several proteins forming the cpe. In case of TST the uncertainty of $q_{\max, \text{ker}}$ (compare section 4.4.4.2) becomes relevant. By definition the maximum free concentration available for binding to the cpe equals c_{lip} . The lipid solubility of TST is sufficiently high that the non-linear part of the isotherm is reached. For FFA $q_{\max, \text{ker}}$ was estimated with higher certainty as due to a higher aqueous solubility roughly 70% saturation of binding sites were achieved (239).

The great importance of considering a corneocyte interactions of not only water soluble but also lipophilic, protein binding molecules shall be explained consulting Vieth and Sladek (219) who provided a kinetic interpretation of the dual sorption theory. They assumed that the kinetics of immobilization are very rapid compared to the diffusion rate of the mobile component so that the diffusion is rate controlling and a local equilibrium between mobile and immobilized species is always maintained throughout the medium. Only the mobile species will be able to participate in the concentration gradient and thus in the diffusion process while the adsorbed species is completely immobilized and does not participate in the diffusive flux. This leads to significant differences in the effective and true diffusion coefficient and a retardation of adsorption equilibrium as some compound is removed from the pool of diffusing species. The magnitude of the affinity constant k , representing the ratio of the rate constant of adsorption and desorption and thus being an indicator of the binding strength, will influence the extent to which the effective diffusion coefficient will be reduced compared to a pure partitioning process. Naegel et al. recently noticed that the corneocyte diffusivity D_{cor} of FFA is overestimated when the interaction with the corneocyte phase is described solely via a partition coefficient (170). Furthermore a

large German multicentre-study aiming at a validation of reconstructed human *epidermis* models failed irrespective of the skin model investigated to predict experimental apparent permeability coefficient of a set of test compounds by established QSAR-analyses (quantitative structure permeability relationship) that base only on molecular weight and lipophilicity parameters such as those mentioned above, or open-source software such as DermWin and Skinperm (254). It may be speculated that predictions may be improved when taking into account protein binding and hydration effects with the help of the theoretical analysis or the proposed experimental procedure.

After the present experimental findings there can be no doubt that hydration plays a central role in SC partitioning of water soluble molecules. Obviously CAF has a higher SC affinity than FFA and TST. At first sight this is contradictory to predictions that foot on a positive correlation between $\log K_{\text{Oct/w}}$ and the apparent permeability coefficient (85, 89, 253). This means that a hydrophilic compound such as CAF permeates the skin poorly due to a low affinity to the highly lipophilic character of the SC. This is evidently true for aqueous donor media. In addition the cited QSARs rely on a lipid permeation pathway that excludes the trans-cellular route.

6.6 CONCLUSION

Equilibration experiments with gradually hydrated SC using a non-aqueous donor medium are an efficient method to investigate the impact of water uptake into the SC on SC partitioning of compounds. Together with keratin binding studies they offer experimental tools to investigate the mechanism of corneocyte interactions of compounds partitioning into the SC. The corneocytes are a distribution compartment for both lipophilic and hydrophilic compounds. Hydrophilic water soluble molecules will predominantly interact with water that is present within healthy SC *in vivo* or additional water that has entered the corneocytes through hydration in the course of occlusive conditions. For lipophilic compounds the aqueous compartment does not play a role in SC partitioning. Although these compounds could be shown to bind to isolated keratin this is probably meaningless for the SC-donor partition coefficient. Due to their low aqueous solubility only a very limited number of molecules will find access to intra-corneocyte proteins. Thus keratin binding is limited by the aqueous solubility of a compound. An involvement of extra-cellular proteins might be of much more importance for SC uptake of lipophilic protein binding molecules.

SUMMARY

Mathematical modeling of skin transport is considered a valuable alternative to *in vitro* and *in vivo* investigations especially considering ethical and economical questions. Mechanistic diffusion models describe skin transport by solving Fick's second law of diffusion in time and space; however models relying entirely on a consistent experimental data set are missing.

A non-steady state-*in silico* model of *in vitro* diffusion experiments was developed. The two-dimensional model membrane consists of a biphasic *stratum corneum* and an additional compartment for the homogeneous viable *epidermis/dermis*. The underlying geometry for the *stratum corneum* is of brick-and-mortar character, meaning that the corneocytes are completely embedded in the lipid phase. All phases are modelled with homogeneous partition and diffusion coefficients.

It was the declared objective of this work to put the model on an experimental basis. This avoids any primary assumptions that are necessary if input data for membrane affinities and diffusion coefficients are estimated from physico-chemical properties of the diffusant such as size and lipophilicity methods, or fitting experimental skin permeation or penetration data to a one-dimensional solution of the diffusion equation.

Therefore methods were developed to measure the partition coefficients between lipids and donor ($K_{lip/don}$), corneocytes and lipids ($K_{cor/lip}$), and viable deeper skin layers and lipids ($K_{DSL/lip}$) and the diffusion coefficients within lipids and DSL (D_{lip} and D_{DSL}) and approximate the diffusion coefficient within the corneocytes (D_{cor}). The data were generated for two model compounds using human female abdominal skin. These are flufenamic acid and caffeine that feature different skin permeation characteristics.

$K_{lip/don}$ was determined in an equilibration experiment with extracted human *stratum corneum* lipids. For the experiment the lipids were put on an inert membrane filter support. The coating of the filters was reproducible as ascertained by measuring the increase of mass and thickness. High performance thin layer chromatography showed that the ratio of cholesterol, cholesterol esters, triglycerides, free fatty acids, and ceramides of the extracted lipids was within the range that could be expected for excised human abdominal skin. Apart from the characteristic composition of the *stratum corneum* lipids the ordering within the bilayers is tantamount to guaranteeing

an efficient barrier structure and transport characteristics. Therefore differential scanning calorimetry (DSC) and wide angle X-ray powder diffraction analysis (WAXD) were performed to analyze the lipid structure. DSC revealed that after extraction the lipids re-crystallized as lamellae with a hexagonal and/or orthorhombic lateral packing. The presence of the orthorhombic phase was then also confirmed by WAXD. Significant amounts of lipids in a non-physiological amorphous or liquid crystalline state were attributed to the high amount of triglycerides that is not seen *in vivo*. This is an artefact due to contamination of the SC lipids with lipids from the subcutaneous fat during surgery and transport.

$K_{\text{cor/lip}}$ and $K_{\text{DSL/lip}}$ were derived from experimental data on *stratum corneum*-donor-, lipid-donor- and *stratum corneum*-viable deeper skin layers partition coefficients ($K_{\text{SC/don}}$, $K_{\text{lip/don}}$ and $K_{\text{SC/DSL}}$) considering volume ratios of the lipid and corneocyte phases that are normally found in human *stratum corneum*.

$K_{\text{SC/don}}$ was determined in equilibration measurements and by non-linear fitting of *stratum corneum* concentration-depth profiles to a one-dimensional solution of the diffusion equation. Both methods returned very similar estimates of $K_{\text{SC/don}}$ (and hence also $K_{\text{cor/lip}}$ and $K_{\text{SC/DSL}}$) for caffeine while for flufenamic acid the estimates varied distinctly. The reason for this behaviour could not finally be identified. It was speculated that depth dependent changes in barrier function, or keratin binding might be involved. The fitting method further revealed a time dependency of $K_{\text{SC/don}}$ hinting at changes of the membrane properties or slow equilibration processes.

Apparent diffusion coefficients in the *stratum corneum* lipids and viable deeper skin layers D_{lip} and D_{DSL} were calculated based on measurements of *steady state* flux across the membrane filter supports coated with *stratum corneum* lipids or dermatomized viable deeper skin layers, respectively. However, this method could not be applied to measure the apparent diffusion coefficient inside the corneocytes. Therefore D_{cor} was estimated based on an approximation, which uses D_{lip} and $K_{\text{cor/lip}}$ (measured as described above) and D_{SC} . D_{SC} was determined from the *steady state* flux across isolated human *stratum corneum* and by non-linear fitting of *stratum corneum* concentration-depth profiles to a one- dimensional solution of the diffusion equation. As with $K_{\text{SC/don}}$ the fitting method hinted at time-dependent changes inside the membrane, as D_{SC} for both caffeine and flufenamic acid was found to decrease within the early hours of skin absorption. This might possibly be due to swelling of the membrane which gradually changes the effective pathlength.

The quality of the model was evaluated by a comparison of concentration-*stratum corneum*-depth-profiles of the experiment with those of the simulation. The calculations were performed at the chair of “Simulation in Technology” at Heidelberg University under Prof. Dr. Gabriel Wittum. The outlined approximation of the corneocyte diffusion coefficient is highly sensitive to membrane geometry in the range of the experimentally determined values for D_{lip} , D_{SC} , and $K_{cor/lip}$ for caffeine and flufenamic acid. Starting with geometrical information that was derived from microscopical data for human skin, the estimate of D_{cor} was later reduced by one order of magnitude for caffeine and two orders of magnitude for flufenamic acid in order to receive an agreement between experiment and simulation.

As a main result of both experiments and simulation the corneocytes were shown to play a decisive role in skin transport for both model compounds. As expected from the different lipophilicity of both drugs flufenamic acid but not caffeine was shown to bind to keratin protein which forms the main body of the corneocytes and makes up for the largest weight fraction of dry *stratum corneum*.

In order to address this phenomenon further mechanisms of compound-corneocyte interactions were investigated in a combined experimental and theoretical approach. Experimental methods were developed to investigate compound-corneocyte interactions in terms of dissolution within water of hydration and protein binding and to quantify the extent of the concurrent mechanisms. The uptake of compounds into water of hydration was measured in a series of equilibration experiments using *stratum corneum* that was either dry or contained a known weight of water in the range of approximately 30 to 800 % wt/wt of dry *stratum corneum*. This was possible by pre-hydrating freeze-dried *stratum corneum* sheets at a constant relative humidity or by bathing within double distilled water and by using a non-aqueous vehicle for the equilibration experiments. Keratin binding was investigated in equilibration studies with keratin powder from bovine hoof and horn.

Results were presented for three compounds: caffeine, flufenamic acid, and testosterone. Two compartmental *stratum corneum* models M1 and M2 were formulated based on experimentally determined input parameters describing the affinity to lipids, proteins and water. M1 features a homogeneous protein compartment and considers protein interactions only via intra-corneocyte water. In M2 the protein compartment is sub-divided into a cornified envelope compartment interacting with inter-cellular lipids and a keratin compartment interacting with intra-

cellular water. As a first estimate the dissolution properties of water inside the membrane were assumed to be identical to bulk water. Binding constants and maximum binding capacities derived from studies with the model protein powdered bovine keratin were used for estimating both the interaction with the keratin compartment as well as the cornified envelope compartment.

For the non-protein binding caffeine which however features a high affinity to the aqueous phase, the impact of the aqueous compartment on *stratum corneum* partitioning was first overestimated but then could successfully be simulated after introducing a bound water fraction that is non-accessible for compound uptake. Only M2 correctly predicted *stratum corneum* partition coefficients of lipophilic, keratin binding compounds (flufenamic acid, testosterone) to depend on concentration. Consequently, lipophilic and hydrophilic compounds interact with corneocytes. The interactions of lipophilic compounds are probably confined to the corneocyte surface. Interactions with intracellular keratin may be limited by a low aqueous solubility of a molecule.

The simple biphasic two layer model of the human skin with homogenous partition and diffusion coefficients that was proposed initially provides a useful first estimate of skin absorption *in vitro*. However, the representation of the corneocyte compartment is probably too simple due to the following reasons that were determined in the course of this work, namely the binding affinity and the maximum binding capacity to corneocyte proteins. Also, for compounds with a high affinity to water the bound water fraction that is not accessible for compound uptake needs to be taken into account. Furthermore, a model of the partitioning and binding schemes inside the *stratum corneum* was proposed and could successfully be applied to explain *stratum corneum* partition coefficients of three model compounds with different *stratum corneum* affinities.

In the future the refinements of the corneocyte phase will have to be integrated in the diffusion model. It should also be used to precise the estimate of the corneocyte diffusion coefficient as now a differentiation between freely mobile and fixed substance is possible.

The model will further have to be validated with additional compounds in order to evaluate whether after including the newly identified parameters it can be used in a predictive way. The prerequisite for advancing from simulation to prediction will be to

find appropriate substitutes for the experimentally measured input parameters. As described, correlations between membrane-solvent- and octanol-water partition coefficients and between diffusion coefficients and compound size are well established. In contrast little is known about adequate estimates of compound binding to corneocyte proteins. In contrast, for another ubiquitous protein, namely serum albumin, there is a variety of binding data available as this is an important pharmacokinetic parameter influencing drug distribution after systemic absorption. Also several QSAR-models for the prediction of binding affinities to human serum albumin are available. Therefore it seems worthwhile to look for a relationship between binding to serum albumin and keratin binding. This could serve as a first orientation whether for the compound under investigation keratin binding needs to be considered in the modeling. It remains to be seen whether apart from that a direct correlation between both parameters can be established which could be employed in a predictive way.

Eventually, the diffusion model should be applicable to predicting skin absorption *in vivo*. Usually only a limited dose of a compound is available to the skin especially if pharmaceutical or cosmetical applications are concerned. With decreasing the volume that is applied to the skin processes inside the formulation such as the depletion of the active ingredient, interaction of formulation components with the skin and evaporation of formulation ingredients gain importance and therefore need to be integrated in the model.

Furthermore formulations for skin delivery are usually multi-component systems. The excipients play a complex role in the constitution of the vehicle and may influence the absorption of the active ingredient in terms of a permeation enhancement as well as a retardation. This is mainly due to complicated interaction of formulation excipients with the skin membrane. These may influence the affinity of the active drug to different membrane compartments as well as the diffusivity inside the membrane. The first step towards the integration of these influences into the model will be to investigate the skin absorption of typical formulation excipients. In this field recent advances include measuring the absorption of enhancers such as propylene glycol, oleic acid and water. Provided that a relationship between excipient concentration and membrane partitioning and diffusion of the active drug can be established the "co-permeation" of both components should be predictable.

And finally, for active ingredients dedicated for a trans-cutaneous delivery to the systemic circulation cutaneous metabolism and systemic distribution will have to be integrated in the model. For the latter problem solutions have been proposed in terms of combining diffusion models of the upper skin layers with pharmacokinetic models of the human body. On the other hand little is known about the consequences of metabolism on the absorption of drugs. Ubiquitous enzymes such as esterases and deaminases are active inside the viable skin layers and also enzymes of the cytochrome P450 family are present. Cutaneous metabolism has also been used as a therapeutic concept for topically applied ester-prodrugs that usually exhibit a higher lipophilicity which is beneficial for the permeation for otherwise poorly absorbed hydrophilic drugs.

ZUSAMMENFASSUNG

Die mathematische Modellierung des Transports von Substanzen über die Haut stellt insbesondere im Hinblick auf ethische und ökonomische Fragen eine wertvolle Alternative zu *in vitro* und *in vivo* Untersuchungen dar. Mechanistisch basierte Modelle beschreiben den Hauttransport mittels orts- und zeitaufgelösten Lösungen des Fick'schen Diffusionsgesetzes. Jedoch fehlen derzeit Modelle, die vollständig auf experimentellen Datensätzen beruhen.

Im Rahmen dieser Arbeit wurde ein nicht-*steady state-in silico* Modell zur Vorhersage von *in vitro* Diffusionsexperimenten über Humanhaut entwickelt. Die zweidimensionale Modellmembran besteht aus einem biphasigen *stratum corneum* und zusätzlich einem homogenen Kompartiment, das die lebende *Epidermis/Dermis* darstellt. Die *stratum corneum*-Geometrie beruht auf dem „Ziegelstein-Mörtel“-Modell. Das heißt, dass die Corneocyten vollständig in die Lipidphase eingebettet sind. Alle Phasen werden mit homogenen Verteilungs- und Diffusionskoeffizienten modelliert.

Es war das erklärte Ziel dieser Arbeit ein Diffusionsmodell vollständig auf Grundlage von experimentellen Daten zu entwickeln. Damit werden primäre Annahmen vermieden, die sonst notwendig sind um Eingangsparameter, die die Membranaffinität und die Diffusionskoeffizienten beschreiben, abzuschätzen. Dies erfolgt meist ausgehend von physikochemischen Eigenschaften der diffundierenden Spezies wie Größe und Lipophilie oder durch Kurvenanpassung gemessener Permeations- und Penetrationsdaten an eine eindimensionale Lösung der Diffusionsgleichung.

Daher wurden im Laufe der Arbeit Methoden entwickelt, um die Verteilungskoeffizienten zwischen Lipiden und Donor ($K_{lip/don}$), Corneocyten und Lipiden ($K_{cor/lip}$), und lebenden tieferen Hautschichten und Lipiden ($K_{DSL/lip}$) sowie die Diffusionskoeffizienten in den Lipiden und lebenden tieferen Hautschichten (D_{lip} und D_{DSL}) zu messen und den Diffusionskoeffizienten in den Corneocyten näherungsweise zu bestimmen. Diese Daten wurden unter Verwendung von humaner weiblicher Bauchhaut für zwei Modellverbindungen generiert. Bei den Modellsubstanzen handelt es sich um Flufenaminsäure und Koffein, die sich in ihren Hautpermeationseigenschaften unterscheiden.

$K_{lip/don}$ wurde mittels Gleichgewichtsversuchen mit extrahierten humanen *stratum corneum*-Lipiden bestimmt. Für diese Experimente wurden die Lipide auf einen

Membranfilter aufgebracht. Dieser Lipidüberzug konnte reproduzierbar hergestellt werden, was durch Messung der Gewichts- und Dickenzunahme sichergestellt wurde. Mittels Hochleistungs-Dünnschichtchromatographie wurde gezeigt, dass das Verhältnis von Cholesterol zu Cholestereestern, Triglyceriden, freien Fettsäuren und Ceramiden in den extrahierten Lipiden in einem Rahmen lag, der allgemein für exzidierte Humanhaut anzunehmen ist. Neben der charakteristischen Zusammensetzung der *stratum corneum*-Lipide ist auch ihre Anordnung innerhalb der Doppelschichten entscheidend für eine effiziente Barriere sowie die Transporteigenschaften. Daher wurde die Lipidstruktur mittels Differenzialscanningkalorimetrie- (DSC) und Weitwinkelröntgenuntersuchungen (WAXD) näher untersucht. Die DSC-Untersuchungen ergaben, dass die Lipide nach Extraktion wieder als Lamellen kristallisieren, wobei ihre hexagonale und/oder orthorhombische lateralen Ordnung erhalten bleibt. Die Anwesenheit der orthorhombischen Phase bestätigte sich auch bei den WAXD-Untersuchungen. Signifikante Anteile der Lipide kristallisierten jedoch in einem nichtphysiologischen amorphen oder flüssigkristallinen Zustand, was dem hohen unphysiologischen Gehalt an Triglyceriden zugeschrieben wurde. Es handelt sich hierbei um ein Artefakt aufgrund von Kontamination der *stratum corneum*-Lipide mit Lipiden des Unterhautfettgewebes während der Entnahme im OP und beim Transport.

$K_{\text{cor/lip}}$ and $K_{\text{DSL/lip}}$ wurden aus experimentell gemessenen Verteilungskoeffizienten zwischen *stratum corneum* und Donor, Lipiden und Donor und *stratum corneum* und den lebenden tieferen Hautschichten ($K_{\text{SC/don}}$, $K_{\text{lip/don}}$ and $K_{\text{SC/DSL}}$) abgeleitet unter Annahme von Lipid- und Corneocytenvolumenanteilen, wie sie normalerweise in Humanhaut zu finden sind.

$K_{\text{SC/don}}$ wurde sowohl in Gleichgewichtsexperimenten bestimmt als auch mittels nichtlinearer Kurvenanpassung aus Konzentrations-Schichttiefenprofilen abgeleitet. Hierzu wurde eine Lösung der Diffusionsgleichung für eine eindimensionale Membran verwendet. Beide Methoden ergaben für Koffein sehr ähnliche Abschätzungen für $K_{\text{SC/don}}$ (und dementsprechend für $K_{\text{cor/lip}}$ und $K_{\text{SC/DSL}}$), während die Abschätzungen für Flufenaminsäure stärker voneinander abwichen. Obwohl der Grund für dieses Verhalten nicht abschließend geklärt werden konnte, wurde spekuliert, dass tiefenabhängige Veränderungen in der Barrierefunktion oder eine Bindung an Keratin hieran beteiligt sind. Die Kurvenanpassung ergab weiterhin eine

zeitabhngige nderung des Parameters $K_{SC/don}$, was auf Vernderungen in der Membran oder eine langsame Gleichgewichtseinstellung hinweisen kann.

Die apparenten Diffusionskoeffizienten in den Lipiden und tieferen Hautschichten D_{lip} und D_{DSL} wurden auf Grundlage des Gleichgewichtsfluxes ber lipidberzogene Membranfilter beziehungsweise dermatomisierte lebende Hautschichten bestimmt. Diese Methode konnte jedoch nicht zur Bestimmung des apparenten Diffusionskoeffizienten in den Corneocyten genutzt werden. D_{cor} wurde aufgrund einer Nherungsformel bestimmt, die $K_{cor/lip}$ und D_{lip} sowie D_{SC} verwendet.

D_{SC} wurde ebenfalls auf Grundlage des Gleichgewichtsfluxes, hier ber isoliertes *stratum corneum*, bestimmt sowie aus nichtlinearer Kurvenanpassung von *stratum corneum* Konzentrations-Schichttiefenprofilen an eine eindimensionale Lsung der Diffusionsgleichung abgeleitet. Wie schon im Fall von $K_{SC/don}$ ergaben sich in der Kurvenanpassung Hinweise, dass es zeitabhngig zu Vernderungen in der Membran kommt, da D_{SC} von sowohl Koffein als auch Flufenaminsure whrend der ersten Stunden der Absorption sank. Diese beruhen vermutlich auf Vernderungen der Pfadlnge durch Quellung der Membran.

Die Qualitt der Vorhersagen wurde im Vergleich von experimentellen und simulierten *stratum corneum*-Konzentrations-Schichttiefenprofilen berprft. Diese Arbeiten wurden am Lehrstuhl fr „Technische Simulation“ der Universitt Heidelberg unter Prof. Dr. Gabriel Wittum durchgefhrt. Die hier skizzierte nherungsweise Bestimmung des Diffusionskoeffizienten in den Corneocyten reagiert im Rahmen der Messdaten fr D_{lip} , D_{SC} und $K_{cor/lip}$ fr Koffein und Flufenaminsure hoch sensibel auf Vernderungen in der Membrangeometrie. Ausgehend von geometrischen Informationen, die mikroskopischen Daten fr Humanhaut entnommen wurden, musste jedoch der abgeschtzte Wert fr D_{cor} spter um eine Zehnerpotenz fr Koffein und zwei Zehnerpotenzen fr Flufenaminsure herab korrigiert werden, damit eine gute bereinstimmung zwischen Experiment und Simulation erzielt werden konnte.

Als ein wichtiges Ergebnis sowohl der Experimente als auch der Simulation konnte gezeigt werden, dass die Corneocyten eine entscheidende Rolle fr den Hauttransport von beiden Modellsubstanzen spielen. Wie aufgrund der unterschiedlichen Lipophilie der beiden Substanzen zu erwarten gewesen war, konnte gezeigt werden, dass Flufenaminsure, jedoch nicht Koffein an Keratin

bindet, ein Protein, das den Hauptgewichtsanteil des lebenden *stratum corneums* ausmacht.

Um diese Fragestellung genauer zu untersuchen, wurden die Mechanismen der Wirkstoff-Corneocyten-Interaktion in einem kombinierten experimentellen und theoretischen Ansatz näher untersucht. Es wurden experimentelle Methoden entwickelt, um die Wirkstoff-Corneocyten-Interaktionen hinsichtlich der Wirkstoffverteilung in Hydratationswasser und Bindung an Proteine zu untersuchen und das Ausmaß der konkurrierenden Mechanismen zu quantifizieren. Die Verteilung in Hydratationswasser wurde in Gleichgewichtsversuchen unter Verwendung von getrocknetem *stratum corneum*, beziehungsweise *stratum corneum*, das bekannte Mengen an Wasser enthielt, quantifiziert. Die enthaltene Wassermenge lag im Bereich von etwa 30-800 Gewichtsprozent bezogen auf trockenes *stratum corneum*. Hierzu wurde gefriergetrocknetes *stratum corneum* bei einer konstanten relativen Luftfeuchtigkeit gelagert oder in doppelt destilliertem Wasser gebadet. Die Keratinbindung wurde in Gleichgewichtsversuchen mit pulverisiertem Keratin vom Rinderhuf und –horn untersucht.

Die Ergebnisse für drei Substanzen, Koffein, Flufenaminsäure und Testosteron, wurden vorgestellt. Zwei Kompartimentmodelle des *stratum corneums* (M1 und M2) wurden formuliert, die, basierend auf experimentell bestimmten Eingangsparametern für die Affinität zu den Lipiden, Proteinen und Wasser, den *stratum corneum*-Donor Verteilungskoeffizienten beschreiben. M1 beinhaltet ein homogenes Proteinkompartiment und nimmt an, dass Proteininteraktionen nur über intra-corneocytäres Wasser stattfinden. In M2 wird das Proteinkompartiment unterteilt in ein Kompartiment der Corneocytenhülle, das in Wechselwirkung mit den interzellulären Lipiden steht und ein Keratinkompartiment, das mit Wasser wechselwirkt. Als erste Abschätzung wurden die Lösungseigenschaften des Wassers in der Membran als identisch zu Bulkwasser angenommen. Die Bindungskonstanten und maximale Bindungskapazitäten wurden aus Studien mit pulverisiertem Rinderkeratin abgeleitet und sowohl für die Abschätzung der Wechselwirkung mit dem Keratinkompartiment als auch mit den Proteinen der Corneocytenhülle verwendet.

Für Koffein, das nicht an Proteine bindet jedoch eine hohe Affinität zur Wasserphase aufweist, wurde der Einfluss des Wasserkompartiments zunächst überschätzt. Die Substanz konnte jedoch erfolgreich modelliert werden, nachdem eine gebundene,

unzugängliche Wasserphase eingeführt wurde. Für lipophile, keratinbindende Verbindungen (Flufenaminsäure und Testosteron) sagte nur M2 die Konzentrationsabhängigkeit des *stratum corneum*-Donor Verteilungskoeffizienten korrekt voraus. Demzufolge interagieren sowohl lipophile als auch hydrophile Substanzen mit den Corneocyten. Die Interaktionen von lipophilen Substanzen sind wahrscheinlich auf die Corneocytenoberfläche begrenzt. Interaktionen mit intrazellulärem Keratin werden wahrscheinlich durch ihre geringe Wasserlöslichkeit limitiert.

Das zunächst vorgeschlagene einfache biphasige Zweischichtmodell der Humanhaut mit homogenen Verteilungs- und Diffusionskoeffizienten erlaubt eine nützliche erste Abschätzung der *in vitro* Hautabsorption. Allerdings ist die Darstellung des Corneocytenkompartiments hier wahrscheinlich zu einfach, da im Laufe der Arbeiten neue Parameter identifiziert wurden, insbesondere die Bindungsaffinität und die maximale Bindungskapazität an die Proteine der Corneocyten. Außerdem muß für Substanzen, die eine hohe Affinität zu Wasser haben eine gebundene, unzugängliche Wasserphase berücksichtigt werden. Darüber hinaus wurde ein Modell der Verteilungs- und Bindungsschemata innerhalb des *stratum corneums* vorgeschlagen und konnte auch erfolgreich angewandt werden um die *stratum corneum* Verteilungskoeffizienten von drei Modellschubstanzen mit unterschiedlichen *stratum corneum* Affinitäten zu erklären.

In Zukunft müssen diese Verfeinerungen der Corneocytenphase in das Diffusionsmodell integriert werden. Sie sollten außerdem verwendet werden die Abschätzung des Corneocyten Diffusionskoeffizienten zu präzisieren, da nun eine Unterscheidung zwischen gebundener und frei beweglicher Substanz möglich ist.

Das Modell muß darüber hinaus mit weiteren Substanzen validiert werden, um einschätzen zu können, ob es nach Einbeziehung der neu identifizierten Parameter als prädiktives Modell verwendet werden kann. Voraussetzung für den Übergang vom Simulations- zum Vorhersagemodell wird sein, einen geeigneten Ersatz für die bisher experimentell bestimmten Eingangsparameter zu finden. Wie bereits beschrieben, gelten Korrelationen zwischen Membran-Donor- und Octanol-Wasser Verteilungskoeffizienten sowie zwischen Diffusionskoeffizienten und Molekülgröße als allgemein etabliert. Im Gegensatz dazu ist wenig bekannt über eine geeignete Abschätzung der Bindungsparameter an die Corneocytenproteine. Im Gegensatz

dazu existieren für eine große Anzahl von Substanzen Bindungsdaten zu einem anderen ubiquitär vorkommenden Protein, nämlich Serumalbumin, da dies ein wichtiger pharmakokinetischer Parameter für die Wirkstoffverteilung im zentralen Kompartiment ist. Ebenso gibt es eine Anzahl von QSAR-Modellen, die die Bindung an humanes Serumalbumin vorhersagen. Daher erscheint es sinnvoll nach einem Zusammenhang zwischen Serumalbumin- und Keratinbindung zu suchen. Dieser könnte zur ersten Orientierung dienen, ob eine Keratinbindung für die jeweils untersuchte Substanz überhaupt für die Modellierung berücksichtigt werden muß. Es bleibt abzuwarten, ob eine direkte Korrelation zwischen den beiden Parametern besteht, die sich in prediktiver Weise für die Modellierung nutzen läßt.

Letztendlich soll das Diffusionsmodell verwendet werden, um die *in vivo* Absorption über die Haut vorherzusagen. Normalerweise steht nur eine limitierte Dosis an Substanz auf der Hautoberfläche zur Verfügung, insbesondere wenn es sich um pharmazeutische oder kosmetische Applikationen handelt. Mit abnehmendem applizierten Volumen gewinnen Prozesse innerhalb der Formulierung wie beispielsweise das Verschwinden des aktiven Bestandteils, Wechselwirkungen zwischen Komponenten des Vehikels mit der Haut und Verdunstung von Formulierungsbestandteilen zunehmend an Bedeutung und müssen daher im Modell berücksichtigt werden.

Darüber hinaus handelt es sich bei den meisten Formulierungen, die auf der Haut angewendet werden, um Multikomponentensysteme. Hilfsstoffe spielen eine komplexe Rolle im Aufbau des Vehikels und können die Absorption des Wirkstoffs sowohl im Sinne einer Permeationsverbesserung als auch einer Retardierung beeinflussen. Das ist hauptsächlich darin begründet, dass komplexe Wechselwirkungen zwischen der Hilfsstoffen der Formulierung und der Haut auftreten. Diese können die Affinität des Wirkstoffs zu einzelnen Bereichen der Haut beeinflussen wie auch die Diffusionsgeschwindigkeit in der Haut. Der erste Schritt diese Mechanismen in das Modell zu integrieren würde es sein, die Absorption häufig eingesetzter Hilfsstoffe zu untersuchen. Fortschritte auf diesem Gebiet wurden erzielt, indem die Absorption von Permeationsverbesserern wie Propylenglycol, Ölsäure und Wasser gemessen wurde. Vorausgesetzt, dass sich eine Beziehung zwischen der Konzentration der Hilfsstoffe in der Haut und dem Verteilungs- und Diffusionskoeffizienten des Wirkstoffs etablieren lässt, kann die "Ko-Permeation" beider Komponenten vorhergesagt werden.

Und schließlich müssen zur Modellierung von Wirkstoffen, die zur transkutanen Applikation und systemischen Wirkung bestimmt sind, außerdem der kutane Metabolismus sowie die systemische Verteilung in das Modell integriert werden. Für letzteres Problem existieren bereits Lösungsansätze, im Rahmen derer ein Diffusionsmodell der oberen Hautschichten mit einem Pharmakokinetischen Modell des menschlichen Körpers kombiniert wird. Auf der anderen Seite ist wenig über die Auswirkung einer enzymatischen Metabolisierung in den lebenden Hautschichten auf die Hautabsorption bekannt. Ubiquitär vorkommende Enzyme wie Esterasen und Deaminasen sind auch in den lebenden Hautschichten aktiv. Daneben gibt es hier außerdem auch Enzyme der Cytochrom P450 Familie. Der kutane Metabolismus wird bereits im Rahmen therapeutischer Konzepte genutzt, da topisch applizierte Ester-prodrugs normalerweise eine erhöhte Lipophilie gegenüber dem eigentlichen Wirkstoff haben und damit einen Vorteil für die Permeation von ansonsten schlecht absorbierbaren hydrophilen Wirkstoffen darstellen.

REFERENCES

1. A.E. Kalinin, A.V. Kajava, and P.M. Steinert. Epithelial barrier function: Assembly and structural features of the cornified cell envelope. *BioEssays*. 24:789-800 (2002).
2. R.J. Scheuplein. Molecular Structure and Diffusional Processes Across Intact Stratum Corneum: Semi-Annual Report. US Army Chemical Research and Development Laboratories, Edgewood Arsenal, MD (1966).
3. E. Jaeckle, U.F. Schaefer, and H. Loth. Comparison of effects of different ointment bases on the penetration of ketoprofen through heat-separated human epidermis and artificial lipid barriers. *Journal of Pharmaceutical Sciences*. 92:1396-1406 (2003).
4. H. Fischer, I. Polikarpov, and A.F. Craievich. Average protein density is a molecular-weight-dependent function. *Protein Science*. 13:2825-2828 (2004).
5. OECD. Test guideline 428: Skin Absorption: *In vitro* Method, OECD, Paris, 2004.
6. OECD. Guidance document for the conduct of skin absorption studies. OECD Series on Testing and Assessment. No 28, Environment Directorate, Paris, 2004.
7. SCCNFP. Basic criteria for the in-vitro assessment of dermal absorption of cosmetic ingredients, 2003.
8. EC. Guidance document on dermal absorption, European comission Health & consumer Protection Directorate - General Directorate E - Food Safety: plant health, animal welfare, international questions E1 - Plant health, 2004.
9. FDA. Guidance for industry: SUPAC-SS In-vitro release testing and in-vivo bioequivalence documentation, Center for Drug Evaluation and Research (CDER), Rockvill, MD, 1997.
10. R.L. Bronaugh, R.F. Stewart, and E.R. Congdon. Methods for *in vitro* percutaneous absorption studies. II. Animal models for human skin. *Toxicology and Applied Pharmacology*. 62:481-488 (1982).
11. H. Raabe, R. Curren, S. Ward, and J. Harbell. Report from an *in vitro* dermal absorption assay workshop, 2005 *In vitro percutaneous absorption expert users workshop*, Gaithersburg, USA, 2005.

12. F.P. Schmook, J.G. Meingassner, and A. Billich. Comparison of human skin or epidermis models with human and animal skin in in-vitro percutaneous absorption. *International Journal of Pharmaceutics*. 215:51-56 (2001).
13. M. Ruet Rossignol. The 7th Amendment to the Cosmetics Directive. *Alternative to Laboratory Animals: ATLA*. 33 Suppl 1:19-20 (2005).
14. F. Netzlaff, C.M. Lehr, P.W. Wertz, and U.F. Schaefer. The human epidermis models EpiSkin, SkinEthic and EpiDerm: an evaluation of morphology and their suitability for testing phototoxicity, irritancy, corrosivity, and substance transport. *European Journal of Pharmaceutics and Biopharmaceutics*. 60:167-178 (2005).
15. M. Schaefer-Korting, U. Bock, W. Diembeck, H.J. Düsing, A. Gamer, E. Haltner-Ukomadu, C. Hoffmann, M. Kaca, H. Kamp, S. Kersen, M. Kietzmann, H.C. Korting, H.-U. Kraechter, C.-M. Lehr, M. Liebsch, A. Mehling, C. Mueller-Goymann, F. Netzlaff, F. Niedorf, M.K. Ruebbelke, U.F. Schaefer, E. Schmidt, S. Schreiber, H. Spielmann, A. Vuia, and M. Weimer. Reconstructed Human Epidermis for Skin Absorption Testing: Results of the German Validation Study. *Alternative to Laboratory Animals: ATLA*. 36:161-187 (2008).
16. J. Powells. Skin physiology. *Foundation Years*. 3:193-196 (2007).
17. K.A. Walters and M.S. Roberts The structure and function of skin. In K.A. Walters (ed.), *Dermatological and transdermal formulations*, Vol. 119, Marcel Dekker, New York, 2002, pp. 1-39.
18. G.P. Moss, J.C. Dearden, H. Patel, and M.T.D. Cronin. Quantitative structure-permeability relationships (QSPRs) for percutaneous absorption. *Toxicology in vitro*. 16:299-317 (2002).
19. K. Kretsos and G.B. Kasting. Dermal capillary clearance: Physiology and modeling. *Skin Pharmacology and Physiology*. 18:55-74 (2005).
20. K. Taira, Y. Narisawa, J. Nakafusa, N. Misago, and T. Tanaka. Spatial relationship between Merkel cells and Langerhans cells in human hair follicles. *Journal of Dermatological Science*. 30:195-204 (2002).
21. Y. Suzuki, J. Nomura, J. Koyama, and I. Horii. The role of proteases in stratum corneum: Involvement in stratum corneum desquamation. *Archives of Dermatological Research*. 286:249-253 (1994).
22. A. Lundstrom, G. Serre, M. Haftek, and T. Egelrud. Evidence for a role of corneodesmosin, a protein which may serve to modify desmosomes during

- cornification, in stratum corneum cell cohesion and desquamation. *Archives of Dermatological Research*. 286:369-375 (1994).
23. P.M. Elias. Stratum corneum defensive functions: An integrated view. *Journal of Investigative Dermatology*. 125:183-200 (2005).
 24. L. Landmann. Epidermal permeability barrier: Transformation of lamellar granule-disks into intercellular sheets by a membrane-fusion process, a freeze-fracture study. *Journal of Investigative Dermatology*. 87:202-209 (1986).
 25. H. Sugiura and M. Nakano. Dry skin and filaggrin. *Skin Research*. 4:12-18 (2005).
 26. G.B. Kasting and N.D. Barai. Equilibrium water sorption in human stratum corneum. *Journal of Pharmaceutical Sciences*. 92:1624-1631 (2003).
 27. P.J. Caspers, G.W. Lucassen, H.A. Bruining, and G.J. Puppels. Automated depth-scanning confocal microspectrometer for rapid in-vivo determination of water concentration profiles in human skin. *Journal of Raman Spectroscopy*. 31:813-818 (2000).
 28. A. Kalinin, L.N. Marekov, and P.M. Steinert. Assembly of the epidermal cornified cell envelope. *Journal of Cell Science*. 114:3069-3070 (2001).
 29. D.C. Schwartzendruber, P. Wertz, and D.T. Downing. Evidence that the corneocyte has a chemically bound lipid envelope. *Journal of Investigative Dermatology*. 88:709-713 (1987).
 30. P.W. Wertz, M. Kremer, and C.A. Squier. Comparison of lipids from epidermal and palatal stratum corneum. *Journal of Investigative Dermatology*. 98:375-378 (1992).
 31. M.A. Lampe, A.L. Burlingame, and J.A. Whitney. Human stratum corneum lipids: Characterization and regional variations. *Journal of Lipid Research*. 24:120-130 (1983).
 32. J.A. Bouwstra, G.S. Gooris, K. Cheng, A. Weerheim, W. Bras, and M. Ponc. Phase behavior of isolated skin lipids. *Journal of Lipid Research*. 37:999-1011 (1996).
 33. J. Bouwstra, G. Pilgram, G. Gooris, H. Koerten, and M. Ponc. New aspects of the skin barrier organization. *Skin Pharmacology and Applied Physiology*. 14:52-62 (2001).

34. J.A. Bouwstra, G.S. Gooris, J.A. van der Spek, and W. Bras. Structural investigations of human stratum corneum by small-angle X-ray scattering. *Journal of Investigative Dermatology*. 97:1005-1012 (1991).
35. G.S.K. Pilgram, A.M. Engelsma-Van Pelt, J.A. Bouwstra, and H.K. Koerten. Electron diffraction provides new information on human stratum corneum lipid organization studied in relation to depth and temperature. *Journal of Investigative Dermatology*. 113:403-409 (1999).
36. F. Netzlaff, K.H. Kostka, C.M. Lehr, and U.F. Schaefer. TEWL measurements as a routine method for evaluating the integrity of epidermis sheets in static Franz type diffusion cells *in vitro*. Limitations shown by transport data testing. *European Journal of Pharmaceutics and Biopharmaceutics* (2005).
37. R.C. Scott, P.H. Dugard, and A.W. Doss. Permeability of abnormal rat skin. *Journal of Investigative Dermatology*. 86:201-207 (1986).
38. M. Fartasch. Epidermal barrier in disorders of the skin. *Microscopical Research and Technology*. 38:361-372 (1997).
39. A.T. Goon, G. Yosipovitch, Y.H. Chan, and C.L. Goh. Barrier repair in chronic plaque-type psoriasis. *Skin Research and Technology*. 10:10-13 (2004).
40. M. Sznitowska and B. Berner. Polar pathway for percutaneous absorption. *Current Problems in Dermatology*. 22:164-170 (1995).
41. S. Yagi, K. Nakayama, Y. Kurosaki, K. Higaki, and T. Kimura. Factors determining drug residence in skin during transdermal absorption: studies on beta-blocking agents. *Biol Pharm Bull*. 21:1195-1201 (1998).
42. N.A. Monteiro-Riviere, A.O. Inman, V. Mak, P. Wertz, and J.E. Riviere. Effect of selective lipid extraction from different body regions on epidermal barrier function. *Pharmaceutical Research*. 18:992-998 (2001).
43. S.K. Rastogi and J. Singh. Lipid extraction and transport of hydrophilic solutes through porcine epidermis. *International Journal of Pharmaceutics*. 225:75-82 (2001).
44. K. Welin-Berger, J.A.M. Neelissen, and J. Engblom. Physicochemical interaction of local anesthetics with lipid model systems - Correlation with *in vitro* permeation and *in vivo* efficacy. *Journal of Controlled Release*. 81:33-43 (2002).
45. G.S.K. Pilgram, J. Van der Meulen, G.S. Gooris, H.K. Koerten, and J.A. Bouwstra. The influence of two azones and sebaceous lipids on the lateral

- organization of lipids isolated from human stratum corneum. *Biochimica et Biophysica Acta - Biomembranes*. 1511:244-254 (2001).
46. P.M. Elias, E.R. Cooper, A. Korc, and B.E. Brown. Percutaneous transport in relation to stratum corneum structure and lipid composition. *Journal of Investigative Dermatology*. 76:297-301 (1981).
 47. H. Loth, G. Hauck, D. Borchert, and F. Theobald. Statistical testing of drug accumulation in skin tissues by linear regression versus contents of stratum corneum lipids. *International Journal of Pharmaceutics*. 209:95-108 (2000).
 48. L. Norlén, I. Nicander, B. Lundh Rozell, S. Ollmar, and B. Forslind. Inter- and intra-individual differences in human stratum corneum lipid content related to physical parameters of skin barrier function *in vivo*. *Journal of Investigative Dermatology*. 112:72-77 (1999).
 49. M. De Jager, W. Groenink, R. Bielsa I Guivernau, E. Andersson, N. Angelova, M. Poncet, and J. Bouwstra. A novel *in vitro* percutaneous penetration model: Evaluation of barrier properties with P-aminobenzoic acid and two of its derivatives. *Pharmaceutical Research*. 23:951-960 (2006).
 50. J.A. Bouwstra, A. de Graaff, G.S. Gooris, J. Nijssse, J.W. Wiechers, and A.C. van Aelst. Water distribution and related morphology in human stratum corneum at different hydration levels. *Journal of Investigative Dermatology*. 120:750-758 (2003).
 51. T. Richter, C. Peuckert, M. Sattler, K. Koenig, I. Riemann, U. Hintze, K.-P. Wittern, R. Wiesendanger, and R. Wepf. Dead but highly dynamic - The stratum corneum is divided into three hydration zones. *Skin Pharmacology and Physiology*. 17:246-257 (2004).
 52. P.V. Raykar, M.-C. Fung, and B.D. Anderson. The role of protein and lipid domains in the uptake of solutes by human stratum corneum. *Pharmaceutical Research*. 5:140-150 (1988).
 53. H.E. Boddé, I. van den Brink, H.K. Koerten, and F.H.N. de Haan. Visualization of *in vitro* percutaneous penetration of mercuric chlorite; transport through intercellular space versus cellular uptake through desmosomes. *Journal of Controlled Release*. 15:227-236 (1991).
 54. B. Yu, K.H. Kim, P.T. So, D. Blankschtein, and R. Langer. Visualization of oleic acid-induced transdermal diffusion pathways using two-photon

- fluorescence microscopy. *Journal of Investigative Dermatology*. 120:448-455 (2003).
55. B. Yu, K.H. Kim, P.T.C. So, D. Blankschtein, and R. Langer. Topographic heterogeneity in transdermal transport revealed by high-speed two-photon microscopy: Determination of representative skin sample sizes. *Journal of Investigative Dermatology*. 118:1085-1088 (2002).
 56. U. Jacobi, T. Tassopoulos, C. Surber, and J. Lademann. Cutaneous distribution and localization of dyes affected by vehicles all with different lipophilicity. *Archives of Dermatological Research*. 297:303-310 (2006).
 57. N. Otberg, H. Richter, H. Schaefer, U. Blume-Peytavi, W. Sterry, and J. Lademann. Variations of Hair Follicle Size and Distribution in Different Body Sites. *Journal of Investigative Dermatology*. 122:14-19 (2004).
 58. J. Lademann, H. Richter, A. Teichmann, N. Otberg, U. Blume-Peytavi, J. Luengo, B. Weiß, U.F. Schaefer, C.-M. Lehr, R. Wepf, and W. Sterry. Nanoparticles - An efficient carrier for drug delivery into the hair follicles. *European Journal of Pharmaceutics and Biopharmaceutics*. 66:159-164 (2007).
 59. R. Alvarez-Román, A. Naik, Y.N. Kalia, R.H. Guy, and H. Fessi. Skin penetration and distribution of polymeric nanoparticles. *Journal of Controlled Release*. 99:53-62 (2004).
 60. A. Vogt, B. Combadiere, S. Hadam, K.M. Stieler, J. Lademann, H. Schaefer, B. Autran, W. Sterry, and U. Blume-Peytavi. 40 nm, but not 750 or 1,500 nm, nanoparticles enter epidermal CD1a⁺ cells after transcutaneous application on human skin. *Journal of Investigative Dermatology*. 126:1316-1322 (2006).
 61. N. Otberg, A. Patzelt, U. Rasulev, T. Hagemeister, M. Linscheid, R. Sinkgraven, W. Sterry, and J. Lademann. The role of hair follicles in the percutaneous absorption of caffeine. *British Journal of Clinical Pharmacology*. 65:488-492 (2008).
 62. F. Hueber, J. Wepierre, and H. Schaefer. Role of transepidermal and transfollicular routes in percutaneous absorption of hydrocortisone and testosterone: *In vivo* study in the hairless rat. *Skin Pharmacology*. 5:99-107 (1992).

63. B. Illel, H. Schaefer, J. Wepierre, and O. Doucet. Follicles play an important role in percutaneous absorption. *Journal of Pharmaceutical Sciences*. 80:424-427 (1991).
64. B.W. Barry. Drug delivery routes in skin: A novel approach. *Advanced Drug Delivery Reviews*. 54: (2002).
65. A. Teichmann, U. Jacobi, M. Ossadnik, H. Richter, S. Koch, W. Sterry, and J. Lademann. Differential stripping: determination of the amount of topically applied substances penetrated into the hair follicles. *The Journal Of Investigative Dermatology*. 125:264-269 (2005).
66. F. Bonté, A. Saunois, P. Pinguet, and A. Meybeck. Existence of a lipid gradient in the upper stratum corneum and its possible biological significance. *Archives of Dermatological Research*. 72:8-82 (1997).
67. H.M. Klimisch and G. Chandra. Use of Fourier transform infrared spectroscopy with attenuated total reflectance for *in vivo* quantitation of polydimethylsiloxanes on human skin. *Journal of the Society of Cosmetic Chemists of Japan*. 37:73-87 (1986).
68. C. Curdy, A. Naik, Y.N. Kalia, I. Alberti, and R.H. Guy. Non-invasive assessment of the effect of formulation excipients on stratum corneum barrier function *in vivo*. *International Journal of Pharmaceutics*. 271:251-256 (2004).
69. M.B. Reddy, A.L. Stinchcomb, R.H. Guy, and A.L. Bunge. Determining dermal absorption parameters *in vivo* from tape strip data. *Pharmaceutical Research*. 19:292-298 (2002).
70. V.H.W. Mak, R.O. Potts, and R.H. Guy. Percutaneous penetration enhancement *in vivo* measured by attenuated total reflectance infrared spectroscopy. *Pharmaceutical Research*. 7:835-841 (1990).
71. V.H.W. Mak, R.O. Potts, and R.H. Guy. Oleic acid concentration and effect in human stratum corneum: Non-invasive determination by attenuated total reflectance infrared spectroscopy *in vivo*. *Journal of Controlled Release*. 12:67-75 (1990).
72. Y.N. Kalia, I. Alberti, A. Naik, and R.H. Guy. Assessment of topical bioavailability *in vivo*: The importance of stratum corneum thickness. *Skin Pharmacology and Applied Skin Physiology*. 14:82-86 (2001).
73. L.K. Pershing, J.L. Nelson, J.L. Corlett, S.P. Shrivastava, D.B. Hare, and V.P. Shah. Assessment of dermatopharmacokinetic approach in the

- bioequivalence determination of topical tretinoin gel products. *Journal of the American Academy of Dermatology*. 48:740-751 (2003).
74. V.P. Shah. IV-IVC for topically applied preparations - A critical evaluation. *European Journal of Pharmaceutics and Biopharmaceutics*. 60:309-314 (2005).
 75. A. Schätzlein and G. Cevc. Non-uniform cellular packing of the stratum corneum and permeability barrier function of intact skin: a high-resolution confocal laser scanning microscopy study using highly deformable vesicles (Transfersomes). *Br J Dermatol*. 138:583-592 (1998).
 76. G. Betz, R. Imboden, and G. Imanidis. Interaction of liposome formulations with human skin *in vitro*. *International Journal of Pharmaceutics*. 229:117-129 (2001).
 77. J. Lademann, H. Richter, K. Golz, L. Zastrow, W. Sterry, and A. Patzelt. Influence of microparticles on the homogeneity of distribution of topically applied substances. *Skin Pharmacol Physiol*. 21:274-282 (2008).
 78. F. Stracke, B. Weiss, C.M. Lehr, K. König, U.F. Schaefer, and M. Schneider. Multiphoton microscopy for the investigation of dermal penetration of nanoparticle-borne drugs. *J Invest Dermatol*. 126:2224-2233 (2006).
 79. K. Koenig and I. Riemann. High-resolution multiphoton tomography of human skin with subcellular spatial resolution and picosecond time resolution. *Journal of Biomedical Optics*. 8:432-439 (2003).
 80. J. Luengo, B. Weiss, M. Schneider, A. Ehlers, F. Stracke, K. König, K.-H. Kostka, C.-M. Lehr, and U.F. Schaefer. Influence of nanoencapsulation on human skin transport of flufenamic acid. *Skin Pharmacology and Physiology*. 19:190-197 (2006).
 81. P.J. Caspers, G.W. Lucassen, and G.J. Puppels. Combined *in vivo* confocal Raman spectroscopy and confocal microscopy of human skin. *Biophys J*. 85:572-580 (2003).
 82. M. Egawa, T. Hirao, and M. Takahashi. *In vivo* estimation of stratum corneum thickness from water concentration profiles obtained with Raman spectroscopy. *Acta Derm Venereol*. 87:4-8 (2007).
 83. A. Tfayli, O. Piot, F. Pitre, and M. Manfait. Follow-up of drug permeation through excised human skin with confocal Raman microspectroscopy. *Eur Biophys J*. 36:1049-1058 (2007).

84. J. Crank. The mathematics of diffusion, Clarendon Press, Oxford, 1976.
85. R.O. Potts and R.H. Guy. Predicting skin permeability. *Pharmaceutical Research*. 9:663-669 (1992).
86. R.O. Potts and R.H. Guy. A predictive algorithm for skin permeability: The effects of molecular size and hydrogen bond activity. *Pharmaceutical Research*. 12:1628-1633 (1995).
87. H. Patel, W.T. Berge, and M.T.D. Cronin. Quantitative structure-activity relationships (QSARs) for the prediction of skin permeation of exogenous chemicals. *Chemosphere*. 48:603-613 (2002).
88. M.S. Roberts, W.J. Pugh, and J. Hadgraft. Epidermal permeability: Penetrant structure relationships. 2. The effect of H-bonding groups in penetrants on their diffusion through the stratum corneum. *International Journal of Pharmaceutics*. 132:23-32 (1996).
89. P.S. Magee. Some novel approaches to modelling transdermal penetration and reactivity with epidermal proteins. In J. Devillers (ed.), *Comparative QSAR*, Taylor & Francis, London, 1998, pp. 137-168.
90. F. Yamashita and M. Hashida. Mechanistic and empirical modeling of skin permeation of drugs. *Advanced Drug Delivery Reviews*. 55:1185-1199 (2003).
91. C.W. Lim, S. Fujiwara, F. Yamashita, and M. Hashida. Prediction of human skin permeability using a combination of molecular orbital calculations and artificial neural network. *Biological Pharmaceutical Bulletin*. 25:361-366 (2002).
92. M.E. Johnson, D. Blankschtein, and R. Langer. Permeation of steroids through human skin. *Journal of Pharmaceutical Sciences*. 84:1144-1146 (1995).
93. I.T. Degim, W.J. Pugh, and J. Hadgraft. Skin permeability data: Anomalous results. *International Journal of Pharmaceutics*. 170:129-133 (1998).
94. G.L. Flynn. Physicochemical determinants of skin absorption. In T.R. Gerrity and C.J. Henry (eds.), *Principles of route-to-route extrapolation of risk assessment*, Elsevier, New York, 1990, pp. 93-127.
95. A. Wilschut, W.F. ten Berge, P.J. Robinson, and T.E. McKone. Estimating skin permeation. The validation of five mathematic skin permeation models. *Chemosphere*. 30:1275-1296 (1994).

96. B.E. Vecchia and A. Bunge. SKin absorption databases and predictive equations. In R. Guy and J. Hadgraft (eds.), *Transdermal drug delivery*, Vol. 123, Marcel Dekker, New York, 2003, pp. 25-55.
97. J.J. Hostynek and P.S. Magee. Modelling *in vivo* human skin absorption. *Quantitative Structure-Activity Relationships*. 16:473-479 (1997).
98. R.J. Scheuplein and I.H. Blank. Mechanism of percutaneous absorption. IV. Penetration of nonelectrolytes (alcohols) from aqueous solutions and from pure liquids. *Journal of Investigative Dermatology*. 60:286-296 (1973).
99. M.S. Roberts, R.A. Anderson, and J. Swarbrick. Permeability of human epidermis to phenolic compounds. *Journal of Pharmacy and Pharmacology*. 29:677-683 (1977).
100. B.M. Magnusson, Y.G. Anissimov, S.E. Cross, and M.S. Roberts. Molecular size as the main determinant of solute maximum flux across the skin. *Journal of Investigative Dermatology*. 122:993-999 (2004).
101. G.B. Kasting, R.L. Smith, and E.R. Cooper. Effect of lipid solubility and molecular size on percutaneous absorption. In B. Schroet and H. Schaefer (eds.), *Skin Pharmacokinetics*, Karger, Basel, 1987, pp. 138-153.
102. W.J. Roberts and K.B. Sloan. Correlation of aqueous and lipid solubilities with flux for prodrugs of 5-fluorouracil, theophylline, and 6-mercaptopurine: A Potts-Guy approach. *Journal of Pharmaceutical Sciences*. 88:515-522 (1999).
103. S. Majumdar, J. Thomas, S. Wasdo, and K.B. Sloan. The effect of water solubility of solutes on their flux through human skin *in vitro*. *International Journal of Pharmaceutics*. 329:25-36 (2007).
104. J. Thomas, S. Majumdar, S. Wasdo, A. Majumdar, and K.B. Sloan. The effect of water solubility of solutes on their flux through human skin *in vitro*: An extended Flynn database fitted to the Roberts-Sloan equation. *International Journal of Pharmaceutics*. 339:157-167 (2007).
105. S.C. Wasdo and K.B. Sloan. Topical delivery of a model phenolic drug: Alkylloxycarbonyl prodrugs of acetaminophen. *Pharmaceutical Research*. 21:940-946 (2004).
106. W.J. Roberts and K.B. Sloan. Application of the transformed Potts-Guy equation to *in vivo* human skin data. *Journal of Pharmaceutical Sciences*. 90:1318-1323 (2001).

107. W.J. Roberts and K.B. Sloan. Prediction of transdermal flux of prodrugs of 5-fluorouracil, theophylline and 6-mercaptopurine with a series/parallel model. *Journal of Pharmaceutical Sciences*. 89:1415-1431 (2000).
108. K.B. Sloan. Prodrugs for dermal delivery. *Advanced Drug Delivery Reviews*. 3:67-101 (1989).
109. G. Winckle, Y.G. Anissimov, S.E. Cross, G. Wise, and M.S. Roberts. An integrated pharmacokinetic and imaging evaluation of vehicle effects on solute human epidermal flux and, retention characteristics. *Pharmaceutical Research*. 25:158-166 (2008).
110. T.F. Wang, G.B. Kasting, and J.M. Nitsche. A multiphase microscopic diffusion model for stratum corneum permeability. I. formulation, solution, and illustrative results for representative compounds. *Journal of Pharmaceutical Sciences*. 95:620-648 (2006).
111. G.B. Kasting. Kinetics of finite dose absorption through skin 1. Vanillylnonanamide. *Journal of Pharmaceutical Sciences*. 90:202-212 (2001).
112. K.D. McCarley and A.L. Bunge. Physiologically relevant one-compartment pharmacokinetic models for skin. 1. Development of models. *Journal of Pharmaceutical Sciences*. 87:470-480 (1998).
113. K.D. McCarley and A.L. Bunge. Physiologically relevant two-compartment pharmacokinetic models for skin. *Journal of Pharmaceutical Sciences*. 89:1212-1235 (2000).
114. K.D. McCarley and A.L. Bunge. Pharmacokinetic models of dermal absorption. *Journal of Pharmaceutical Sciences*. 90:1699-1719 (2001).
115. M.B. Reddy, K.D. Mccarley, and A.L. Bunge. Physiologically relevant one-compartment pharmacokinetic models for skin. 2. Comparison of models when combined with a systemic pharmacokinetic model. *Journal of Pharmaceutical Sciences*. 87:482-490 (1998).
116. R.H. Guy and J. Hadgraft. Prediction of drug disposition kinetics in skin and plasma following topical administration. *Journal of Pharmaceutical Sciences*. 73:883-887 (1984).
117. R.H. Guy, J. Hadgraft, and H.I. Maibach. A pharmacokinetic model for percutaneous absorption. *International Journal of Pharmaceutics*. 11:119-129 (1982).

118. K. Kretsos, M.A. Miller, G. Zamora-Estrada, and G.B. Kasting. Partitioning, diffusivity and clearance of skin permeants in mammalian dermis. *International Journal of Pharmaceutics*. 346:64-79 (2008).
119. S.K. Chandrasekaran, P.S. Campbell, and T. Watanabe. Application of the "dual sorption" model to drug transport through skin. *Polymer Engineering and Science*. 20:36-39 (1980).
120. Y.G. Anissimov and M.S. Roberts. Diffusion modeling of percutaneous absorption kinetics. 1. Effects of flow rate, receptor sampling rate, and viable epidermal resistance for a constant donor concentration. *Journal of Pharmaceutical Sciences*. 88:1201-1209 (1999).
121. G.B. Kasting and M.A. Miller. Kinetics of finite dose absorption through skin 2: Volatile compounds. *Journal of Pharmaceutical Sciences*. 95:268-280 (2006).
122. K. Kubota, E. Koyama, and E.H. Twizell. Dual sorption model for the nonlinear percutaneous permeation kinetics of timolol. *Journal of Pharmaceutical Sciences*. 82:1205-1208 (1993).
123. H. Tang, D. Blankschtein, and R. Langer. Prediction of steady-state skin permeabilities of polar and nonpolar permeants across excised pig skin based on measurements of transient diffusion: Characterization of hydration effects on the skin porous pathway. *Journal of Pharmaceutical Sciences*. 91:1891-1907 (2002).
124. A.C. Watkinson, A.L. Bunge, J. Hadgraft, and A. Naik. Computer simulation of penetrant concentration-depth profiles in the stratum corneum. *International Journal of Pharmaceutics*. 87:175-182 (1992).
125. A.B. Gumel, K. Kubota, and E.H. Twizell. A sequential algorithm for the non-linear dual-sorption model of percutaneous drug absorption. *Mathematical Biosciences*. 152:87-103 (1998).
126. Y.G. Anissimov and M.S. Roberts. Diffusion modeling of percutaneous absorption kinetics: 2. Finite vehicle volume and solvent deposited solids. *Journal of Pharmaceutical Sciences*. 90:504-520 (2001).
127. Y.G. Anissimov and M.S. Roberts. Diffusion modeling of percutaneous absorption kinetics. 3. Variable Diffusion and Partition coefficients, Consequences for stratum corneum depth profiles and desorption kinetics. *Journal of Pharmaceutical Sciences*. 93:470-487 (2004).

128. F. Pirot, Y.N. Kalia, A.L. Stinchcomb, G. Keating, A. Bunge, and R.H. Guy. Characterization of the permeability barrier of human skin *in vivo*. Proceedings of the National Academy of Sciences of the United States of America. 94:1562-1567 (1997).
129. J.E. Rim, P.M. Pinsky, and W.W. Van Osdol. Finite element modeling of coupled diffusion with partitioning in transdermal drug delivery. Annals of Biomedical Engineering. 33:1422-1438 (2005).
130. K. Tojo, C.C. Chiang, and Y.W. Chien. Drug Permeation Across the Skin: Effect of Penetrant Hydrophilicity. Journal of Pharmaceutical Sciences. 76:123-126 (1987).
131. J. Kruese, D. Golden, S. Wilkinson, F. Williams, S. Kezic, and J. Corish. Analysis, interpretation, and extrapolation of dermal permeation data using diffusion-based mathematical models. Journal of Pharmaceutical Sciences. 96:682-703 (2007).
132. R. Manitz, W. Lucht, K. Strehmel, R. Weiner, and R. Neubert. On mathematical modeling of dermal and transdermal drug delivery. Journal of Pharmaceutical Sciences. 87:873-879 (1998).
133. H.F. Frasch and A.M. Barbero. Steady-state Flux and lag time in the stratum corneum lipid pathway: Result from finite element models. Journal of Pharmaceutical Sciences. 92:2196-2107 (2003).
134. M.E. Johnson, D. Blankschtein, and R. Langer. Evaluation of solute permeation through the stratum corneum: lateral bilayer diffusion as the primary transport mechanism. Journal of Pharmaceutical Sciences. 86:1162-1172 (1997).
135. S. Mitragotri. Modeling skin permeability to hydrophilic and hydrophobic solutes based on four permeation pathways. Journal of Controlled Release. 86:69-92 (2003).
136. A.M. Barbero and H.F. Frasch. Transcellular route of diffusion through stratum corneum: Results from finite element models. Journal of Pharmaceutical Sciences. 95:2186-2194 (2006).
137. A.S. Michaels, S.K. Chandrasekaran, and J.E. Shaw. Drug permeation through human skin: Theory and *in vitro* experimental measurement. American Institute for Chemical Engineers. 21:985-996 (1975).

138. P. Poulin and K. Krishnan. Molecular structure-based prediction of human abdominal skin permeability coefficients for several organic compounds. *Journal of Toxicology and Environmental Health - Part A*. 62:143-159 (2001).
139. G.C. Charalambopoulou, P. Karamertzanis, E.S. Kikkinides, A.K. Stubos, N.K. Kanellopoulos, and A.T. Papaioannou. A study on structural and diffusion properties of porcine stratum corneum based on very small angle neutron scattering data. *Pharmaceutical Research*. 17:1085-1091 (2000).
140. S. Mitragotri, M.E. Johnson, D. Blankschtein, and R. Langer. An analysis of the size selectivity of solute partitioning, diffusion, and permeation across lipid bilayers. *Biophysical Journal*. 77:1268-1283 (1999).
141. T.-F. Wang, G.B. Kasting, and J.M. Nitsche. A multiphase microscopic diffusion model for stratum corneum permeability. II. Estimation of physicochemical parameters, and application to a large permeability database. *Journal of Pharmaceutical Sciences*. 96:3024-3051 (2007).
142. M. Heisig, R. Lieckfeldt, G. Wittum, G. Mazurkevich, and G. Lee. Non steady-state descriptions of drug permeation through stratum corneum. I. The biphasic brick-and-mortar model. *Pharmaceutical Research*. 13:421-426 (1996).
143. A.M. Barbero and H.F. Frasch. Modeling of diffusion with partitioning in stratum corneum using a finite element model. *Annals of Biomedical Engineering*. 33:1281-1292 (2005).
144. K. George, K. Kubota, and E.H. Twizell. A two-dimensional mathematical model of percutaneous drug absorption. *BioMedical Engineering Online*. 3: (2004).
145. K. George. A two-dimensional mathematical model of non-linear dual-sorption of percutaneous drug absorption. *BioMedical Engineering Online*. 4: (2005).
146. L.A. Chen, G.B. Lian, and L.A. Han. Use of "bricks and mortar" model to predict transdermal permeation: Model development and initial validation. *Industrial and Engineering Chemistry Research*. 47:6465-6472 (2008).
147. A.L. Stinchcomb, F. Pirot, G.D. Touraille, A.L. Bunge, and R.H. Guy. Chemical uptake into human stratum corneum *in vivo* from volatile and non-volatile solvents. *Pharmaceutical Research*. 16:1288-1293 (1999).

148. J.E. Rim, P.M. Pinsky, and W.W. van Osdol. Using the method of homogenization to calculate the effective diffusivity of the stratum corneum. *Journal of Membrane Science*. 293:174-182 (2007).
149. D. Feuchter, M. Heisig, and G. Wittum. A geometry model for the simulation of drug diffusion through the stratum corneum. *Computing and Visualization in Science*. 9:117-130 (2006).
150. J.M. Nitsche, T.F. Wang, and G.B. Kasting. A two-phase analysis of solute partitioning into the stratum corneum. *Journal of Pharmaceutical Sciences*. 95:649-666 (2006).
151. H.F. Frasch and A.M. Barbero. The transient dermal exposure: theory and experimental examples using skin and silicone membranes. *Journal of Pharmaceutical Sciences*. 97:1578-1592 (2008).
152. M. Heisig, D. Feuchter, A. Nägel, and G. Wittum. Numerical simulation of drug diffusion through a three-dimensional model stratum corneum, CRS, 2005.
153. Y.N. Kalia, F. Pirot, and R.H. Guy. Homogeneous transport in a heterogeneous membrane: water diffusion across human stratum corneum *in vivo*. *Biophysical Journal*. 71:2692-2700 (1996).
154. S.E. Cross, B.M. Magnusson, G. Winckle, Y. Anissimov, and M.S. Roberts. Determination of the effect of lipophilicity on the *in vitro* permeability and tissue reservoir characteristics of topically applied solutes in human skin layers. *Journal of Investigative Dermatology*. 120:759-764 (2003).
155. A. Henning, D. Neumann, K.H. Kostka, C.M. Lehr, and U.F. Schaefer. Influence of Human Skin Specimens Consisting of Different Skin Layers on the Result of *in vitro* Permeation Experiments. *Skin Pharmacol Physiol*. 21:81-88 (2008).
156. M.E. Johnson, D.A. Berk, D. Blankschtein, D.E. Golan, R.K. Jain, and R.S. Langer. Lateral diffusion of small compounds in human stratum corneum and model lipid bilayer systems. *Biophysical Journal*. 71:2656-2668 (1996).
157. B.D. Anderson, W.I. Higuchi, and P.V. Raykar. Heterogeneity effects on permeability - partition coefficient relationships in human stratum corneum. *Pharmaceutical Research*. 5:566-573 (1988).
158. B.D. Anderson and P.V. Raykar. Solute structure-permeability relationships in human stratum corneum. *Journal of Investigative Dermatology*. 93:280-286 (1989).

159. S. Mitragotri. In situ determination of partition and diffusion coefficients in the lipid bilayers of Stratum corneum. *Pharmaceutical Research*. 17:1026-1029 (2000).
160. S. Mitragotri. A theoretical analysis of permeation of small hydrophobic solutes across the stratum corneum based on scaled particle theory. *Journal of Pharmaceutical Sciences*. 91:744-752 (2002).
161. R.J. Scheuplein. Mechanism of percutaneous absorption. II. Transient diffusion and the relative importance of various routes of skin penetration. *Journal of Investigative Dermatology*. 48:79-88 (1967).
162. W.R. Lieb and W.D. Stein. Biological membranes behave as non-porous polymeric sheets with respect to the diffusion of non-electrolytes. *Nature*. 224:240-243 (1986).
163. W.J. Pugh, I.T. Degim, and J. Hadgraft. Epidermal permeability - penetrant structure relationship. 4. QSAR of permeant diffusion across human stratum corneum in terms of molecular weight, H-bonding and electron charge. *International Journal of Pharmaceutics*. 197:203-211 (2000).
164. D. Neumann, O. Kohlbacher, C. Merkwirth, and T. Lengauer. A Fully Computational Model for Predicting Percutaneous Drug Absorption. *Journal of chemical information and modeling*. 46:424-429 (2006).
165. B.M. Magnusson, W.J. Pugh, and M.S. Roberts. Simple rules defining the potential of compounds for transdermal delivery or toxicity. *Pharmaceutical Research*. 21:1047-1054 (2004).
166. W.J. Albery and J. Hadgraft. Percutaneous absorption: theoretical description. *Journal of Pharmacy and Pharmacology*. 31:129-139 (1979).
167. M.E. Hatcher and W.Z. Plachy. Dioxygen diffusion in the stratum corneum: an EPR spin label study. *Biochimica et Biophysica Acta*. 1149:73-78 (1993).
168. K.J. Packer and T.C. Sellwood. Proton magnetic resonance studies of hydrated stratum corneum. Part 2. - Self diffusion. *Journal of the Chemical Society, Faraday Transactions 1: Physical Chemistry in Condensed Phases*. 74:1592-1606 (1978).
169. R.J. Phillips, W.M. Deen, and J.F. Brady. Hindered transport in fibrous membranes and gels: effect of solute size and fiber configuration. *Journal of Colloid Interface Science*. 139:363-373 (1990).

170. A. Naegel, S. Hansen, D. Neumann, C.M. Lehr, U.F. Schaefer, G. Wittum, and M. Heisig. In-silico model of skin penetration based on experimentally determined input parameters. Part II: Mathematical modelling of in-vitro diffusion experiments. Identification of critical input parameters. *European Journal of Pharmaceutics and Biopharmaceutics*. 68:368-379 (2008).
171. E. Abignente and P. de Caprariis. Flufenamic acid. In K. Florey (ed.), *Analytical profiles of drug substances*, Vol. 11, Academic Press, New York, London, 1982, p. 324.
172. M.U. Zubair, M.M.A. Hassan, and I.A. Al-Meshal. Caffeine. In K. Florey (ed.), *Analytical profiles of drug substances*, Vol. 15, Academic Press, Inc., London, 1986.
173. H. Wagner, K.H. Kostka, C.M. Lehr, and U.F. Schaefer. Drug distribution in human skin using two different *in vitro* test systems: comparison with *in vivo* data. *Pharmaceutical Research*. 17:1475-1481 (2000).
174. A.M. Kligman and E. Christophers. Preparation of Isolated Sheets of Human Stratum Corneum. *Archives of Dermatological Research*. 88:702-705 (1963).
175. M. de Jager, W. Groenink, J. van der Spek, C. Janmaat, G. Gooris, M. Poncet, and J. Bouwstra. Preparation and characterization of a stratum corneum substitute for *in vitro* percutaneous penetration studies. *Biochimica et Biophysica Acta*. 1758:636-644 (2006).
176. F. Netzlaff, M. Kaca, U. Bock, E. Haltner-Ukomadu, P. Meiers, C.-M. Lehr, and U.F. Schaefer. Permeability of the reconstructed human epidermis model Episkin® in comparison to various human skin preparations. *European Journal of Pharmaceutics and Biopharmaceutics*. 66:127-134 (2007).
177. F. Theobald. In-vitro Methoden zur biopharmazeutischen Qualitätsprüfung von Dermatika unter Berücksichtigung der Lipidzusammensetzung des Stratum Corneum, *Saarbruecken*, Universität des Saarlandes, Saarbruecken, 1998.
178. M. Schaefer-Korting, U. Bock, A. Gamer, A. Haberland, E. Haltner-Ukomadu, M. Kaca, H. Kamp, M. Kietzmann, H.C. Korting, H.-U. Kraechter, C.-M. Lehr, M. Liebsch, A. Mehling, F. Netzlaff, F. Niedorf, M.K. Ruebbelke, U. Schaefer, E. Schmidt, S. Schreiber, K.-R. Schroeder, H. Spielmann, and A. Vuia. Reconstructed human epidermis for skin absorption testing: Results of the German prevalidation study. *Alternatives to Laboratory Animals: ATLA*. 34:283-294 (2006).

179. E. Jaeckle. Stratum Corneum analoge Lipidmischungen als Diffusionsmedien, ihre Eigenschaften und deren Beeinflussung durch Salbengrundlagen, Saarland university, Saarbrücken, 1996.
180. C. Surber, K.-P. Wilhelm, M. Hori, H.I. Maibach, and R.H. Guy. Optimization of topical therapy: Partitioning of drugs into stratum corneum. *Pharmaceutical Research*. 7:1320-1324 (1990).
181. D. van der Merwe and J.E. Riviere. Comparative studies on the effects of water, ethanol and water/ethanol mixtures on chemical partitioning into porcine stratum corneum and silastic membrane. *Toxicology in vitro*. 19:69-77 (2005).
182. J. Hadgraft. Calculations of drug release rates from controlled release devices. The slab. *International Journal of Pharmaceutics*. 2:177-194 (1979).
183. C. Herkenne, A. Naik, Y.N. Kalia, J. Hadgraft, and R.H. Guy. Pig ear skin ex vivo as a model for *in vivo* dermatopharmacokinetic studies in man. *Pharmaceutical Research*. 23:1850-1856 (2006).
184. H.S. Carslow and J.C. Jaeger. Conduction of heat in soils, Clarendon Press, Oxford, 1959.
185. Sun. Numerical Computation Guide, Sun Microsystems Inc., Paolo Alto, 2000.
186. S.E. Cross, W.J. Pugh, J. Hadgraft, and M.S. Roberts. Probing the effect of vehicles on topical delivery: understanding the basic relationship between solvent and solute penetration using silicone membranes. *Pharmaceutical Research*. 18:999-1005 (2001).
187. J.A. Bouwstra, G.S. Gooris, M.A. Salomons-de Vries, J.A. Van der Spek, and W. Bras. Structure of human stratum corneum as a function of temperature and hydration: A wide-angle X-ray diffraction study. *International Journal of Pharmaceutics*. 84:205-216 (1992).
188. M.W. De Jager, G.S. Gooris, I.P. Dolbnya, W. Bras, M. Ponec, and J.A. Bouwstra. The phase behaviour of skin lipid mixtures based on synthetic ceramides. *Chemistry and Physics of Lipids*. 124:123-134 (2003).
189. H. Tanojo, J.A. Bouwstra, H.E. Junginger, and H.E. Bodde. Thermal analysis studies on human skin and skin barrier modulation by fatty acids and propylene glycol. *Journal of Thermal Analysis and Calorimetry*. 57:313-322 (1999).

190. C.L. Silva, S.C.C. Nunes, M.E.S. Eusebio, A.A.C.C. Pais, and J.J.S. Sousa. Thermal behaviour of human stratum corneum: A differential scanning calorimetry study at high scanning rates. *Skin Pharmacology and Physiology*. 19:132-139 (2006).
191. K. De Paepe, A. Weerheim, E. Houben, D. Roseeuw, M. Poncet, and V. Rogiers. Analysis of Epidermal Lipids of the Healthy Human Skin: Factors Affecting the Design of a Control Population. *Skin Pharmacology and Physiology*. 17:23-30 (2004).
192. P.W. Wertz, D.C. Swartzendruber, K.C. Madison, and D.T. Downing. Composition and morphology of epidermal cyst lipids. *Journal of Investigative Dermatology*. 89:419-425 (1987).
193. D. Bommannan, R.O. Potts, and R.H. Guy. Examination of stratum corneum barrier function *in vivo* by infrared spectroscopy. *Journal of Investigative Dermatology*. 95:403-408 (1990).
194. B. Mueller, Y.G. Anissimov, and M.S. Roberts. Unexpected clobetasol propionate profile in human stratum corneum after topical application *in vitro*. *Pharmaceutical Research*. 20:1835-1837 (2003).
195. W. Abraham and D.T. Downing. Preparation of model membranes for skin permeability studies using stratum corneum lipids. *Journal of Investigative Dermatology*. 93:809-813 (1989).
196. D. Kuempel, D.C. Swartzendruber, C.A. Squier, and P.W. Wertz. *In vitro* reconstitution of stratum corneum lipid lamellae. *Biochimica et Biophysica Acta*. 1372:135-140 (1998).
197. H. Wagner, K.H. Kostka, C.M. Lehr, and U.F. Schaefer. pH profiles in human skin: influence of two *in vitro* test systems for drug delivery testing. *European Journal of Pharmaceutics and Biopharmaceutics*. 55:57-65 (2003).
198. R. Lange-Lieckfeldt and G. Lee. Use of a model lipid matrix to demonstrate the dependence of the stratum corneum's barrier properties on its internal geometry. *Journal of Controlled Release*. 20:183-194 (1992).
199. M.W. De Jager, G.S. Gooris, I.P. Dolbnya, M. Poncet, and J.A. Bouwstra. Modelling the stratum corneum lipid organisation with synthetic lipid mixtures: The importance of synthetic ceramide composition. *Biochimica et Biophysica Acta*. 1664:132-140 (2004).

200. L. Norlén, A. Emilson, and B. Forslind. Stratum corneum swelling. Biophysical and computer assisted quantitative assessments. Archives of Dermatological Research. 289:506-513 (1997).
201. A.D. Jones, I.P. Dick, J.W. Cherrie, M.T.D. Cronin, J.J. van de Sandt, D.J. Esdaile, S. Iyengar, W.F. ten Berge, S.C. Wilkinson, C.S. Roper, S. Semple, C. de Heer, and F.M. Williams. CEFIC workshop on methods to determine dermal permeation for human risk assessment. European Chemical Industry Council (2004).
202. F.M. Williams. EDETOX. Evaluations and predictions of dermal absorption of toxic chemicals. International Archives of Occupational and Environmental Health. 77:150-151 (2004).
203. Commission Proposal for a Regulation of the European Parliament and of the Council concerning the Registration, Evaluation, Authorisation and Restrictions of Chemicals (REACH), Establishing a European Chemicals Agency and amending Directive 1999/45/EC on the classification, packaging and labelling dangerous preparations and Regulation (EC) from 29 October 2003, COM, Vol. 644, Commission of the European Communities, Brussels, 2003, p. final.
204. R.H. Guy and J. Hadgraft. Transdermal drug delivery: A simplified pharmacokinetic approach. International Journal of Pharmaceutics. 24:267-274 (1985).
205. G. Gienger, A. Knoch, and H.P. Merkle. Modeling and numerical computation of drug transport in laminates: Model case evaluation of transdermal delivery system. Journal of Pharmaceutical Sciences. 75:9-15 (1986).
206. M. Wolf. Mathematisch-physikalische Berechnungs- und Simulationsmodelle zur Beschreibung und Entwicklung therapeutischer Systeme, University of Bonn, 1993.
207. M. Schmauder. Diffusion through the human skin - an unexpected application of a PDE-black-box-solver. ZAMM. 75:707-708 (1995).
208. K. Sugibayashi, T. Hayashi, T. Hatanaka, M. Ogihara, and Y. Morimoto. Analysis of simultaneous transport and metabolism of ethyl nicotinate in hairless rat skin. Pharmaceutical Research. 13:855-860 (1996).
209. K. Sugibayashi, T. Hayashi, and Y. Morimoto. Simultaneous transport and metabolism of ethyl nicotinate in hairless rat skin after its topical application:

- The effect of enzyme distribution in skin. *Journal of Controlled Release*. 62:201-208 (1999).
210. P. Boderke, K. Schittkowski, M. Wolf, and H.P. Merkle. Modeling of diffusion and concurrent metabolism in cutaneous tissue. *Journal of Theoretical Biology*. 204:393-407 (2000).
 211. K. Kubota, F. Dey, S.A. Matar, and E.H. Twizell. A repeated-dose model of percutaneous drug absorption. *Applied Mathematical Modelling*. 26:529-544 (2002).
 212. H.F. Frasch. A random walk model of skin permeation. *Risk Analysis*. 22:265-276 (2002).
 213. T. Yotsuyanagi and W.I. Higuchi. A two phase series model for the transport of steroids across the fully hydrated stratum corneum. *Journal of Pharmacy and Pharmacology*. 24:934-941 (1972).
 214. D.A. Edwards and R. Langer. A linear theory of transdermal transport phenomena. *Journal of Pharmaceutical Sciences*. 83:1315-1334 (1994).
 215. B. Yu, C.-Y. Dong, P.T.C. So, D. Blankschtein, and R. Langer. *In vitro* visualization and quantification of oleic acid induced changes in transdermal transport using two-photon fluorescence microscopy. *Journal of Investigative Dermatology*. 117:16-25 (2001).
 216. K.M. Hanson, M.J. Behne, N.P. Barry, T.M. Mauro, E. Gratton, and R.M. Clegg. Two-photon fluorescence lifetime imaging of the skin stratum corneum pH gradient. *Biophysical Journal*. 83:1682-1690 (2002).
 217. K. Abdulmajed, C.M. Heard, C. McGuigan, and W.J. Pugh. Topical delivery of retinyl ascorbate co-drug. 2. Comparative skin tissue and keratin binding studies. *Skin Pharmacology and Physiology*. 17:274-282 (2004).
 218. P. Talreja, N.K. Kleene, W.L. Pickens, T.F. Wang, and G.B. Kasting. Visualization of the lipid barrier and measurement of lipid pathlength in human stratum corneum. *AAPS Pharmaceutical Sciences*. 3:E13 (2001).
 219. W.R. Vieth and K.J. Sladek. A model for diffusion in a glassy polymer. *Journal of Colloid Science*. 20:1014-1033 (1965).
 220. E. Nelson. *Dynamical Theories of Brownian Motion*, Princeton University Press, 2001.
 221. A.C. Williams and B.W. Barry. Penetration enhancers. *Advanced Drug Delivery Reviews*. 56:603-618 (2004).

- 222. R. Panchagnula, H. Desu, A. Jain, and S. Khandavilli. Effect of lipid bilayer alteration on transdermal delivery of a high-molecular-weight and lipophilic drug: studies with paclitaxel. *Journal of Pharmaceutical Sciences*. 93:2177-2183 (2004).
- 223. A.K. Jain, N.S. Thomas, and R. Panchagnula. Transdermal drug delivery of imipramine hydrochloride. I. Effect of terpenes. *Journal of Controlled Release*. 79:93-101 (2002).
- 224. M. Sznitowska, S. Janicki, and A.C. Williams. Intracellular or intercellular localization of the polar pathway of penetration across stratum corneum. *Journal of Pharmaceutical Sciences*. 87:1109-1114 (1998).
- 225. K.D. Peck, A.-H. Ghanem, and W.I. Higuchi. Hindered diffusion of polar molecules through and effective pore radii estimates of intact and ethanol treated human epidermal membrane. *Pharmaceutical Research*. 11:1306-1314 (1994).
- 226. B. Yu, K.H. Kim, P.T. So, D. Blankschtein, and R. Langer. Evaluation of fluorescent probe surface intensities as an indicator of transdermal permeant distributions using wide-area two-photon fluorescence microscopy. *J Pharm Sci*. 92:2354-2365 (2003).
- 227. A. Weerheim and M. Ponc. Determination of stratum corneum lipid profile by tape stripping in combination with high-performance thin-layer chromatography. *Archives of Dermatological Research*. 293:191-199 (2001).
- 228. K. Walkley. Bound water in stratum corneum measured by differential scanning calorimetry. *Journal of Investigative Dermatology*. 50:225-227 (1972).
- 229. J.R. Hansen and W. Yellin. NMR and infrared spectroscopy studies of stratum corneum hydration. In H.H.G. Jellinek (ed.), *Water structure at the water-polymer interface*, Plenum Press, New York, 1972, pp. 19-28.
- 230. M.I. Foreman. A proton magnetic resonance study of water in human stratum corneum. *Biochimica et Biophysica Acta*. 437:599-603 (1976).
- 231. D.A. Van Hal, E. Jeremiasse, H.E. Junginger, F. Spies, and J.A. Bouwstra. Structure of fully hydrated human stratum corneum: A freeze-fracture electron microscopy study. *Journal of Investigative Dermatology*. 106:89-95 (1996).

232. G.C. Charalambopoulou, T.A. Steriotis, T. Hauss, A.K. Stubos, and N.K. Kanellopoulos. Structural alterations of fully hydrated human stratum corneum. *Physica B: Condensed Matter*. 350: (2004).
233. T.P. Banning and C.M. Heard. Binding of doxycycline to keratin, melanin and human epidermal tissue. *International Journal of Pharmaceutics*. 235:219-227 (2002).
234. C.M. Heard, B.V. Monk, and A.J. Modley. Binding of primaquine to epidermal membranes and keratin. *International Journal of Pharmaceutics*. 257:237-244 (2003).
235. U. Hagedorn-Leweke and B.C. Lippold. Accumulation of sunscreens and other compounds in keratinous substrates. *European Journal of Pharmaceutics and Biopharmaceutics*. 46:215-221 (1998).
236. H. Wagner, K.H. Kostka, C.M. Lehr, and U.F. Schaefer. Correlation between stratum corneum/water-partition coefficient and amounts of flufenamic acid penetrated into the stratum corneum. *Journal of Pharmaceutical Sciences*. 91:1915-1921 (2002).
237. C. Surber, K.-P. Wilhelm, H.I. Maibach, L.L. Hall, and R.H. Guy. Partitioning of chemicals into human stratum corneum: Implications for risk assessment following dermal exposure. *Fundamental and Applied Toxicology*. 15:99-107 (1990).
238. P. Meares. The diffusion of gases through polyvinyl acetate. *Journal of the American Chemical Society*. 76:3415-3422 (1954).
239. S. Hansen, A. Henning, A. Naegel, M. Heisig, G. Wittum, D. Neumann, K.H. Kostka, J. Zbytovska, C.M. Lehr, and U.F. Schaefer. In-silico model of skin penetration based on experimentally determined input parameters. Part I: Experimental determination of partition and diffusion coefficients. *European Journal of Pharmaceutics and Biopharmaceutics*. 68:352-367 (2008).
240. R.L. Anderson and J.M. Cassidy. Variation in physical dimensions and chemical composition of human stratum corneum. *Journal of Investigative Dermatology*. 61:30-32 (1973).
241. S. Sobue, K. Sekiguchi, and T. Nabeshima. Intracutaneous distributions of fluconazole, itraconazole, and griseofulvin in Guinea pigs and binding to human stratum corneum. *Antimicrobial Agents and Chemotherapeutics*. 48:216-223 (2004).

242. H. Takahashi. Problems with the topical antimycotics. *Japanese Journal of Medical Mycology*. 35:331-334 (1994).
243. S.P. Banks Schlegel and C.C. Harris. Tissue-specific expression of keratin proteins in human esophageal and epidermal epithelium and their cultured keratinocytes. *Experimental Cell Research*. 146:271-280 (1983).
244. P.G. Chu and L.M. Weiss. Keratin expression in human tissues and neoplasms. *Histopathology*. 40:403-439 (2002).
245. J. Kubilus, M.J. MacDonald, and H.P. Baden. Epidermal proteins of cultured human and bovine keratinocytes. *Biochimica et Biophysica Acta*. 578:484-492 (1979).
246. Y. Katz and J.M. Diamond. A method for measuring nonelectrolyte partition coefficients between liposomes and water. *Journal of Membrane Biology*. 17:69-86 (1974).
247. Y. Katz and J.M. Diamond. Nonsolvent water in liposomes. *Journal of Membrane Biology*. 17:87-100 (1974).
248. A.L. Bunge and R.L. Cleek. A new method for estimating dermal absorption chemical exposure: 2. Effect of molecular weight and octanol-water partitioning. *Pharmaceutical Research*. 12:88-95 (1995).
249. S. Yadav, N.G. Pinto, and G.B. Kasting. Thermodynamics of water interaction with human stratum corneum I: Measurement by isothermal calorimetry. *Journal of Pharmaceutical Sciences*. 96:1585-1597 (2007).
250. A. Alonso, J.V. Da Silva, and M. Tabak. Hydration effects on the protein dynamics in stratum corneum as evaluated by EPR spectroscopy. *Biochimica et Biophysica Acta - Proteins and Proteomics*. 1646:32-41 (2003).
251. I.H. Blank, J. Moloney, 3rd, A.G. Emslie, I. Simon, and C. Apt. The diffusion of water across the stratum corneum as a function of its water content. *Journal of Investigative Dermatology*. 82:188-194 (1984).
252. G. Imokawa, H. Kuno, and M. Kawai. Stratum corneum lipids serve as a bound-water modulator. *Journal of Investigative Dermatology*. 96:845-851 (1991).
253. M.D. Barratt. Quantitative structure-activity relationships for skin permeability. *Toxicology in vitro*. 9:27-37 (1995).
254. M. Schaefer-Korting, U. Bock, W. Diembeck, H.-J. Duesing, A. Gamer, E. Haltner-Ukomadu, C. Hoffmann, M. Kaca, H. Kamp, S. Kersen, M. Kietzmann,

H.C. Korting, H.-U. Kraechter, C.-M. Lehr, M. Liebsch, A. Mehling, C. Mueller-Goymann, F. Netzlaff, F. Niedorf, M.K. Ruebbelke, U. Schaefer, E. Schmidt, S. Schreiber, H. Spielmann, A. Vuia, and M. Weimer. The use of reconstructed human epidermis for skin absorption testing: Results of the validation study. *Alternatives to Laboratory Animals: ATLA*. 36:161-187 (2008).

ABBREVIATIONS

Definitions are given for the symbols used in the main text in alphabetical order.

aqu	aqueous corneocyte domain
c_i	concentration
CAF	caffeine
$c_{\max,i}$	Langmuir saturation constant (maximum binding capacity)
cor	corneocytes
cpe	cornified protein envelope
D_{cor}	diffusion coefficient within corneocytes
DCM	dichloro methane
don	Donor
SC,dry	usually freeze-dried SC, $\omega_{\text{aqu}} = 0$
FFA	flufenamic acid
SC,hyd	hydrated SC
k_i	Langmuir binding affinity (adsorption coefficient)
K_{ij}	partition coefficient
ker	keratin
lip	intercellular SC lipid bilayers
$K_{\text{Oct/w}}$	logarithmical octanol water partition coefficient
LVP	low viscous paraffin
M1	compartmental model 1
M2	compartmental model 2
MW	molecular weight
pK_a	acid constant
pro	SC proteins (= ker + cpe)
$q_{\max,i}$	protein maximum loading capacity
s_i	saturation concentration
SC	stratum corneum
Soer,7.4	Soerensen phosphate buffer pH 7.4
TST	testosterone
V_i	volume
w_i	weight

w_0	weight of substance in incubation solution before equilibration
w_{End}	weight of substance in incubation solution after equilibration
ρ_i	density
$\Gamma_{i,j}$	interface
Ω_i	compartment
ϕ_j^i	volume fraction V_i/V_j
ω_j^i	weight fraction w_i/w_j
$\omega_{\text{SC,dry}}^{\text{aqu, bound}}$	weight fraction of bound aqueous phase per weight of dry SC
c_0	initial concentration of substance within the incubation solution
c_{exSC}	concentration within the bottom layer of the <i>stratum corneum</i> , i.e. the last pool of tape-strips
c_{inDSL}	concentration within the topmost layer of the viable deeper skin layers, i.e. the first pool of cryo-cuts
D_i	apparent diffusion coefficient, $i \in I$
dc/dx	concentration gradient
Der	dermis
DSL	viable deeper skin layers
Epi	epidermis
h	membrane thickness
I	index set $\{\text{aqu, cor, cpe, Der, don, DSL, Epi, lip, ker}\}$
J_{ss}	steady state flux
$K_{i/j}$	partition coefficient $i \neq j$ and $i, j \in I$
k_p	apparent permeability coefficient
w_0	weight of substance within the incubation solution before equilibration
w_{End}	weight of substance within the incubation solution after equilibration
w_i	dry weight of skin compartment i
w_{Ex}	weight of substance extracted from a skin compartment
M1	compartmental model 1
M2	compartmental model 2
MW	molecular weight
pK_a	acid constant

CURRICULUM VITAE

Personal Information

Name	Steffi Hansen
Address	Rentrischer Strasse 3, 66123 Saarbrücken
Born	18.03.1981, Rostock
Nationality	German

School

09/1987-07/1991	5. POS Villis Lacis, Rostock
09/1991-07/1997	Albert-Schweitzer-Gymnasium, Rostock
09/1997-07/1999	Ernst-Barlach-Gymnasium, Rostock

Undergraduate Studies

10/1999-10/2003	Pharmacy, Ernst-Moritz-Arndt-University, Greifswald
-----------------	---

Master thesis

11/2003-04/2004	Department of Pharmaceutical Technology, Ernst-Moritz-Arndt-University, Greifswald “Charakterisierung eines Ferrofluids für das magnetische drug-targeting”
-----------------	---

PhD-thesis

01/2005-12/2008	Department of Biopharmaceutics and Pharmaceutical Technology, Saarland University, Saarbrücken
-----------------	--

LIST OF PUBLICATIONS

Publications in peer-reviewed journals:

S. Hansen, A. Henning, A. Naegel, M. Heisig, G. Wittum, D. Neumann, K.H. Kostka, J. Zbytovska, C.M. Lehr, U.F. Schaefer, In silico model of skin penetration based on experimentally determined input parameters. Part I: Experimental determination of partition and diffusion coefficients, *European Journal of Pharmaceutics and Biopharmaceutics* **68** (2008) 352-367.

A. Naegel, S. Hansen, D. Neumann, C.-M. Lehr, U.F. Schaefer, G. Wittum, M. Heisig, In silico model of skin penetration based on experimentally determined input parameters. Part II: Mathematical modelling of in-vitro diffusion Experiments. Identification of critical input parameters, *European Journal of Pharmaceutics and Biopharmaceutics* **68** (2008) 368-79.

S. Hansen, A. Naegel, M. Heisig, G. Wittum, D. Neumann, K.H. Kostka, P. Meiers C.M. Lehr, U.F. Schaefer, *The role of corneocytes in skin transport revised – a combined experimental and computational approach*, *Pharmaceutical Research* **26** (2009) 1379-97.

Book chapters:

U.F. Schaefer, S. Hansen, M. Schneider, J. Luengo, C.M. Lehr, *Models for Skin Absorption and Skin Toxicity Testing*, in: C. Ehrhardt, K.-J. Kim (Eds.), *Drug absorption Studies. In situ, in vitro and in silico models*, Springer, New York, 2008, pp 3-33.

Conference Contributions – Oral presentations:

S. Hansen, K.H. Kostka, D. Neumann, C.-M. Lehr, U.F. Schäfer, Experimental determination of partition coefficients important for modeling skin penetration.

Controlled Release Society German Chapter Annual Meeting 2006, Jena, Germany, February 23-24 2006

S. Hansen, A. Henning, A. Nägel, D. Feuchter, M. Heisig, G. Wittum, D. Neumann, C.-M. Lehr, U.F. Schäfer, Experimental determination of partition and diffusion coefficients important for *in silico* modeling of skin penetration.

33rd Annual Meeting and Exposition of the Controlled Release Society, Vienna, Austria, July 22-26 2006

S. Hansen, Cutaneous absorption – *in vitro* studies.

Galenos Course Intensive Program, SKIN BARRIER FUNCTION “Cutaneous absorption and Environmental Factors”, Claude Bernard University, Lyon, France, September 16 - October 2 2007

S. Hansen, Cutaneous absorption – *in vitro* studies.

Galenos Course Intensive Program, SKIN BARRIER FUNCTION “Cutaneous absorption and Environmental Factors”, Claude Bernard University, Lyon, France, October 12-26 2008

S. Hansen, *In vitro* and *in silico* methods for investigating (per)cutaneous absorption. APGI Skin and Formulation 3rd Symposium/ Skin Forum 10th Annual Meeting, Versaille, France, March, 09-10 2009

Conference Contributions – Poster presentations:

S. Hansen, A. Henning, A. Nägel, D. Feuchter, M. Heisig, G. Wittum, D. Neumann, C.-M. Lehr, U.F. Schäfer, Description of skin transport on the basis of experimentally determined partition and diffusion coefficients and their use for *in silico* modeling of skin penetration.

6th International Conference and Workshop on Cell Culture and *in vitro* Models for Drug Absorption and Delivery, Saarbruecken, Germany, March 1-10 2006

S.Hansen, A. Henning, A. Nägel, D.Feuchter, M. Heisig, G. Wittum, D. Neumann, C.-M. Lehr, U.F. Schäfer, Experimental determination of partition and diffusion coefficients important for modeling skin penetration

10th International Conference Perspectives in Percutaneous Penetration, La Grande Motte, France, April 18-22 2006

S.Hansen, A. Nägel, D.Feuchter, M. Heisig, G. Wittum, D. Neumann, C.-M. Lehr, U.F. Schäfer, Partition and diffusion – the experimental basis for *in silico* modeling of skin absorption.

Deutsche Pharmazeutische Gesellschaft Doktorandentagung, Nürnberg-Heroldsberg, Germany, September 6-8 2006

L. Kolackova, S. Hansen, C.-M. Lehr, P. Dolezal, U.F. Schäfer, Comparison of permeation of various drugs from a lipophilic donor solution through human skin.

Pharmaceutical Sciences World Congress, Amsterdam, Netherlands, April 20-25 2007

A. Naegel, S. Hansen, D. Neumann, C.-M. Lehr, U.F. Schaefer, G. Wittum, M. Heisig, *In silico* model of skin penetration based on experimentally determined input parameters.

Occupational and Environmental Exposures of Skin to Chemicals, Golden, Colorado USA, June 17-20 2007

S. Hansen, A. Naegel, M. Heisig, G. Wittum, D. Neumann, K.H. Kostka, C.M. Lehr, U.F. Schäfer, Partition and diffusion - The experimental basis for *in silico* modeling of skin absorption.

14th Congress on Alternatives to Animal Testing, Linz, Austria, September 28-30 2007

O. Frings, S.Hansen, C.-M. Lehr, U.F. Schäfer, Quantification of keratin binding of drug substances.

Deutsche Pharmazeutische Gesellschaft Jahrestagung, Erlangen, Germany, Oktober 10-12 2007:

S.Hansen, A. Nägel, M. Heisig, G. Wittum, D. Neumann, C.-M. Lehr, U.F. Schäfer, Investigation of the influence of hydration on the stratum corneum-donor partition coefficient.

7th International Conference and Workshop on Cell Culture and *in vitro* Models for Drug Absorption and Delivery, Saarbruecken, Germany, February 20-29 2008

S.Hansen, A. Nägel, M. Heisig, G. Wittum, D. Neumann, C.-M. Lehr, U.F. Schäfer, Keratin binding and partitioning into the aqueous domain – an experimental and theoretical evaluation of compound interactions with corneocytes,

11th International Conference Perspectives in Percutaneous Penetration, La Grande Motte, France, March 25-29 2008

S.Hansen, A. Nägel, M. Heisig, G. Wittum, D. Neumann, C.-M. Lehr, U.F. Schäfer, Experimental and theoretical investigation of corneocyte-drug interactions: effect of hydration on stratum corneum partitioning of caffeine.

34rd Annual Meeting and Exposition of the Controlled Release Society, New York, USA, July 12-16 2008

S. Hansen, T. Hahn, C.M. Lehr, U.F. Schäfer, One step further towards computer assisted simulation of percutaneous absorption to avoid animal experiments –the combination of experiment and simulation effectively helps to identify new important parameters.

15th Congress on Alternatives to Animal Testing, Linz, Austria, September 19-21 2008

S. Hansen, A. Naegel, M. Heisig, G. Wittum, D. Neumann, C.M. Lehr, U.F. Schäfer, Compartmental analysis of drug-corneocyte interaction – an evaluation of critical parameters.

American Association of Pharmaceutical Scientists, USA, November 16-20 2008

Teaching experience

S. Hansen, A. Henning, J. Luengo-Contreras, U.F. Schäfer, Lab-course I. Skin barrier and drug delivery.

6th International Conference and Workshop on Cell Culture and *in vitro* Models for Drug Absorption and Delivery, Saarbruecken, Germany, March 1-10 2006

S. Hansen, A. Henning, S. Schmitt, A. Melero, U.F. Schäfer, Labcourse I. Skin barrier and drug delivery.

7th International Conference and Workshop on Cell Culture and *in vitro* Models for Drug Absorption and Delivery, Saarbruecken, Germany, February 20-29 2008

S. Hansen, A. Henning, U.F. Schäfer, Pharmaceutical Technology. Labcourse for pharmacy students in their basic study period.

S. Hansen, S. Taetz, B. Wahl, T. Hahn, Semisolid formulations. Labcourse for pharmacy students in their advanced study period.

S. Hansen, C.-M. Lehr, Interdisciplinary lecture course in Biopharmaceutics. Skin drug delivery I and II. Winter semester 2008/2009.

Awards

A. Naegel, S. Hansen, D. Neumann, C.-M. Lehr, U.F. Schaefer, G. Wittum, M. Heisig, *In silico* model of skin penetration based on experimentally determined input parameters.

Occupational and Environmental Exposures of Skin to Chemicals, Golden, Colorado USA, June 17-20 2007: (poster award: best in category "skin exposure")

DANKSAGUNG

Zunächst bedanke ich mich bei Herrn Prof. Dr. Claus-Michael Lehr für die Bereitstellung des Themas und die Gewährung vielfacher Möglichkeiten meine Arbeiten auf internationalen Kongressen vorzustellen. Des Weiteren danke ich Herrn Prof. Dr. Volkhard Helms für die Anfertigung des Zweitgutachtens, sowie den anderen Mitgliedern der Prüfungskommission.

Ein besonderer Dank geht an meinen Betreuer Herrn Dr. Ulrich Schäfer, der mir immer wissenschaftlich und moralisch mit Rat und Tat zur Seite stand.

Besondere Freude hat mir die interdisziplinäre Arbeit mit Herr Dr. Dirk Neumann vom Zentrum für Bioinformatik der Universität des Saarlandes und dem Arbeitskreis „Technische Simulation“ der Universität Heidelberg um Herrn Prof. Dr. Gabriel Wittum und Herrn Dr. Michael Heisig sowie insbesondere meinem Mit-Doktoranden Herrn Arne Nägel gemacht. Ich denke diese und auch die Arbeit von Herrn Arne Nägel sind den Ideen und Anstrengungen aller zu verdanken.

Einige weitere Leute sollen nicht unerwähnt bleiben, die mir bei der Durchführung bestimmter Experimente geholfen haben:

- Herr Peter Meiers, der mir als Techniker an unserem Institut die Lipidanalytik abgenommen hat und mir bei der Interpretation der Ergebnisse weitergeholfen hat.
- Herrn Dr. Karl-Heinz Kostka und seinem Team der plastischen Chirurgie des Caritas-Krankenhaus, Lebach und natürlich all ihren Patienten für das Überlassen der exzidierten Humanhaut
- Frau Jarmila Zbytovska für die Durchführung der Röntgenkristallographischen Untersuchungen an den Lipidproben
- Frau Lenka Kolackova, die im Rahmen des Erasmus/Sokrates Programms ihre Diplomarbeit bei uns angefertigt hat, für die Entwicklung der UV-Analytik

Keine Arbeit ist möglich ohne Finanzierung. In diesem Fall waren die DFG (Deutsche Forschungsgemeinschaft; DFG Grant BIZ 4/1) und die ZEBET (Zentralstelle zur Erfassung und Bewertung von Ersatz- und Ergänzungsmethoden zum Tierversuch) beteiligt, denen ich ganz herzlich für die Förderung danke.

Eine wichtige Rolle während der letzten vier Jahre haben die Kollegen im Arbeitskreis Biopharmazie und Pharmazeutische Technologie gespielt, insbesondere Andi, Barbara, Eva, Katharina, Michael, Sebastian und Stephan. Die wissenschaftliche Unterstützung aber in besonderem Maße auch die gute Laune und Kameradschaftlichkeit, die sie verbreitet haben, waren für das Gelingen der Arbeit von großer Wichtigkeit.

Ein letzter Dank geht an meine Familie dafür, dass sie mich immer meinen Weg gehen lassen hat, auch wenn der mich weit weg von meiner Heimat Mecklenburg-Vorpommern geführt hat. Sie hat mich immer in meinen Entscheidungen bestärkt und mich mit allen Mitteln unterstützt.